Pyrolysis of torrefied *Acacia nilotica* and application of biochar for removal of methylene blue dye from aqueous solution

Thesis submitted in partial fulfillment

For the Award of Degree

DOCTOR OF PHILOSOPHY

By

Satyansh Singh

DEPARTMENT OF CHEMICAL ENGINEERING & TECHNOLOGY
INDIAN INSTITUTE OF TECHNOLOGY
(BANARASHINDUUNIVERSITY)
VARANASI-221005
INDIA

Roll. No: 15041010

2020

I would like to dedicate this thesis to my family who has supported and encouraged me throughout this endeavor: thank you for your love and support throughout my entire life and helping me to realize who I am today

CERTIFICATE

It is certified that the work contained in the thesis titled "**Pyrolysis of torrefied *Acacia nilotica* and application of biochar for removal of methylene blue dye from aqueous solution**" by **Satyansh Singh** has been carried under my supervision and that this work has not been submitted elsewhere for a degree.

It is further certified that the student has fulfilled all the requirements of Comprehensive Examination, Candidacy and SOTA for the award of Ph.D. Degree.

Dr. Jyoti Prasad Chakraborty
(Supervisor)
Department of Chemical Engineering & Technology
Indian Institute of Technology (BHU), Varanasi-221005

Prof. Monoj Kumar Mondal
(Co-supervisor)
Department of Chemical Engineering &Technology
Indian Institute of Technology (BHU), Varanasi-221005

DECLARATION BY THE CANDIDATE

I, **Satyansh Singh**, certify that the work embodied in this Ph.D. thesis is my own bonafide work carried out by me under the supervision of **Dr. Jyoti Prasad Chakraborty** and co-supervision of **Prof. Monoj Kumar Mondal** for a period of 5 years from July 2015 to September 2020 at Department of Chemical Engineering & Technology, Indian Institute of Technology (BHU), Varanasi, India. The matter embodied in this Ph.D. thesis has not been submitted for the award of any other degree/diploma.

I declare that I have faithfully acknowledged, given credit to and referred to the research workers wherever their works have been cited in the text and the body of the thesis. I further certify that I have not willfully lifted up some other's work, paragraph, text, data, results, etc. reported in the journals, books, magazines, reports, dissertations, theses, etc., or available at web-sites and included them in this Ph. D. thesis and cited as my own work.

Date: …….

Place: Varanasi **(Satyansh Singh)**

CERTIFICATE FROM THE SUPERVISOR

This is to certify that the above statement made by the candidate is correct to the best of our knowledge.

Dr. Jyoti Prasad Chakraborty
(Supervisor)
Department of Chemical Engineering & Technology
Indian Institute of Technology (BHU), Varanasi-221005

Prof. Monoj Kumar Mondal
(Co-supervisor)
Department of Chemical Engineering & Technology
Indian Institute of Technology (BHU), Varanasi-221005

Head
Department of Chemical Engineering & Technology
Indian Institute of Technology
(BHU), Varanasi–221005

COPYRIGHT TRANSFER CERTIFICATE

.

Title of Thesis: "Pyrolysis of torrefied *Acacia nilotica* and application of biochar for removal of methylene blue dye from aqueous solution"

Candidate's Name: Satyansh Singh

Copyright Transfer

The undersigned hereby assigns to the Indian Institute of Technology (Banaras Hindu University) all rights under copyright that may exist in and for the above thesis submitted for the award of the Ph. D. degree.

Date:

Place: **(Satyansh Singh)**

ACKNOWLEDGEMENT

I take this opportunity to express my deep sense of gratitude and indebtedness to my esteemed supervisor **Dr. Jyoti Prasad Chakraborty**, and **Prof. Monoj Kumar Mondal** who helped enormously and always inspired me by their indispensable guidance and encouragement during the whole dissertation work. They always supported and strengthened me in many direct and indirect ways.

I am highly grateful to **Prof. V. L. Yadav**, Professor, Department of Chemical Engineering and Technology, Indian Institute of Technology, Banaras Hindu University, for providing necessary facilities and encouragement during the research work.

I express my sincere thanks to all DPGC and RPEC members for their direct or indirect motivation and assistance from different corners during my research work at institute. Further, I would like to thank **Mr. Vinay Kumar** of Chemical Engineering Department, for providing me valuable support and encouragement during the research work.

Also I express my sincere thanks to all faculty members of the Department of Chemical Engineering and Technology, Indian Institute of technology, Banaras Hindu University for their help during the research work. I am very thankful to all technical and non-technical staff of Department of Chemical Engineering & Technology, Indian Institute of technology, Banaras Hindu University.

I feel loss of words to express my most heartfelt and cordial thanks to my friends **Ms. Bineeta Singh, Mr. Shobhit dixit, Mr. Sudhakar Saroj, Mr. Anuj Kumar Prajapati, Mr. Rishikesh Kumar Singh, Mr. Devesh Kumar Srivastava, Mr. Goutam Kishore Gupta, Mr. Pramendra Gaurh, Mr. Deoashish Panjiara and Ms. Zeenat Arif**

who have always been a source of inspiration for me and who stood by my side at the toughest times.

The whole credit of my achievements goes to my father **Late Mr. Giraja Shankar Singh**, mother **Smt. Vanshraji Devi**, and brother **Amrit Kumar Singh** who were always there for me in my difficulties. It was their unshakable faith in me that has always helped me to proceed further.

Finally I wish to extend a warm thank all those who could not find a separate name but have helped directly and indirectly.

Date:

Varanasi **(Satyansh Singh)**

Table of Contents

Title of the thesis

List of Figure

List of Tables

List of Abbreviations

ANSI	American National Standards Institute	RT	Retention time
ANOVA	Analysis of variance	RSM	Response surface methodology
ASTM	American Society for testing and materials	SEM	Scanning electron microscope
AC	Ash content (wt %)	SGF	Sweeping gas flow rate
BBD	Box-Behnken design	TGA	Thermogravimetric analysis
BD	Bulk density	HR	Heating rate
BL	Biomass loading	V_p	Volume of biomass (m^3)
BET	Brunauer–Emmett–Teller	V_c	Sample cell volume (m^3)
C	Cohesion coefficient	V_R	Reference volume (m^3)
CCD	Central composite design	V_L	Volume of measuring cylinder (m^3)
CCI	Carr compressibility index	VCT	Vapour cooling temperature
CI	Combustibility index (MJ/kg)	T	Temperature
CrI	Crystallinity index (%)	TAN	Torrefied *Acacia nilotica*
CHNS	Carbon Hydrogen Nitrogen Sulphur	TANX-Y-Z	Torrefied biomass at optimum condition
Db	Dry basis	X	Optimum temperature
d_{gm}	Geometric mean diameter (mm)	Y	Optimum retention time
DAN	Dry *Acacia nilotica*	Z	Optimum heating rate
DTG	Differential thermogravimetry	XRD	X-Ray diffraction (XRD)
d_i	Aperture diagonal of i^{th} screen	ρ_b	Bulk density (kg/m^3)
d_{i-1}	Aperture diagonal of next larger screen	ρ_{Tb}	Tapped density (kg/m^3)
EY	Energy yield (%)	ρ_p	Particle density (kg/m^3)
EDX	Energy dispersive X-ray (EDX)	k	Scherrer constant (0.90)
FC	Fixed carbon (Wt %)	λ	X-ray wavelength (0.15406 nm)
Fr	Feed rate	β	FWHM of peak
FR	Fuel ratio	k	Rate constant
FTIR	Fourier transform infrared spectroscopy	α	fractional conversion
FWHM	Full width at half maximum	m_0	Initial mass of the sample (mg)
HHV	Higher heating value (MJ/kg)	m_t	Mass of sample at any time t (mg)
HR	Hausner ratio	m_f	Final mass of the sample (mg)
I_{002}	Crystalline intensity of diffraction	E_a	Activation energy

	plane (002)
I_{am}	Amorphous intensity of diffraction plane (002)
L_{002}	crystal size
M_i	Mass retained on i^{th} screen (kg)
M_1	Initial mass of sample (kg)
m_c	Mass of empty cylinder
m_p	Mass of geometrical shape (kg)
P_1	Pressure after pressurizing the reference volume (Pa)
P_2	Pressure after including V_C (Pa)
m_g	Total mass of cylinder with sample (kg)
m_t	Total mass of cylinder with sample after tapping (kg)
GC-MS	Gas chromatography-mass spectroscopy
PO-DAN	Pyrolysis oil from raw biomass pyrolysis at optimum condition
PO-TAN	Pyrolysis oil from torrefied biomass pyrolysis at optimum condition

	(kJ/mol)
E_α	Activation energy at different conversion (kJ/mol)
A	Pre-exponential factor (s^{-1})
R	Universal gas constant
β	Heating rate (K/min)
T	Temperature (K)
T_α	Temperature at different conversion (K)
T_p	Peak temperature in the DTG curve (K)
ΔH	Change in enthalpy (kJ/mol)
ΔG	Change in Gibbs free energy (kJ/mol)
ΔS	Change in entropy (J/mol.K)
K_B	Boltzmann constant ($1.381*10^{-23}$ J/K)
h	Plank constant ($6.626*10^{-34}$ J.s),

Preface

This thesis explores the pyrolysis of torrefied *Acacia nilotica* in a tubular fixed-bed reactor under nitrogen environment. The process was optimized using response surface methodology coupled with central composite design, in order to obtain the maximum yield of pyrolysis oil. Due to the fast-growing population, technological advancement and higher standard of living of people, demand for energy as well as the price of fossil-derived fuels like petrol and diesel are increasing. Also, the fossil fuel reserves are neither sustainable nor clean sources of energy. Among the available renewable sources of energy, incidentally, biomass has gathered significant attention due to its copious amount, low market value, and carbon neutrality. However, biomass is associated with many inherent shortcomings like higher moisture content, lower higher heating value, higher O/C and H/C ratio and hygroscopic nature, which makes biomass inferior to fossil derived fuels.

So, I decided my research objective to pretreat the biomass using torrefaction process and then preform the pyrolysis of treated biomass. The physicochemical characteristics of products from pyrolysis of treated and raw biomass were compared. Finally, the efficacy of biochar from treated and raw biomass was tested towards removal of aqueous methylene blue.

I express my deep sense of gratitude and indebtedness to my esteemed supervisors **Dr. Jyoti Prasad Chakraborty** and **Prof. Monoj Kumar Mondal**, for their guidance and encouragement during the PhD dissertation work.

So, it is hoped that this PhD work will help to understand the integrated torrefaction-pyrolysis process for better utilization of biomass as source of energy. For ease of understanding to the readers, this thesis has divided in eight chapters.

Satyansh Singh

Chapter 1

Introduction

1.1 Background and problem statement

The economic and social development of a nation is decided by the resources and its utilization for production of energy. The demand for energy in the world is increasing day by day due to increasing global population and ever-increasing living standard of people (Singh et al., 2020a). Considering worldwide population from 2015 to 2040, World Bank predicted that total population will increase from 7.3 to 9.1 billion (Fig. 1.1a). In recent years the world is facing major energy crisis. According to international energy outlook (IEA) 2016, total world energy consumption is projected to rise from 549 quadrillion Btu in 2015 to 812 quadrillion Btu in 2040 with an increase of around 48% (Fig. 1.1b) (Mokheimer et al., 2017). To fulfill our energy demand, we are highly dependent on the conventional sources of energy like coal, petroleum and natural gas. Fig. 1.2 clearly shows that fossil-derived fuels contribute to 87 % of total energy demand in India, while it contributes to 81.2 % of total energy demand of the world. The use of conventional energy resources like coal and crude petroleum produce greenhouse gases which severely affect the environment by increasing the temperature level of the earth. According to international energy outlook (IEA) 2016, world energy related CO_2 emission increases from 32.2 billion metric ton in 2012 to 43.2 billion metric ton in 2040 with an increase of around 34% (Mokheimer et al., 2017). The reserves of fossil fuel such as coal, petroleum, and natural gas are limited and large exploitation along with complete dependence on the fossil fuel can diminish the fossil fuel reserve. Also, application of fossil fuels severely affects the

environment by harmful emission such as SO_x, NO_x, greenhouse gas (CO_2) and particulate matters (Chen et al., 2011; Phanphanich & Mani, 2011; Yue et al., 2017).

Hence, the world is moving towards the exploration of non- conventional energy sources. The major thrust on research and technology of present era is how to extract maximum amount of energy from renewable energy resources in the most efficient, economical, and sustainable way. Though we have wind, solar, geothermal, hydrothermal etc. as renewable energy sources, however, among them biomass is the most abundant worldwide and easily available. The consideration of biomass as a carbon-neutral fuel and its quality to emit lesser amount of sulfur and nitrogen makes it important source for the production of bio-energy (Giudicianni et al., 2013).

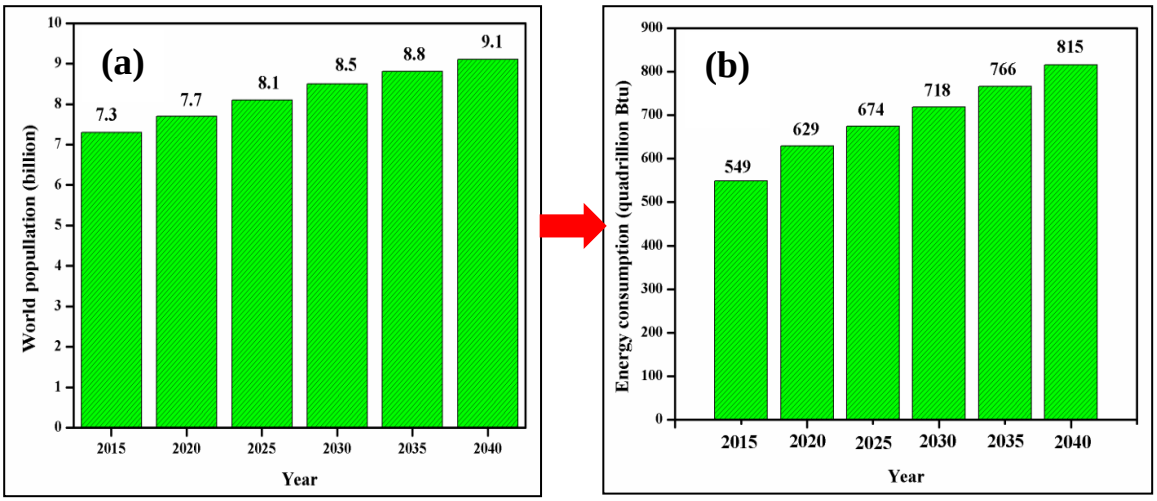

Figure 1.1 (a) Trend of increase in world population from 2015 to 2020 and **(b)** increase in demand of energy from 2015 to 2020

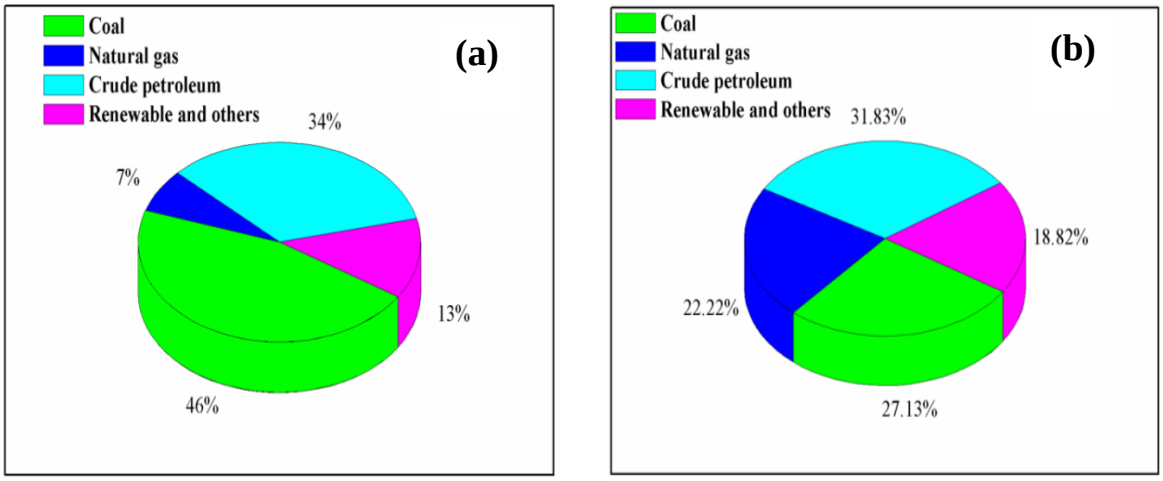

Figure 1.2 Major sources of energy in **(a)** India and **(b)** World

1.2. Biomass as a source of renewable energy

As the name suggests, biomass is biological mass i.e., the organic matter which is derived from living or recently living organism is called biomass. It can be microorganism, plant or animal in a given area of the ecosystem at a particular time. Various examples of biomass include food crops, crops for energy like switch grass or prairie perennials, crop residues like corn stover, wood waste and by-products (both mill residues and traditionally noncommercial biomass in the woods), and animal manure. In recent years the concept of biomass has widened and includes construction debris, municipal solid waste, algae, yard waste and food waste. Woody biomass is preferred over food crop biomass since it contains larger amount of energy than food crop biomass and lower application of fertilizer and pesticides for woody biomass (van der Stelt et al., 2011).

1.2.1 Components of biomass

Basic components of biomass can be classified as lignocellulosic and non-lignocellulosic. The lignocellulosic part of the biomass consists of mainly non-starch and fibrous part of the plants which are mainly polymer and joined with each other to different degree and with varying composition depending on the type and source of biomass. It consists of cellulose, hemicellulose and lignin which account for 40-60, 20-40 and 10-25 wt % of the total lignocellulosic biomass (Agbor et al., 2011; Carere et al., 2008; Chandra et al., 2007; Yang et al., 2007). Typical composition of various biomass samples are presented in Table 1.1. Non- lignocellulosic part of the biomass, on other hand, contains non-cellulosic material like sugar, starch, protein and fat. Cellulose, hemicellulose, and lignin are the main fiber cell-wall components present in the biomass and they show different reactivity during thermochemical conversion processes (Chen et al., 2013).

Table: 1.1 Constituents of selected biomass (wt% composition)

Biomass	**Cellulose (%)**	**Hemicellulose (%)**	**Lignin (%)**	**References**
Wheat straw	41.3	30.8	7.7	(Bridgeman et al., 2008)
Reed Canary Grass	42.6	29.7	7.6	(Bridgeman et al., 2008)
Rice Straw	34.0	27.2	14.2	(Mohan et al., 2006)
Birch Wood	40.0	25.7	15.7	(Mohan et al., 2006)
Corn cobs	50.5	31.0	15.0	(Worasuwannarak et al., 2007)
Cotton linter	89.7	1.0	2.7	(Dorez et al., 2014)

Sugar cane	51.8	27.6	10.7	(Dorez et al., 2014)
Switch grass	35.8	21.5	21.1	(Jung et al., 2015)
Bamboo	54.6	11.4	21.7	(Dorez et al., 2014)
Willow	42.4	20.6	21.1	(Stolarski et al., 2013)
Coconut	51.3	11.7	30.7	(Dorez et al., 2014)

1.2.1.1 Cellulose

Long chain polymers of saturated linear polysaccharide (glucose) which are linked together by inter-molecular and intra-molecular hydrogen bonding are called cellulose (Ghetti et al., 1996; Pordesimo et al., 2005; Tillman, 2000) Cellulose molecules are having fibrous macromolecular structures with smooth surface and composed of semi crystalline arrays of b-1,4 glucan chains having molecular weight of 500,000 in which D- Glucose is linked together by β-Glucosidic linkage (Chen & Kuo, 2010; Raveendran & Ganesh, 1998). Crystalline structure of cellulose provides higher packing density which increases the strength of biomass (Mohan et al., 2006).

1.2.1.2 Hemicellulose

Hemicelluloses, also known as polyose (Mohan et al., 2006) are generally heteropolysaccharides like hexoses which contain glucose, mannose and galactose which account for 25-35% by mass in dry wood, 28% in softwood, and 35% in hardwood (Mohan et al., 2006; Raveendran & Ganesh, 1998; Scurlock et al., 2000). Hemicelluloses are those polysaccharides which provide strength to the plant wall. The important constituents of hemicellulose are xyloglucons, xylans mannans, glucomannans and β-glucanes. Hemicelluloses are highly branched, amorphous and irregular in structure and cracks are

found on the surface which makes it weakest part of the biomass (Huber et al., 2006; Raveendran & Ganesh, 1998; Yang et al., 2007). Hemicellulose has lower degree of polymerization in comparison to cellulose hence it undergoes thermal degradation easily.

1.2.1.3 Lignin

The third major constituent of biomass is lignin whose amount depends on the type of biomass (23-33% for softwood and 16-25% for hardwood) (Bridgewater, 2004; Mohan et al., 2006). Three dimensional irregular, amorphous polymers which are dominant in C-O-C and C-O linkage are generally known as lignin and mainly attached with four or more phenylpropane unit and different type of alcohol such as p-coumaryl, coniferyl and sinapyl as a basic constituent of lignin (Goyal et al., 2008; Huber et al., 2006; Jenkins et al., 1998; Khan et al., 2009; Mohan et al., 2006; Tillman, 2000). Lignin having hemispherical shape (Raveendran & Ganesh, 1998) embedded into the cellulose, consists of large group of aromatic polymers and it acts as a binder for the agglomeration of cellulosic component of biomass and it hold the micro fibrils with greater rigidity and provide strength to the cell wall of the biomass (Goyal et al., 2008; Mohan et al., 2006; Scurlock et al., 2000; Yaman, 2004). Thermal degradation of lignin occurs at wide range of temperature since different oxygen functional groups have different thermal stability.

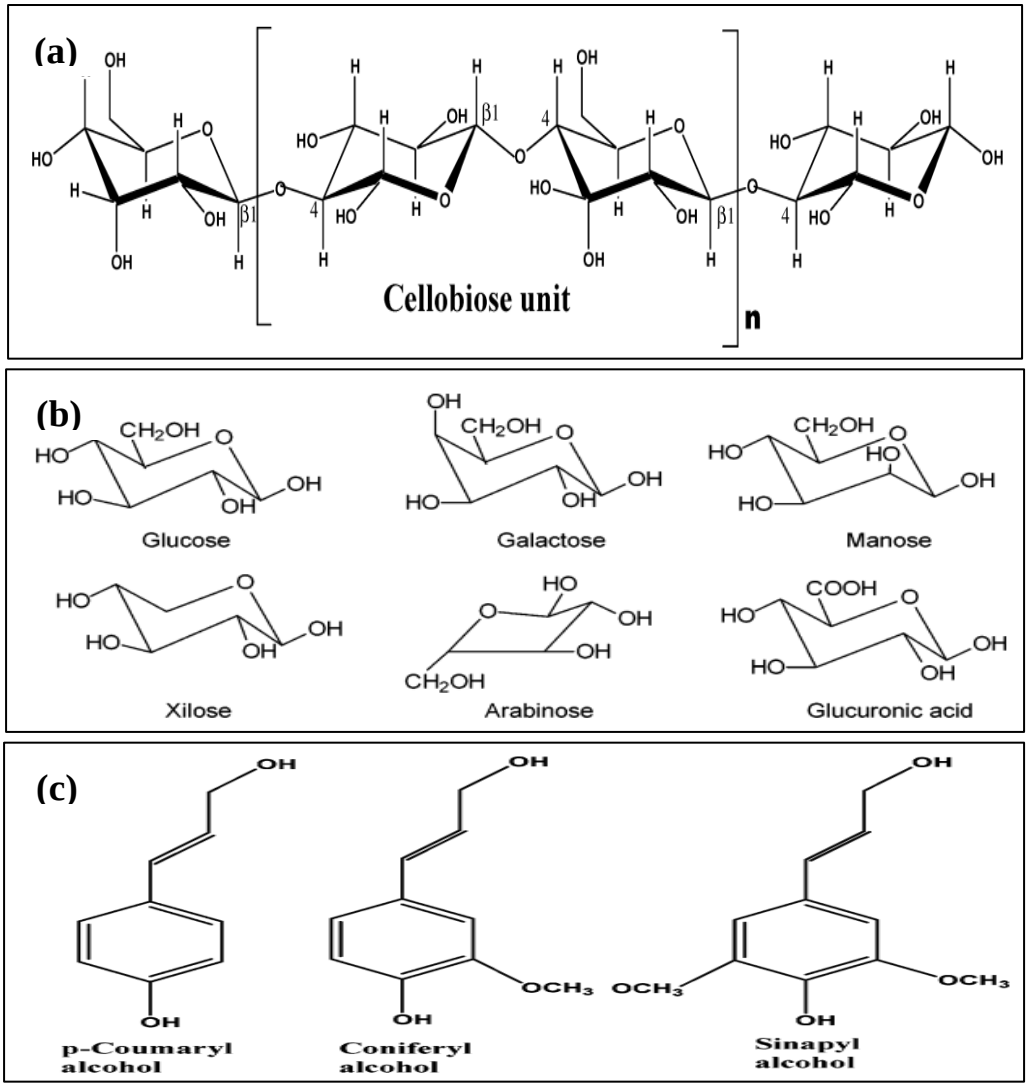

Figure 1.3 Major constituents of biomass **(a)** cellulose **(b)** hemicellulose and **(c)** lignin

1.2.1.4 Organic extractives

Biomass also contains some organic extractive materials. These materials can be identified in polar solvent (water, alcohol, methylene chloride) as well as non-polar solvent (toluene, n-hexane). The common extractive materials which are present in biomass are waxes (polyalkanes which is solid at room temperature), fats (polyalkanes which may be solid or

liquid at room temperature), alkaloids, proteins (amino acid, amines and carboxylic acid), phenolic, gum, resins (Mohan et al., 2006). These extractive materials act as intermediates in metabolism and as energy reserves. These extractive materials protect the biomass from external attack of microbes and insects (Mohan et al., 2006).

1.2.1.5 Inorganic minerals

Many inorganic minerals or metals are also present in biomass, which get concentrated in biochar after thermochemical process like torrefaction and pyrolysis. The common minerals present in the biomass are potassium (K), magnesium (Mg), calcium (Ca), phosphorus (P), and sodium (Na). The presence of these inorganic materials opens a wide range of application of bio char in different fields like catalysis, adsorption and fertilizer production.

1.3 Extraction of energy from biomass

Generally, energy from biomass can be extracted via two processes such as thermochemical conversion and biological conversion. However, thermochemical conversion of biomass has gained dominance over biological conversion because of its fast and efficient nature, higher conversion efficiency (Singh et al., 2020b), etc.

1.3.1Thermochemical conversion of biomass

1.3.1.1 Pyrolysis of biomass

Pyrolysis is the thermal decomposition of lignocellulosic biomass in the presence of inert atmosphere. Temperature during the pyrolysis may vary from 200-1000 ℃. The term devolatilization is also used as equivalent to pyrolysis but it is usually understood that devolatilization implies the presence of an oxidizing agent. The major products from

pyrolysis of biomass are bio-oil (liquid), biochar (solid) and noncondensable gases (Goyal et al., 2008). The process parameters which generally affect pyrolysis are temperature, retention time, heating rate, atmosphere inside the reactor, pressure and type of reactor. The products from pyrolysis of biomass depend on the process parameters and the composition of biomass. The pyrolysis gas contains mainly hydrogen, carbon dioxide, carbon monoxide, methane and light saturated and unsaturated hydrocarbons (Volpe et al., 2018). The liquid product from pyrolysis consists mainly of polyaromatic hydrocarbons (PAH), oxygenated aromatic compounds such as phenol and water (due to the moisture content of the fuel) (Yang et al., 2015). It is also called pyrolysis oil or bio-oil and can be upgraded to hydrocarbon liquid fuels for combustion engines, or directly used for power generation or heat (Kumar et al., 2020).

1.3.1.2 Combustion of biomass

Combustion means the complete oxidation of the biomass feedstock (Demirbas, 2007) in presence of stoichiometric or excess air/oxygen. It is one of the most traditional processes for extraction of energy from lignocellulosic biomass (Zhang et al., 2010). The process produces very hot gases that can be used to generate steam or to provide heat to a Sterling engine. The combustion process of biomass is far better known than the other thermochemical processes as far as the heat generation is concerned; however, many harmful gaseous products (NOx and SOx emissions) are generated during combustion of biomass.

1.3.1.3 Liquefaction of biomass

The liquefaction of biomass is similar to pyrolysis, while, it differs in operating conditions (Zhang et al., 2010). The process takes place at low temperatures (250-350 °C) and high pressure (100-200 bar) (Demirbaş, 2000). During liquefaction, biomass gets converted to water and fragments of small molecules which finally get converted into bio-oil by re-polymerization reaction (Demirbaş, 2001). With respect to pyrolysis, liquefaction has been considered as more complex and challenging process because of operating conditions, feedstock conditions and operational cost (Demirbaş, 2001).

1.3.1.4 Gasification of biomass

The gasification of biomass is an endothermic process where carbonaceous biomass is transformed mainly into mixture of combustible gases such as CO, CO_2, CH_4, and H_2 in presence of partial supply of O_2, CO_2 and H_2O (Zhang et al., 2010). When O_2 is used in gasification process, it is similar to combustion; however, partial combustion of biomass takes place in case of gasification. Also, the aim of combustion is to generate heat from biomass, while, gasification is used for generation of valuable gaseous products which can be used for direct combustion or can be used for other purposes (Rezaiyan & Cheremisinoff, 2005). In addition, gasification can be considered as more environmental-friendly process because of lower emissions of toxic gases like SOx and NOx (Rezaiyan & Cheremisinoff, 2005).

1.4 Demerits of raw biomass

Regardless of large availability, easy accessibility, and inexpensive in nature, biomass is burdened with many inherent disadvantages. Table 1.2 presents various drawbacks

associated with raw biomass and their effect on process as well as products. These drawbacks hinder the direct application of biomass in thermochemical conversion processes. It is therefore essential to improve the quality of biomass through pretreatment process and check the suitability of treated biomass in term of fuel and flow properties, before it can be used in thermochemical conversion process efficiently.

Table: 1.2 Demerits of raw biomass (adopted from (Bach & Skreiberg, 2016), (Dai et al., 2019))

Parameter	Associated drawbacks
High moisture content	• Reduces the efficiency of the process • Increases drying energy requirement • Increases corrosion because of condensation of water in flue gas • Possibility of biological degradation • Reduces the heating value • Increases storage and transportation cost
Heterogeneity	• Creates wide variation in the property
High Oxygen content	• Reduces the number of high energy C-H bond • Reduces heating value and thermal stability • Creates poor energy density
Poor Grindability	• Increases the grinding energy • Poor grindability produces coarser particle
Hygroscopic nature	• Prone to biological degradation due to absorption of moisture
Low bulk and energy density	• Increases the storage and transportation cost • High feeding capacity required

1.5 Pretreatment of raw biomass

The raw biomass commonly requires certain physical and chemical modification to improve its inherent characteristics prior to its utilization in any thermochemical processes such as pyrolysis, gasification, combustion, etc. Generally, the pretreatment of biomass can be done through four methods namely; (1) physical methods, (2) thermal treatment, (3) chemical treatment, and (4) biological treatment (Kumar et al., 2020). Fig. 1.4 represents various types of pretreatment steps and their effects on structure of biomass.

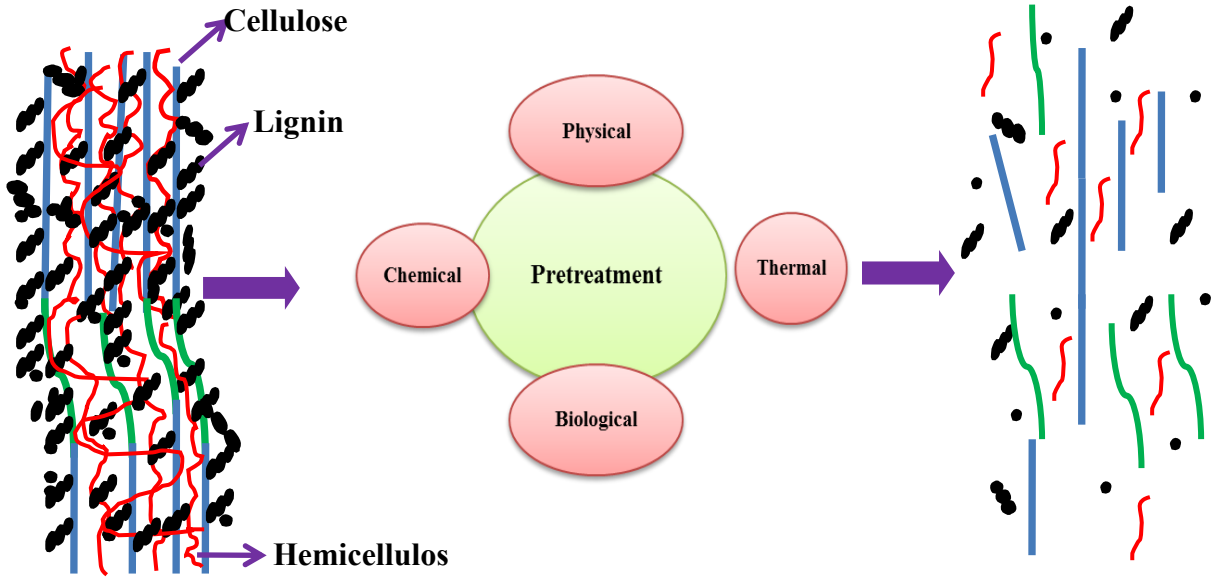

Figure 1.4 Effect of pretreatment on structure of biomass

.1.5.1 Physical pretreatment

Generally, the physical pretreatment of biomass is associated with size reduction and/or densification. The size reduction of biomass particles facilitates better heat and mass transfer during thermochemical conversion process (Kumar et al., 2020). The size reduction of biomass also decreases the crystallinity of biomass (Alvira et al., 2010). The size reduction of biomass requires variety of resources such as milling, grinding, extrusion, and chopping machine which makes the process costly (Kumar et al., 2020). The prime concern of size reduction is to disintegrate the large biomass particles into smaller particles having uniform particle size and enhanced surface area. The higher surface area of biomass facilitates easy access to bacterial and enzymatic degradation of biomass, while in case of thermochemical processes, it provides better heat and mass transfer which provide uniform temperature distribution inside the particles (Kan et al., 2016). The densification of biomass increases the density and simplifies its storage and transportation. The densification of biomass is performed through compaction process by applying mechanical force on biomass and converting it into solid lumps called as briquettes.

1.5.2 Biological pretreatment

The biological pretreatment of biomass has been considered as the most economic, cost effective and environmental-friendly pretreatment process as it occurs at ambient temperature and atmospheric pressure and does not involve any chemical (Sindhu et al., 2016; Vasco-Correa et al., 2016). There are various microorganisms such as bacteria and fungi which have high potential to degrade biomass; however white and brown rot fungi have been utilized for pretreatment of biomass (Yang et al., 2011; Yu et al., 2013). Due to

action of microorganism, the complex lignocellulosic biomass unit such as lignin and cellulose break into their monomeric units through degradation or depolymerization. Subsequently, the activation energy of pretreated biomass decreases during thermochemical conversion (Vasco-Correa et al., 2016). The biological pretreatment process has certain drawbacks such as (1) time-consuming process, (2) microorganisms are very temperature-sensitive, (3) large space is required for biological pretreatment, (4) some amount of biomass can be consumed by microorganisms which lead to the decrease in mass yield of pretreated biomass (Agbor et al., 2011). These drawbacks limit the application of biological pretreatment process at industrial scale.

1.5.3 Chemical pretreatment

Chemical pretreatment of biomass is an important method that may overcome the recalcitrant nature of biomass. It involves the treatment of biomass with different kind of chemicals. Chemical treatment of biomass facilitates decomposition and decreases the thermal stability of biomass. Generally, acid and alkali treatment are the most prevalent treatments which fall under chemical pretreatment method. The biomass as a feedstock in thermochemical conversion process contains many inorganic minerals such as chlorides, sulphates, phosphates, and carbonates, etc. (Kumar et al., 2020). These minerals might affect the thermochemical processes through its catalytic activity or soluble minerals may be present in the products. For instance, presence of minerals in bio-oil may decrease the stability and create aging and corrosiveness in bio-oil through polymerization or condensation reaction. Therefore, removal of these minerals is of prime importance to increase the applicability of bio-oil. The pretreatment of biomass with dilute acids such as H_2SO_4, HNO_3, H_3PO_4 and HCl can be potentially used to remove the minerals present in

biomass (Lloyd & Wyman, 2005). The acid pretreatment of biomass basically cleaves the chemical bonds associated with hemicellulose, cellulose and lignin. In similar manner, the alkali pretreatment of biomass may also be carried out with the help of chemicals such as NaOH, KOH, and $Ca(OH)_2$. The alkali pretreatment of biomass facilitates the removal of lignin and increases the digestibility of cellulose (Kumar et al., 2020). Basically, the alkali treatment of biomass breaks the ester and glycosidic bonds between hemicellulose and lignin, while keeping most of the cellulosic part of biomass intact (Mohammed et al., 2017a). The treatment of biomass with alkali results in swelling of cellulose, which can reduce the degree of polymerization and decrystallization of cellulose leading to increase in surface area of biomass (Baruah et al., 2018). The major challenge associated with chemical treatment is corrosion of process reactor system for pretreatment, disposal of chemicals, and cost of chemicals which may increase the overall cost of chemical pretreatment process (Mohammed et al., 2017a).

1.5.4 Thermochemical pretreatment

The thermochemical pretreatment of biomass generally involves two processes; drying and torrefaction (Edelmann et al., 2005). Drying is used to remove the surface moisture from the biomass.

1.5.4.1 Torrefaction of biomass

Torrefaction is defined as the mild pyrolysis in the temperature range of 200-300 ^{0}C under the atmospheric pressure in the presence of inert with a low heating rate (< 20 ^{0}C/min). The retention time of biomass in the reactor should be around 15-60 min. After the torrefaction process, quantity of initial biomass reduces up to 40% and energy decreases around 10-

15% (Granados et al., 2016). Torrefaction occurs via drying, decomposition, devolatilization and depolymerization of biomass. In drying process most of the bound water is released and this takes place below 200 ^{0}C. According to Deng et al. (Deng et al., 2009a) during torrefaction, drying is supposed to be more destructive since it breaks the inter and intra molecular hydrogen bonds, C-O and C-H bonds which lead to the removal of hydrophilic and oxygenated compounds and makes the biomass black in color, hydrophobic in nature and high energy dense. Main products of torrefaction are torrefied biomass in solid form, permanent gases like hydrogen (H_2), Carbon dioxide (CO_2), Carbon monoxide (CO) and hydrocarbon like Methane (CH_4). Along with these products a condensable mixture containing mostly water, organic compound and lipid are also produced. Among all three products, torrefied biomass is the main product since it accounts for 70% weight of the total biomass and retains around 90% of the total energy of the biomass (Bach & Skreiberg, 2016). Unlike pyrolysis, the main aim of torrefaction is to maximize the yield of solid product, hence torrefaction is performed under low heating rate (Chen & Kuo, 2011). The main objective of torrefaction process is to enhance the quality of biomass for thermochemical process like pyrolysis and gasification. A torrefied biomass is quite suitable for pelletization, briquetting, pyrolysis, gasification and co-firing in thermal power plants (Bridgeman et al., 2010b; Felfli et al., 2005b). The limitations associated with biomass may be removed by torrefaction. It makes the biomass moisture free, hydrophobic solid product, decreases grinding energy, increases energy density, decreases O/C ratio and makes the biomass suitable for storage and transportation. Along with above improvements, it also enhances the particle size distribution, combustion with less smoke; in gasifier, combustion shifted to higher temperature zone, and increases

resistance to biological degradation. Torrefaction makes biomass brittle by removing fibrous and tenacious structure and hydrophobic nature. Due to this, grinding energy requirement for biomass reduces. Due to hydrophobic nature of torrefied biomass, it absorbs less moisture than the raw biomass which is around 3% (Chen et al., 2016b; Granados et al., 2016). Addition to above property, torrefaction provides uniformity, resistance to biological decomposition when exposed to external environment and high energy density to biomass (Granados et al., 2016). The decrease of O/C ratio and increase of energy density of biomass is mainly due to removal of volatile matter and light gases during torrefaction process.

1.6 Characteristics of torrefied biomass

Torrefaction is used as a pretreatment process to upgrade the quality of raw biomass. The most valuable product from torrefaction, considering it as a pretreatment, is torrefied biomass. The quality of torrefied biomass can be examined by its fuel and flow properties. The fuel properties of torrefied biomass can be interpreted by proximate and ultimate analyses, higher heating value, chemical composition and surface morphology. In addition, some fuel properties are also derived from proximate and ultimate analyses such as volatile ignitability, combustibility index, and fuel ratio. The flow properties of torrefied biomass such as Hausner ratio, cohesion coefficient, Carr compressibility index, and angle of repose play an important role during blending of torrefied biomass with other biomass, plastics co-pyrolysis and coal in co-firing in thermal power plants. The flow characteristics of raw and torrefied biomass can be characterized by Hausner ratio (HR), cohesion coefficient (C), Carr compressibility index (CCI) and angle of repose (Lumay et al., 2012). The angle of repose is defined as the steepest angle at which a stack of biomass particle can remain

stable without slumping (Rous et al., 2014). It may range from 0^o to 90^o. Different methods such as revolving cylinder method, tilting box method and fixed funnel method for analyzing the angle of repose have been described in literature (Cai et al., 2017; Rous et al., 2014). However, in this thesis ASTM-C144 associated with fixed funnel method was employed to investigate angle of repose. In fixed funnel method (Fig. 1.5), the biomass particles obtained after sieving were poured very slowly through a funnel which was fixed through a stand at a certain height (H) from the base. The biomass coming out of funnel takes the shape of a cone. The pouring from the funnel was stopped when cone pile touched the lower tip of the funnel which was at a predetermined height (H). By measuring the radius of base of the cone, the angle of repose can be calculated using Eqs. (1.1). Szalay et al. (Szalay et al., 2015) derived a correlation for cohesion coefficient and concluded that cohesion coefficient depends on angle of repose and particle size of biomass. The cohesion coefficient was calculated by Eqs. (1.2). HR and CCI vary with densities (bulk and tapped density) of biomass. HR and CCI of DAN and TAN were obtained by employing Eqs. (1.3) and (1.4).

$$Angle\ of\ repose\ (\theta) = tan^{-1}\left(\frac{H}{R}\right) \quad Where\ R = D/2 \tag{1.1}$$

$$Cohesion\ coefficient\ (C) = \frac{1}{2}d\left(\sqrt{cos^2\theta + \frac{4sin\theta}{d}} - cos\theta\right) \tag{1.2}$$

$$Hausner\ ratio\ (HR) = \frac{\rho_{Tb}}{\rho_b} \tag{1.3}$$

$$Carr\ compressibility\ index\ (CCI) = \left(1 - \frac{\rho_b}{\rho_{Tb}}\right) \times 100 \tag{1.4}$$

To evaluate the suitability of torrefied biomass as good quality solid bio-fuel, Conag et al. (Conag et al., 2017) mentioned combustion indices such as fuel ratio (FR), combustibility index (CI) and volatile ignitability (VI) and they were enumerated by using Eqs. (1.5)-(1.6).

$$\textit{Fuel ratio, } FR = \frac{FC_{db}}{VM_{db}} \tag{1.5}$$

$$\textit{Combustibility index CI (MJ/kg)} = \frac{HHV_{db}}{FR} \times (115 - Ash_{db}) \times \frac{1}{105} \tag{1.6}$$

$$\textit{Volatile ignitability, VI (MJ/kg)} = \left[\frac{HHV_{db} - 0.338FC_{db}}{VM_{db} + M_{db}} \right] \times 100 \tag{1.7}$$

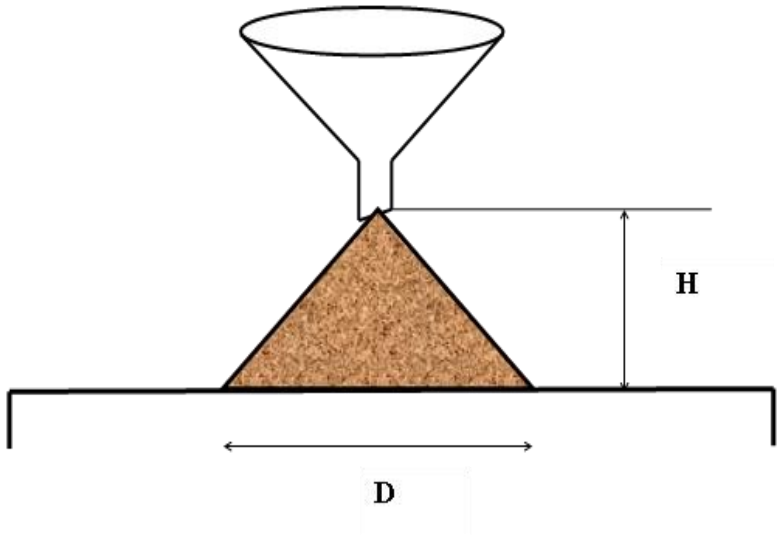

Figure 1.5 Schematic for calculation angle of repose

1.7 Application of biochar from pyrolysis of biomass

The pyrolysis of biomass yields three types of products, namely, bio-oil, biochar, and gaseous products. Nowadays, biochar has gathered colossal attention in wastewater treatment processes because it is chemically stable and environmentally friendly (Lyu et al., 2018; Zhang et al., 2020). It is a low cost adsorbent having high surface area, porosity, and higher carbon content (Trakal et al., 2014). The high functionality of biochar surface imparts adsorption potential for toxic substances present in wastewater (Uchimiya et al., 2010). Biochar from thermochemical processes has also been chemically engineered to improve its adsorption capacity (Lyu et al., 2018). However, chemically treated biochars have certain limitations, such as cost and associated problems of release of chemicals (Lyu et al., 2018).

1.8 Structure of thesis

This thesis entitled "**Pyrolysis of torrefied *Acacia nilotica* and application of biochar for removal of methylene blue dye from aqueous solution**" has been divided into eight chapters.

Chapter 1 is related to introduction section where general information about limitations of fossil derived fuels, basic information about biomass, extraction of energy from biomass, limitations of biomass, pretreatment of biomass, and application of biochar has been discussed.

Chapter 2 contains the detailed literature review of torrefaction process, pyrolysis process, and application of biochar for removal of methylene blue dye.

Chapter 3 is related to the torrefaction of *Acacia nilotica* in fixed-bed reactor and investigation of fuel and flow properties of torrefied biomass. The physicochemical

characteristics of raw biomass, torrefied biomass and coal have been compared to check the suitability of torrefied biomass in pyrolysis process.

Chapter 4 is related to pyrolysis of raw and torrefied biomass in thermogravimetric analyzer followed by estimation of kinetic parameters, thermodynamic parameters, and solid state reaction mechanism.

Chapter 5 is related to the optimization of process parameters (temperature, retention time, and heating rate) for torrefaction process using response surface methodology. The physicochemical characteristics of raw biomass and torrefied biomass obtained at optimum condition have been compared.

Chapter 6 is related to the pyrolysis of torrefied biomass obtained at optimum condition of torrefaction. The process parameters (temperature, retention time, heating rate, and sweeping gas flow rate) have been optimized using response surface methodology for maximum yield of pyrolysis oil. The pyrolysis of raw biomass at obtained optimum condition is also performed and characteristics of pyrolysis products (pyrolysis oil, biochar and pyrolytic gases) have been compared with products from pyrolysis of torrefied biomass at optimum condition.

Chapter 7 is related to the comparative study for removal of methylene blue dye from aqueous solution using biochar as an adsorbent from pyrolysis of raw and torrefied biomass obtained at optimum condition of pyrolysis for maximum pyrolysis oil yield.

Chapter 8 is related to the summary of results from thesis and scope of future work.

Chapter 2

Literature review and objectives

In this chapter literature review related to the torrefaction of biomass, optimization of torrefaction process for high grade torrefied biomass, pyrolysis of raw and torrefied biomass, and optimization of process parameters such as temperature, retention time, heating rate, sweeping gas flow rate, particle size, etc. have been discussed. Finally, the literature related to application of biochar from pyrolysis of raw biomass towards removal of methylene blue dye from aqueous solution has been systematically discussed. This chapter-2 has been divided into three parts: (1) literature review on torrefaction of biomass and optimization of torrefaction process, (2) literature review on pyrolysis of raw and torrefied biomass and optimization of process parameters, (3) literature review on application of biochar from pyrolysis of biomass for removal of aqueous methylene blue. Based on the literature review objectives of present research work have been decided.

2.1 Literature review

2.1.1 Torrefaction of biomass and optimization of torrefaction process

2.1.1.1 Torrefaction of biomass

Torrefaction is thermochemical pretreatment process that occurs in the temperature range of 200 to 300 ℃ in an oxygen free environment at atmospheric pressure (Niu et al., 2019). Torrefaction can alleviate the undesired characteristics of biomass such higher moisture content, lower energy density and HHV, lower fixed carbon, hydrophobicity, higher grinding energy (Chen & Kuo, 2011).

2.1.1.1.1 Effect of torrefaction on proximate and ultimate analysis of biomass

The effect of torrefaction on proximate and ultimate analysis of various biomasses has been mentioned in Table 2.1. The proximate analysis of torrefied biomass at different torrefaction condition revealed the significant decrease in volatile matter and at the same time increase in fixed carbon content and ash content was observed due to torrefaction. The ultimate analysis demonstrates the higher carbon content and lower oxygen and hydrogen content in torrefied biomass as compared to the raw biomass. Also, the trend in results of proximate and ultimate analysis intensifies with increase in severity of torrefaction process (increase in process temperature and retention time). The cleavage of oxygen containing functional groups present in biomass consequently release of light volatile matter during torrefaction is responsible for change in results of proximate and ultimate analysis (Wannapeera et al., 2011b). The decrease in volatile matter during torrefaction is the result of catalytic effect of inorganic minerals present on biomass (Sadaka & Negi, 2009). The higher carbon content in torrefied biomass as compared to oxygen and hydrogen depicts the higher energy value of torrefied biomass as compared to raw biomass (Couhert et al., 2009). The increase in energy value of torrefied biomass makes it suitable for biofuel production. The ash content of torrefied biomass is higher than raw biomass; however, increase in ash content is lower than the increase in fixed carbon content. The ash content is the inherent characteristics of biomass selected for torrefaction. Thus, the ash content of biomass has relative effect on the obtained torrefied products (Bridgeman et al., 2008). The increase in ash content on torrefied can results in accumulation of metallic minerals which may act as catalyst during pyrolysis of torrefied biomass (Yildiz et al., 2015). The

elemental analysis also revealed that the atomic ratios H/C and O/C of torrefied biomass are lower than raw biomass. The decrease in these ratios facilitates the application of torrefied for biofuel production.

Table 2.1 Effect of torrefaction on proximate and ultimate analysis of biomass

Biomass	**Proximate analysis**			**Ultimate analysis**				**References**
	VM (wt%)	FC (wt%)	AC (wt%)	C (wt%)	H (wt%)	O (wt%)	N (wt%)	
Beech wood (raw) *PS =50-500 μm	84.20	15.50	0.30	47.20	6.00	45.20	0.40	(Couhert et al., 2009)
Torrefaction at T (240 ℃) RT (1 h) PS = 50-500 μm	80.60	19.20	0.35	51.70	5.40	42.90	0.00	
Torrefaction at T (260 ℃) RT (1 h) PS = 50-500 μm	75.70	24.20	0.40	54.40	5.20	40.40	0.00	
Leucaena (raw) PS < 75 μm	86.10	13.10	0.80	50.10	7.40	41.80	0.70	(Wannapeera et al., 2011b)
Torrefaction at T (200 ℃) RT (0.5 h) PS < 75 μm	85.30	14.00	0.70	51.70	7.10	40.50	0.70	
Torrefaction at T (225 ℃) RT (0.5 h) PS < 75 μm	84.30	14.90	0.80	52.40	7.10	39.80	0.70	
Torrefaction at T (250 ℃) RT (0.5 h) PS < 75 μm	82.20	16.90	0.90	53.00	6.40	39.90	0.70	
Torrefaction at T (275 ℃) RT (0.5 h) PS < 75 μm	73.80	24.90	1.30	57.20	5.50	36.50	0.80	
Willow (raw) PS = NR	87.60	10.70	1.70	47.20	6.10	44.80	0.34	(Bridgeman et al., 2008)
Torrefaction at T (230 ℃) RT (0.5 h) PS = **NR	82.10	16.10	1.80	50.70	6.20	39.50	0.20	

Torrefaction at T (250 ℃) RT (0.5 h) PS = NR	79.80	18.40	1.90	51.70	6.10	38.70	0.20	
Torrefaction at T (270 ℃) RT (0.5 h) PS = NR	79.30	18.60	2.10	53.40	6.10	37.20	0.20	
Torrefaction at T (290 ℃) RT (0.5 h) PS = NR*	77.20	20.50	2.30	54.70	6.00	36.40	0.10	
Pine (raw) PS= 20.94-70.59 mm (length)	85.98	13.76	0.27	47.20	6.64	45.76	0.17	(Phanphanich & Mani, 2011)
Torrefaction at T (225 ℃) RT (0.5 h) PS= 20.94-70.59 mm (length)	84.78	14.95	0.27	49.47	6.07	44.03	0.15	
Torrefaction at Temp (250 ℃) RT (0.5 h) PS= 20.94-70.59 mm (length)	82.52	17.24	0.25	51.46	5.86	42.02	0.14	
Torrefaction at T (275 ℃) RT (0.5 h) PS= 20.94-70.59 mm (length)	76.40	23.26	0.35	54.91	6.20	38.17	0.20	
Torrefaction at T (300 ℃) RT (0.5 h) PS= 20.94-70.59 mm (length)	58.72	40.85	0.43	63.67	5.58	29.99	0.20	
Sawdust (raw) PS= 20-30 mesh	73.15	13.02	0.38	40.85	6.17	39.07	0.03	(Chen et al., 2011)
Torrefaction at (230 ℃) RT (0.5 h) PS= 20-30 mesh	69.10	19.84	8.62	45.92	5.20	37.01	0.53	
Torrefaction at T (250 ℃) RT (0.5 h) PS= 20-30 mesh	64.79	23.74	9.21	47.16	5.01	0.55	35.52	
Torrefaction at T (270 ℃) RT (0.5 h) PS= 20-30 mesh	57.07	30.15	10.63	50.67	4.77	30.81	0.65	
Torrefaction at (290 ℃), RT (0.5 h)	49.68	35.71	12.54	52.22	4.41	27.72	0.71	

PS= 20-30 mesh								
Read canary grass (raw) PS = NR	82.50	12.10	5.50	48.60	6.80	37.30	0.30	(Bridgeman et al., 2008)
Torrefaction at T (250 ℃) RT (0.5 h) PS = NR	80.30	13.30	6.40	50.30	6.30	37.00	-	
Torrefaction at T (270 ℃) RT (0.5 h) PS = NR	76.60	16.10	7.30	52.20	6.00	37.30	0.10	
Torrefaction at (290 ℃) RT (0.5 h) PS = NR	70.50	21.30	8.30	54.30	6.10	45.20	0.10	
Wheat straw (raw) PS = NR	76.40	17.30	6.30	47.30	6.80	37.70	0.80	(Bridgeman et al., 2008)
Torrefaction at T (250 ℃) RT (0.5 h) PS = NR	77.00	15.60	7.40	49.60	6.10	35.60	0.90	
Torrefaction at T (270 ℃) RT (0.5 h) PS = NR	65.20	26.50	8.40	51.90	5.90	33.20	0.80	
Torrefaction at T (290 ℃) RT (0.5 h) PS = NR	51.80	38.00	10.20	56.40	5.60	27.60	1.00	
Miscanthus (raw) PS < 4 mm and PS > 10 mm	78.4	12.9	1.3	49.3	6.4	44.3	0.00	(Bridgeman et al., 2010a)
Torrefaction at T (290 ℃) RT (10min) PS < 4 mm and PS > 10 mm	63.8	32.6	1.4	55.8	5.8	38.4	0.00	
Torrefaction at T (240 ℃) RT (1 h) PS < 4 mm and PS > 10 mm	76.4	20.0	1.3	53.7	6.0	40.3	0.00	
Torrefaction at T (240 ℃) RT (10min) PS < 4 mm and PS > 10 mm	81.3	15.0	1.2	50.6	6.0	43.4	0.00	
Torrefaction at T (290 ℃) RT (1 h)	60.00	35.50	1.90	63.4	5.70	30.90	0.00	

PS < 4 mm and PS > 10 mm								
Eucalyptus (raw) PS < 5 mm	84.00	-	0.70	49.00	6.10	44.60	0.20	(Arias et al., 2008a)
Torrefaction at T (240 ℃) RT (0 h) PS < 5 mm	80.50	-	0.50	49.20	6.20	44.30	0.20	
Torrefaction at T (240 ℃) RT (0.25 h) PS < 5 mm	78.70	-	0.50	51.20	5.90	42.70	0.10	
Torrefaction at T (240 ℃) RT (0.5 h) PS < 5 mm	75.40	-	0.70	53.10	6.10	40.60	0.10	
Torrefaction at T (240 ℃) RT (1 h) PS < 5 mm	74.50	-	1.00	53.00	5.90	40.90	0.10	
Torrefaction at T (240 ℃) RT (2 h) PS < 5 mm	73.30	-	0.90	54.20	5.90	39.70	0.10	
Torrefaction at T (240 ℃) RT (3 h) PS < 5 mm	74.10	-	1.00	53.80	6.00	40.00	0.10	

*****PS: Particle size, **NR: not reported

2.1.1.1.2 Effect of torrefaction on mass yield, energy yield and higher heating value of biomass

The mass yield, energy yield, and higher heating value are the crucial indicator of biomass for its practical evaluation during thermochemical conversion process (Dai et al., 2019). The mass and energy yield can be calculated by using Eqs. (1) and (2) (Bridgeman et al., 2010a; Yan et al., 2009). The mass yield, energy yield, and higher heating value of different biomass are mentioned in Table 2.2. It was observed that mass yield decreases with increase in temperature and retention time during torrefaction process. The

decomposition of volatile matter in liquid and gaseous products at higher temperature and retention time is responsible for decrease in mass yield (Chew & Doshi, 2011; Dai et al., 2019). The major decomposition of hemicellulose takes place during torrefaction (Arias et al., 2008a). Thus, it was also observed that, the mass yield of herbaceous biomass is lower that the woody biomass during torrefaction due to higher hemicellulose content in herbaceous biomass (Bridgeman et al., 2008; Prins et al., 2006b). The increase in temperature and retention time during torrefaction causes increase in higher heating value of torrefied biomass. The increase in carbon content and decrease in oxygen content as a result of torrefaction is accountable for increase in higher heating value of torrefied biomass since, C-C bond has higher energy content as compared to C-H or C-O bonds (Phanphanich & Mani, 2011). The energy yield being a function of mass yield, HHV of torrefied and raw biomass signifies the amount of energy lost during torrefaction. The wide variation in energy yield of herbaceous biomass was observed due to large variation in volatile matter and hemicellulose content (Deng et al., 2009b). It was also observed that temperature has more pronounced effect on energy yield as compared to retention time. Thus, lower or higher temperature range along with shorter retention time can minimize the loss of energy through torrefaction (Chew & Doshi, 2011).

$$\text{Mass yield} = \frac{\text{Mass}_{\text{torrefied biomass}}}{\text{Mass}_{\text{raw biomass}}} \times 100 \quad (1.1)$$

$$\text{Energy yield} = \text{Mass yield} \times \frac{\text{HHV}_{\text{torrefied biomass}}}{\text{HHV}_{\text{raw biomass}}} \quad (1.2)$$

Phanphanich et al. (Phanphanich & Mani, 2011) investigated the mass and energy yield of pine chips and logging residues in the temperature range of 225-300 ℃ at a retention time of 0.5 h and reported that the mass yield varies in the range of 52-89%,while energy yield

varies in the range of 71-94%. Pimchuai et al. (Pimchuai et al., 2010) performed the torrefaction of water hyacinth, peanut husk, rice husk and bagasse in the temperature range of 250-300 ℃ and retention time in the range of 1-2 h. They reported that mass and energy yield fell in the range of 41-79% and 55-98%, respectively. The mass and energy yield and HHV of torrefied biomass depends on types of biomass, temperature, retention time and types of process reactor (Niu et al., 2019).

Table 2.2 Effect of torrefaction on mass yield, energy yield and higher heating value of biomass

Biomass	Torrefaction condition	Mass yield (%)	Energy yield (wt%)	HHV (MJ/kg)	References
Leucaena	T (200 ℃) RT (0.5 h) *PS < 75 μm	91.0	94.1	21.0	(Wannapeera et al., 2011b)
	T (225 ℃) RT (0.5 h) PS < 75 μm	86.5	90.3	21.2	
	T (250 ℃) RT (0.5 h) PS < 75 μm	73.0	76.2	21.2	
	T (275 ℃) RT (0.5 h) PS < 75 μm	54.5	61.2	22.0	
Pine	T (230 ℃) RT (1.0 h) PS = **NR	92.4	96.5	18.0	(Pach et al., 2002)
	T (250 ℃) RT (1.0 h) PS = NR	88.2	94.3	18.5	
	T (280 ℃) RT (1.0 h) PS = NR	78.1	93.9	20.8	
Willow	T (230 ℃) RT (0.5 h)	95.1	96.0	20.2	(Bridgeman et al., 2008)

	PS = NR				
	T (250 ℃) RT (0.5 h) PS = NR	89.6	92.2	20.6	
	T (270 ℃) RT (0.5 h) PS = NR	79.8	85.3	21.4	
	T (290 ℃) RT (0.5 h) PS = NR	72.0	78.8	21.9	
Wood briquette	T (220 ℃) RT (0.5 h) PS = NR	94.0	95.9	20.4	(Felfli et al., 2005a)
	T (250 ℃) RT (0.5 h) PS = NR	74.0	78.3	21.2	
	T (270 ℃) RT (0.5 h) PS = NR	56.0	63.7	22.7	
Sugarcane bagasse	T (230 ℃) RT (1.0 h) PS = NR	87.5	96.4	17.0	(Pach et al., 2002)
	T (250 ℃) RT (1.0 h) PS = NR	78.9	92.0	18.0	
	T (280 ℃) RT (1.0 h) PS = NR	68.6	82.9	18.7	
Cotton stalk	T (200 ℃) RT (0.5 h) PS = 25 mm	63.8	83.4	23.9	(Wang et al., 2011)
	T (250 ℃) RT (0.5 h) PS = 25 mm	33.8	45.3	24.5	
	T (300 ℃) RT (0.5 h) PS = 25 mm	30.0	41.0	25.0	
Sawdust	T (250 ℃) RT (1.0 h) PS = NR	67.2	72.4	19.5	(Pimchuai et al., 2010)
	T (270 ℃) RT (1.0 h) PS = NR	59.5	67.1	20.4	
	T (300 ℃) RT (1.0 h) PS = NR	42.0	55.1	23.8	

Wheat straw	T (200 ℃) RT (0.5 h) PS = 25 mm	47.56	56.0	19.8	(Wang et al., 2011)
	T (250 ℃) RT (0.5 h) PS = 25 mm	41.24	51.0	20.8	
	T (300 ℃) RT (0.5 h) PS = 25 mm	31.61	40.6	21.6	
Rice straw	T (200 ℃) RT (0.5 h) PS = 25 mm	59.8	59.9	17.1	(Deng et al., 2009b)
	T (250 ℃) RT (0.5 h) PS = 25 mm	40.3	42.4	18.0	
	T (300 ℃) RT (0.5 h) PS = 25 mm	36.5	39.9	18.6	
Reed canary grass	T (250 ℃) RT (0.5 h) PS = NR	83.0	85.1	20.0	(Bridgeman et al., 2008)
	T (270 ℃) RT (0.5 h) PS = NR	72.0	76.8	20.8	
	T (290 ℃) RT (0.5 h) PS = NR	61.5	68.7	21.8	

*****PS: Particle size, **NR: not reported

2.1.1.1.3 Effect of torrefaction on grindability and moisture absorption capacity of biomass

As a result of torrefaction, the fibrous structure of biomass is broken and smaller and spherical size particle are obtained which enhances the flow characteristics of biomass (Arias et al., 2008a; Wang et al., 2011). Thus, torrefaction makes the biomass brittle which enhances its grinding properties and lower the grinding energy as a result smaller particle size distribution are obtained (Deng et al., 2009b; Repellin et al., 2010). The grinding

energy of torrefied biomass was noted to 10-20% lower than the raw biomass, and this grinding energy can be compared with grinding energy of coal (Ciolkosz & Wallace, 2011; Phanphanich & Mani, 2011). Hence, torrefaction facilitate grindability and flowability of biomass. Repellin et al. (Repellin et al., 2010) performed the grinding of spruce and beech at different torrefaction temperature (180-280 ℃ for beech and 160-280 ℃ for spruce) and retention time (5-60 min for beech and 5 min for spruce) using ultra centrifugal mill (Retsch ZM1) coupled with 0.5 mm grid and found that grinding energy decreased with increase in temperature and retention time. However, small decrease in grinding energy was noted when retention time increased beyond 20 min. Bridgeman et al. (Bridgeman et al., 2010a) confirmed that temperature during torrefaction had most significant impact on grindability of torrefied biomass followed by retention time and particle size. Mani et al. (Mani et al., 2004) confirmed that higher moisture content in torrefied biomass increased its grinding energy due to more shear strength. Wang et al. (Wang et al., 2011) investigated the grinding energy for cotton stalk and wheat straw and reported that beyond 250 ℃, temperature had almost no significance on grinding energy.

The hygroscopic characteristics of biomass is highly depends on the composition (cellulose, hemicellulose and lignin content) of biomass (Niu et al., 2019). Among the composition of biomass, hemicellulose has the strongest affinity toward water absorption while, lignin has the least affinity towards water (Björk & Rasmuson, 1995). Due to torrefaction, the decomposition of majority of hemicellulose along with reduction in H/C and O/C ratios, the torrefied biomass has hydrophobic characteristics as compared to raw biomass. The cleavage of hydroxyl bonds associated with hemicellulose is mainly accountable for hydrophobic characteristics of torrefied biomass (Kanwal et al., 2019;

Phanphanich & Mani, 2011). The hydrophobic nature of torrefied biomass facilitates its transport and storage without bacterial deterioration like raw biomass (Yan et al., 2009). The water absorption capacity of biomass decreases with increase in temperature during torrefaction (Pimchuai et al., 2010). Ciolkosz et al. (Ciolkosz & Wallace, 2011) summarized the mechanism of hydrophobic characteristics of biomass due to torrefaction. They reported that decomposition of hemicellulose during torrefaction leads to unbind the cellulose and lignin. This causes discharge of water molecules present in cell wall. The decomposition of hemicellulose brings the brittle characteristics in cellulose and lignin. The breakdown of hydroxyl groups present in hemicellulose decreases the tendency of formation of hydrogen bond with water molecules. Non-polar molecules are formed as a result of hemicellulose decomposition. The hydrophobic characteristics of biomass can be estimated by using Equilibrium Moisture Content (ECM) as proposed by Acharjee et al. (Acharjee et al., 2011) and Yan et al. (Yan et al., 2009). The torrefied biomass having lower ECM has lower risk of biological degradation as compared to torrefied biomass with higher ECM (Yan et al., 2009). Thus, it can be concluded that torrefaction significantly reduced the grinding energy and moisture absorption capacity of native biomass. The reduction in grinding energy of biomass due to torrefaction increased the energy efficiency of process and reduction in moisture absorption capacity can lead to lower bacterial degradation resulting in longer storage of native biomass.

2.1.1.2 Optimization of torrefaction process

The torrefaction process depends on temperature, retention time, heating rate, type of biomass, process reactor system, particle size, etc. Among these parameters temperature and retention time has most significant impact on torrefaction process (Asadullah et al.,

2014). Also, the torrefaction process is generally used as a pretreatment process to upgrade the quality of native biomass; hence yield of upgraded biomass (torrefied biomass) with enhanced properties is the desired output from torrefaction. However, the yield and quality of torrefied biomass shows opposite trend during torrefaction process. With increase in temperature and retention time the quality of torrefied biomass (HHV, fixed carbon, H/C and O/C ratios) enhances while, yield of torrefied biomass decreases (Singh et al., 2019b). Thus, it is of prime importance to find a balance between quality and quantity of torrefied biomass. The process outcomes such as mass and energy yield are very sensitive to temperature and retention time. A small variation in temperature and retention time can cause significant variation in mass and energy yield (Koukios, 1993). The desired value of process parameters can be established through optimization of process parameters. Asadullah et al. (Asadullah et al., 2014) carried out the torrefaction of palm kernel shell between 200-350 ℃, retention time 10-60 min and sweeping gas flow between 100-1000 mL/min. They reported the optimum condition of torrefaction for maximum yield (73%) and HHV (24.5 MJ/kg) of torrefied biomass at 300 ℃, retention time (20 min) and sweeping gas flow rate (300 mL/min). Buratti et al. (Buratti et al., 2018) investigated the torrefaction of coffee chaff and spent coffee ground between 220-300 ℃, retention time 20-60 min and heating rate between 5-25 ℃/min and optimize the weight loss and HHV using response surface methodology. The optimum value for coffee chaff was found at 271.7 ℃, retention time (20 min) and heating rate (5 ℃/min) and for spent coffee ground the optimum value was found at 256 ℃, retention time (20 min) and heating rate (25 ℃/min). Table 2.3 represents the optimization of torrefaction process for different biomass.

Table 2.3 Optimization of process parameters for torrefaction of different biomass

Biomass	Independent Variable	Dependent variable	Optimization Tool	Optimum condition	Optimum Value of dependent variable	References
Palm kernel shell	T (200-350 ℃), RT (10-60 min) SGF (100-1000mL/min)	Solid yield HHV	-	T (300 ℃), RT (20 min), SGF (300 mL/min)	Solid yield (73%), HHV (24.5 MJ/kg)	(Asadullah et al., 2014)
Greenhouse crop residue	T (200-300 ℃), RT (15-60 min)	Energy# yield	ANFIS modeling	T(263 ℃), RT (15 min)	-	(Iáñez-Rodríguez et al., 2017)
Coffee Chaff	T (220-300 ℃), RT (20-60 min) HR (5-25 ℃/min)	Weight loss and Heating value	RSM based BBD	T(271.7 ℃), RT (20 min), HR (5 ℃/min)	Weight loss (28.7%), HHV (23.60 MJ/kg)	(Buratti et al., 2018)
Spent coffee ground	T (220-300 ℃), RT (20-60 min) HR (5-25 ℃/min)	Weight loss and Heating value	RSM based BBD	T (256.7 ℃), RT (20 min) HR (25 ℃/min)	Weight loss (21.6%), HHV (28.18 MJ/kg)	(Buratti et al., 2018)
Empty fruit bunch	T (200-300 ℃), RT (15-60 min)	HHV yield	RSM	T (230 ℃), RT (40 min)	121.1%	(Chin et al., 2013)
Oil palm trunk	T (200-300 ℃), RT (15-60 min)	HHV yield	RSM	T(300 ℃), RT (45 min)	109.2%	(Chin et al., 2013)
Acacia spp.	T (200-300 ℃), RT (15-60 min)	HHV yield	RSM	T (260 ℃), RT (30 min)	131.4%	(Chin et al., 2013)
Macaranga spp.	T (200-300 ℃), RT (15-60 min)	HHV yield	RSM	T (280 ℃), RT (45 min)	131.0%	(Chin et al., 2013)
Cotton stalk	T (260-320 ℃), RT (10-60 min) BD (125-175 kg/m^3)	HHV and carbon content	RSM based BBD	T (305 ℃), RT (32 min) BD (158 kg/m^3)	HHV (19.7 MJ/kg), Carbon content (64%)	(Kutlu & Kocar, 2018)
Rice straw	T (210-290 ℃), RT (20-60 min)	Energy yield	RSM based CCD	T (210 ℃), RT (20	91.3%	(Nam & Capareda, 2015)

				min)		
Cotton stalk	T (210-290 ℃), RT (20-60 min)	Energy yield	RSM based CCD	T (210 ℃), RT (20 min)	99.4%	(Nam & Capareda, 2015)

the definition of energy yield has been defined in section 2.1.1.1.2 (Eq. 1.2)

2.1.2 Pyrolysis of raw and torrefied biomass and optimization of process parameters

2.1.2.1 Pyrolysis of raw biomass and optimization of process parameters

Pyrolysis is a process that can potentially be used to harness energy and various chemicals from biomass (Akhtar & Amin, 2012). The pyrolysis is a thermochemical conversion process which can convert the biomass into solid, liquid, and gaseous products in an inert atmosphere depending upon the process parameters such as temperature, heating rate and retention time. The amount of solid, liquid and gaseous products from pyrolysis depends on the process parameters (Akhtar & Amin, 2012). Generally the pyrolysis process takes place between 500-800 ℃ (Akhtar & Amin, 2012). Depending upon the process parameters, the pyrolysis can be classified as slow pyrolysis, fast pyrolysis, and flash pyrolysis (Dai et al., 2019). The flash pyrolysis is characterized by higher heating rate (> 1000 ℃/s) and lower retention time (< 0.5 s) (Bahng et al., 2009). The flash pyrolysis process requires an experimental set-up equipped with high quality equipment for the control of process. In this regard, slow and fast pyrolysis has gathered huge attention for production of biochar and bio-oil from biomass (Dai et al., 2019). The slow pyrolysis is characterized by low heating

rate (0.1-1 ℃/s) and longer retention time (300-550 s). While, fast pyrolysis generally occurs between heating rate of 10-200 ℃/s, and retention time between 0.5-10 s (Ben & Ragauskas, 2013; Guedes et al., 2018; Jahirul et al., 2012). Biochar and bio-oil has been considered as the main product from slow and fast pyrolysis, respectively (Guedes et al., 2018). During pyrolysis process biomass went through primary and secondary cracking reactions through heat and mass transfer. The primary reactions during pyrolysis consist of degradation of hemicellulose, cellulose and lignin content of biomass.. The primary products and intermediates are the major products during primary reactions. The intermediates formed during primary reactions are further cracked during secondary reaction of pyrolysis. The primary reactions during pyrolysis follow the dehydration and charring mechanism; while, secondary reactions follows the volatilization and degradation of intermediates (Akhtar & Amin, 2012; Zaror & Pyle, 1982). The yield of bio-oil during pyrolysis of biomass is governed by many factors such as process temperature, retention time, heating rate, sweeping gas flow rate, particle size of feedstock, minerals present in biomass, initial moisture content of biomass and composition of feedstocks (Akhtar & Amin, 2012). Tsai et al. (Tsai et al., 2007) investigated the pyrolysis of rice husk and reported that the yield of bio-oil increased from 11.26 wt% to 35.92 wt%, once the temperature increased from 400 to 500 ℃. However, the yield of bio-oil increased with lower rate to 40 wt% at a temperature of 800 ℃. Lazzari et al. (Lazzari et al., 2016) performed the mango seed pyrolysis in the temperature range of 450 to 650 ℃. The maximum yield of bio-oil (38.8 wt %) was obtained at 650 ℃. Jung et al. (Jung et al., 2008) investigated the pyrolysis of saw dust from bamboo and reported that the yield of bio-oil increased from 56% to 72% , once the temperature increased from 350 to 405 ℃.

On further increase in temperature up to 510 ℃, the yield of bio-oil decreased to 61%. With increase in temperature during pyrolysis, the bio-oil yield increased up to maximum value and after that bio-oil yield decreased due to secondary cracking of volatiles at higher temperature (Isahak et al., 2012). Ates et al. (Ateş et al., 2004) investigated the pyrolysis of sesame stalk and varied the heating rate from 100-700 ℃/min. they observed that maximum yield of bio-oil was obtained at a heating rate of 500 ℃/min. Tsai et al. (Tsai et al., 2007) varied the heating rate form 100-500 ℃/min during pyrolysis of rice husk in a fixed bed reactor. They reported that maximum bio-oil yield was obtained at a heating rate of 200 ℃/min and further increase in heating rate has negligible impact on bio-oil yield. Morali et al. (Moralı & Şensöz, 2015) carried out the pyrolysis of hornbean shell and varied the heating rate from 7-50 ℃/min. They observed that the variation in yield of bio-oil was almost negligible and effect of heating rate on pyrolysis was minimal in the tested conditions of pyrolysis.

Table 2.4 Optimization of process parameters for pyrolysis of different biomass

Biomass	**Desired outcomes**	**Optimum condition**	**Optimization tool**	**References**
Napier grass	Bio-oil yield (50.57 wt%)	T: 600 ℃, HR; 50 ℃/min, SGF: 5 L/min	RSM based CCD	(Mohammed et al., 2017c)
Oil Palm Fiber	Bio-oil yield (50.57 wt%)	T: 536.5 ℃, RT: 23.88 min, AC loading: 86.21 g	RSM based CCD	(Abas et al., 2018)
Bambara groundnut	Bio-oil yield (36.49 wt%)	T: 600 ℃, HR: 50 ℃/min, SGF: 11 L/min	RSM based CCD	(Mohammed et al., 2017b)
Sagwan sawdust	Bio-oil yield (48.70 wt%)	T: 640 ℃, SGF: 180 mL/min, Bed height: 8 cm	RSM based BBD	(Gupta & Mondal, 2019)

Food waste	Bio-oil yield (30.24 wt%)	T: 400 ℃, RT: 30 min, SGF: 50 mL/min	RSM based CCD	(Kadlimatti et al., 2019)
Perennial grass	Bio-oil yield (38.1 wt%)	T: 550 ℃, HR: 20 ℃/min, SGF: 226 mL/min	RSM based CCD	(Saikia et al., 2018)
Neem press seed cake	Bio-oil yield (52.1 wt%)	T: 512.5 ℃, RT: 60 min, SGF: 0.5 L/min	RSM based BBD	(Dhanavath et al., 2019)
Pine needles	Bio-oil yield (27.6 wt%)	T: 547 ℃, HR: 50 ℃/min, VCT: 15 ℃, SGF: 1.85 L/min	RSM based CCD	(Mandal et al., 2018)
Euphorbia rigida	Bio-oil yield (35.3 wt%)	T: 600 ℃, HR: 200 ℃/min, SGF: 100 mL/min	RSM based CCD	(Kılıç et al., 2014)
Pearl Millet	Bio-oil yield (48.27 wt%)	T: 400 ℃, SGF: 200 mL/min, PS:1.5 mm	RSM based CCD	(Boubacar Laougé et al., 2020)
Sida cordifolia L.	Bio-oil yield (48 wt%)	T: 400 ℃, SGF: 200 mL/min, PS:1.5 mm	RSM based CCD	(Boubacar Laougé et al., 2020)
Rice husk	Biochar yield (37.71 wt%)	T: 300 ℃, HR: 20 ℃/min, RT: 5400 s, BL: 500 g	Taguchi method	(Vieira et al., 2020)
Rice husk	HHV of biochar (23.41 MJ/kg)	T: 500 ℃, HR: 10 ℃/min, RT: 5400 s, BL: 125 g	Taguchi method	(Vieira et al., 2020)
Rice husk	Fixed carbon of biochar (60.10 wt%)	T: 500 ℃, HR: 5 ℃/min, RT: 7200 s, BL: 500 g	Taguchi method	(Vieira et al., 2020)
Palm fruit empty bunch	Bio-oil yield (45.29 wt%)	T: 628.2 ℃, SGF: 0.259 L/min	Central rotational compound design	(Ferreira et al., 2020)
Poplar saw dust	Bio-oil yield (30.45	T: 528.44 ℃, HR: 750	RSM based CCD	(Ates & Erginel, 2016)

	wt%)	℃/min, Pressure: 1 bar		
Oil palm trunk	Bio-oil yield (42.05 wt%)	T: 446.11 ℃, RT: 119.98 min, moisture content: 9.26%	RSM based BBD	(Oramahi et al., 2015)
Waste mixture (10% pine, 10% scrap tyres, 80% recycled plastic)	Bio-oil yield (54.9 wt%)	T: 426 ℃, RT: 28 min, Pressure: 0.2 MPa	RSM (experimental factorial design)	(Pinto et al., 2013)
Coffee silverskin	Organic phase yield (15.2 wt%)	T: 560 ℃, SGF: 49 mL/min	RSM based CCD	(Polidoro et al., 2018)
Salwood	Bio-oil yield (44.78 wt%)	T: 540 ℃, SGF: 155 cm^3/min, Feed rate: 0.45 kg/h	RSM based BBD	(Charusiri & Numcharoenpinij, 2017)
Sugarcane bagasse	Bio-oil yield (53.4 wt%)	T: 560 ℃, RT: 77 s, Particle size: 0.5 to 0.85 mm	Simplex method	(Vecino Mantilla et al., 2014)
Palm Empty fruit bunch	Bio-oil yield (48.4 wt%)	T: 540 ℃, RT: 31 s, Particle size: less than 0.5 mm	Simplex method	(Vecino Mantilla et al., 2014)
Cascabela thevetia seed	Bio-oil yield (45.26 wt%)	T: 525 ℃, HR: 75 ℃/min, SGF: 75 mL/min	RSM based CCD	(Mishra et al., 2020)

2.1.2.2 Pyrolysis of torrefied biomass

2.1.2.2.1 Effect of torrefaction on kinetics of biomass during pyrolysis

The torrefaction process can alter the kinetic parameters resulting in change in rate of heat and mass transfer due to decomposition of biomass during torrefaction. The torrefied

biomass displayed the better behavior than raw biomass due to lower moisture content, H/C and O/C ratios and fractured and brittle structure (Dai et al., 2019). Since, the torrefaction as a pretreatment process can alleviate the undesired characteristics of raw biomass such as higher moisture content, lower energy density, higher oxygen content, higher grinding energy and tendency to absorb the moisture, added energy provided during torrefaction can offset due to enhanced characteristics of raw biomass (Dai et al., 2019). Ren et al. (Ren et al., 2013a) and Martin-Lara et al. (Martín-Lara et al., 2017) performed the TGA analysis of raw and torrefied biomass to investigate the pyrolysis characteristics. They reported that activation energy for pyrolysis of torrefied biomass was lower as compared to raw biomass due to decomposition of biomass during torrefaction. Martin-Lara et al. (Martín-Lara et al., 2017) also reported that for torrefied biomass obtained at mild torrefaction condition, the first order, single kinetic model was followed however, for severe torrefaction condition multi step kinetic model was followed. Hu et al. (Hu et al., 2018) performed the pyrolysis of raw and pellets from torrefied corn stalk. They observed that considerable amount of volatiles were lowered and rate of decomposition of biomass had increased due to torrefaction. Ru et al. (Ru et al., 2015) reported that the activation energy of hemicellulose and cellulose significantly reduced due to torrefaction, while for lignin, slight change in activation energy was observed. This showed that with increase in temperature during torrefaction, contribution of hemicellulose and cellulose decreased while contribution of lignin increased during decomposition of torrefied biomass during pyrolysis.

2.1.2.2.2 Effect of torrefaction on product distribution during pyrolysis of biomass

The integrated torrefaction-pyrolysis process can be a promising route for upgradation of quality of bio-oil obtained from pyrolysis of biomass. However, yield of bio-oil from pyrolysis of torrefied biomass is lower that the raw biomass because lighter component of biomass has already been converted into gaseous and liquid condensate (water, CO_2, CO, acids, etc.) during torrefaction process (Boateng & Mullen, 2013a; Chen et al., 2016c; Prins et al., 2006a). Table 2.5 represents the effect of torrefaction on quality of bio-oil obtained from pyrolysis of torrefied biomass. Boateng et al. (Boateng & Mullen, 2013a) performed the pyrolysis of torrefied biomass and reported that yield of bio-oil decreased and biochar yield increased however, quality of bio-oil has increased due to lower acidic content and higher energy content. Ukaew et al. (Ukaew et al., 2018) performed torrefaction of rice straw in the temperature range of 225-275 ℃ and retention time of 30 min followed by pyrolysis of torrefied rice straw. They reported that bio-oil yield decreased by quarter as compared to raw rice straw. However, bio-oil from pyrolysis of torrefied rice straw has lower water content, oxygenated and acids compounds as compared to raw rice straw. Pyrolysis of torrefied biomass favors the cross-linking reaction resulting in higher char yield and lower bio-oil yield (Wannapeera et al., 2011b). Zeng et al. (Zheng et al., 2013) performed the pyrolysis of raw and torrefied corncob and analyzed the composition of bio-oil by employing GC-MS analyzer. They reported that the bio-oil from pyrolysis of torrefied corncob has lower yield, acidic, furfural and aldehydes derivative compounds as compared to bio-oil from raw corncob. The higher heating value and pH of bio-oil were improved after torrefaction. They reported that intense devolatilization, cross-linking

reactions and charring of torrefied corncob was mainly accountable for decrease in yield of bio-oil. Xin et al. (Xin et al., 2018) performed the torrefaction of herbaceous residue having high moisture content between temperature 210-280 ℃ and retention time of 60 min followed by pyrolysis of torrefied herbaceous residue. They reported that torrefaction reduces the oxygen and acids derived compound in the bio-oil. Chen et al. (Chen et al., 2017) reported that torrefaction as a pretreatment can significantly reduce the acidic compounds and increase the phenol derivative compounds in the bio-oil from pyrolysis of torrefied biomass. Thus, it can be concluded that the yield of bio-oil from pyrolysis of torrefied biomass is lower as compared to pyrolysis of native biomass. However, the quality of bio-oil has improved due to torrefaction supporting the feasibility of integrated torrefaction-pyrolysis process for production of high quality bio-oil.

Table 2.5 Effect of torrefaction on quality of bio-oil obtained from pyrolysis of torrefied biomass

Biomass	**Torrefaction condition**	**Pyrolysis condition**	**Important findings***	**References**
Arecanut husk	T; 200-300 ℃, HR; 10 ℃/min, RT; 30 min	T; 300-600 ℃, HR; 40 ℃/min	The bio-oil yield decreased from 32 to 21 %, O/C ratio of bio-oil decreased from 0.36 to 0.28	(Gogoi et al., 2017)
Loblolly pine	T; 273-330 ℃, RT; 2.5 min	T; 500 ℃, Fr; 150 g/h	O/C ratio of bio-oil decreased from 0.63 to 0.31, while, HHV of bio-oil increased from 20 to 26.3 MJ/kg	(Meng et al., 2012)
Cotton stalk	T; 220-280 ℃, RT; 30 min	T; 500 ℃	Acid and furan content of bio-oil decreased, while, phenolic and ketone derivatives increased from 0.53-8.25, 0.59-6.41 %, respectively.	(Chen et al., 2015a)
Rice straw	T; 225-275 ℃,	T; 450-500 ℃,	Oxygenated, acid, aldehydes,	(Zheng et

	RT; 30 min	HR; 1000 ℃/sec	ketones, and sugar derivative compounds as well as water content of bio-oil decreased	al., 2012)
Yunnan pine	T; 210-300 ℃, RT; 30 min	T; 500 ℃	The bio-oil yield decreased from 37 to 20 %, phenolic and hydrocarbon derivatives increased, while, acid, aldehydes and ketone derivative compounds decreased	(Zheng et al., 2017)
Rice straw	T; 240 ℃, RT; 60 min	T; 550 ℃	Phenolic compounds increased from 28 to 42 %, while, acid, aldehydes, ketone and furan derivative compounds decreased	(Dong et al., 2018)
Corncob	T; 210-300 ℃, RT; 20-60 min	T; 600 ℃, HR; 20000 K/sec (catalytic pyrolysis)	The yield of bio-oil increased to 82 % from 51 %, aromatic compounds increased	(Zheng et al., 2014)
Corn stalk	T; 200-290 ℃, RT; 30 min	T; 550 ℃	Bio-oil yield decreased as compared to raw biomass	(Wang et al., 2018b)
Herbaceous residue	T; 210-280 ℃, RT; 60 min	T; 600 ℃, HR; 50 ℃/min	Phenol, acid, ketone, ester and furan derivative compounds are the main components of bio-oil and collectively contribute 72.1 % of total compounds detected.	(Xin et al., 2018)

*important findings are mentioned with respect to the pyrolysis of raw biomass at similar pyrolysis conditions

2.1.3 Application of biochar from pyrolysis of biomass for removal of aqueous methylene blue

The removal of methylene blue (MB) dye from real or synthetic wastewater using adsorption process has gathered huge attention in recent years due to simple operation, utilization of abundant and low cost adsorbent as well as high removal efficiency towards

MB removal (Santoso et al., 2020). In addition, adsorption process inhibit the generation of secondary pollutant which can generated via degradation or oxidation of MB dye (Katheresan et al., 2018; Salleh et al., 2011). Biochar obtained from pyrolysis of biomass or biomass waste can act as an adsorbent for removal of MB from wastewater (Santoso et al., 2020). The biochar derived from biomass can have similar properties to activated carbon. Hagemann et al. (Hagemann et al., 2018) discussed the two carbon based pyrogenic materials biochar and activated carbon that possess similar preparation technique, terminology and their applications. Biochar was used as a soil amendment agent in agriculture however; recently it has got more attention as an adsorbent towards wastewater treatment (Hagemann et al., 2018). Sun et al. (Sun et al., 2013) used three feedstocks namely, eucalyptus, palm bark, and anaerobic digestion residue for preparation of biochar from pyrolysis at 400 ℃. They reported the adsorption capacity of 2.0, 2.95, and 9.77 mg/g for eucalyptus, palm bark, and anaerobic digestion residue, respectively towards MB removal. Ahmed et al. (Ahmed et al., 2019) reported the adsorption capacity of 512.67 mg/g towards MB removal for biochar derived from seaweed by performing pyrolysis process at 800 ℃. Ji et al. (Ji et al., 2019) reported the adsorption capacity of 78.6 mg/g towards MB removal for biochar derived from fallen leaf by performing pyrolysis process at 500 ℃. Table 2.6 represents the application of biochar derived from pyrolysis of different biomass. The large number of functional groups associated with biochar, porous structure and high surface area of biochar are accountable for removal of MB from wastewater (Que et al., 2018). Thus, with increase in the scope of integrated torrefaction-pyrolysis process, it is imperative to check the efficacy of biochar from pyrolysis of

torrefied biomass towards aqueous methylene blue removal. It might offset the extra energy provided during torrefaction during integrated torrefaction-pyrolysis process.

Table 2.6 Application of biochar from pyrolysis raw biomass towards aqueous methylene blue removal

Feedstock	Pyrolysis condition	Duration of experiment (min)	Adsorbent dose (g/L)	Initial Conc. (mg/L)	pH	Adsorption capacity (mg/g)	Ref.
Eucalyptus sawdust	T: 400 ℃, RT: 30 min	240	8	15	NR	0.957	(Sun et al., 2013)
Palm bark	T: 400 ℃, RT: 30 min	240	8	15	NR	1.217	(Sun et al., 2013)
Municipal solid waste	T: 400-500 ℃, RT: 30 min	240	2	50	6.5	21.83	(Sumalinog et al., 2018)
Tea waste mixed with sewage sludge	T: 300 ℃, RT: 2 h	1440	NR	100	-	8.945	(Fan et al., 2016)
Mixed municipal discard material	T: 400 ℃, RT: 30 min	360	5	10	5	1.798	(Hoslett et al., 2020)
Mixed municipal discard material	T: 400 ℃, RT: 30 min	360	5	25	5	2.732	(Hoslett et al., 2020)
Mixed municipal discard material	T: 400 ℃, RT: 30 min	360	5	50	5	2.960	(Hoslett et al., 2020)
Mixed municipal discard material	T: 400 ℃, RT: 30 min	360	5	75	5	5.018	(Hoslett et al., 2020)
Mixed municipal discard	T: 400 ℃, RT: 30	360	5	100	5	7.254	(Hoslett et al., 2020)

material	min						
Eucalyptus Sheathiana bark	T: 500 ℃, RT: 2 h	150	10	100	11.3	104.2	(Dawood et al., 2016)
Wheat straw	T: 550 ℃, RT: 5 min	50	-	100	8-9	12.03	(Liu et al., 2012)

NR: not reported

2.2 Objectives

The detailed literature review showed that torrefaction has been successfully employed as a pretreatment process to upgrade the quality of raw biomass. However, work related to the optimization of process parameters for maximum energy yield and higher heating value of torrefied biomass considering both at the same time has scarcely reported. Also, little attention has been given to the effect of heating rate on torrefaction process. The in-depth analysis of kinetics and solid reaction mechanism during pyrolysis of torrefied biomass has been scarcely reported. The literature review showed that pyrolysis of raw and optimization process parameters for maximum bio-oil yield have been extensively reported. However, pyrolysis of torrefied biomass has been scarcely reported. The optimization of process parameters for maximum bio-oil yield from pyrolysis of torrefied biomass has not been reported yet. The biochar from pyrolysis of raw biomass has been extensively used as an adsorbent for removal of methylene blue dye from wastewater. However efficacy of biochar from pyrolysis of torrefied biomass towards methylene blue dye removal has not been tested. In order to fulfill the above mentioned research gaps, the present thesis has the following objectives:

- Pretreatment of raw *Acacia nilotica* using torrefaction and investigation of fuel and flow properties to check the suitability of torrefied *Acacia nilotica* for pyrolysis process
- Investigation of kinetic and thermodynamic parameters and solid reaction mechanism of pyrolysis of torrefied *Acacia nilotica* using thermogravimetric analysis
- Optimization of process parameters (temperature, retention time and heating rate) for torrefaction of *Acacia nilotica* for maximum energy yield and higher heating value using response surface methodology
- The pyrolysis of torrefied *Acacia nilotica* obtained at optimum condition of torrefaction and optimization of process parameters (temperature, heating rate, retention time and sweeping gas flow rate) for maximum yield of pyrolysis oil using response surface methodology. Also, the comparative study of products obtained from pyrolysis of raw and torrefied *Acacia nilotica* at optimum condition of pyrolysis
- Application and comparative study of biochar obtained from pyrolysis of raw and torrefied *Acacia nilotica* at optimum condition of pyrolysis towards removal of aqueous methylene blue dye

Chapter 3

Torrefaction of woody biomass (*Acacia nilotica*): Investigation of fuel and flow properties to study its suitability as a good quality solid fuel

General background

This chapter aimed to investigate the torrefaction of *Acacia nilotica* in a quartz tube fixed-bed reactor to examine the suitability of torrefied *Acacia nilotica* as a good quality solid fuel. Temperature and retention time varied from 220-280 ℃ and 20-60 min, while, heating rate was kept constant at 15 ℃/min. The fuel (volatile ignitability (VI), combustibility index (CI), fuel ratio (FR)), and flow (Hausner ratio (HR), cohesion coefficient (C), Carr compressibility index (CCI), angle of repose,) properties were investigated for raw and torrefied biomass. Torrefied *Acacia nilotica* was also characterized through TGA, FTIR, SEM-EDX and ICP-MS analysis. For moisture sorption test, contact angle was measured. Finally, torrefied *Acacia nilotica* was compared with coal using published literature.

3.1 Introduction

Over the last few decades, the rapid increase in world population, industrialization and high living standard of people, created a huge gap between demand and supply of energy (Song et al., 2018). To fulfill the energy demand, only coal contributes 38 % of total electricity generation of the world in 2017 (Magalhães et al., 2019). The reserves of fossil fuel such as coal, petroleum, and natural gas are limited and large exploitation along with complete dependency on the fossil fuel can diminish the fossil fuel reserve. Also, application of fossil fuels severely affects the environment by harmful emission such as SO_x, NO_x, greenhouse gas (CO_2) and particulate matters (Yue et al., 2017). The most promising way to solve the problem is to use and extract energy from renewable resources (Yang et al., 2019).

Though we have wind, solar, geothermal, hydrothermal etc. as renewable energy sources, however, among them biomass is most abundant worldwide and easily available. The consideration of biomass as a carbon-neutral fuel and its quality to emit lesser amount of sulfur and nitrogen makes it important source for the production of bio-energy (Giudicianni et al., 2013). *Acacia nilotica*, a kind of forest tree, has vast availability in India, Australia, African, and South East Asian countries (Bargali & Bargali, 2009). It is a tropical tree having height around 7 to 18 m and diameter around 20 to 30 cm (Raj et al., 2015). These trees are fast growing, generally found in waste and barren land having low productivity and it does not compete with land application for food production. It is also considered as an important plant having economic value since it is a medicinal plant and good source of tannins and gums (Bargali & Bargali, 2009; Saratale et al., 2019). In addition, it is a good source of timber wood and used as a fuel and fodder for animals in rural areas in India.

Acacia nilotica is dispersed all over India along national highways, railway lines, forest areas, roadsides, farmlands, tank foreshores, farm fields, village grazing lands and wastelands. The total wood production from *Acacia nilotica* is 167 tonnes per hectare, while, total pod generation from *Acacia nilotica* is 0.6 million tonnes per year (Pandey & Sharma, 2005; Singh et al., 2019b; Singh et al., 2020b). As a fuelwood it is considered as an excellent material as it has high calorific value (~20 MJ/kg) and lesser smoke emission tendency (Pandey & Sharma, 2005). It is also used in pulp and paper industry and as a fuel in textile and brick kiln (Singh et al., 2020b). Also, the charcoal made from *Acacia nilotica* has superior properties from the other biomass species. Different part of *Acacia nilotica* tree (leaf, seed and bark) are used as adsorbent and feedstock for pyrolysis process (Garg et al., 2016; Gupta & Lataye, 2019).

Regardless of large availability and easy accessibility, biomass is allied with many inherent disadvantages as discussed in Chapter 1. Due to these drawbacks, at present, the global annual energy achieved from biomass is approximately 10% of the overall energy consumption (Chen & Kuo, 2010; van der Stelt et al., 2011). It is therefore essential to improve the quality of biomass through pretreatment process and check the suitability of treated biomass in term of fuel and flow properties, before it can be used in thermochemical conversion process efficiently. Flow characteristics of biomass play an important role when it comes to blending biomass with other biomass, plastic materials during co-pyrolysis, and coal in co-firing process in thermal power plants. However, application of biomass in co-pyrolysis, combustion and co-firing is difficult to attain due difference in fuel and flow behavior of coal and biomass. In the past, various pretreatment

methods have been explored to improve the quality of biomass. Among the various processes, torrefaction provides a promising route for the upgradation of biomass.

Torrefaction is defined as a mild pyrolysis process with the temperature zone of 200-300 ℃ at atmospheric pressure with inert medium at a low heating rate of (< 20 ℃/min) and retention time around 15-60 min (Keivani et al., 2018; Kutlu & Kocar, 2018; Manouchehrinejad et al., 2018). Many literatures are available that discuss the properties of torrefied biomass as good quality solid biofuel as discussed in Chapter 2. However, focus given on the study of fuel properties such as volatile ignitability (VI), combustibility index (CI), fuel ratio (FR) and flow properties such as Hausner ratio (HR), cohesion coefficient (C), Carr compressibility index (CCI) and angle of repose for raw and torrefied biomass and variation of these properties with process parameter during torrefaction is very less. To check the suitability of torrefied biomass as better quality solid biofuel or as a blend with coal, various tests have been performed. The fuel (volatile ignitability (VI), combustibility index (CI), fuel ratio (FR)), and flow (Hausner ratio (HR), cohesion coefficient (C), Carr compressibility index (CCI), angle of repose,) properties, particle size, density, moisture sorption (open environment test and contact angle test) of torrefied biomass were analyzed. Also, the characteristics of torrefied biomass at different conditions were analyzed through TGA, FTIR, SEM-EDX and ICP-MS analysis. Finally, the characteristics of torrefied biomass were compared with properties of coal using published literature.

3.2 Experimental section

3.2.1 Materials

The wooden block of *Acacia nilotica*, about 1 ft in diameter was collected from village close to Banaras Hindu University (BHU) campus, Uttar Pradesh, India. The collected biomass was chopped into smaller with the help of an axe and further, fine particles between 0.7 to 1.25 mm were obtained after subsequent cutting (Cutting machine; Retsch model SM 300, Germany) and screening. The surface moisture of the biomass was removed by sun drying. After that biomass sample was again kept in an oven kept at 80 ℃ for overnight and then kept in air tight container prior to experiments. In the present work, dried *Acacia nilotica* is labeled as DAN and torrefied *Acacia nilotica* is labeled as TAN-X-Y-Z, where X indicates the torrefaction temperature, Y indicates the retention time and Z indicates the heating rate. For example, TAN-250-60-15 indicates torrefied *Acacia nilotica* which was obtained by torrefaction at 250 ℃, 60 min retention time and 15 ℃/min heating rate.

3.2.2 Experimental setup and procedure for torrefaction

The schematic diagram of the experimental setup is shown in Fig. 3.1. It consists of temperature controller unit and a fixed-bed reactor (Inner diameter = 2.5 cm, length = 80 cm) made up of quartz, split tube furnace (NSW-104 New Delhi), recirculating bath (Eyela CA-1112CE, Japan), and a counter-current condenser unit. In each experiment, 10 g of biomass sample was loaded into the reactor on a support of ceramic wool. The height of sample in the reactor was around 10 cm. A K- type thermocouple was inserted into the

reactor for measuring the temperature of torrefaction. The tip of the thermocouple just touched the upper surface of sample. The reactor was then purged by nitrogen gas (99.999% purity, Ashish Enterprise, Varanasi) at a flow rate of 45 mL/min using mass flow controller (Bronkhorst, Netherlands) for 30 min to remove oxygen trapped into the bed. Then, the furnace was turned on and heating rate was measured from control panel of furnace. The torrefaction of biomass was carried out between 220-280 ℃ with retention time between 20-60 min at a heating rate of 15 ℃/min. In each case, when the retention time was over the furnace automatically started cooling. The solid residue (torrefied biomass) was taken out of the reactor when room temperature reached. All the experiments were performed twice and average values were reported.

The solid yield of biomass is calculated as:

$$\textit{Solid yield (SY)} = \frac{m_{TAN}}{m_{DAN}} \qquad (3.1)$$

where m_{TAN} is the mass of torrefied *Acacia nilotica* at different process parameter and m_{DAN} is the mass of dried *Acacia nilotica*.

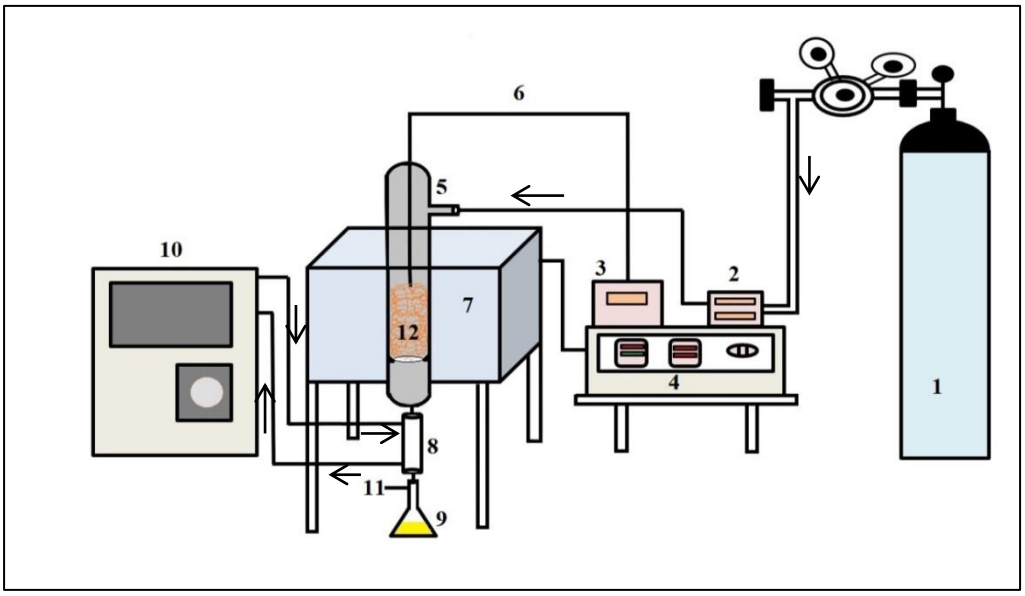

Figure 3.1 Schematic diagram of experimental set-up: 1-nitrogen cylinder, 2-mass flow controller, 3-temperature measuring unit, 4- split tube furnace (NSW-104) controller, 5-long tube fixed bed reactor, 6-K-type thermocouple, 7- split tube furnace (NSW-104), 8-condenser, 9-oil collector, 10- chiller (Eyela CA-1112CE), 11-gas collector, 12-biomass with ceramic wool bed (Singh et al., 2020b).

Table 3.1 List of controlled and measured variable during experiment

Variable	Range/value
Controlled variable	
Heating rate (℃/min)	15
Sweeping gas flow rate (mL/min)	40
Particle size (mm)	0.7-1.25
Pressure	Atmospheric
Measured variable	
Temperature (℃)	220-280
Retention time (min)	20-60

Table 3.2 Specifications/detail of instruments/variables used in experimental setup and procedure

Variable/analysis	**Instrument name/specification**	**Measurement Range**	**Uncertainty (%)**
Temperature (℃)	K-type thermocouple	-270 to 1370 ℃	±1.1 ℃
Split tube furnace (NSW-104)	Single heating zone (length 455 mm)	Max. 900 ℃	
	Micro processing PID controller		
	Work on 220 volt AC 50 Hz		
Heating rate (℃/min)	Set from control panel of furnace	-	±0.15 ℃/min
Retention time (min)	Set from control panel of furnace	-	Nil
Nitrogen flow rate (mL/min)	Mass flow controller (Bronkhorst)	0 to 200 mL/min	±0.30 % mL/min
Weighing machine	Sartorius weighing machine (BSA224S-CW)	Max. 250 g	±0.1 mg
Initial drying of sample	Laboratory Universal Hot air oven	Max. 260 ℃	±5 ℃
Proximate analysis	Muffle furnace	Max. 900 ℃	±5 ℃
Recirculating bath	Eyela CA-1112CE	-20 to 30 ℃	±2 ℃
Cutting machine	Retsch model SM 300	-	-

3.2.3 Physicochemical properties of raw and torrefied biomass

3.2.3.1 Proximate and ultimate analyses

Proximate analysis of biomass can be used to calculate moisture, volatile matter, fixed carbon, and ash content of the biomass sample. All these parameters were expressed on wet basis and dry basis and calculated using different ASTM standards mentioned in Table 3.3. The aim of ultimate analysis was to calculate the elemental composition (CHNS) of DAN and TAN. The Element analyzer (EURO EA3000, EURO VECTOR instrument and software, ITALY) was used to execute ultimate analysis. Oxygen bomb calorimeter (Rajdhani Scientific, NSTTS Co., New Delhi, India) was employed to evaluate the heating value of DAN and TAN.

The energy density ratio and energy yield can be calculated using Eqs. (3.2) and (3.3):

$$\textit{Energy density ratio (EDR)} = \frac{HHV_{db,TAN}}{HHV_{db,DAN}} \tag{3.2}$$

$$\textit{Energy yield (EY)} = SY \times EDR \tag{3.3}$$

The CHO index derived from the ultimate analysis of biomass to explain the oxidation state of carbon present in organic matter as recommended by Mann et al. (Mann et al., 2015). It can be calculated as:

$$\textit{CHO index} = \frac{2[O]-[H]}{[C]} \tag{3.4}$$

where [O], [H] and [C] are the mole fraction of oxygen, hydrogen, and carbon present in the organic material respectively.

Table 3.3 Different ASTM standards used to calculate engineering properties of torrefied biomass

Physical parameter	ASTM standard used
Bulk density	ASTM E873-82
Moisture content	ASTM E871
Ash content	ASTM E1755
Volatile matter	ASTM E872
Heating value	ASTM D240
Angle of repose	ASTM C144

3.2.3.2 Density, porosity, and particle size of raw and torrefied biomass

The density of biomass can be of three types: the bulk density, the tapped density, and the particle density. ASTM standard E873-82 is used to calculate the bulk density of biomass. The standard includes pouring the biomass sample into a standard-size container. In this study, a measuring cylinder of 500 ml is filled with biomass gently. The excess material over the cylinder was removed by a scale to level the biomass at the top of the measuring cylinder. The mass of the biomass present in the cylinder was weighed, and bulk density was calculated using the Eqs. (3.5). The tapped bulk density of biomass can be calculated by tapping the cylinder containing the biomass until it reaches a constant volume (tap around 100 times). The tapped density (ρ_{Tb}) was calculated using Eqs. (3.6). For calculation of particle density of biomass, it can be given a particular geometrical shape like cube, cuboid, sphere, and cylinder, etc. The mass of the shape and volume can be

calculated, and division of both gives the particle density of biomass. The porosity of biomass sample can be defined as the pore spaces present in the bulk samples of biomass, and it can be calculated using the following Eqs. (3.8).

Bulk density, ρ_b (kg/m^3) = $\frac{m_g - m_c}{V_L}$ (3.5)

Tapped density, ρ_{Tb} (kg/m^3) = $\frac{m_t - m_c}{V_L}$ (3.6)

Particle density, ρ_p (kg/m^3) = $\frac{m_p}{V_p}$ (3.7)

$\varepsilon_0 = 1 - \frac{\rho_b}{\rho_p}$ (3.8)

where $\rho_b$is the bulk density, ρ_{Tb} is the tapped density, ρ_p is the density of particle, m_g is the total mass of cylinder and biomass (kg), m_c is the mass of empty cylinder (kg), m_t is the total mass of cylinder and biomass after tapping (kg), m_p is the mass of geometrical shape (kg) and Vp is the volume of geometrical shape (m^3), V_L is the volume of measuring cylinder (m^3) and ε_0 is the porosity of biomass.

However, the biomass particle having irregular shape, the volume of particle can be calculated by deploying Eqs. (3.9) given by Tooyserkani et al.(Tooyserkani et al., 2013).

$Vp = Vc - V_R\left(\frac{P_1}{P_2} - 1\right)$ (3.9)

where Vp is the volume of biomass (m^3), V_C is the sample cell volume (m^3), V_R is the reference volume (m^3), P_1 is the pressure after pressurizing the reference volume (Pa), and P_2 is the pressure after including V_C (Pa).

For particle size distribution, unsieved DAN obtained after grinding was torrefied at 220, 250, and 280 ℃; then DAN and TAN was sieved and analyzed. Both, DAN and TAN were passed through a series of sieves having opening sizes (22, 25, 30, 36, 44, 52, 60 and 85 BSS) using a screen shaker. The sieves are arranged in the stack with largest opening at the top and smallest opening at the bottom. Size distribution for DAN and TAN was analyzed by employing the procedure given by American National Standards Institute (ANSI). After completion of shaking process, biomass sample accumulated on every single screen has been weighed. Geometric mean diameter (d_{gm}) for DAN and TAN was determined by employing the co-relation given by Cai et al. (Cai et al., 2017) in Eqs. (3.10).

$$d_{gm} = log^{-1}\left(\frac{\sum M_i . log\sqrt{d_i . d_{i-1}}}{\sum M_i}\right) \quad (3.10)$$

where d_i is diagonal of screen apertures of i^{th} screen, d_{i-1} is diagonal of the screen apertures in the next larger screen, and M_i is the mass retained on the i^{th} screen.

3.2.3.3 Moisture sorption test of raw and torrefied biomass

3.2.3.3.1 Open environment test

In this work, the characteristics of DAN and TAN for moisture sorption were performed in an open environment (relative humidity 60 %). For calculation of amount of moisture absorbed with respect to time, the sample DAN, TAN220-40, TAN250-40, and TAN280-40 were analyzed for the purpose. Weighed samples were kept for five days in an open environment. After estimated time, the samples were taken and weighed and percentage moisture absorbed was calculated using Eqs. (3.11):

$$\% \text{ moisture absorbed} = \frac{M_{Bi} - M_A}{M_A} \times 100 \qquad i = 1 \text{ to } 5 \text{ days} \qquad (3.11)$$

where M_A is the initial mass of the sample (kg), and M_{Bi} is the mass of sample after i^{th} day (kg).

3.2.3.3.2 Contact angle measurement

To check the water absorption characteristics, water contact angle of DAN and TAN were measured using contact angle analyzer (KRUSS, DSA25 Series, Hamburg, Germany). De-ionized water was used as a probe liquid. For contact angle measurement pellets from DAN and TAN were made and contact angle was recorded using a sessile drop method at room temperature.

3.2.3.4 Flowability and combustion indices of raw and torrefied biomass

The flow characteristics of DAN and TAN was investigated using Hausner ratio (HR), cohesion coefficient (C), Carr compressibility index (CCI) and angle of repose, while, fuel characteristics of DAN and TAN was investigated by fuel ratio (FR), combustibility index (CI), and volatile ignitability (VI). The detail about flow and fuel characteristics has been discussed in Chapter 1.

3.2.3.5 Analytical instruments used to characterize raw and torrefied biomass

Thermogravimetric analyzer (Perkin Elmer STA 6000) was used to investigate the thermal behavior and mass loss characteristics. 5 mg of DAN and TAN was heated from 25 to 800 ℃ in the presence of nitrogen atmosphere, at a flow rate of 20 mL/min and a constant

heating rate of 5 ℃/min. Fourier Transform Infrared Spectroscopy (FTIR) was done using (FTIR, Varian 1000, USA) for qualitative analysis of functional group present in DAN and TAN after torrefaction. Oven dried Potassium Bromide (KBr) was used to make the pellets to reduce the interference from water. The spectra were recorded from 4000 to 400 cm^{-1} wavenumber. The surface morphology and elemental analysis of DAN and TAN220-40, TAN250-40, and TAN280-40) were studied by scanning electron microscopy (SEM, model JEOL JSM5410, Japan). Metal content present in DAN and TAN was determined by using inductively coupled plasma-mass spectrometer (ICP-MS Perkin Elmer Optima 7000 DV series). Sample were digested in nitric acid and diluted with double distilled water so that metal concentration falls into the detection limit.

3.3 Results and discussion

3.3.1 Solid product and energy yield of torrefied biomass

The outcomes of torrefaction process are torrefied *Acacia nilotica* as solid product, condensable liquid and gaseous products. The amount of each product varies with operating conditions such as process temperature and retention time of biomass inside the reactor. Fig. 3.2 shows the variation of solid yield with temperature and retention time during torrefaction. When process temperature during torrefaction increases, the significant cleavage of hydroxyl group associated with biomass takes place. As a result, the amount of condensable liquid product with more water vapour increases with process temperature at fixed retention time. As an example, the solid yield was 61.82% and 43.03%, when the biomass was torrefied at 220 and 280 ℃, respectively, at a constant retention time of 40 min. Hence, effectively, the solid yield decreased by 30.40% due to increase of process

temperature at constant retention time. Moreover, solid yield also decreased with increase in retention time (Strandberg et al., 2015). The solid yield decreased from 60.10% to 51.23%, when the retention time was increased from 20 to 60 min, at torrefaction temperature of 250 ℃. It was observed that temperature had more pronounced effect than the retention time on torrefaction process. Subsequently, fuel and flow characteristics of torrefied *Acacia nilotica* should also be more process temperature reliant than retention time. Keeping this in mind, all the properties of torrefied *Acacia nilotica* at three temperature (220, 250, and 280 ℃) at 40 min retention time are calculated. The solid product yield from torrefaction often varies with biomass and its constituents. The biomass with higher fraction hemicellulose produces less solid product, as hemicellulose decomposition occurs at comparatively lower temperatures than cellulose and lignin (Bach & Skreiberg, 2016; Granados et al., 2016). The energy yield which is a product of solid yield and ratio of HHV of TAN to DAN indicates the amount of energy preserved in biomass after torrefaction. The energy yield of TAN220-40, TAN250-40, and TAN280-40 is found to be 74.10, 62.99, and 45.36 %, respectively. It shows that with increase in temperature the energy yield decreases since at higher temperature, dehydrogenation and deoxygenation of biomass become more prominent.

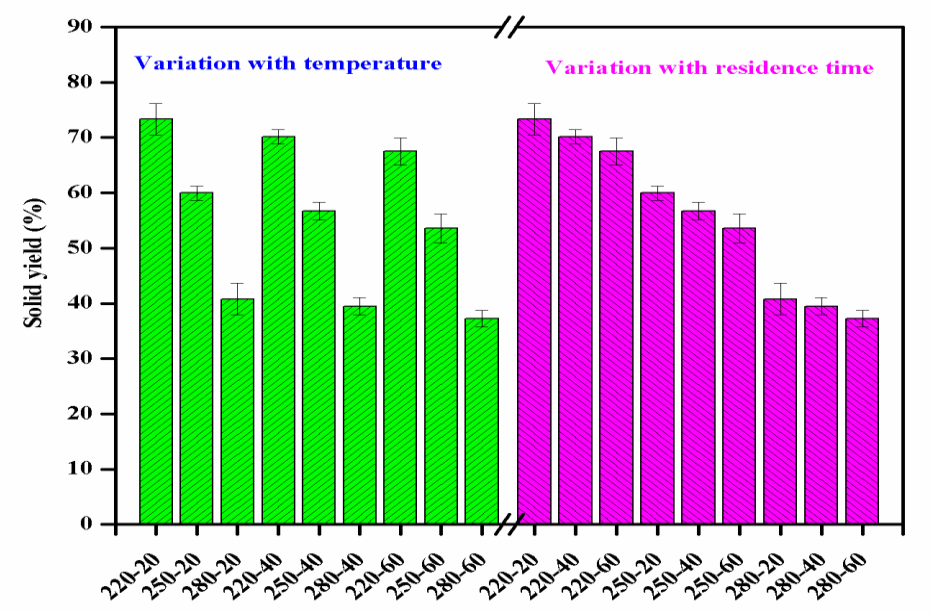

Figure 3.2 Variation of solid yield with temperature and retention time

The choice of optimum parameter for upgradation of DAN through torrefaction is based on the balance between higher heating value and energy yield of TAN. In this study, torrefaction at 250 ℃, and retention time 40 is recommended since the energy yield of TAN is 62.99 % and higher heating value is 22.54 MJ/kg.

3.3.2 Physicochemical Characteristic of raw and torrefied products

The results from physicochemical analysis are presented in Table 3.4. It shows that both the moisture content and the volatile matter decreased with increase in temperature during process. The moisture content of biomass decreased from 6.18% (DAN) to 0.88% (TAN280-40). Besides, the volatile matter also decreased from 81.77% (DAN) to 36.84% (TAN280-40). Vassilev et al. (Vassilev et al., 2013) revealed that biomass having higher

volatile matter is well suited for production of bio-oil through pyrolysis. The amount of volatile matter released from biomass depends on the temperature, retention time and heating rate during the process (Cai et al., 2017). It should be mentioned that the quantity of bio-oil could be reduced if TAN (low volatile matter) is pyrolyzed as compared to DAN (high volatile matter); however, the quality of bio-oil will be improved due to decreased O/C ratio as evident from Fig. 3.3. The ash content of biomass increased from 0.69% for DAN to 1.87% for TAN280-40. The fixed carbon increased from 11.35% for DAN to 60.40% for TAN280-40. The increase in fixed carbon and ash content of biomass was perceived after torrefaction since devolatilization of biomass increases with increase in temperature which results in relative decrease in moisture content and volatile matter and relative increase in fixed carbon and ash content of biomass. With increase in temperature, rate of release of light volatile matter (light hydrocarbon like methane, ethane, etc.) from biomass increases which affects the properties obtained from proximate analysis of biomass. During the torrefaction, release of hydrogen and oxygen in form of condensable liquid and gaseous products are more pronounced than release of carbon. The higher carbon content in biomass after torrefaction is accountable for increase in HHV of TAN. The higher heating values obtained for DAN, TAN220-40, TAN250-40, and TAN280-40 are 19.31, 20.77, 22.54, and 24.76 MJ/kg, respectively. Similar results for HHV were also obtained by Chen et al. (Chen et al., 2015c), Chen et al. (Chen et al., 2011) and Phanphanich et al. (Phanphanich & Mani, 2011) for same kind of biomass.

Table 3.4 Proximate and ultimate analysis of raw and torrefied biomass

Analysis	**DAN**	**TAN220-40**	**TAN250-40**	**TAN280-40**	**Coal sample[#]**
Proximate analysis (wt %)					
Moisture content	6.18	2.52	1.86	0.88	2.67
Ash content	0.69 (0.73)	1.24 (1.27)	1.39 (1.41)	1.87 (1.88)	6.63 (6.81)
Volatile matter	81.77 (87.15)	58.57 (60.08)	46.07 (46.94)	36.84 (37.16)	39.58 (40.66)
Fixed carbon*	11.35 (12.09)	36.66 (37.60)	50.66 (51.62)	60.40 (60.93)	51.12 (52.52)
Ultimate analysis (wt %)					
Carbon	43.84	50.31	58.62	64.75	76.48
Hydrogen	7.88	6.75	5.24	4.85	5.24
Nitrogen	0.42	0.63	0.69	0.64	2.32
Oxygen*	47.86	42.31	35.45	29.76	8.27
Sulphur	ND	ND	ND	ND	1.06
Higher heating value (MJ/kg)	19.31 (20.58)	20.77 (21.30)	22.54 (22.96)	24.76 (24.97)	30.42 (31.25)
Energy density ratio	-	1.19	1.11	1.05	-
Energy yield (%)	-	74.10	62.99	45.36	-

*Calculated by difference; ND Not detected; values in the parentheses are based on dry basis; # data for coal sample has been taken from (Shabbar & Janajreh, 2013).

The van Krevelen diagram may be used to compare the elemental composition of biomass with that of coal. In this diagram, the atomic ratio of hydrogen to carbon (H/C) is plotted against the atomic ratio of oxygen to carbon (O/C). Fig. 3.3 shows the van Krevelen diagram for DAN, TAN220-40, TAN250-40, and TAN280-40. As the temperature increases during torrefaction, the amount of oxygen and hydrogen present in biomass decreased with the relative increase in carbon content. The carbon content of DAN,

TAN220-40, TAN250-40, and TAN280-40 is found to be 43.84, 50.31, 58.62, and 64.75 wt%, respectively. Thus, with increase in temperature during torrefaction the carbon content of resulting solid product increases. The increase in carbon content of TAN is attributed to higher heating value of TAN. However, the solid yield decreases with increase in temperature (Fig. 3.2). Therefore, a balance between carbon content of TAN and solid product yield should be established. Hence, torrefaction at 250 ℃ and 40 min retention time is considered optimum for further studies. In addition, properties of TAN also move towards the properties of coal suggesting that TAN may be used as a substitute of coal. The ICP-MS was performed to analyze the effect of torrefaction on the metal content of DAN. The results are presented in Table 3.5. In can be observed that TAN is enriched in Sodium (Na), potassium (K), calcium (Ca), magnesium (Mg), iron (Fe), aluminum (Al), nickel (Ni) and cobalt (Co) while some elements such as chromium, Zink, and beryllium were not detected. The concentration of detected elements increased with increase in temperature during torrefaction. Presence of elements in TAN might be responsible for higher reactivity of TAN than the DAN. Also, TAN may be used as an agent for soil amendment (Gupta et al., 2018; Mullen et al., 2010).

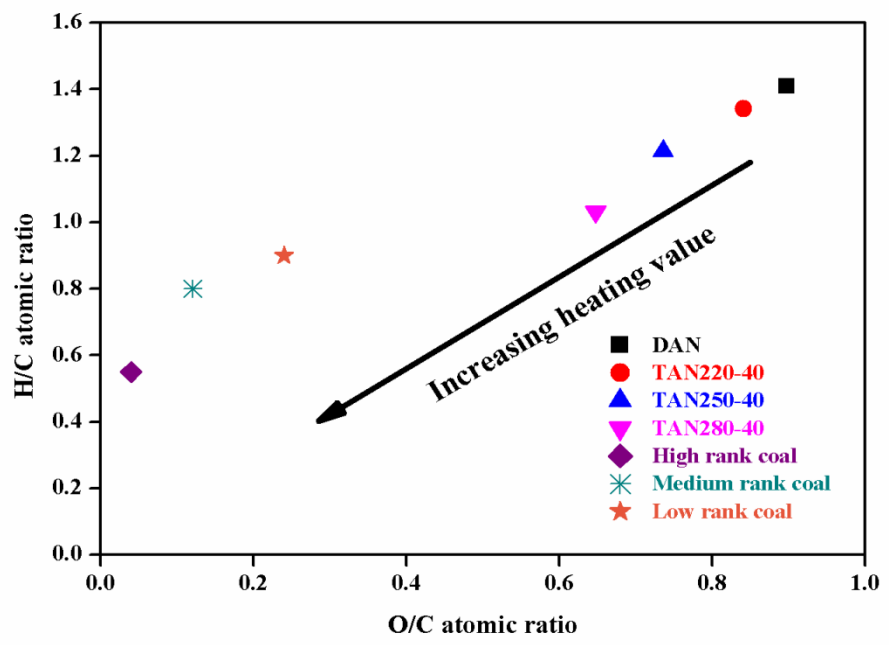

Figure 3.3 Van Krevelen diagram for raw and torrefied biomass

The range of CHO index can be from −4 to +4 (Cai et al., 2017). Higher value of CHO index depicts more oxidized compounds, while lower CHO index depicts reduced molecules of oxidized compounds. The CHO index obtained for DAN, TAN220-40, TAN250-40, and TAN280-40 are -0.34, -0.34, -0.55 and -0.58, respectively. The typical value of CHO index for biomass varies between -0.50 to + 0.05 (Cai et al., 2017; Mann et al., 2015). This index decreases with increasing temperature of torrefaction and are presented in Table 3.6. This clearly shows that the oxygen content of biomass decreases during this process. A positive value of CHO index for any biomass suggests that the amount of oxygen present in biomass is quite high (Cai et al., 2017; Mann et al., 2015).

Table 3.5 ICP-MS analysis of raw and torrefied biomass

Elements	**Concentration[@] of elements in different sample**				
	DAN	**TAN220-40**	**TAN250-40**	**TAN280-40**	**Coal sample****
Na	219	238	316	387	209
K	29	45	88	142	974
Mg	107	122	176	284	252
Ca	642	880	1097	1864	1081
Al	27	32	73	155	6931
Fe	23	40	88	143	5591
Ni	3	4	4	8	9.8
Cr	ND	ND	ND	ND	11.7
Mn	2	2	3	5	12.3
Zn	ND	ND	ND	ND	12.5
Co	6	6	6	10	1.13
Be	ND	ND	ND	ND	0.52

@ Concentration of elements are presented in ppm; ND not detected; ** data for coal has been taken from (Balarama Krishna et al., 2015)

Color is an important parameter for biomass fuel, like the biomass having dark color, is known for its high ash content. The color of DAN and TAN indicates the severity of process. The color of treated biomass has a direct relation with its calorific value, darker the treated biomass higher will be the calorific value. Fig. 3.4 shows the physical appearance of DAN, TAN220-40, TAN250-40, and TAN280-40. It can be clearly observed that TAN obtained at higher temperature had darker color and higher calorific value. In industries associated with biomass, color can be a time-saving parameter to judge the quality of biomass by preventing lab scale testing of properties like moisture content,

calorific value and hydrophobicity. Tooyserkani et al. (Tooyserkani et al., 2013) suggested that pellets made from bark of wood were darker in color.

Figure 3.4 Color appearance of raw and torrefied biomass

3.3.3 Density, porosity, and particle size raw and torrefied biomass

Three type of densities namely bulk, tapped and particle density and porosity of DAN and TAN were calculated using equations (3.5), (3.6), (3.7), and (3.8). Density is a key physical parameter for crafting a system for storage, handling, and transport of biomass. Bulk density of biomass varies with moisture content, particle dimension (size and shape), and surface morphology (Bhagwanrao & Singaravelu, 2014; S. Lam et al., 2008). The variation

of density and porosity of DAN and TAN obtained at different temperature is given Table 3.6. Results showed that densities (bulk, tapped and particle) of DAN and TAN were reduced at higher process temperature, while, porosity of biomass increased due to removal of volatile content present in biomass. The porosity of DAN and TAN280-40) were 0.79 and 0.83, respectively. These results are well supported by the results obtained by Conag et al. (Conag et al., 2017) for bulk and tapped density of biomass.

Table 3.6 Fuel and flow properties, different types of densities of DAN and TAN

Properties	**DAN**	**TAN220-40**	**TAN250-40**	**TAN280-40**	**Coal sample**
Fuel properties/indices[$]					
FR	0.13	0.62	1.09	1.63	1.29
CI (MJ/kg)	147.40	38.99	24.67	17.37	24.96
VI (MJ/kg)	15.76	15.69	15.65	15.37	31.15
H/C	0.17	0.13	0.08	0.07	0.06
O/C	1.09	0.84	0.60	0.45	0.10
VM/FC	7.20	1.59	0.90	0.60	0.77
CHO index	−0.34	−0.34	−0.55	−0.58	-
Flow properties[$$]					
Angle of repose (°)	39.36	38.79	36.15	32.51	36.8
HR	1.29	1.27	1.21	1.18	1.10
CCI	22.85	21.44	17.35	15.86	9.23
C	0.40	0.39	0.36	0.33	0.28
Bulk density (kg/m^3)	230.82	210.34	190.18	172.84	727
Tapped density (kg/m^3)	299.21	267.77	230.13	205.43	801

Particle density (kg/m^3)	1220	1150	1110	1050	1500
Porosity	0.81	0.81	0.82	0.83	-
Particle size (mm)	0.50	0.48	0.46	0.45	-

$ data for fuel properties of coal has been taken from (Shabbar & Janajreh, 2013); $$ data for flow properties of coal has been taken from (Lu et al., 2015).

The dimensions (size and shape) of biomass particles have significant consequence on the mixing, fluidization, and surface area. It also affects the heat and mass transfer along with flow behavior of biomass particles. Hence, the thermochemical process involving various dimensions of biomass can have different efficiency and energy requirement. The particle size of biomass feedstocks highly affects the thermochemical conversion process. Generally biomass has irregular shape and size which creates difficulties in the precise measurement of dimension (length, width, and thickness). The precise description of biomass dimension is crucial for processing, handling, and storage. Sieve analysis is a major technique for characterization of particle size (geometric mean diameter) of DAN and TAN. According to Eqs. (3.10), the geometric mean diameters of DAN, TAN220-40, TAN250-40, and TAN280-40 are found to be 0.50, 0.48, 0.46 and 0.45 mm, respectively. The screen analysis of DAN, TAN220-40, TAN250-40, and TAN280-40 is shown in Fig. 3.5 (a) and (b). It was observed that at higher temperature during torrefaction the fraction of smaller particle increases and uniformity in the particle size was obtained. Smaller particle obtained after torrefaction have lower heat resistance in further thermochemical process. Based on the results of screen analysis, SEM analysis, and density of TAN, it may be predicted that comminution of TAN becomes easier than the DAN. SEM analysis

revealed that tenacious and fibrous structure of biomass is removed after torrefaction and pores were seen on the surface of biomass. Based on this observation, it may be noted that comminution of TAN is likely to be less energy-intensive process. In addition, decrease in density of biomass after torrefaction also favors easier comminution of TAN. Similar finding were reported by Arias et al. (Arias et al., 2008b), and Tumuluru et al. (Tumuluru & Heikkila, 2019). Tumuluru et al. (Tumuluru & Heikkila, 2019) optimized the grinding process using response surface methodology taking moisture content and grinder speed as input variables. They reported that at constant grinder speed of 20 Hz, specific grinding energy (kWh/ton) requirement would be lowered by 39.1 % if the moisture content was reduced from 20 wt% to 10 wt %. In the present work the moisture content for TAN220-40, TAN250-40, and TAN280-40 was decreased by 59.22, 69.90, and 85.76 %, respectively, as compare to the native biomass (DAN). Based on these observations, it can be mentioned that the comminution of TAN may be easier than that of DAN. Fig. 3.5 (b) shows the cumulative mass (wt%) retained on the screen and it was observed that mass of uniform particle size on each screen is obtained in case of TAN in contrast to DAN having unequal proportion of biomass on each screen. The larger biomass particle offers larger mass transfer and heat transfer resistance.

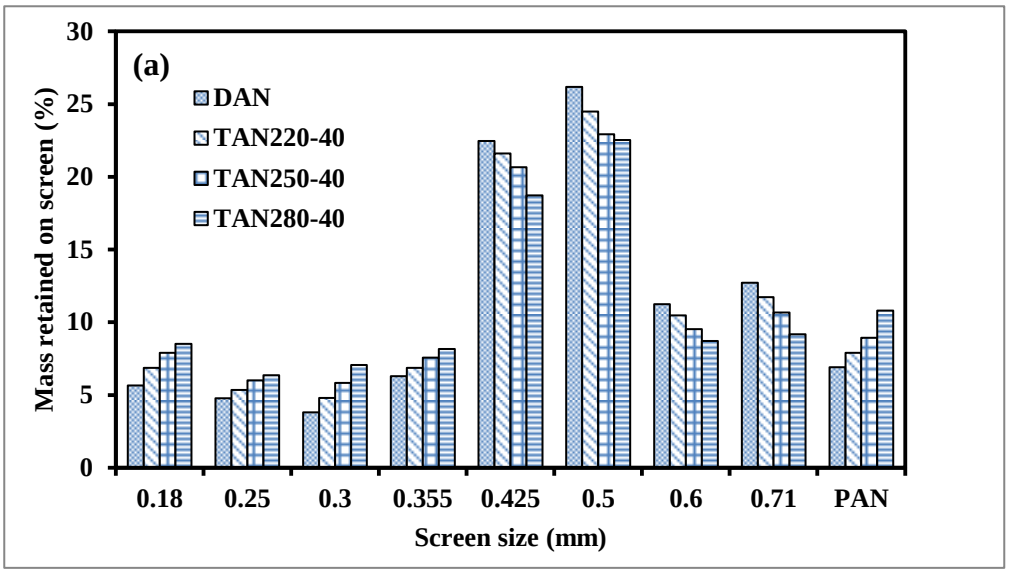

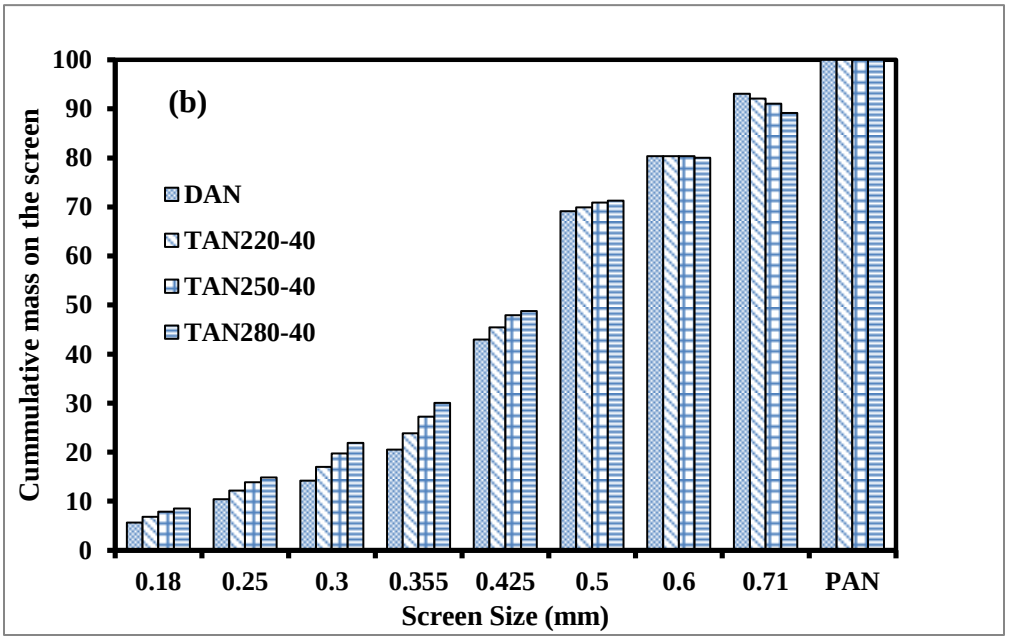

Figure 3.5 (a) Particle size distribution of raw and torrefied biomass **(b)** Cumulative mass distribution for raw and torrefied biomass

3.3.4 Moisture sorption characteristics of raw and torrefied biomass

The biomass has hydrophilic characteristics due to which it absorbs moisture when kept in open environment which causes biological degradation. Major constituents of biomass are hemicellulose, cellulose, and lignin. Each of these components contain hydroxyl group (-OH). Due to presence of this hydroxyl group biomass forms hydrogen bond with moisture, which makes it hygroscopic in nature. This higher moisture content in the biomass is undesirable since it leads to low energy efficiency, high energy loss, and higher emission when the biomass is used in thermochemical conversion process along with higher transport, storage and handling cost (Bach & Skreiberg, 2016).

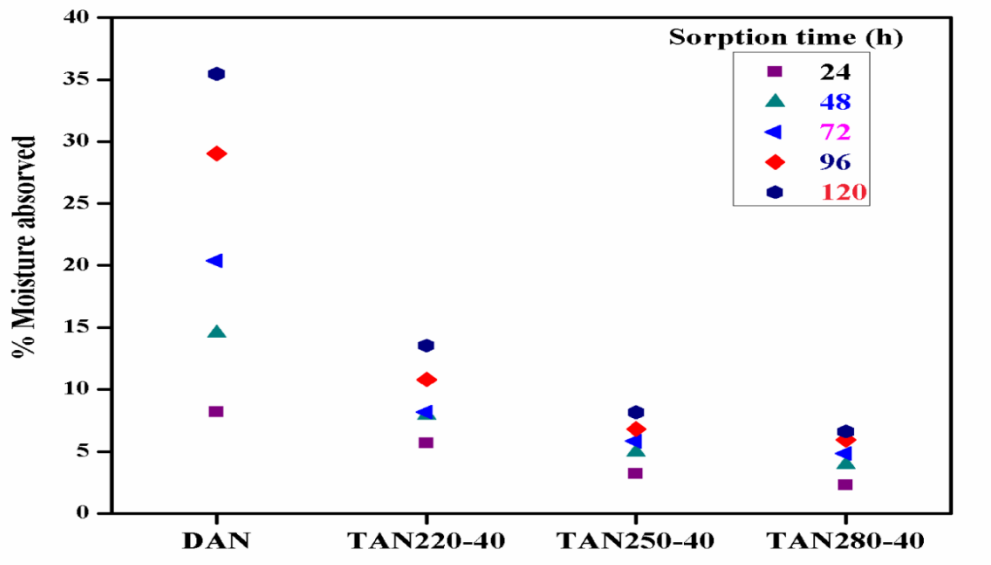

Figure 3.6 (a) Moisture sorption test of raw and torrefied biomass in open environment

Fig. 3.6 (a) shows the percentage of moisture absorbed in DAN and TAN220-40, TAN250-40, and TAN280-40. After five days, percentage of moisture absorbed by DAN, TAN220-40, TAN250-40, and TAN280-40 is 35.44%, 13.52%, 8.15% and 6.61% respectively. The torrefaction of biomass makes it hydrophobic in nature so that it absorbs minimal amount of moisture and becomes more stable when stored in an open environment. During torrefaction, hydroxyl group (-OH) associated with biomass is ruptured resulting in lower affinity of biomass to associate with water through hydrogen bonding (Bach & Skreiberg, 2016). Torrefaction makes the biomass unsaturated which have non-polar properties. In addition, the tar present in the liquid condensate might get condensed on the surface and block the pores present in the TAN which can further reduce the water absorption capacity of TAN through capillary action (Ohm et al., 2015)**.** This implies that the torrefaction can improve the logistic characteristics of biomass. The hydrophobic nature of TAN was also confirmed by contact angle measurement. For hydrophobic character the value of contact angle should be close to 90° (Strandberg et al., 2015). Fig. 3.6 (b) shows the contact angle of DAN and TAN. The contact angle from left and right side of the meniscus for DAN, TAN220-40, TAN250-40, and TAN280-40 was found to be 46.5-47.8°, 64.9-64.3°, 70.3-70.1° and 79.9-77.5° respectively. Thus, it can be concluded that hydrophobic characteristics of biomass increases with increase in temperature during torrefaction.

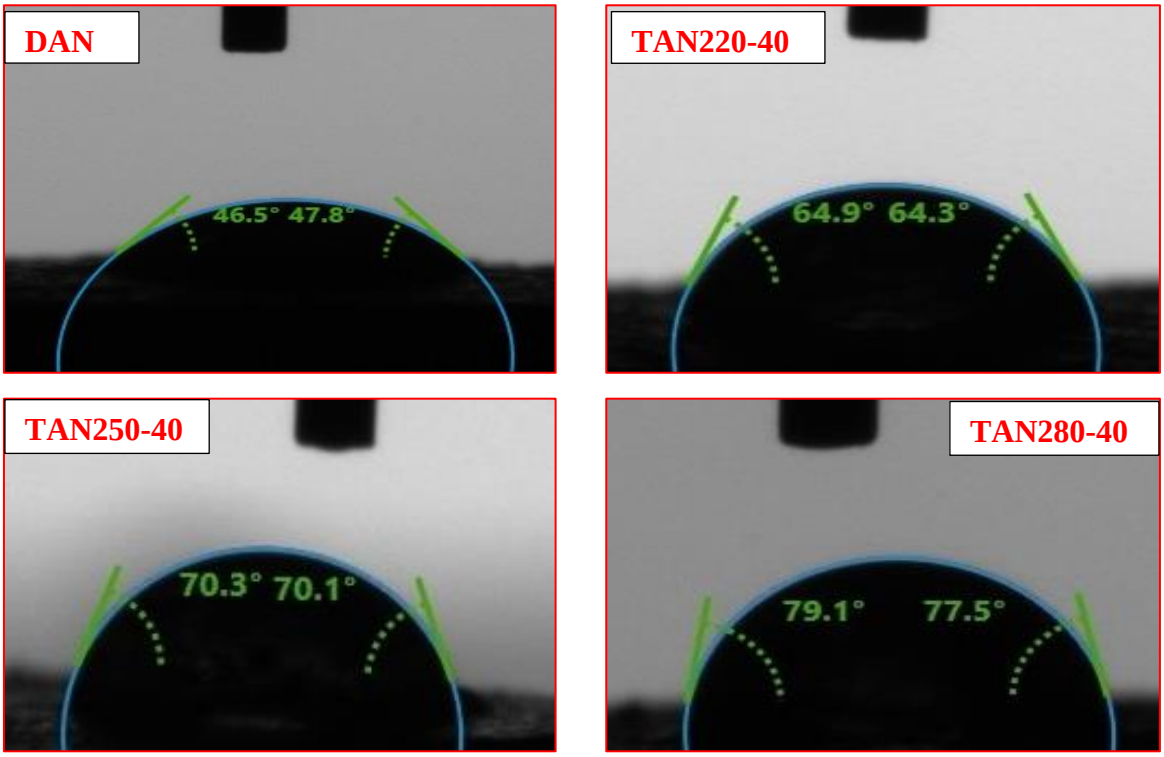

Figure 3.6 (b) Moisture sorption test of raw and torrefied biomass using contact angle measurement

3.3.5 Flowability of raw and torrefied biomass

Flowability is the property of biomass which depicts the ease of motion of biomass from one point to other during the process. The flowability is an important characteristic of biomass which plays a crucial role during its utilization in conversion and co-conversion processes. The flow characteristics of DAN and TAN are shown in Table 3.6. The flow behavior of DAN and TAN based on Hausner ratio (HR), cohesion coefficient (C), Carr compressibility index (CCI) and angle of repose were analyzed and compared from Table 3.7 obtained from literature. The angle of repose for DAN, TAN220-40, TAN250-40, and TAN280-40 are 39.36, 38.79, 36.15, and 32.51 respectively. The calculated value of

Hausner ration in this work for DAN, TAN220-40, TAN250-40, and TAN280-40 are 1.29, 1.27, 1.21 and 1.18, respectively, while, Carr compressibility index of DAN, TAN220-40, TAN250-40, and TAN280-40 are 22.85, 21.44, 17.35 and 15.86, respectively. The cohesion coefficient of DAN, TAN220-40, TAN250-40, and TAN280-40 are 0.40, 0.39, 0.36, and 0.33, respectively. During the course of torrefaction, solid product obtained at higher temperature has lower angle of repose and has better flowing property than the DAN.

Table 3.7 Characteristic flow properties of biomass (Lumay et al., 2012; Szalay et al., 2015)

Flow property	Angle of repose (degree)	Hausner ratio (HR)	Carr compressibility index (CCI)
Excellent	25-30	1.00-1.11	≤ 10
Good	31-35	1.12-1.18	11-15
Fair	36-40	1.19-1.25	16-20
Passable	41-45	1.26-1.34	21-25
Poor	46-55	1.35-1.45	26-31
Very Poor	56-65	1.46-1.59	32-37
Very very Poor	>66	>1.60	>38

The TAN at a higher temperature has better flowing property than DAN or low temperature torrefied material. The Carr compressibility index of DAN, TAN220-40, TAN250-40, and TAN280-40 are 22.85, 21.44, 17.35 and 15.86 respectively. The TAN at higher temperature has lower tendency to agglomerate resulting in better flow behavior in

comparison to DAN. Cohesion coefficient signifies the cohesive and frictional force of biomass particles (Szalay et al., 2015)**.** The cohesion coefficient of DAN, TAN220-40, TAN250-40, and TAN280-40 are 0.40, 0.39, 0.36, and 0.33, respectively, which revealed that cohesive force in case of TAN is lower than the DAN resulting in better flow behavior of TAN as compared to DAN.

3.3.6 Combustion indices of raw and torrefied biomass

Table 3.6 presents the combustion indices of DAN and TAN. The combustion indices are generally used to define quality of torrefied biomass after thermochemical conversion processes. Fuel ratio (FR), combustibility index (CI), and volatile ignitability (VI) are determined using equations (1.5), (1.6), and (1.7), respectively. The fuel ratio of DAN increased after torrefaction due to increase in fixed carbon and simultaneous decrease in volatile content of biomass. In case of coal, the recommended range for fuel ratio is 0.5-3.0. The TAN obtained at 280 ℃ and 40 min retention time having the fuel ratio 1.63 which makes it suitable for firing in power plants along with coal. The higher fuel ratio causes an incomplete burning of fuel which reduces the efficiency of boiler when such fuel is used during its operation. During the process, the fuel with a fuel ratio greater than two may cause problems with ignition and flammability. The published combustibility index and volatile ignitability ranges are: combustibility index should be below 23MJ/kg and volatile ignitability should be above 14.5MJ/kg (Ohm et al., 2015). The value of combustibility index and volatile ignitability of DAN are 147.40 MJ/kg and 15.76 MJ/kg, respectively. It means that, without prior treatment DAN cannot be suited as an alternative energy source. The calculated value of combustibility index for TAN220-40, TAN250-40, and TAN280-40 are 38.99, 24.67, and 17.37 MJ/kg, respectively. The calculated value of

VI for TAN220-40, TAN250-40, and TAN280-40 are 15.69, 15.65, and 15.37 MJ/kg, individually. Similar kind results were obtained by Singh et al. (Singh et al., 2019a). It shows that TAN obtained at 280 ℃ has nearly comparable characteristics like coal, and it can be used as a substitute source of energy and also, TAN can be blended with coal.

3.3.7 Thermogravimetric analysis

Fig. 3.7 (a) shows the thermogravimetric analysis of DAN and TAN. The plot revealed that, in case of TAN, fixed amount decomposition attained at higher temperature. For DAN, mass loss of 20% was attained at 280 ℃, however, the same amount of mass loss was observed at 336, 351, and 496 ℃ in case of TAN220-40, TAN250-40, and TAN280-40, respectively. This shifting of decomposition temperature for TAN might be due to breakdown of hemicellulose and retaining most of the cellulose and lignin. The different components of biomass have range of temperature for thermal decomposition. Hemicellulose and cellulose, generally decomposed at between 200-350 ℃, while lignin decomposed between 280-600 ℃ (Ren et al., 2013a). For hemicellulose and cellulose, substantial weight loss was observed from 268 ℃ to 355 ℃ (Yang et al., 2007). The DTG curve of DAN and TAN are presented in Fig. 3.7 (b). At around 300 ℃, a shoulder in DTG curve of biomass corresponds to degradation of hemicellulose (Müller-Hagedorn et al., 2003; Yang et al., 2007). In present work similar kind of shoulder is appeared in case of DAN Fig. 3.7 (b). However, in case of TAN220-40, TAN250-40 and TAN280-40, the shoulder cannot be observed, which revealed that the hemicellulose of DAN has decomposed in course of torrefaction. In DTG curve, the peak associated with maximum mass loss corresponds to cellulose content of biomass (Yang et al., 2007). Around 340 ℃,

similar peaks attributed to cellulose can be perceived in case of DAN and TAN which signifies lesser decomposition of cellulose in comparison to hemicellulose during torrefaction. However, intensity of peak for TAN decreases as the temperature increases during the process.

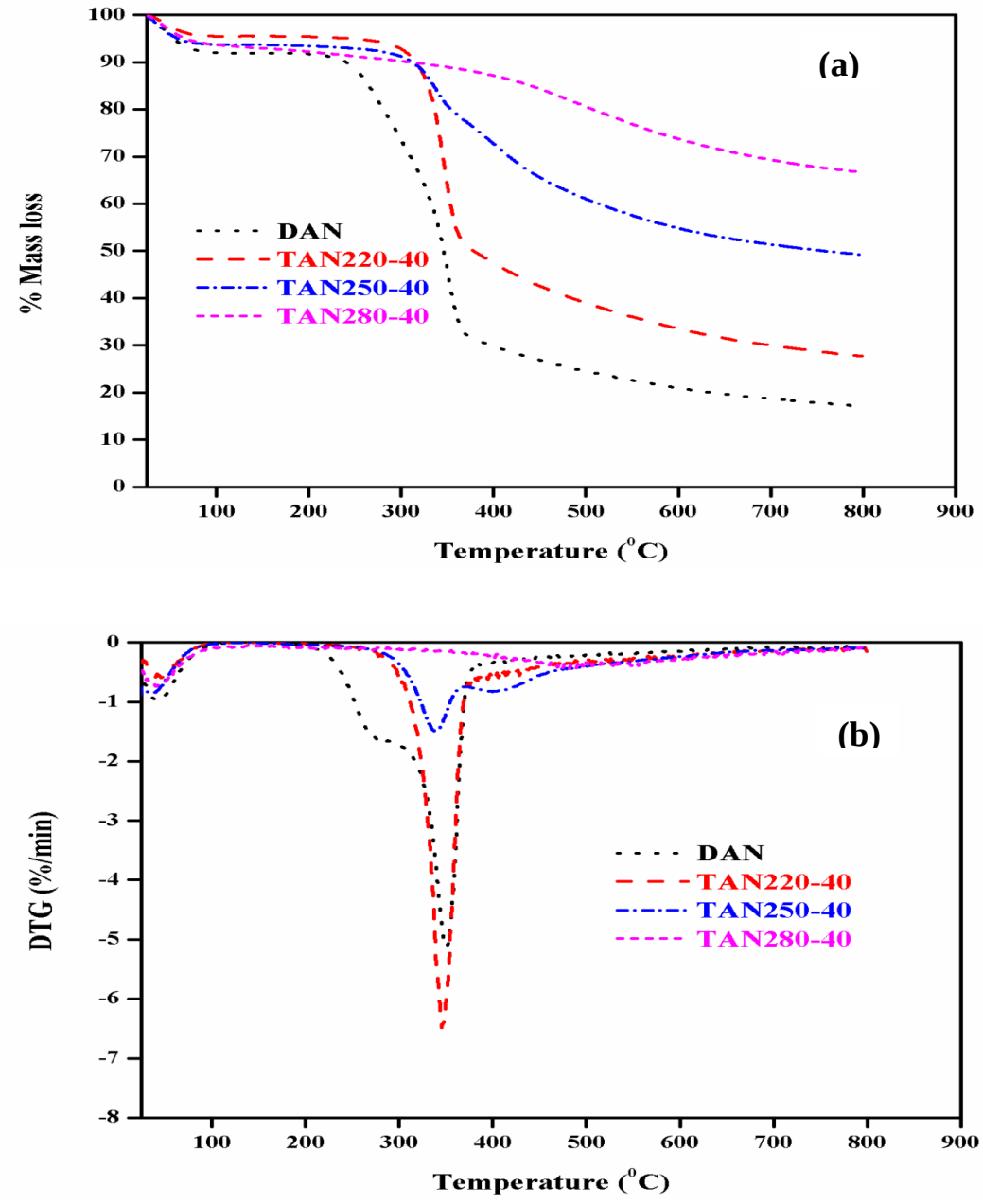

Figure 3.7 Thermogravimetric analysis of raw and torrefied biomass (a) TGA analysis (b) DTG analysis

3.3.8 FTIR analysis of raw and torrefied biomass

The analysis of various chemical functional groups present in DAN and corresponding changes in then after torrefaction was analyzed by employing Fourier transform infrared spectroscopy (FTIR) (Fig. 3.8). The breakdown of hemicellulose during torrefaction is mainly accountable for alteration in chemical structure of DAN. The distinctive peak among 3300-3100 cm^{-1} ascribed the stretching vibration of hydroxyl group (-OH) associated with hemicellulose of biomass. It also confirmed the hydrogen bond present between alcohol and phenol groups associated with hemicellulose and cellulose component of biomass (Min et al., 2011). Decrease in intensity from 3300-3100 cm^{-1} waveband inferred the breaking of hydrogen bond present between alcohol and phenol. This increases the durability of biomass against the moisture and biological attacks along with make it suitable for long storage, easy handling, and transportation.

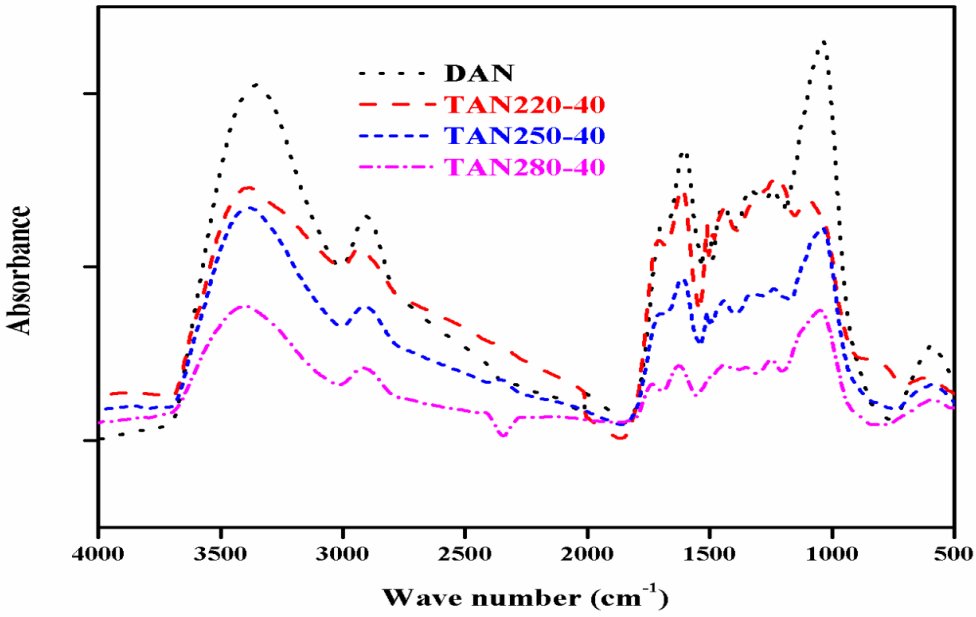

Figure 3.8 FTIR analysis of raw and torrefied biomass

The specific peaks between 2900-2750 cm^{-1}, 1750-1500 $cm^{-1,}$ and 1200-1000 cm^{-1} were observed due to stretching vibration in C=O bond, C=C bond, C-H bond, and C-O-C bond respectively (Azargohar et al., 2014; Keiluweit et al., 2010; Sharma et al., 2001).With increase in temperature during torrefaction, the in intensity of peaks reaffirming the rupture of chemical bonds such as C=O, C-O-C, CHO- etc. present in the biomass. Reduction in peak intensity from 1750-1500 cm^{-1} corresponds to cleavage of ester group associated with hemicellulose through deacetylation reaction (Carrasco & Roy, 1992). The characteristic peak between wavenumber 600-700 cm^{-1}, attributed to existence of aromatic compounds with mono and cyclic groups (Gomez-Serrano et al., 1996).

3.3.9 SEM-EDX analysis of raw and torrefied biomass

The scanning electron microscopy (SEM) analysis of DAN, TAN220-40, TAN250-40 and TAN280-40 at 2K magnification is depicted in Fig. 3.9 to investigate the impact of torrefaction on biomass morphology. The effect of torrefaction could be clearly perceived in Fig. 3.9 (c), (e), and (g). Hemicelluloses are typically branched polysaccharides comprising solid bulky and branched xylem tissues (Ibrahim et al., 2013). Hemicellulose is elucidated by a branched arrangement associated with the DAN. Nevertheless, in the case of TAN, this branched structure began to disappear, indicating hemicellulose degradation during torrefaction (Fig. 3.9 (c), (e), and (g)). The formation of pores is visible for TAN220-40, TAN250-40, and TAN280-40. An increase in the pore size with increasing temperature could be seen from Fig. 3.9 (g) where the biomass was torrefied at 280 ℃ for 40 min. The appearance of pores on the surface of TAN was ascribed its lower density than the DAN which can increase the surface area and lower grinding energy as compared to DAN. Ibrahim et al. (Ibrahim et al., 2013), and Bach et al. (Bach & Skreiberg, 2016)

mentioned the similar kind of results. Along with SEM analysis, energy dispersive X-ray (EDX) was also performed to identify elements present on the surface of DAN and TAN. EDX images of DAN, TAN220-40, TAN250-40, and TAN280-40 are depicted in Fig. 3.9 (b) (d) (f) and (h), respectively. The results revealed that with increase in severity of the torrefaction process, peaks corresponding to nitrogen, calcium, magnesium and potassium are appearing in TAN220-40, TAN250-40, and TAN280-40 with high intensity. However, in case of DAN, only carbon, oxygen and potassium can be seen. Presence of these elements in the TAN makes it suitable for soil amendment to increase the fertility of soil (Gupta et al., 2018; Mullen et al., 2010).

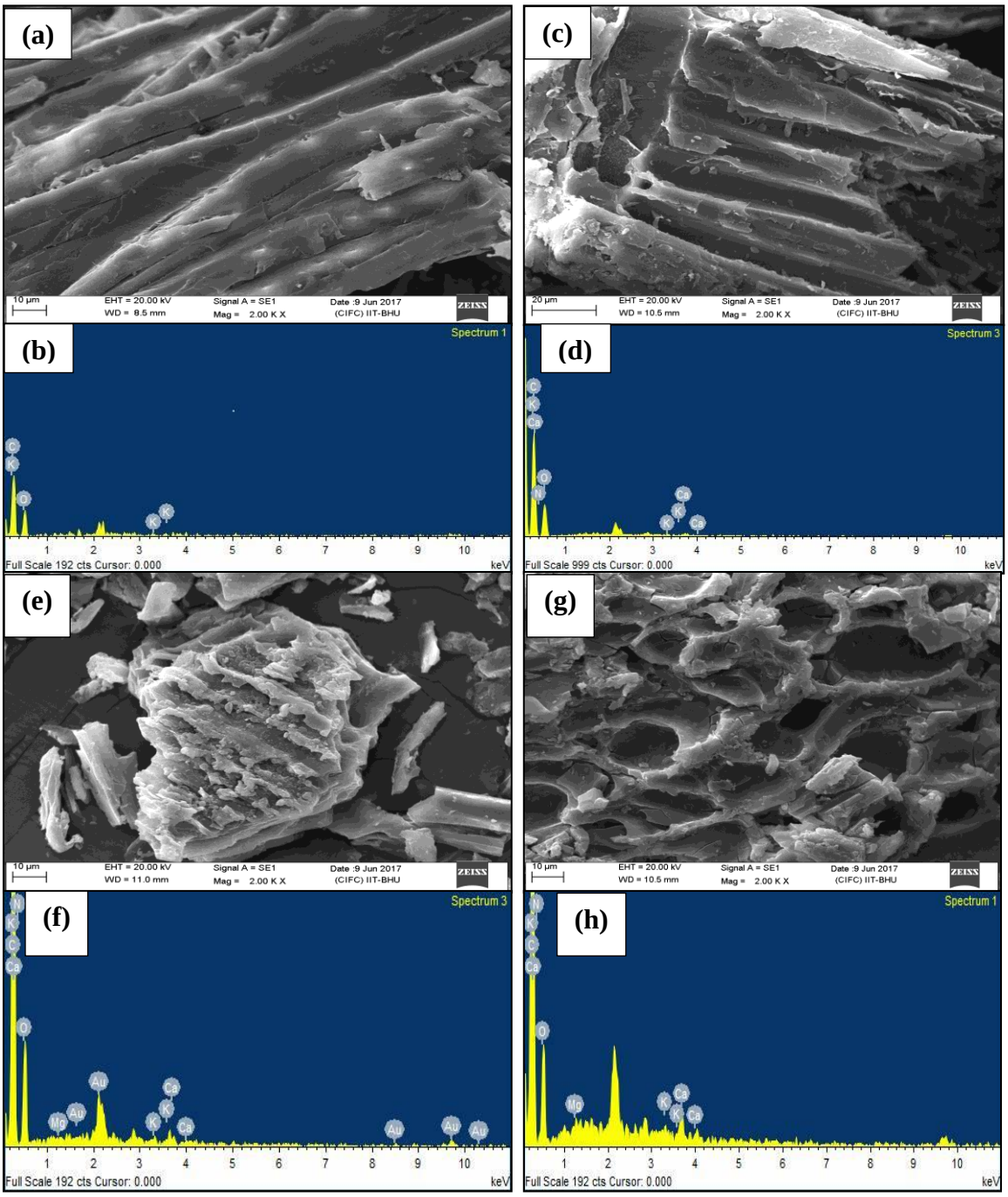

Figure 3.9 SEM and EDX images of raw and torrefied biomass: (a) and (b) DAN, (c) and (d) TAN220-40, (e) and (f) TAN250-40 and (g) and (h) TAN280-40

3.4. Conclusions

Experimental investigation of torrefaction of *Acacia nilotica* within a temperature range of 220- 280 ℃ and retention time between 20-60 min was performed. Various properties which validate good quality of solid fuel from biomass were examined. Results showed that temperature during torrefaction had more pronounced effect on solid yield as compared to retention time. Fuel and flow characteristics of *Acacia nilotica* has been improved after torrefaction and are closure to the properties of coal. The higher heating value (HHV) increased by 28.2 % when DAN was torrefied at 280 ℃ for 40 min. TAN was found to be less hygroscopic as moisture reabsorbed was 6.61 % (TAN280-40, 120 h) as compared to 35.44 % (DAN, 120 h). Also, the contact angle of TAN280-40 (79.1°/77.5°) was close to 90° confirming the hydrophobic nature. The bulk density of TAN was suitable for use as briquette and co-firing with coal in thermal plants with HR value less than 1.29 and CCI less than about 23. There was significant decrease in volatile matter (57.4 %) with simultaneous increase in fixed carbon content (~4 times). Hence, less volatile matter and high fixed carbon make TAN a better solid fuel. TGA results showed that devolatilization temperature shifted to higher value and residual char yield increases when TAN was pyrolysed. ICP-MS analysis revealed that TAN enriched by important elements such as sodium (Na), potassium (K), calcium (Ca), magnesium (Mg) etc. making it suitable for soil amendment. Finally, *Acacia nilotica* exhibited better performance as compared to other woody biomass because of enhanced HHV, low ash content etc.

Chapter 4

Intrinsic kinetics, thermodynamic parameters and reaction mechanism of non-isothermal degradation of torrefied *Acacia nilotica* using isoconversional methods

General background

This chapter aimed to examine the suitability of torrefied *Acacia nilotica* for bio-energy generation by investigating its kinetic and thermodynamic parameters as well as reaction mechanism during pyrolysis based on thermogravimetric analysis. Thus, torrefaction of *Acacia nilotica* was performed in a fixed bed reactor at 220, 250 and 280 ℃, with constant retention time (40 min) and heating rate (15 ℃/min). Pyrolysis of dried *Acacia nilotica* (DAN), torrefied *Acacia nilotica* obtained at 220 ℃ (TAN220), 250 ℃ (TAN250) and 280 ℃ (TAN280) was performed using thermogravimetric analyzer at three different heating rate viz. 5, 10 and 15 K/min. Further, isoconversional models namely, Kissinger-Akahira-Sunose (KAS), Ozawa-Wall-Flynn (OWF), Friedman and Starink were employed to calculate the kinetic parameters (activation energy and pre-exponential factor) of DAN and TAN. Using kinetic parameters obtained from KAS method, thermodynamic parameters (enthalpy, Gibbs free energy, and entropy) were calculated at a heating rate of 10 K/min. Reaction mechanism during pyrolysis of DAN and TAN was predicted using Criado method (Z-master plot).

4.1 Introduction

The energy from biomass can be extracted through biological (enzymatic digestion and fermentation), and thermochemical (torrefaction, liquefaction, pyrolysis, gasification etc.) conversion routes; however later has gained dominance due to its fast and efficient nature (Dacres et al., 2019). The torrefied biomass exhibits improved characteristics than raw biomass in terms of less moisture content, higher HHV, lower H/C and O/C ratio. Torrefaction also improves the grindability and lowers the water sorption characteristics of biomass (Bach et al., 2017a; Bach et al., 2017b; Chen et al., 2016b; Ren et al., 2013a). Eventually, there are two ways through which energy can be extracted from the torrefied biomass viz. either direct use of treated biomass in pyrolysis and gasification or co-pyrolysis, co-gasification with other biomass, plastic and municipal waste. Besides, these days blending of torrefied biomass with coal in thermal power plants are common practice (Bada et al., 2014; Kastanaki et al., 2002; Moghtaderi et al., 2004; Pan et al., 2000; Vuthaluru, 2004; Zhang et al., 2007).

So, in order to explore the torrefied biomass and to achieve the best utilization for bio-energy generation, kinetic and thermodynamic parameters along with model prediction of reaction mechanism become essential. The recommendations suggested by the kinetic committee of the International Confederation for Thermal Analysis and Calorimetry (ICTAC), the thermogravimetric analysis (TGA) is one of the most prevalent and effective methods to describe the thermal decomposition behavior and kinetics of biomass and coal conversion (Vyazovkin et al., 2011). Through TGA and DTG data, kinetic parameters such as activation energy and pre-exponential factor can be investigated. Furthermore, the thermodynamic parameters may also be interpreted based on the kinetic parameters.

The kinetic parameters (activation energy, pre-exponential factor), thermodynamic parameters (enthalpy, Gibbs free energy, and entropy) and reaction mechanism are very important for design, optimization, and scaling of process reactor and parameters (Hu et al., 2018). The behavior of torrefied biomass towards thermochemical conversion might be different from raw biomass. Also, during blending of torrefied biomass with coal in thermal power plant, the process will be affected by the distinctive kinetic, thermodynamic parameters and reaction mechanism followed individually by torrefied biomass and coal. So, the deep in-sight about the kinetic, thermodynamic parameter as well as reaction mechanism of torrefied biomass is required.

4.2 Materials and methods

4.2.1 Material collection, preparation, and characterization

The detailed discussion about material collection, preparation and characterization such as proximate and ultimate analysis has been discussed in Chapter 3. The proximate, ultimate, HHV and other parameters are presented in Table 3.1 of Chapter 3 and the relevant discussion is carried out in subsequent sections. The hemicellulose, cellulose, and lignin components of biomass were determined following the protocol mentioned by Bledzki et al. (Bledzki et al., 2010). Extractive component was calculated by difference.

4.2.2 Experimental procedure for torrefaction and pyrolysis of torrefied biomass

The torrefaction of biomass was carried out in a laboratory fixed bed reactor at 220, 250, and 280 ℃ with a retention time of 40 min, and a heating rate of 15 ℃/min. The schematic

diagram of the experimental setup, detailed procedure has been discussed in Chapter 3. The thermogravimetric analyzer (NETZSCH TG 209F1 Libra) was used to carry out pyrolysis of DAN, TAN220, TAN250, TAN280 at three different heating rates 5, 10, 15 K/min, between the temperature ranges from 298 to 1073 K. Nitrogen gas (99.99%, purity), at a flow rate of 20 mL/min was used as a carrier. 5 mg of each biomass sample was taken. In each experiment, initially, nitrogen gas was purged into the TGA for 20 min at an initial temperature to avoid undesirable oxidation of sample during pyrolysis. The sample was kept for 20 min at 1073 K when the experiment was over.

4.2.3 Kinetic study

The chemical composition and physical characteristics vary from one biomass to another. Consequently, pyrolysis becomes a complex process and various biomass shows different behavior (Huang et al., 2016; Sriram & Swaminathan, 2018). The TGA and DTG data were used to obtain the kinetic and thermodynamic parameters for thermal degradation of DAN and TAN during pyrolysis. The general pyrolysis reaction can be represented as (Kaur et al., 2018; Slopiecka et al., 2012):

$$\text{Biomass} \xrightarrow{k} \text{Bio-char} + \text{volatile}$$

A general expression for non-isothermal kinetics for solid decomposition can be expressed as follows:

$$\frac{d\alpha}{dt} = k\,(T)\,f\,(\alpha) \qquad (4.1)$$

where, k is the rate constant, and α is the fractional conversion during thermal decomposition of solid biomass. Biomass conversion can be defined as follows:

$$\alpha = \frac{m_0 - m_t}{m_0 - m_f} \quad (4.2)$$

where, m_0 is the initial mass of the sample, m_t is the mass of sample at any time t, and m_f is the final mass of the sample.

The rate constant is a function of temperature and may be expressed as follows:

$$k\,(T) = Ae^{-E_a/RT} \quad (4.3)$$

where E_a is activation energy, A is pre-exponential factor and R is universal gas constant.

Combining Eqs. (4.1) and (4.3) gives the fundamental expression (4.4) for the analytical method to calculate kinetic parameters, on the basis of TGA data.

$$\frac{d\alpha}{dt} = Ae^{-E_a/RT}\, f\,(\alpha) \quad (4.4)$$

The TGA analysis was carried out at a constant heating rate given as:

$$\beta = \frac{dT}{dt} \quad (4.5)$$

The conversion can be expressed as the function of temperature. However, the temperature is dependent on the heating rate also. Therefore,

$$\frac{d\alpha}{dT} = \frac{d\alpha}{dt}\frac{dt}{dT} \quad (4.6)$$

$$\frac{d\alpha}{dT} = \frac{d\alpha}{dt}\frac{1}{\beta} \quad (4.7)$$

Combining Eqs. (4.4) and (4.7)

$$\frac{d\alpha}{dT} = \frac{A}{\beta}\, e^{-E_a/RT}\, f\,(\alpha) \quad (4.8)$$

Integrating both sides of Eqs. (4.8) gives:

$$g(\alpha) = \int_0^{\alpha} \frac{d\alpha}{f(\alpha)} = \frac{A}{\beta} \int_0^{T} e^{-E_a/RT} dT \quad (4.9)$$

where, $g(\alpha)$ is the integral function of conversion α. The kinetic model $f(\alpha)$ is an algebraic expression related with a physical model which describes the kinetics of the solid state reaction. Functional forms of $f(\alpha)$ and $g(\alpha)$ representing different reaction mechanism are listed in Table 4.1. These expressions can be used to predict the reaction mechanism, reflected by the dynamic TGA curves. In the present study, the activation energy was obtained from non-isothermal TGA. The methods used to determine the kinetic parameters are isoconversional or model free methods. The kinetic parameters were estimated from numerous plots at different heating rates at same level of conversion.

4.2.4 Model-free isoconversional methods

The thermal decomposition of biomass is very complex process and it is characterized by multiple reactions with different rates. Thus, simple kinetic model cannot be applicable for such reactions. To investigate the in-depth analysis of thermal decomposition of biomass, isoconversional models are frequently used. The isoconversional models used in present work are: (1) Kissinger-Akahira-Sunose (KAS) method, (2) Ozawa-Wall- Flynn (OWF) method, (3) Friedman method, and (4) Starink method.

4.2.4.1. The Kissinger-Akahira-Sunose (KAS) method

KAS method predicted the relationship between heating rate and activation energy through non-isothermal linear integral as per the Eqs. (4.10)

$$\ln\left(\frac{\beta}{T_\alpha{}^2}\right) = \ln\left(\frac{AR}{E_\alpha g(\alpha)}\right) - \frac{E_\alpha}{RT_\alpha} \quad (4.10)$$

where T_α is the temperature at conversion α. The plot between $\ln\left(\frac{\beta}{T_\alpha{}^2}\right)$ and $\frac{1}{T_\alpha}$, at a constant value of conversion gives a straight line, whose slope can be used to calculate activation energy.

4.2.4.2 The Ozawa-Wall- Flynn (OWF) method

OWF method can be derived by integrating Eqs. (4.11), and then Doyle's approximation was implied over temperature integral. The resulting equations are obtained as Eqs. (4.12) and (4.13). At every conversion three points for $\ln\beta$ and $\frac{1}{T_\alpha}$ can be obtained at three heating rates. The plot between these points will give a straight line having slope $(-1.052\frac{E_a}{R})$ which can be used to compute activation energy.

$$\frac{d\alpha}{dT} = \frac{A}{\beta} e^{-E_a/RT} f(\alpha) \quad (4.11)$$

$$\ln\beta = \ln\left(\frac{AE_\alpha}{Rg(\alpha)}\right) - 5.3305 - 1.052\frac{E_\alpha}{RT_\alpha} \quad (4.12)$$

or

$$\ln\beta = \ln\left(\frac{0.0048AE_\alpha}{Rg(\alpha)}\right) - 1.052\frac{E_\alpha}{RT_\alpha} \quad (4.13)$$

4.2.4.3. Friedman method

The Friedman equation can be derived by rearranging Eqs. (4.14) and then taking natural logarithm on both sides, Eqs. (4.15) and (4.16) can be deduced.

$$\frac{d\alpha}{dT} = \frac{A}{\beta} e^{-E_a/RT} f(\alpha) \quad (4.14)$$

$$\beta \frac{d\alpha}{dT} = \text{A } e^{-E_a/RT_\alpha} f(\alpha) \quad (4.15)$$

$$\ln\left(\beta \frac{d\alpha}{dT}\right) = \ln [A\ f\ (\alpha)]\ - \frac{E_\alpha}{RT_\alpha} \quad (4.16)$$

The plot between $\ln\left(\beta \frac{d\alpha}{dT}\right)$ and $\frac{1}{T_\alpha}$ will give a straight line having slope, $(-\frac{E_\alpha}{R})$ which can be used to compute activation energy.

4.2.4.4. Starink method

Starink analyzed the KAS and OWF methods to get the following equation.

$$\ln\left(\frac{\beta}{T_\alpha{}^S}\right) = \text{C} - \frac{BE_\alpha}{RT_\alpha} \quad (4.16)$$

where, S and B take different values. By using temperature integral approximation, Starink obtained the value of S and B as 1.92, and 1.0008 respectively. Then Eqs. (4.16) can be rewritten as:

$$\ln\left(\frac{\beta}{T^{1.92}}\right) = \text{C} - 1.0008\ \frac{E_\alpha}{RT_\alpha} \quad (4.17)$$

At every conversion, three points for $\ln\left(\frac{\beta}{T^S}\right)$ and $\frac{1}{T_\alpha}$ can be obtained at three heating rates. The plot between these points will give a straight line having slope, $(-1.0008\frac{E_\alpha}{R})$ which can be used to compute activation energy.

4.2.5 Prediction of reaction model

The model for solid state reaction during pyrolysis of biomass is investigated by Z-master plot associated with Criado method (Eqs. 4.18) (Criado, 1978). Master plots are the plots which depend on the reaction kinetic model however they are independent of kinetic parameters like activation energy and pre-exponential factor (Dhyani et al., 2017).

$$\frac{Z(\alpha)}{Z(0.5)} = \frac{f(\alpha)\times g(\alpha)}{f(0.5)\times g(0.5)} = \left(\frac{T_\alpha}{T_{0.5}}\right)^2 \times \frac{(d\alpha/dT)_\alpha}{(d\alpha/dT)_{0.5}} \quad (4.18)$$

The above Equation is employed to generate the master plots equivalent to various solid-state reaction mechanism as mentioned in Table 4.1. In this Equation, the term [$f(\alpha) \times g(\alpha)/f(0.5)\times g(0.5)$] will give a theoretical curve, which signifies the characteristics of each reaction mechanism. While, the term [$(T_\alpha/T_{0.5})^2 \times ((d\alpha/dT)_\alpha/(d\alpha/dT)_{0.5})$] will reduce to a curve obtained from experimental values. The conversion value α = 0.5 is selected as a reference value, at which, master plot from all the reaction mechanism and experimental curve will intersect to each other at the value of $[Z(\alpha)/Z(0.5)]$ = 1. The principal reaction mechanism for experimental value is decided by comparing the theoretical and experimental curves. The theoretical curve which is closest to the experimental curve is selected as reaction mechanism (Dhyani et al., 2017; Mishra et al., 2015; Poletto et al., 2012).

Table 4.1 Models of pyrolysis reaction with different values of $f(\alpha)$ and g (α)

Solid state process	**Mechanism**	$f(\alpha)$	$g(\alpha)$
One dimensional diffusion	D1	$1/(2\alpha)$	α^2
Two-dimensional diffusion (Valensi model)	D2	$[-\ln(1-\alpha)]^{-1}$	$(1-\alpha)\ln(1-\alpha)+\alpha$
Three-dimensional diffusion (Jander model model)	D3	$\frac{3}{2}(1-\alpha)^{2/3}\,[1-(1-\alpha)^{1/3}]^{-1}$	$[1-(1-\alpha)^{1/3}]^2$
Three-dimensional diffusion (Ginstlinge-Brounshtein model)	D4	$\frac{3}{2}[(1-\alpha)^{1/3}-1]^{-1}$	$1-\frac{2}{3}\alpha-(1-\alpha)^{2/3}$
Contracting cylinder	F2	$2(1-\alpha)^{1/3}$	$1-(1-\alpha)^{1/2}$
Contracting sphere	F3	$(1-\alpha)^{2/3}$	$1-(1-\alpha)^{1/3}$
Power law	P2/3	$\frac{2}{3}\alpha^{-1/2}$	$\alpha^{3/2}$
Power law	P2	$2\alpha^{1/2}$	$\alpha^{1/2}$
Power law	P3	$3\alpha^{2/3}$	$\alpha^{1/3}$
Power law	P4	$4\alpha^{3/4}$	$\alpha^{1/4}$
Avrami-Erofeev	A1	$\frac{1}{2}(1-\alpha)\,[-\ln(1-\alpha)]^{1/3}$	$[-\ln(1-\alpha)]^{2/3}$
Avrami-Erofeev	A2	$2(1-\alpha)\,[-\ln(1-\alpha)]^{1/2}$	$[-\ln(1-\alpha)]^{1/2}$
Avrami-Erofeev	A3	$3(1-\alpha)\,[-\ln(1-\alpha)]^{2/3}$	$[-\ln(1-\alpha)]^{1/3}$
Avrami-Erofeev	A4	$4(1-\alpha)\,[-\ln(1-\alpha)]^{3/4}$	$[-\ln(1-\alpha)]^{1/4}$
1st order random nucleation having one nucleus on individual particle	R1	$(1-\alpha)$	$-\ln(1-\alpha)$
2nd order random nucleation having two nucleus on individual particle	R2	$(1-\alpha)^2$	$(1-\alpha)^{-1}-1$
3rd order random nucleation having three nucleus on individual particle	R3	$(1-\alpha)^3$	$\frac{1}{2}[(1-\alpha)^{-2}-1]$

4.2.6 Estimation of pre-exponential factor and thermodynamic parameter

Using isoconversional methods discussed earlier in section 2.5, activation energy was calculated at different level of conversion; however, the pre-exponential factor and reaction mechanism given by isoconversional method is not reliable (Dhyani et al., 2017). For pre-exponential factor Kissinger's method was used given by Eqs. (4.19). Kissinger's method is employed at different heating rate; however it gives only a single value of activation energy for overall conversion process. Thus it was not used to calculate activation energy in this study. Once, the activation energy is known at different value of conversion, Eqs. (4.20) can be used to calculate pre-exponential factor. In this study, activation energy obtained from KAS method was used to calculate pre-exponential factor.

$$\ln\left(\frac{\beta}{{T_p}^2}\right) = \ln\left(\frac{AR}{E}\right) - \frac{E}{RT_p} \tag{4.19}$$

$$A=\beta . E_\alpha .\text{Exp}\left(\frac{E_\alpha}{RT_p}\right)/(R.{T_p}^2) \tag{4.20}$$

Once the activation energy and pre-exponential factor was known at different level of conversion, the thermodynamic parameters such as change in enthalpy (ΔH), change in Gibbs free energy (ΔG), and change in entropy (ΔS) were calculated using the equation (4.21)-(4.23).

$$\Delta H = E_\alpha - RT_\alpha \tag{4.21}$$

$$\Delta G = E_\alpha + R.\, T_p .\ln\left(\frac{K_B.T_m}{h.A}\right) \tag{4.22}$$

$$\Delta S = \frac{\Delta H - \Delta G}{T_p} \tag{4.23}$$

where, K_B is the Boltzmann constant (1.381*10 $^{-23}$ J/K), h is the Plank constant (6.626 *10 $^{-23}$ J.s), and T_p, is the peak temperature in the DTG curve.

4.3 Results and discussion

4.3.1. Yield of product and physicochemical characteristics of DAN and torrefied biomass

Table 4.2 represents the yield of solid product at 220, 250, and 280 ℃ with a constant retention time of 40 min and a heating rate of 15 ℃/min. The detailed discussion about product yield and physicochemical characteristics of DAN and TAN has been discussed in Chapter 3. Table 4.2 represents the fiber analysis of DAN and TAN. The hemicellulose, cellulose, lignin, and extractives present in DAN are 28.51, 41.66, 23.90, and 5.95%, respectively. The hemicellulose and extractives content decreased while the lignin content increased with increasing temperature during torrefaction. On the other hand, the cellulose content increased at lower temperature (TAN-220) and then goes on decreasing on further increase in temperature. Hemicellulose, cellulose, and extractives decreased by 69.34, 21.84, and 53.61%, respectively. Though, lignin content increased by 57.27%. Hence, it was noted that, in the course of torrefaction, the decomposition of hemicellulose is more pronounced than the decomposition of cellulose and lignin.

Table 4.2 Fiber analysis of DAN and torrefied biomass and solid yield during torrefaction

Analysis	**DAN**	**TAN-220**	**TAN-250**	**TAN-280**
Fiber analysis(wt %, dry basis)				
Hemicellulose	28.64±0.95	25.49±0.77	17.38±0.56	10.52±1.52
Cellulose	41.66±0.90	44.51±1.89	38.38±1.04	33.61±0.82
Lignin	24.20±0.43	27.71±1.49	41.25±1.24	54.24±1.41
Extractive*	5.50±0.48	2.29±0.23	2.99±0.24	1.63±0.26
Solid yield (wt%)	-	71.28	57.09	42.71

* calculated by difference

4.3.2 Thermogravimetric analysis

The pyrolysis behavior of DAN, TAN-220, TAN-250, and TAN-280 at a heating rate of 5, 10, and 15 K/min is shown in Figs 4.1 (a-d) and Figs 4.2 (a-d). The whole degradation process can be categorized into three major stages: (1) drying, (2) devolatilization, and (3) char formation. The first stage is accompanied with the elimination of surface moisture and some light volatile compounds (Saikia et al., 2018), and it was noticed that mass loss owing to moisture for torrefied biomass (TAN-220, TAN-250, and TAN-280) is slightly lesser than the DAN. The second stage is associated with the devolatilization process which was accompanied by major mass loss from biomass due to degradation of the major portion of hemicellulose and cellulose. At, the third stage, lignin decomposition is more pronounced. The TGA curve in this zone has a flat and long tail. Accordingly, the mass loss in this stage is lower than the second stage. Considering a fixed amount of mass loss for example 10%, for DAN and torrefied biomass (TAN-220, TAN-250, and TAN-280), at a heating rate of 5 K/min, it was attained at 520, 572, 586, and 610 K, respectively. It shows that

decomposition shifted to a higher temperature in case of TAN and extent of the shift in temperature increases with increase in temperature during torrefaction. The decomposition of hemicellulose and cellulose takes place between 200-350 ℃, whereas; lignin decomposes in a wider range of temperature between 280-600 ℃ (Ren et al., 2013a; Yang et al., 2007). It was noticed from Table 4.2 that major fraction of hemicellulose degraded along with limited degradation of cellulose during torrefaction. This may be the reason for shifting of onset devolatilization temperature in case of TAN. Additionally, inconsistency in thermal degradation of biomass component is also responsible for deviation in residual char yield. The residual char yield after pyrolysis of DAN and torrefied biomass (TAN-220, TAN-250, and TAN-280) at a heating rate of 5 K/min, was observed to be 17.09, 27.76, 49.30, and 66.72%, respectively. In addition, slight variation in residual char yield was also observed due to the variation of heating rate. The higher residual char yield in case of TAN may be due to large mass loss through decomposition of hemicellulose and lignin and also due to the cross-linkage reaction during the pyrolysis of TAN (Park et al., 2013; Ren et al., 2013a; Wannapeera et al., 2011a). Thus, it may be mentioned that higher the torrefaction temperature, higher will be the char yield during pyrolysis.

Figs. 4.2 (a-d) present the DTG curve of DAN and torrefied biomass (TAN-220, TAN-250, and TAN-280). In DTG curve, the presence of shoulder on the left side of the plot describes the degradation of hemicellulose in the biomass and is typically noted at around 573 K (Müller-Hagedorn et al., 2003; Yang et al., 2007). In case of DAN, similar shoulders appear at 548, 563, and 573 K at a heating rate of 5, 10, and 15 K/min, respectively, as shown in Fig. 4.2 (a). On the other hand, the similar shoulder disappeared in case of torrefied biomass (TAN-220, TAN-250, and TAN-280) (Figs.4.2 (b-d)), suggesting that

major fraction of hemicellulose has already being degraded in the course of torrefaction. Yang et al. (Yang et al., 2007) reported that peaks appeared in the DTG curve with maximum weight loss signifies the occurrence of cellulose in the biomass. The temperature noted at the peaks in DTG curve for DAN was 623, 639, and 642 K at a heating rate of 5, 10, and 15 K/min, respectively, as shown in Fig.4.2 (a). For torrefied biomass (TAN-220) the cellulose peak temperature was noted at 622, 634, and 639 K, at a heating rate of 5, 10, and 15 K/min, respectively (Fig. 4.2 (b)). However, in case of torrefied biomass (TAN-250), peak temperature was noted at 611, 623, and 623 K, at a heating rate of 5, 10, and 15 K/min, respectively. In addition, another peak to the right side of the cellulose peak can be observed at 677, 688, and 695 K, at a heating rate of 5, 10, and 15 K/min, respectively (Fig.4.2 (c)). The appearance of second peak may be attributed to the degradation of lignin. Conversely, in case of torrefied biomass (TAN-280), in place of hemicellulose and cellulose peak, a broader peak at 769, 783, and 798 K, at a heating rate of 5, 10, and 15 K/min, respectively, were observed (Fig.4.2 (d)). These broader peaks are associated with the degradation of lignin. Similar results were also observed by Tong et al. (Tong et al., 2018) Furthermore, comparing the peak intensity of DAN and torrefied biomass (TAN-220, TAN-250, and TAN-280) at particular heating rate say 5 K/min, it was found to be 5.12, 6.11, 1.49 and 0.41 wt%/min, respectively. The increase in peak intensity of TAN-220 (Fig.4.2 (b)) than the DAN may be due to higher amount of relative cellulose content in TAN-220 than the DAN as presented in Table 4.2. On further increase in temperature, there was decrease in peak intensity.

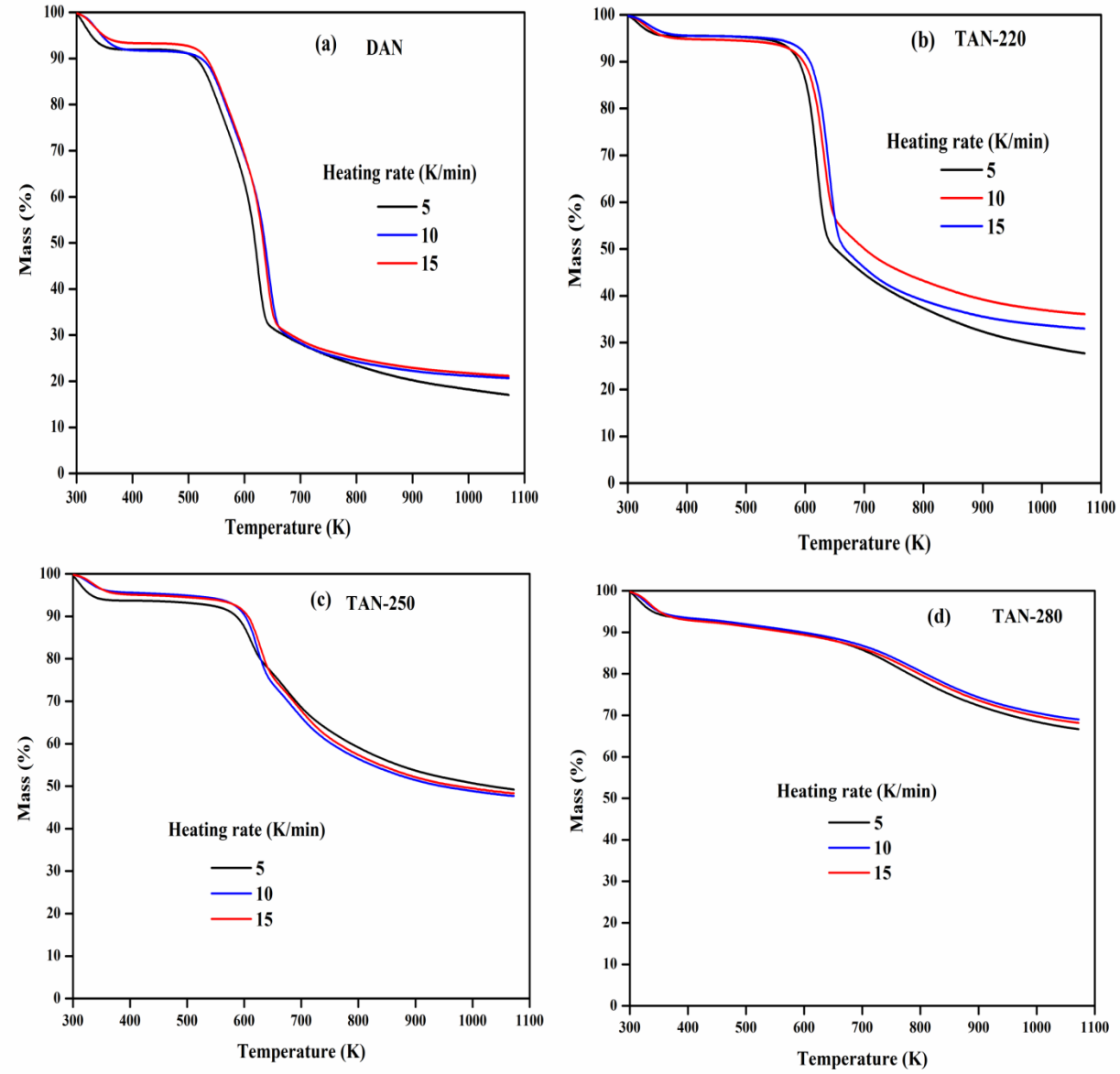

Figure 4.1 TGA analysis of DAN and torrefied biomass at different heating rate: (a) DAN (b) TAN-220 (c) TAN-250, and (d) TAN-280.

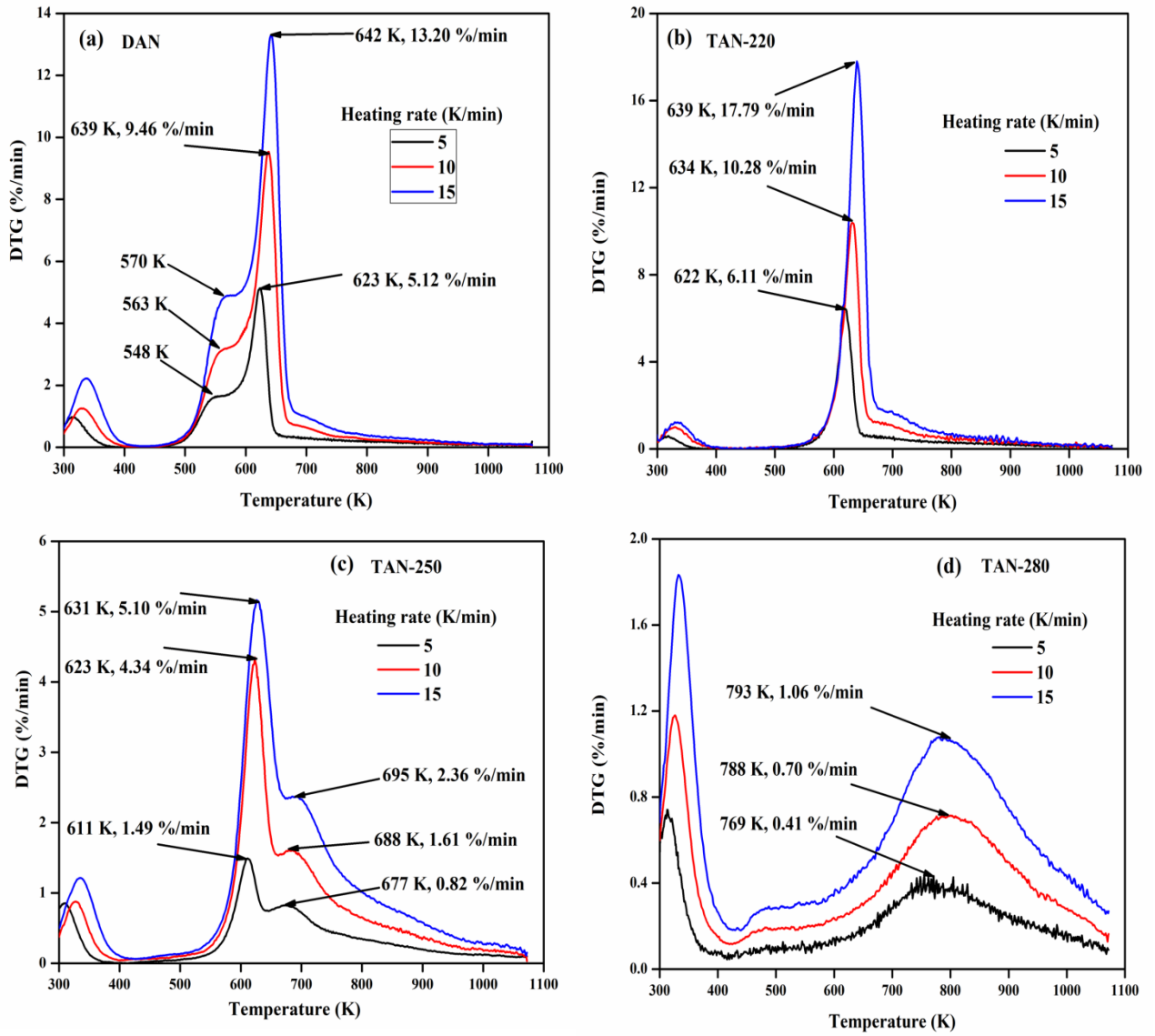

Figure 4.2 DTG analysis of DAN and torrefied biomass at different heating rate: (a) DAN (b) TAN-220 (c) TAN-250, and (d) TAN-280.

4.3.3 Kinetic analysis

The estimation of the kinetic parameters is very useful for efficient design and scaling of process reactors at industrial level (Kaur et al., 2018). The decomposition kinetic analysis of DAN and torrefied biomass (TAN-220, TAN-250, and TAN-280) was performed by applying four isoconversional methods such as KAS, OWF, Friedman and Starink at different degree of conversion ranging from 0.1 to 0.9. The isoconversional plots obtained from four methods for DAN and torrefied biomass (TAN-220, TAN-250, and TAN-280) are shown in Figs. 4.3, 4.4, 4.5 and 4.6. It can be seen that, with an increase in conversion, the slope of isoconversional lines are also changing. The slopes of these lines are used to obtain the activation energy. Thus, the value of activation energy also changes accordingly as presented in Table 4.3. The variation of activation energy with the degree of conversion is shown in Fig. 4.7. The activation energy obtained from KAS, Friedman, and Starink methods for DAN and torrefied biomass (TAN-220, TAN-250, and TAN-280) are comparable. However, slightly higher activation energy was noticed in case of OWF method as depicted by Table 4.3. The difference in activation energy from different method may be due to the assumptions and approximation adopted by different methods (Kaur et al., 2018). For example, in case of OWF method, for integral term $\int_0^T \exp\left(\frac{-E}{RT}\right) dT$, the analytical solution is not possible. Thus, Doyle's approximation was used, though Friedman method does not adopt any such approximation (Doyle, 1962; Yuan et al., 2017). The value of activation energy changes with conversion during the pyrolysis, illustrating the multi-stage kinetics rather than single stage and complexity of process during biomass conversion through pyrolysis. Therefore, the overall decomposition of biomass is

established by a multi-stage reaction mechanism where every single stage added partially to global mechanism depending upon the extent of decomposition.

The activation energy is the minimum amount of energy required to proceed a reaction. Thus, higher activation energy hinders the start of a reaction. Activation energy is also useful in deciding the reactivity of fuel (Kaur et al., 2018). The activation energy of DAN and torrefied biomass (TAN-220, TAN-250, and TAN-280) was calculated using KAS, OWF, Friedman and Starink methods as discussed in section 2.5. For DAN, the calculated value of activation energy from these methods varied within 211.49-221.58 kJ/mol. The activation energy for decomposition of torrefied biomass (TAN-220, TAN-250, and TAN-280) varied within 241.58-261.83, 185.06-198.89, and 121.83-132.98 kJ/mol, respectively. The activation energy of component of biomass (hemicellulose, cellulose and, and lignin) are different. Vamvuka et al. (Vamvuka et al., 2003) reported the activation energy of cellulose, hemicellulose, and lignin in the range of 145-285, 90-125 and 30-39 kJ/mol individually. The highest activation energy was reported for cellulose, followed by hemicellulose and then lignin. Thus the biomass having higher amount of cellulose will have higher activation energy. The relative amount of cellulose in TAN-220 is higher than the DAN as presented in Table 4.2. Accordingly, higher activation energy in case of TAN-220 than the DAN was noticed. On further increasing the temperature during torrefaction, the degradation of cellulose also becomes significant. Thus activation energy of TAN-250 and TAN-280 are lower than DAN. The lower activation energy of TAN-280 makes it suitable for thermochemical conversion. In addition, it can be used in co-firing with other biomass or coal etc.

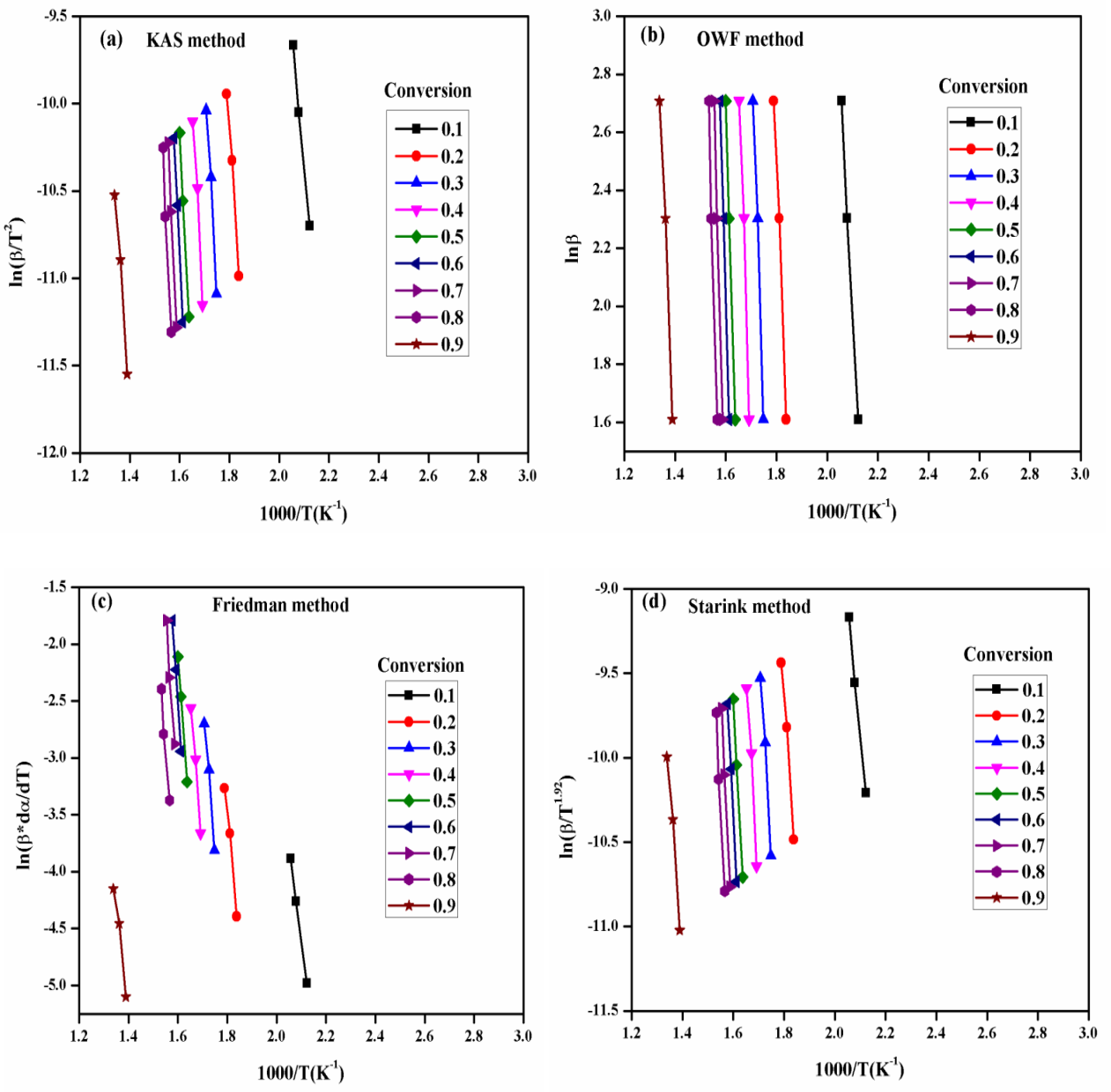

Figure 4.3 Kinetic plots for DAN using (a) KAS, (b) OWF, (c) Friedman, and (d) Starink models.

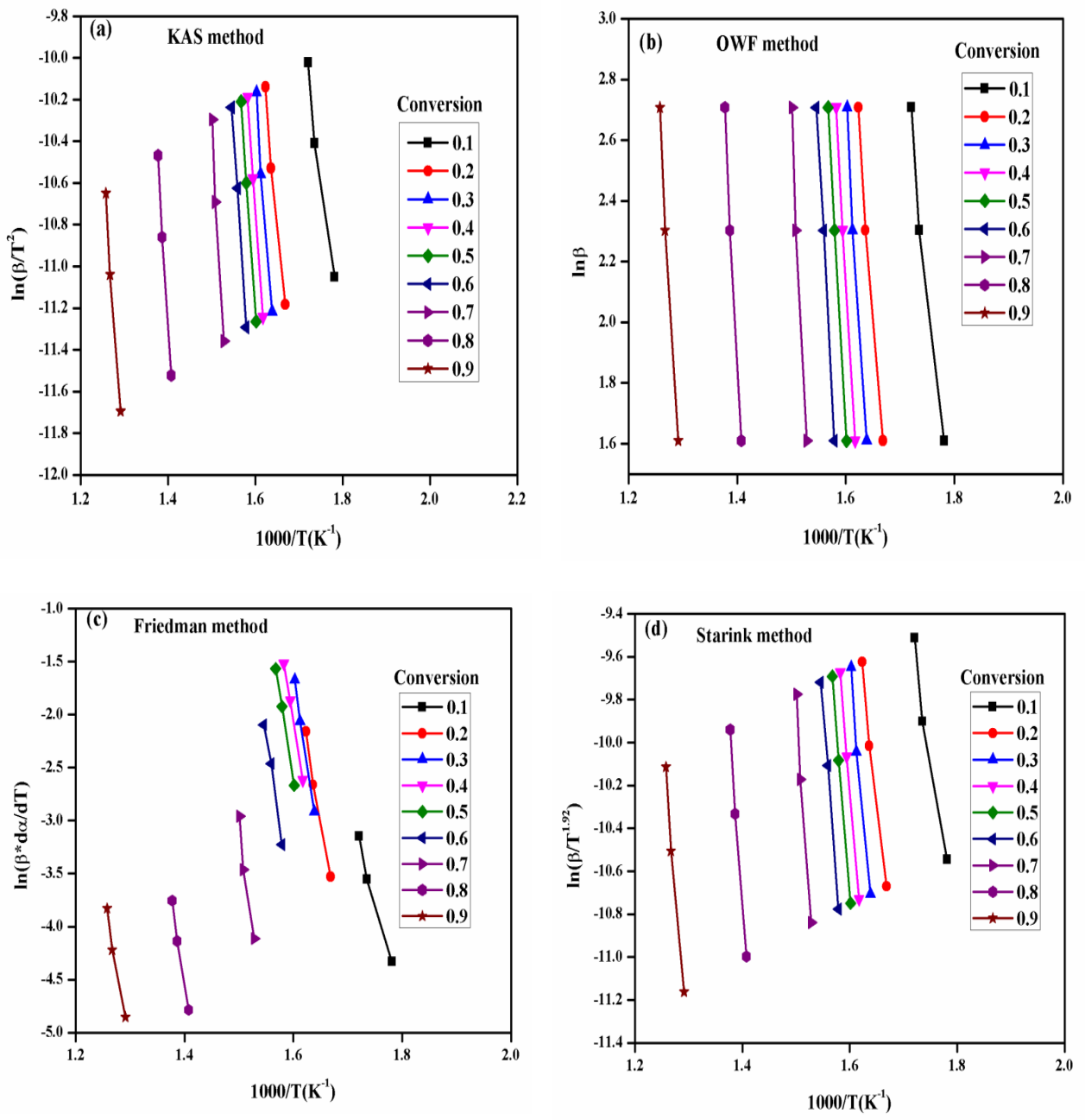

Figure 4.4 Kinetic plots for TAN-220 using (a) KAS, (b) OWF, (c) Friedman, and (d) Starink models.

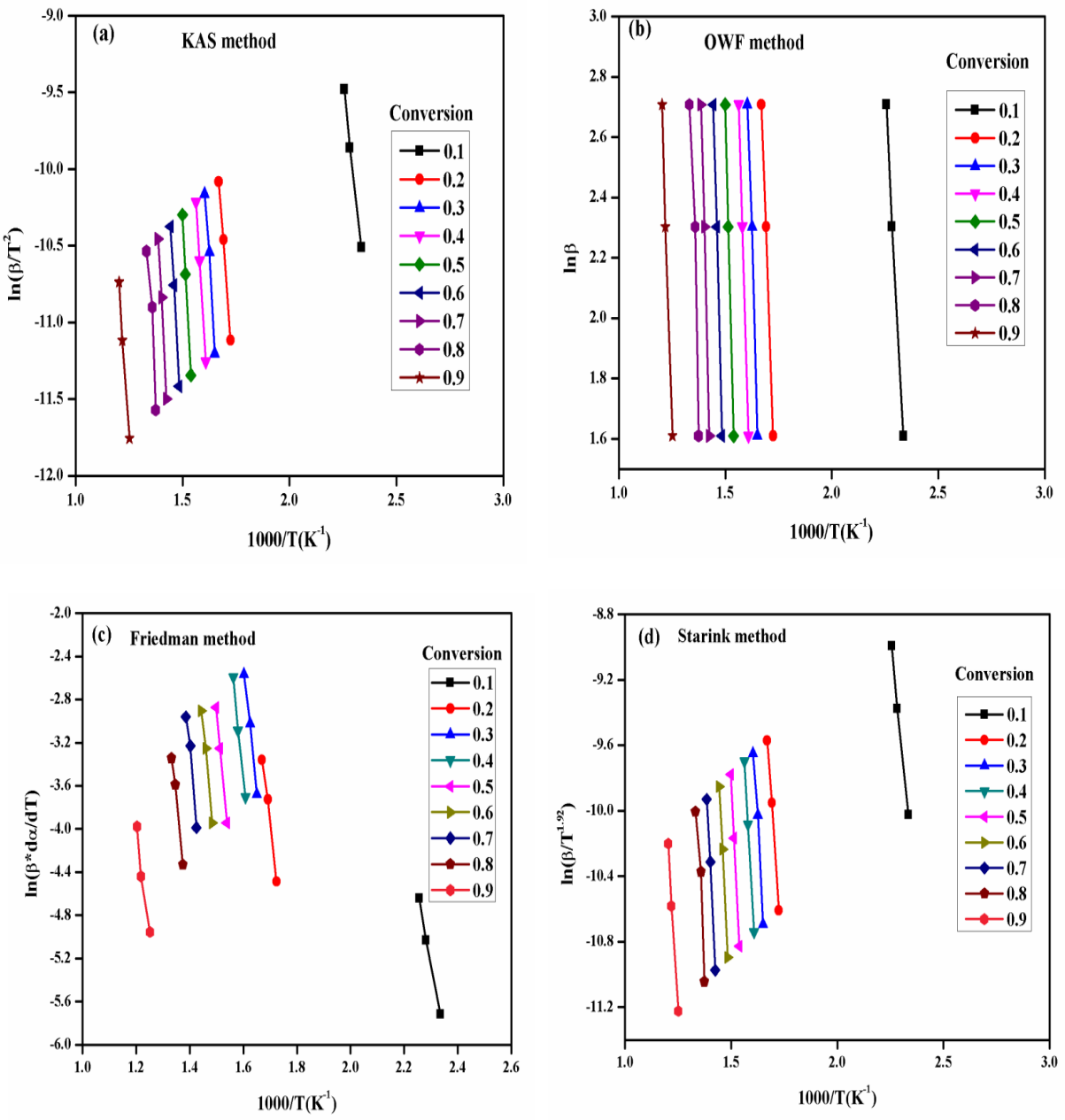

Figure 4.5 Kinetic plots for TAN-250 using (a) KAS, (b) OWF, (c) Friedman, and (d) Starink models.

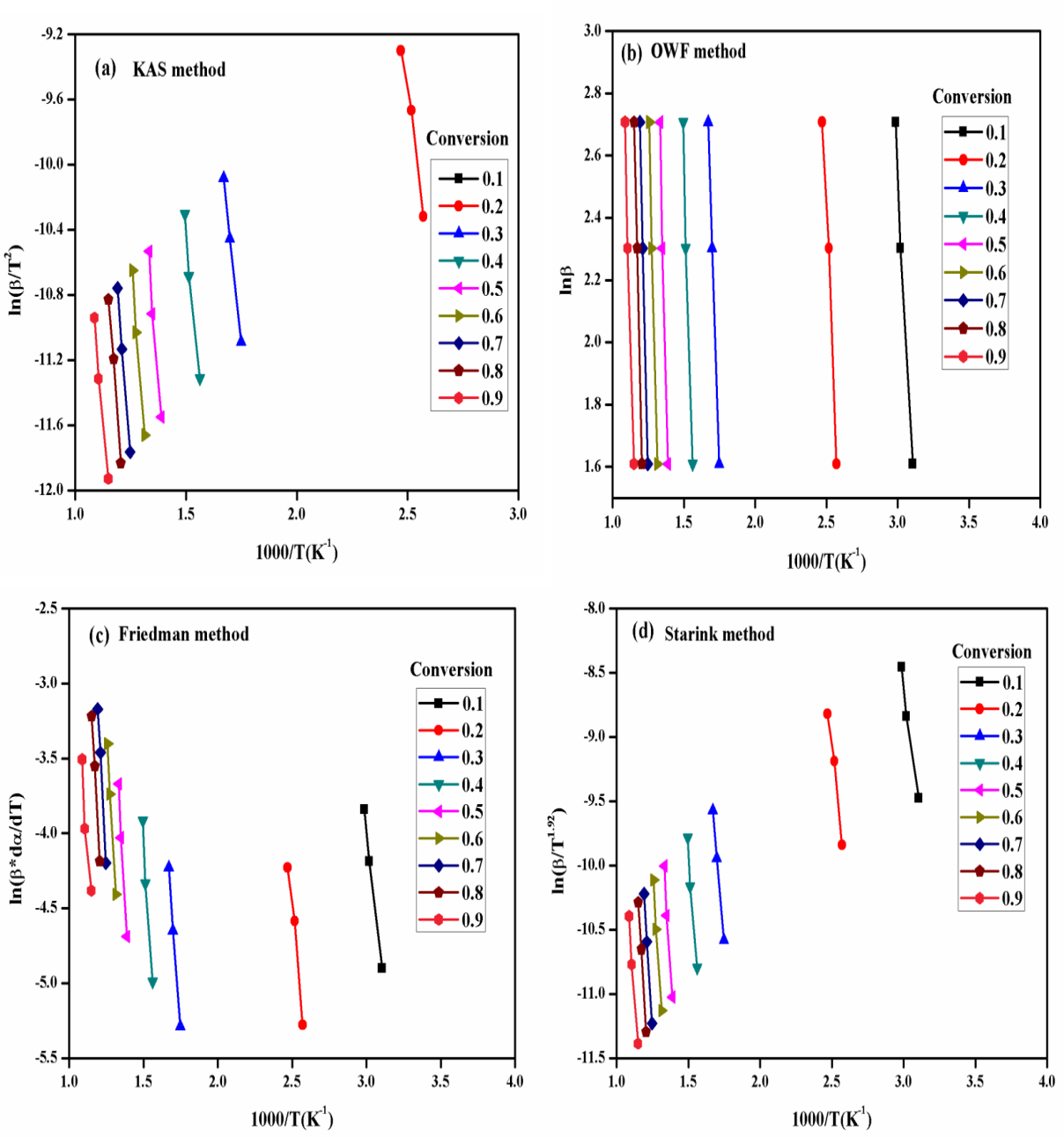

Figure 4.6 Kinetic plots for TAN-280 using (a) KAS, (b) OWF, (c) Friedman, and (d) Starink models.

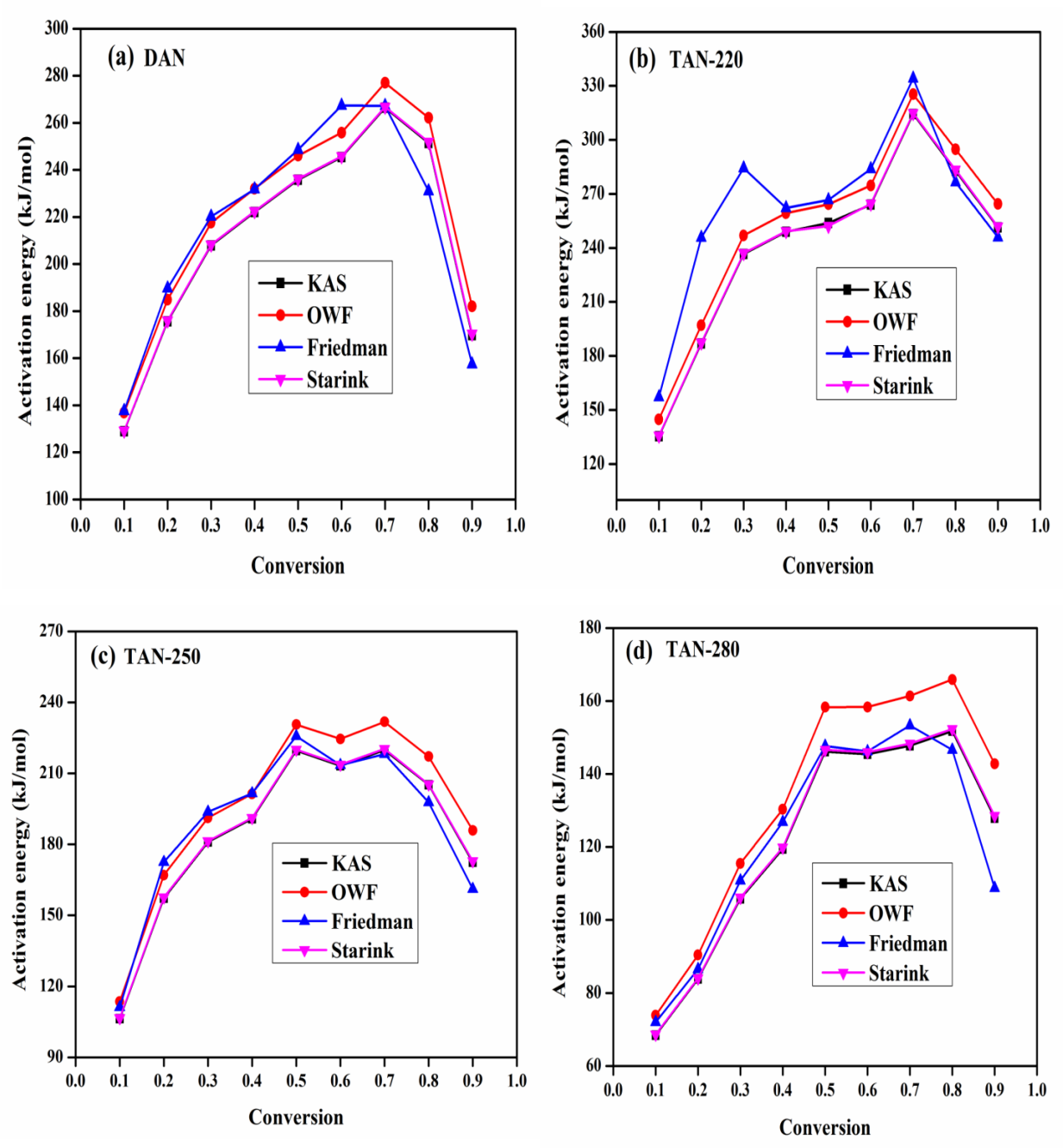

Figure 4.7 Variation of activation energy with conversion using different models: (a) DAN, (b) TAN-220 (c) TAN-250, and (d) TAN-280.

Table 4.3 The activation energy of DAN and torrefied biomass at different level of conversion using KAS, OWF, Friedman and Starink methods

Conversion	KAS method		OWF method		Friedman method		Starink method	
	E (kJ/mol)	R^2	E (kJ/mol)	R^2	E (kJ/mol)	R^2	E (kJ/mol)	R^2
DAN								
0.1	128.89	0.9966	136.84	0.9970	137.67	0.9993	129.21	0.9966
0.2	175.68	0.9900	184.84	0.9910	189.74	0.9873	176.04	0.9901
0.3	207.89	0.9806	217.52	0.9823	220.22	0.9810	208.29	0.9807
0.4	222.09	0.9804	232.03	0.9832	231.85	0.9926	222.49	0.9809
0.5	235.78	0.9992	246.05	0.9992	248.57	0.9992	236.20	0.9992
0.6	245.41	0.9970	255.83	0.9972	267.41	0.9981	245.82	0.9970
0.7	266.40	0.9929	276.98	0.9934	267.21	0.9656	266.82	0.9929
0.8	251.46	0.9882	262.18	0.9891	230.97	0.9792	251.88	0.9882
0.9	169.81	0.9853	182.01	0.9873	157.45	0.9729	170.30	09854
Average	**211.49**		**221.58**		**216.78**		**211.89**	
TAN-220								
0.1	135.29	0.9760	144.77	0.9789	157.20	0.9865	135.66	0.9761
0.2	186.95	0.9893	197.05	0.9904	245.77	0.9910	187.35	0.9894
0.3	236.64	0.9873	246.90	0.9883	284.35	0.9979	237.04	0.9874
0.4	248.88	0.9991	259.28	0.9920	262.14	0.9990	249.30	0.9991
0.5	253.79	0.9991	264.27	0.9992	266.64	0.9996	252.20	0.9991
0.6	264.06	0.9969	274.70	0.9971	283.84	0.9892	264.48	0.9969
0.7	314.44	0.9768	325.41	0.9783	334.18	0.9497	314.88	0.9769
0.8	282.87	0.9935	294.80	0.9940	276.53	0.9941	283.34	0.9936
0.9	251.34	0.9878	264.37	0.9889	245.85	0.9856	251.85	0.9878
Average	**241.58**		**252.39**		**261.83**		**241.78**	
TAN-250								
0.1	106.37	0.9973	113.61	0.9976	111.15	0.9985	106.66	0.9973

0.2	157.23	0.9975	167.03	0.9976	172.55	0.9904	157.62	0.9973
0.3	180.94	0.9783	191.17	0.9806	193.80	0.9918	181.35	0.9998
0.4	190.84	0.9998	201.33	0.9998	201.57	0.9949	191.26	0.9998
0.5	219.65	0.9930	230.60	0.9993	225.79	0.9999	220.09	0.9993
0.6	213.20	0.9972	224.56	0.9975	213.46	0.9919	213.66	0.9972
0.7	219.84	0.9923	231.76	0.9931	218.15	0.9596	220.32	0.9924
0.8	205.14	0.9915	217.12	0.9869	197.77	0.9899	205.32	0.9853
0.9	172.38	0.9939	185.91	0.9947	161.16	0.9636	172.92	0.9940
Average	**185.06**		**198.89**		**188.37**		**185.46**	
TAN-280								
0.1	68.42	0.9874	73.87	0.9891	72.00	0.9968	68.64	0.9874
0.2	83.81	0.9846	90.41	0.9868	86.54	0.9784	84.07	0.9847
0.3	105.77	0.9993	115.49	0.9994	110.80	0.9966	106.16	0.9993
0.4	119.48	0.9818	130.33	0.9846	126.83	0.9779	119.91	0.9819
0.5	146.14	0.9797	158.34	0.9824	147.71	0.9869	146.62	0.9796
0.6	145.44	0.9875	158.35	0.9893	146.17	0.9958	145.96	0.9876
0.7	147.74	0.9994	161.38	0.9995	153.28	0.9947	148.29	0.9994
0.8	151.78	0.9941	165.89	0.9951	146.64	0.9904	152.34	0.9942
0.9	127.93	0.9886	142.78	0.9907	108.73	0.9243	128.52	0.9887
Average	**121.83**		**132.98**		**122.07**		**122.27**	

4.3.4 Prediction of reaction mechanism (Criado analysis)

Criado analysis was employed to investigate the reaction mechanism during pyrolysis of DAN and torrefied biomass (TAN-220, TAN-250, and TAN-280) at a different level of conversion at a heating rate of 10 K/min. The standard kinetic models selected are

mentioned in Table 4.1. The master plots for DAN and torrefied biomass is shown in Fig. 4.8 (a-d) at conversion from 0.1 to 0.9.

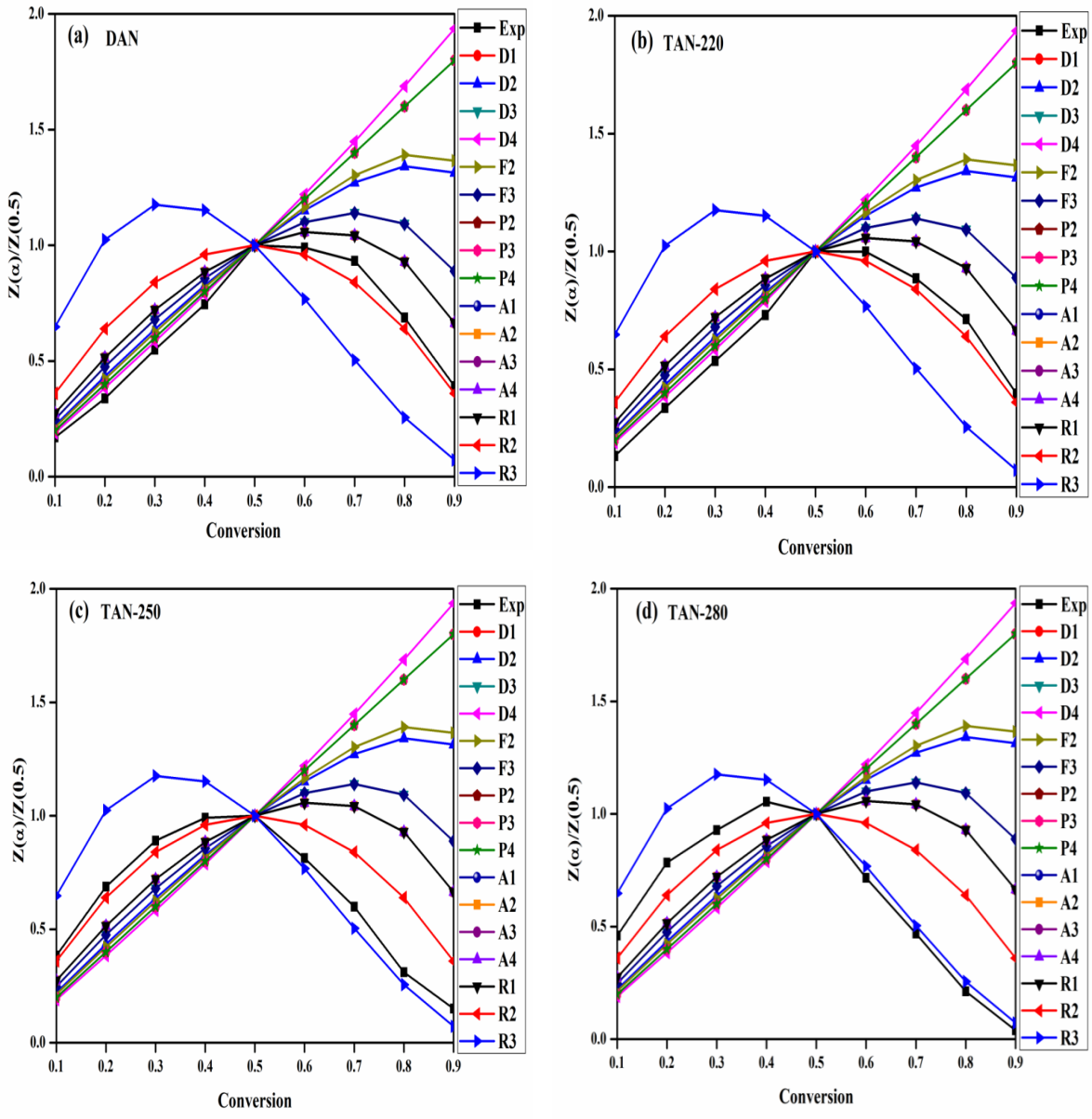

Figure 4.8 Theoretical and experimental plots for prediction of solid state reaction mechanism using Criado method (Z-master plot): (a) DAN, (b) TAN-220 (c) TAN-250, and (d) TAN-280.

4.3.4.1 Reaction mechanism at lower conversion ($\alpha < 0.5$)

Table 4.4 represents the decomposition mechanism followed by DAN and torrefied biomass (TAN-220, TAN-250, and TAN-280). For DAN and torrefied biomass (TAN-220) at conversion less than 0.5, the closest match with the theoretical curve is associated with D1, D2, D3 and D4 mechanism which corresponds to one dimensional diffusion model, two-dimensional diffusion (Valensi model), three-dimensional diffusion (Jander model) and three-dimensional diffusion (Ginstlinge-Brounshtein model), respectively. Whereas, torrefied biomass (TAN-250) follows the R2 model which corresponds to 2^{nd} order random nucleation having two nucleus on individual particle (R2) and torrefied biomass (TAN-280), followed the R2 and R3 model, which corresponds to 2^{nd} order random nucleation having two nucleus on individual particle and 3^{rd} order random nucleation having three nucleus on individual particle (R3), respectively, for the conversion less than 0.5. In case of DAN and torrefied biomass (TAN-220), the dominance of diffusion model may be due to higher volatile content. However, in case of torrefied biomass (TAN-250 and TAN-280), the volatile matter is already released in the course of torrefaction. Accordingly, random nucleation models become prominent. These results are in good agreement with the published results obtained by Doddapaneni et al. (Doddapaneni et al., 2016), Mishra et al. (Mishra et al., 2015), Poletto et al. (Poletto et al., 2012), and Vlaev et al. (Vlaev et al., 2003). Diffusion models are associated with the diffusion of gaseous products from the reactant samples. As the conversion increases, the thickness of the product layer around the sample increases. This layer around the sample can hinder the transfer of heat from the external source. Accordingly, the decomposition of the sample will be affected. Therefore, diffusion becomes the rate-determining step during the pyrolysis process at low conversion.

4.3.4.2 Reaction mechanism at higher conversion ($\alpha > 0.5$)

For higher degree of conversion (from 0.5 to 0.9), the reaction mechanism was followed by DAN and TAN are presented in Table 4.4. For DAN at conversion greater than 0.5, the closest match with the theoretical curve is associated with R2, which corresponds to 2nd order random nucleation having two nuclei on individual particle and Avrami-Erofeev models (A1, A2, A3, and A4) which is associated with nucleation and growth. Whereas, torrefied biomass (TAN-220) follows the R2 model which corresponds to 2nd order random nucleation having two nuclei on individual particle (R2) and torrefied biomass (TAN-250 and TAN-280) both followed R3 model, which corresponds to 3rd order random nucleation having three nuclei on individual particle (R3). During the decomposition process, higher conversion was achieved at relatively higher temperature. At higher temperature, cleavage of some ordered cellulose may take place which gets converted into chain of lower molecular mass. This chain of lower molecular mass might act as a site for random nucleation growth and degradation reaction.

Table 4.4 Predicted models for DAN and torrefied biomass (TAN-220, TAN-250, and TAN-280)

Biomass	**Solid state process**	
	Conversion < 0.5	**Conversion > 0.5**
DAN	Diffusion models (D1, D2, D3 and D4) D1 $f(\alpha) = 2(1-\alpha)\,[-\ln(1-\alpha)]^{1/2}$ $g(\alpha) = [-\ln(1-\alpha)]^{1/2}$ D2 $f(\alpha) = [-\ln(1-\alpha)]^{-1}$ $g(\alpha) = (1-\alpha)\ln(1-\alpha) + \alpha$ D3 $f(\alpha) = \frac{3}{2}(1-\alpha)^{2/3}\,[1-(1-\alpha)^{1/3}]^{-1}$ $g(\alpha) = [1-(1-\alpha)^{1/3}]^2$ D4 $f(\alpha) = \frac{3}{2}[(1-\alpha)^{1/3}-1]^{-1}$	2nd order random nucleation having two nucleus on individual particle (R2) R2 $f(\alpha) = (1-\alpha)^2$ $g(\alpha) = (1-\alpha)^{-1} - 1$ Avrami-Erofeev models (A1, A2, A3 and A4) A1 $f(\alpha) = \frac{1}{2}(1-\alpha)\,[-\ln(1-\alpha)]^{1/3}$ $g(\alpha) = [-\ln(1-\alpha)]^{2/3}$ A2 $f(\alpha) = 2(1-\alpha)\,[-\ln(1-\alpha)]^{1/2}$ $g(\alpha) = [-\ln(1-\alpha)]^{1/2}$

	$g(\alpha) = 1-\frac{2}{3}\alpha - (1-\alpha)^{2/3}$	A3 $f(\alpha) = 3(1-\alpha)\,[-\ln(1-\alpha)]^{2/3}$ $g(\alpha) = [-\ln(1-\alpha)]^{1/3}$ A4 $f(\alpha) = 4(1-\alpha)\,[-\ln(1-\alpha)]^{3/4}$ $g(\alpha) = [-\ln(1-\alpha)]^{1/4}$
TAN-220	Diffusion models (D1, D2, D3 and D4) D1 $f(\alpha) = 2(1-\alpha)\,[-\ln(1-\alpha)]^{1/2}$ $g(\alpha) = [-\ln(1-\alpha)]^{1/2}$ D2 $f(\alpha) = [-\ln(1-\alpha)]^{-1}$ $g(\alpha) = (1-\alpha)\ln(1-\alpha) + \alpha$ D3 $f(\alpha) = \frac{3}{2}(1-\alpha)^{2/3}\,[1-(1-\alpha)^{1/3}]^{-1}$ $g(\alpha) = [1-(1-\alpha)^{1/3}]^2$ D4 $f(\alpha) = \frac{3}{2}[(1-\alpha)^{1/3}-1]^{-1}$ $g(\alpha) = 1-\frac{2}{3}\alpha - (1-\alpha)^{2/3}$	2nd order random nucleation having two nucleus on individual particle (R2) R2 $f(\alpha) = (1-\alpha)^2$ $g(\alpha) = (1-\alpha)^{-1} - 1$
TAN-250	2nd order random nucleation having two nucleus on individual particle (R2) $f(\alpha) = (1-\alpha)^2$ $g(\alpha) = (1-\alpha)^{-1} - 1$	3rd order random nucleation having three nucleus on individual particle (R3) $f(\alpha) = (1-\alpha)^3$ $g(\alpha) = \frac{1}{2}[(1-\alpha)^{-2} - 1]$
TAN-280	2nd order random nucleation having two nucleus on individual particle (R2) R2 $f(\alpha) = (1-\alpha)^2$ $g(\alpha) = (1-\alpha)^{-1} - 1$ 3rd order random nucleation having three nucleus on individual particle (R3) R3 $f(\alpha) = (1-\alpha)^3$ $g(\alpha) = \frac{1}{2}[(1-\alpha)^{-2} - 1]$	3rd order random nucleation having three nucleus on individual particle (R3) $f(\alpha) = (1-\alpha)^3$ $g(\alpha) = \frac{1}{2}[(1-\alpha)^{-2} - 1]$

4.3.5 Thermodynamic parameters

The thermodynamic parameters were calculated by using Eqs. (4.20-4.23) based on apparent activation energy obtained from the KAS method at a heating rate of 10 K/min and corresponding values are presented in Table 4.5. Furthermore, the low value of heating rate was selected to avoid the effect of interaction between the constituents, which shows the pronounced effect at a higher heating rate (Yuan et al., 2017). The values of pre-

exponential factor for DAN and torrefied biomass (TAN-220, TAN-250, and TAN-280) at different conversion, obtained using KAS method at a heating rate of 10 K/min ranges from 10^{10} to 10^{18}, 10^{10} to 10^{25}, 10^{8} to 10^{18} and 10^{3} to 10^{9}, respectively. Pre-exponential factor depicts the nature of the complex associated with the reaction. The low value of pre-exponential factor signifies the closed complex whereas high value signifies the simple complex (Kaur et al., 2018; Yuan et al., 2017). Turmanova et al. (Turmanova et al., 2008) investigated that the value of empirical pre-exponential factor for first-order reaction generally varies from 10^{4} to 10^{18} s^{-1}. The variation in pre-exponential factor may be due to the complex nature of biomass and also due to complex thermal degradation of biomass. It was also noted that the value of pre-exponential factor is in line with the value of activation energy. At particular conversion, higher pre-exponential factor was noted at higher value of activation energy.

The Enthalpy is a thermodynamic property which signifies the total heat content of a system. In case of biomass pyrolysis, it represents the total amount of heat taken by the biomass for its conversion into different products like bio-char, bio-oil, and gases (Daugaard & Brown, 2003). The change in enthalpy with different level of conversion calculated from KAS method at 10 K/min is given in Table 4.5. The enthalpy for DAN and torrefied biomass (TAN-220, TAN-250, and TAN-280) varies from 124.97-261.18, 130.60-309.04, 102.72-214.14, and 65.66-144.69 kJ/mol, respectively. It was noticed that at each level of conversion, the difference of energy between the activation energy and enthalpy for DAN and torrefied biomass (TAN-220, TAN-250, and TAN-280) was ~2-6, ~5-6, ~4-7, and ~3-7 kJ/mol. This difference is attributed to the difference between activated complex formed during the decomposition and initial, DAN and TAN. Mehmood

et al. (Mehmood et al., 2017) illustrated that difference of activation energy and enthalpy suggested that product formation can be achieved by providing 2-6, 5-6, 4-7, and 3-7 kJ/mol of energy in case of DAN and TAN, respectively. Vlaev et al. and Loy et al. (Loy et al., 2018; Vlaev et al., 2007) illustrated that lower difference between the activation energy and enthalpy favors the formation of an activated complex which finally leads to bioenergy production through pyrolysis.

Gibbs free energy (ΔG) indicates the total increase in energy of a system for the formation of the activated complex (Kaur et al., 2018; Turmanova et al., 2008). The change in ΔG at each conversion value calculated using KAS method at 10 K/min is given in Table 4.5. The ΔG for DAN and torrefied biomass (TAN-220, TAN-250, and TAN-280) varies from 164.33-199.59, 162.78-163.47, 158.71-162.48, and 211.20-216.51 kJ/mol, respectively. It can confer that, DAN, the variation in ΔG is higher; however, for TAN the value of ΔG, remains almost constant for all value of conversion from 0.1 to 0.9. A positive value of ΔG for DAN and torrefied biomass (TAN-220, TAN-250, and TAN-280) reveals the unfavorable reactions that consume a considerable amount of energy to occur (Mallick et al., 2018). Similar results of ΔG for different biomass have been reported by Xu et al. (Xu & Chen, 2013) for rice straw, Ahmad et al. (Ahmad et al., 2017) for para grass, and Huang et al. (Huang et al., 2018) for sewage sludge.

The entropy, being a state function, represents the degree of disorder or randomness associated with the reaction system. The change in entropy (ΔS) at different value of conversion is given in Table 4.5. It was found that ΔS for DAN and torrefied biomass (TAN-220 and TAN-250) has both positive and negative values varies in the range of −44.96 to 96.42, −51.82 to 230.24, and −13.03 to 88.81 J/mol.K, respectively. The larger

value of ΔS indicates that biomass sample is away from the thermodynamic equilibrium, while smaller value of ΔS means that biomass sample is acquiring a new state which is approaching it to state of thermodynamic equilibrium. However, TAN-280 has only negative ΔS in the range of −2.20 to −0.43 J/mol.K. The negative value of entropy is the result of disordered nature of product formed through bond dissociation. The low value of entropy also suggests that material has just passed through some physical and chemical changes, which bring the material to the state of thermodynamic equilibrium during the pyrolysis process (Kaur et al., 2018; Yuan et al., 2017).

Table 4.5 Thermodynamic parameters for pyrolysis of DAN and torrefied biomass at a heating rate of 10 K/min

Conversion	A (s^{-1})	ΔH (kJ/mol)	ΔG (kJ/mol)	ΔS (J/mol.K)
DAN				
0.1	1.42×10^{10}	124.97	164.33	−62.13
0.2	1.33×10^{11}	171.18	199.54	−44.96
0.3	6.88×10^{13}	203.17	199.36	5.45
0.4	1.07×10^{15}	217.22	199.33	27.52
0.5	1.51×10^{16}	230.73	199.32	48.72
0.6	9.69×10^{16}	243.22	199.32	63.71
0.7	5.53×10^{18}	261.20	199.35	96.42
0.8	3.11×10^{17}	246.18	199.32	72.93
0.9	4.23×10^{10}	163.83	199.59	−56.56
TAN-220				
0.1	5.61×10^{10}	130.60	163.47	−51.82
0.2	1.39×10^{15}	181.97	162.93	30.01
0.3	2.18×10^{19}	231.59	162.78	108.48
0.4	2.33×10^{20}	243.77	162.79	127.67

0.5	6.04×10^{20}	248.63	162.79	135.33
0.6	4.40×10^{21}	258.84	162.81	151.39
0.7	7.39×10^{25}	309.04	163.00	230.24
0.8	1.67×10^{23}	277.00	162.86	179.95
0.9	3.76×10^{20}	244.91	162.78	129.48
TAN-250				
0.1	2.62×10^{8}	102.72	162.48	−95.73
0.2	6.99×10^{12}	152.31	160.45	−13.03
0.3	7.76×10^{14}	175.82	159.72	25.79
0.4	5.51×10^{15}	185.57	159.44	41.86
0.5	1.64×10^{18}	214.15	158.71	88.81
0.6	4.58×10^{17}	207.50	158.87	77.91
0.7	1.70×10^{18}	213.91	158.71	88.43
0.8	9.32×10^{16}	198.98	159.07	63.94
0.9	1.42×10^{14}	165.55	159.97	8.93
TAN-280				
0.1	3.70×10^{3}	65.66	216.51	−2.20
0.2	4.57×10^{4}	80.50	215.16	−1.60
0.3	1.56×10^{6}	100.87	213.61	−1.06
0.4	1.38×10^{7}	113.98	212.80	−0.82
0.5	9.21×10^{8}	139.96	211.45	−0.48
0.6	8.26×10^{8}	138.91	211.49	−0.49
0.7	1.18×10^{9}	140.87	211.38	−0.47
0.8	2.23×10^{9}	144.69	211.20	−0.43
0.9	5.24×10^{7}	120.40	212.34	−0.71

4.4 Conclusions

Torrefaction of *Acacia nilotica* was performed in a fixed bed reactor at three different temperatures 220, 250 and 280 ℃, keeping retention time and heating rate constant. The TGA of DAN and TAN was performed at three different heating rate viz. 5, 10 and 15 K/min. Based on the result of TGA analysis, kinetic, thermodynamic parameters and reaction mechanism during pyrolysis of DAN and TAN were investigated. Compositional analysis showed that at lower temperature during torrefaction, the relative cellulose content in the torrefied biomass (TAN-220) is higher than the DAN, while, it goes on decreasing on further increase in temperature. The higher cellulose content attributed to higher activation energy of TAN-220 than DAN. The average activation energy of torrefied biomass obtained at 280 ℃ (TAN-280) is 42.39% lower than the DAN. Slight difference between activation energy and enthalpy favors the formation of activated complex. Accordingly, bio-energy generation through pyrolysis can be positively attained. It was noticed that at lower conversion value ($\alpha \leq 0.5$) the diffusion mechanism was rate determining for DAN and TAN-220, however, for TAN-250 and TAN-280, the 2nd order random nucleation model is dominant for rate determination. At higher conversion ($\alpha \geq 0.5$), DAN and TAN-220 follow the 2nd order random nucleation and Avrami-Erofeev models, while, in case of TAN-250 and TAN-280, 3rd order random nucleation is dominant. Finally, it can be concluded that the behavior of DAN and TAN towards thermochemical is quite different. The TAN has much improved properties than the DAN which makes it good quality solid fuel for bio-energy generation. Also, it can be blended with coal in thermal power plants.

Chapter 5

Optimization of process parameters for torrefaction of A*cacia nilotica* using response surface methodology and characteristics of torrefied biomass as upgraded fuel

General background

This chapter dealt with the optimization of process parameters for torrefaction *Acacia nilotica* (TAN) using response surface methodology. The temperature (220-280 ℃), retention time (20-60 min), and heating rate (5-15 ℃/min) were selected as independent variables and energy yield and higher heating value of TAN were selected as dependent variables. The ANOVA and regression analysis were used to study the fitness of developed model using central composite design technique. In addition, the characteristics of torrefied biomass at optimized condition were tested using TGA, FTIR, XRD, BET, and SEM analysis and compared with DAN. Moreover, the fuel characteristics like fuel ratio (FR), combustibility index (CI), volatile ignitability (VI), flow behavior through angle of repose, Hausner ratio (HR), Carr compressibility index (CCI), cohesion coefficient (C), moisture sorption ability and densities (bulk, tapped and particle) of TAN at optimized condition and DAN were also compared.

5.1 Introduction

Torrefaction is used as a pretreatment step which produces high-quality solid biofuel as torrefied biomass. This torrefied biomass can be used in different thermochemical conversion processes like pyrolysis, gasification and combustion to increase the quality of products such as high-grade bio-oil (Dai et al., 2019) and producer gas (Bach et al., 2019) with the lower harmful emission (Louwes et al., 2017) during the process. Therefore, the overall efficiency of the thermochemical process can be increased by using torrefied biomass (Dai et al., 2019). The process of torrefaction depends not only on biomass structure (amount of cellulose, hemicellulose and lignin) and ash content (Lee et al., 2012) but also depends on the process parameters like temperature, heating rate, retention time (Buratti et al., 2018), particle size (Dai et al., 2019). Chen et al. (Chen & Kuo, 2011) suggested that torrefaction process is highly influenced by temperature rather than retention time. Generally, as the temperature increases during torrefaction, more volatiles are released due to the conversion of oxygen-containing compound. The variation of solid yield and higher heating value (HHV) of torrefied biomass with retention time is marginal at fixed temperature (Buratti et al., 2018). Also, EY and HHV of solid product are important outcomes of the process. However, energy yield (EY) and HHV reflect opposite trend, when process parameters are varied during the process. Thus, optimizing the process parameters and a balance between EY and HHV becomes quite important for energy densification and energy utilization. Optimization may reduce operational cost regarding scale-up of the process at industrial level. Thus considering torrefied *Acacia nilotica* (TAN) as desired product from torrefaction, optimization of process parameters such as temperature, retention time and heating rate for HHV and EY of TAN was performed using

RSM. The ANOVA and regression analysis were used to study the fitness of developed model using central composite design technique. Response surface methodology (RSM) is one of the most prevalent and promising techniques to develop, improve, and optimize the process parameters and their interaction effect on the process with a minimum number of experiments. It was developed by Box and Wilson in 1951 (Dhanavath et al., 2017). It is a statistical and mathematical (Gholami et al., 2019) technique having a multivariable non-linear model, which generally is used to optimize the process parameters. In it, a mathematical model is developed which, best fits the experimental data (Cotana et al., 2015). The optimum values of responses are obtained using developed model.

5.2 Material and methods

5.2.1 Sample preparation

The detailed discussion about the collection of *Acacia nilotica* and preparation of dried *Acacia nilotica* (DAN) has been discussed in Chapter 3.

5.2.2 Experimental design using RSM

For optimization of parameters, RSM was used. A three-factor face central composite design, a kind of RSM technique was used to optimize the response in the process. The central composite design technique is well suited for fitting a quadratic surface, which usually works well for any process optimization. This technique is being widely used since it provides a minimum number of experimental run for optimizing the response variable and an easy way to estimate the interaction between different parameters. Assuming the experiments will be performed in a single day with one block, twenty experiments have to

be performed, which may be derived from Eqs. (5.1) (Tan et al., 2008), comprising eight factorial points (2^n), six axial points (2n) and six replicates at center points (n_c).

$$N = 2^n + 2n + n_c = 2^3 + 2(3) + 6 = 20 \quad (5.1)$$

where N is the total number of experiments that have to be performed, n is the number of independent variables and n_c is the number of replicates at central points.

The central point varies between 3 to 10 and it can be used to predict experimental error and reproducibility of data. Temperature (A), retention time (B) and heating rate (C) of range 220-280 ℃, 20-60 min and 5-15 ℃/min, respectively were selected as independent variables. Code -1, 0 and +1 were the value of temperature (220, 250 and 280 ℃), retention time (20 min, 40 min and 60 min) and heating rate (5, 10, and 15 ℃/min). HHV and EY of TAN were chosen as response and both the responses have to be maximized. The matrix of experimental design is given in Table 5.1. The experimentally calculated HHV and EY are incorporated in design expert software (Stat-Ease Design-Expert version-11) as the actual value. While predicted and residual values obtained by software. Data obtained from the experiments were used to optimize the selected parameter. The suggested mathematical model having highest polynomial degree was chosen from central composite design and also it should not be aliased (B. Gratuito et al., 2008).

Once the experiments have been performed, the response variables (HHV and EY of TAN) were correlated with independent parameters (temperature, retention time and heating rate). The general relationship between response and independent variable is given as:

$$Y = f (X_1, X_2, X_3, \ldots\ldots, X_n) \quad (5.2)$$

where Y is the response variable, f is the function relating response to independent variable and X_1, X_2, X_3,…….. X_n are the n independent variables which affect the response.

Following the second order polynomial equation as suggested by central composite design technique, the generalized form of second order polynomial equation is given as:

$$Y = b_0 + \sum_{i=1}^{k} b_i X_i + \sum_{i=1}^{k} b_{ij} X_i^2 + \sum_{i_{i>j}}^{k} \sum_{j}^{k} b_{ij} X_i X_j \quad (5.3)$$

where i is the linear coefficient, j is the quadratic coefficients, b is the regression coefficient, k is the number of factors that were studied and optimized in the study.

The ANOVA and regression analysis were used to study the fitness of regression model at 95% confidence level using Design-Expert software. This analysis was used to check the deviation of mean. Set of experimental data were analyzed in accordance with several variables like p value, degree of freedom (DF), F value, determination coefficient (R^2), predicted determination of coefficient (R^2_{pred}) and adjusted determination of coefficient (R^2_{adj}) to check the statistical fitness of the model. From ANOVA, F and p values are used to examine the importance of terms appeared in the model equation. F value suggests that variation in responses can be demonstrated by regression equation, whereas, p value specifies, whether F value is large enough to ascertain statistical importance of the developed model. For that matter, p value for model should be less than 0.05 and p value for lack of fit test should be greater than 0.05 (Dhanavath et al., 2017). Three dimensional RSM plots and contour plots were incorporated to analyze the effect of each variable and their interaction with HHV and EY of TAN.

5.2.3 Experimental setup and torrefaction procedure

The detail about the experimental set-up and torrefaction process has been discussed in Chapter 3. The torrefaction of DAN was carried out following the experimental matrix given in Table 5.1. The TAN is considered as the main product in this study. The TAN yield was calculated using Eqs. (5.4).

$$\text{TAN yield (wt\%)} = \frac{\text{Weight of TAN (g)}}{\text{Weight of DAN (g)}} \times 100 \quad (5.4)$$

Energy yield is a function of solid product yield and their HHV. EY can be calculated using Eqs. (5.5).

$$\text{Energy yield} = (\text{TAN yield}) \times \frac{\text{HHV}_{\text{db,TAN}}}{\text{HHV}_{\text{db,DAN}}} \quad (5.5)$$

Table 5.1 Experimental design matrix and actual, predicted and residual value of responses obtained using RSM

	Level of actual variable			**Actual, predicted and residual value of response**					
Run	T (^{o}C)	RT (min)	HR (^{o}C/min)	**HHV (MJ/kg)**			**EY (%)**		
				Actual value	Predicted value	Residual value	Actual value	Predicted Value	Residual value
1	250	40	10	22.46	22.51	-0.0453	70.02	69.75	0.2677
2	250	40	10	22.38	22.44	-0.0557	70.52	69.85	0.5722
3	250	40	10	21.77	21.98	-0.2151	69.78	69.39	0.3857
4	220	60	15	20.71	20.71	0.0030	75.55	76.01	-0.4545
5	220	20	15	19.61	19.49	0.1190	75.95	74.83	1.1200
6	250	40	5	23.02	22.68	0.3369	71.31	70.17	1.1300
7	220	20	5	19.97	20.02	-0.0530	76.35	76.98	-0.6337

8	280	20	15	24.39	24.33	0.0600	49.72	49.28	0.4374
9	250	60	10	23.58	23.36	0.2249	71.96	71.18	0.7754
10	280	40	10	25.36	25.25	0.1109	49.76	50.77	-1.0100
11	220	40	10	20.32	20.30	0.0249	75.57	75.36	0.2054
12	250	40	10	22.54	22.72	-0.1766	70.32	69.65	0.5799
13	250	40	10	21.99	22.11	-0.1347	69.88	69.67	0.2165
14	280	60	5	26.19	26.34	-0.1530	51.72	52.64	-0.9187
15	280	20	5	24.73	24.77	-0.0370	53.21	52.55	0.6553
16	220	60	5	21.18	21.27	-0.0940	76.04	76.28	-0.2366
17	250	40	10	22.77	22.94	-0.1724	71.23	70.98	0.2544
18	250	20	10	21.87	21.96	-0.0891	68.97	70.55	-1.5800
19	280	60	15	25.89	25.87	0.0190	52.08	51.25	0.8345
20	250	40	15	21.98	22.18	-0.2011	66.47	68.40	-1.9400

5.2.4 Characteristics of raw and torrefied biomass

The detailed discussion about proximate and ultimate analysis, fuel and flow properties, density, thermogravimetric analysis, Scanning electron microscopy, FTIR analysis has been discussed in Chapter 3. Additionally, the Brunauer–Emmett–Teller (BET) surface area of TAN252-60-5 was determined on an ASAP 2020 adsorption apparatus (Micromeritics, USA). Nitrogen gas was used as an adsorbate. Prior to analysis, the torrefied biomass sample was degassed at −180 ℃ for 24 h. The crystallinity of the DAN and TAN at optimized condition was investigated using X-ray diffractometer (mini flux II, Rigaku, Japan) with a scanning rate of 5^o per min with a step size of 0.02^o in the range of 0

to 80^{o} (2θ). The crystallinity index and crystal size were calculated using following Eqs. (5.6)

$$\text{CrI (\%)} = \left(\frac{I_{002}-I_{am}}{I_{002}}\right) \times 100 \quad (5.6)$$

where CrI denotes crystallinity index; I_{002} and I_{am} denote crystalline and amorphous intensity, respectively of diffraction plane (002).

$$L_{002} = \frac{k \times \lambda}{\beta \times \cos\theta} \quad (5.7)$$

where L_{002} denotes the crystal size, k denotes the Scherrer constant (0.90), λ denotes the X-ray wavelength, usually which is 0.15406 nm, β denotes the full width at half maximum (FWHM) of peak, and θ denotes the diffraction angle plane (002) (Zheng et al., 2015).

5.3 Results and discussion

5.3.1 Solid product yield and Energy yield

The fraction of each product depends on operating parameter like temperature, retention time, heating rate. Maximum and minimum solid yield (73.82% and 38.13%) were obtained at temperature (220 and 280 ℃), retention time (20 and 60 min), and heating rate (5 ℃/min), respectively. The cause of decrease in solid yield with temperature has been discussed in Chapter 3. EY gives an indication about the amount of energy preserved in biomass after torrefaction. The EY of TAN decreases with temperature at constant retention time and heating rate. Maximum and minimum EY (76.35% and 49.72%) were obtained at temperature (220 and 280 ℃), retention time (20 min), and heating rate (5 and 15 ℃/min), respectively. As the retention time increases, the yield of liquid and non-condensable gases increased. At a fixed temperature and longer retention time, biomass is

exposed for longer duration, hence, yield of liquid and gas enhanced. Higher retention time also favors the devolatilization reaction, which can increase the yields of liquid product and gases.

5.3.2 Response surface analysis for HHV and EY of Torrefied biomass

The relation between experimental and predicted values of HHV and EY of TAN are shown in Fig. 5.1 (a) and (b), respectively. It shows that both values are close to each other, indicating that the developed model is well suited to establish the relation between dependent and independent variables during torrefaction process. This relationship can also be justified by the value of correlation coefficient (R^2), which varies between zero to one. The value of coefficient close to one indicates lesser error in developed model.

(a) **(b)**

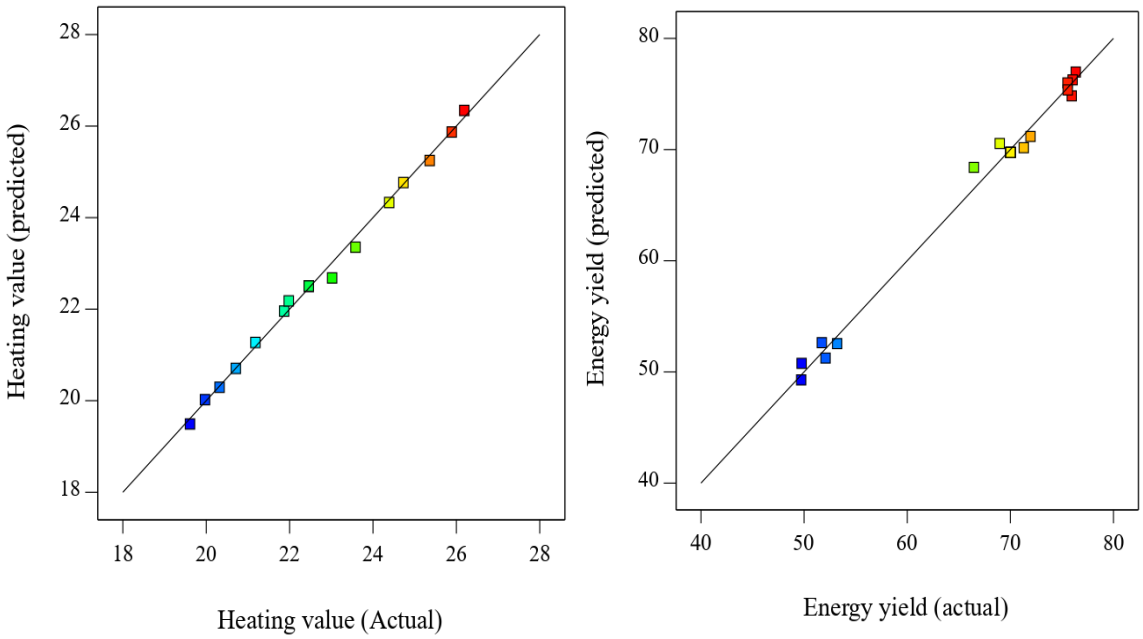

Figure 5.1 Relationship between actual and predicted values of model (a) HHV and (b) EY

For present model, values of correlation coefficients for HHV and EY of TAN are 0.9957 and 0.9921, respectively, indicating a good correlation between independent and dependent variables. The relation between dependent parameter (HHV) and independent parameters (temperature (A), retention time (B), and heating rate (C)) obtained in this study is:

$$Y_{HHV}\ (MJ/kg) = +21.2581 - 0.7266A - 0.0284B - 0.0277C + 0.0001AB + 0.0001AC$$

$$- 0.00008BC + 0.00002A^2 + 0.0003B^2 - 0.0002C^2 \quad (5.8)$$

The statistical analysis of HHV is given in Table 5.2. The significance of each independent variable on the response can be analyzed using F-value and p-value. For a significant model, the p-value should be less than 0.05 and F- value should be large. For present model, p-value and F-values are <0.0001 and 256.54 for HHV, suggesting that the developed model is applicable. The p-value and F-value of model can also be used to compare the linear term (A, B, C), interaction term (AB, AC, BC), and quadratic term (A^2, B^2, C^2). For HHV of TAN linear term (A, B and C) and quadratic term (A^2) are significant having p-value <0.0001, <0.0001 0.0009, and 0.0270 respectively. The F-value of all the significant terms (A, B, C, and A^2) is 2099.53, 166.72, 21.56 and 6.70, respectively. It can be concluded that for HHV of TAN, temperature has a larger effect on the process than retention time and heating rate.

Table 5.2 ANOVA for quadratic model of response: **HHV and EY**

Source	Sum of square	Degree of freedom	Mean of square	F-value	p-value	Remark
HHV						
Model	67.47	9	7.50	256.54	< 0.0001	Significant
A-Temperature	61.36	1	61.36	2099.53	< 0.0001	
B- Retention time	4.87	1	4.87	166.72	< 0.0001	
C-Heating rate	0.6300	1	0.6300	21.56	0.0009	
AB	0.0528	1	0.0528	1.81	0.2085	
AC	0.0045	1	0.0045	0.1544	0.7026	
BC	0.0006	1	0.0006	0.0210	0.8878	
A^2	0.1958	1	0.1958	6.70	0.0270	
B^2	0.0634	1	0.0634	2.17	0.1716	
C^2	0.0147	1	0.0147	0.5040	0.4940	
Residual	0.2922	10	0.0292			
Lack of Fit	0.2922	5	0.0584	4.58	0.0569	
Pure Error	0.0000	5	0.0000			
Cor Total	67.76	19				
R^2 0.9957		Adjusted R^2 0.9918		Predicted R^2 0.9681		
EY						
Model	1724.53	9	191.61	139.88	< 0.0001	Significant
A-Temperature	1512.10	1	1512.10	1103.88	< 0.0001	
B- Retention time	0.9912	1	0.9912	0.7236	0.4149	
C-Heating rate	7.82	1	7.82	5.71	0.0380	
AB	0.3121	1	0.3121	0.2279	0.6434	

AC	0.6280	1	0.6280	0.4584	0.5137	
BC	1.76	1	1.76	1.29	0.2831	
A^2	122.70	1	122.70	89.57	< 0.0001	
B^2	3.44	1	3.44	2.51	0.1440	
C^2	0.5822	1	0.5822	0.4250	0.5292	
Residual	13.70	10	1.37			
Lack of Fit	13.70	5	2.74	6.68	0.0647	
Pure Error	0.0000	5	0.0000			
Cor Total	1738.23	19				
R^2 0.9921		Adjusted R^2 0.9850		Predicted R^2 0.9244		

Three dimensional (3D) and contour plots of response at optimized condition were obtained in this study to verify the dependence of HHV of TAN with different process parameters like temperature, retention time and heating rate (Fig. 5.2). In case of three independent variables, it is not possible to show the effect of all variable on the response simultaneously. Hence the effect of two variables keeping third as constant is shown in this study. Figs. 5.2 (a) and (b) show the 3D and contour plots for variation of HHV of TAN with respect to temperature and retention time. It can be seen that at a constant heating rate of 5 ℃/min, the HHV of TAN increases up to a maximum value, with increase in temperature and retention time. Similar results can be obtained in case of variation of HHV of TAN with temperature and heating rate at a constant retention time of 60 min (Figs. 5.2 (c) and (d)). It can be concluded that maxima of HHV of TAN can be obtained in case of

higher temperature, retention time and heating rate. A flat 3D surface can be seen in Figs. 5.2 (e) and (f) confirming that HHV of TAN does not vary too much with an increase in retention time and heating rate at particular temperature (250 ℃). In can be mentioned that torrefaction is more temperature driven process than retention time and heating rate. Thus, properties like HHV and EY are highly dependent on temperature than the retention time and heating rate. With an increase in temperature, relative increase in carbon content and a decrease in oxygen content lead to increase in HHV of biomass.

(a) **(b)**

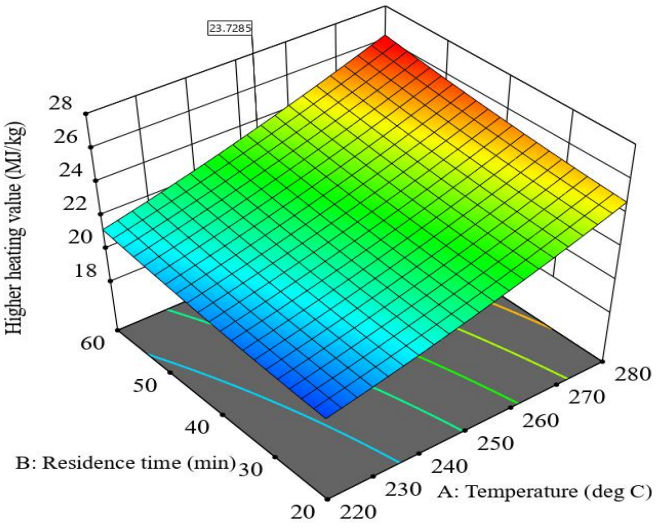

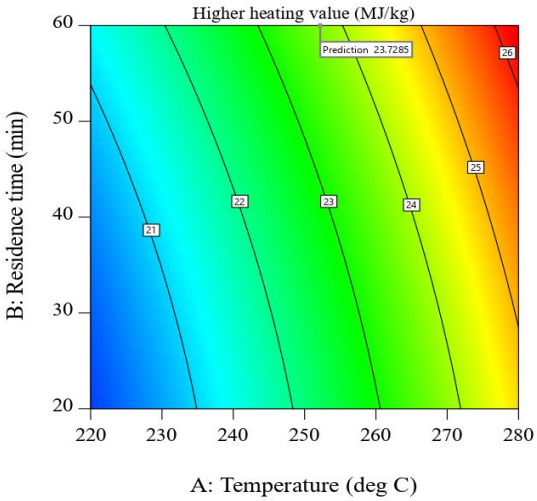

(c)

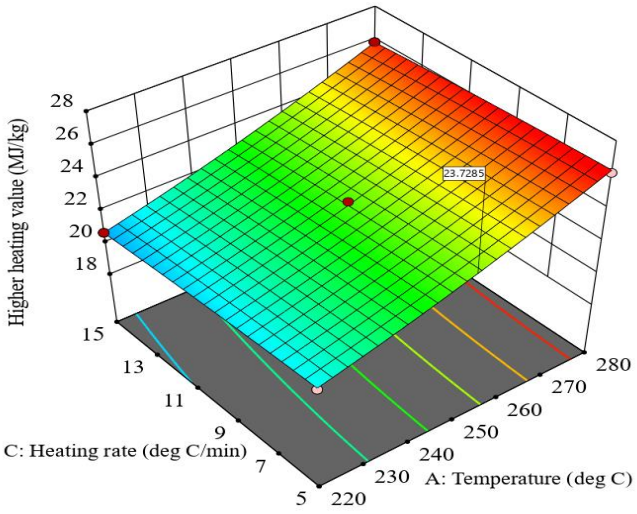

(d)

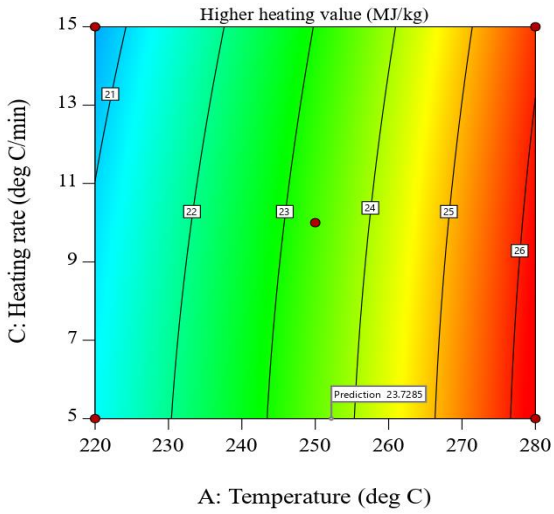

(e)

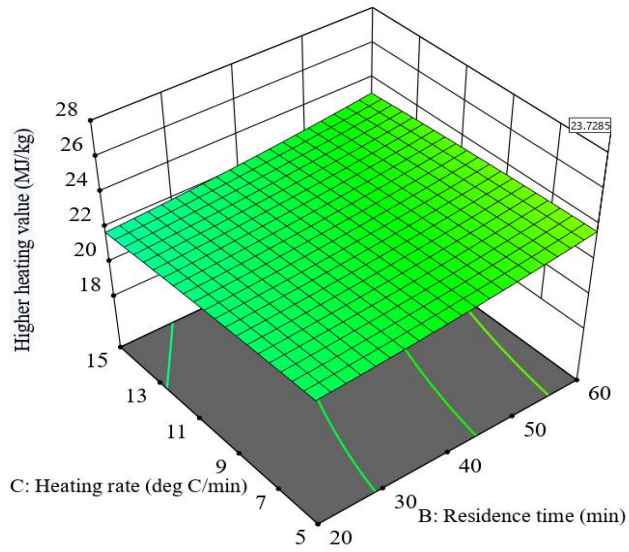

(f)

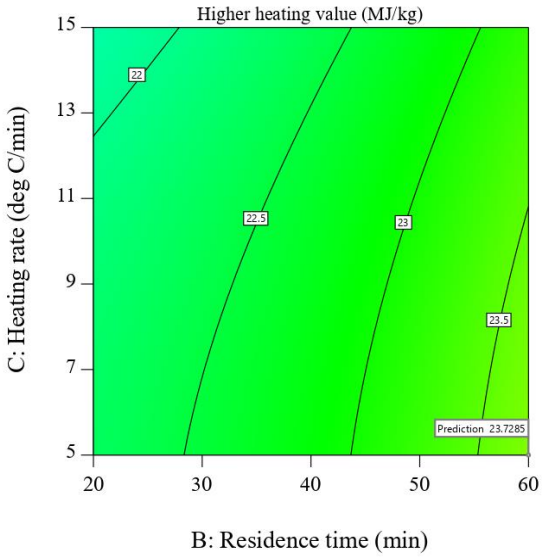

Figure 5.2 Three dimensional response surface and contour plots of HHV showing the effect of (a) and (b) temperature and retention time; (c) and (d) temperature and heating rate; (e) and (f) heating rate and retention time.

For EY, relation between dependent and independent (temperature, retention time and heating rate) variable is as follows:

$$Y_{EY}(\%) = +3.3065A - 0.3372B + 0.4703C + 0.0003AB - 0.0018AC + 0.0046BC$$

$$- 0.0074A^2 + 0.0027B^2 - 0.0184C^2 - 287.3708 \quad (5.9)$$

The statistical analysis for EY is given in Table 5.2. For developed model in case of EY, p-value and F-value are <0.0001 and 139.88, suggesting that developed model is significant. For EY of TAN, linear term (A and C), and quadratic term (A^2) are significant, having p-values <0.0001, 0.0380, and <0.0001, respectively. In case of EY, the F values for significant terms (A, C, and A^2) are 1103.88, 5.71, and 89.57, respectively. The dependency related to temperature is similar to HHV; however EY has the different trend relative to retention time and heating rate. In case of EY, the process is more dependent on heating rate than retention time.

Fig. 5.3 shows the 3D and contour plots for response EY at optimized condition with respect to independent variables. Figs. 5.3 (a), (b) and (c), (d) show the coupled effect of temperature- retention time at constant heating rate of 5 ℃/min and temperature-heating rate at constant retention time of 60 min, respectively on EY. It was found that the maximum value of EY can be obtained at lower temperature, retention time and heating rate during torrefaction process. A flat 3D surface can be seen confirming that EY of TAN does not vary too much with an increase in retention time and heating rate at a particular temperature (Figs. 5.3 (e) and (f)). At lower temperature, the degradation of hemicellulose is less and almost insignificant for cellulose and lignin (Dai et al., 2019) due to lower rate of devolatilization. Hence, mass loss is very small.

(a)

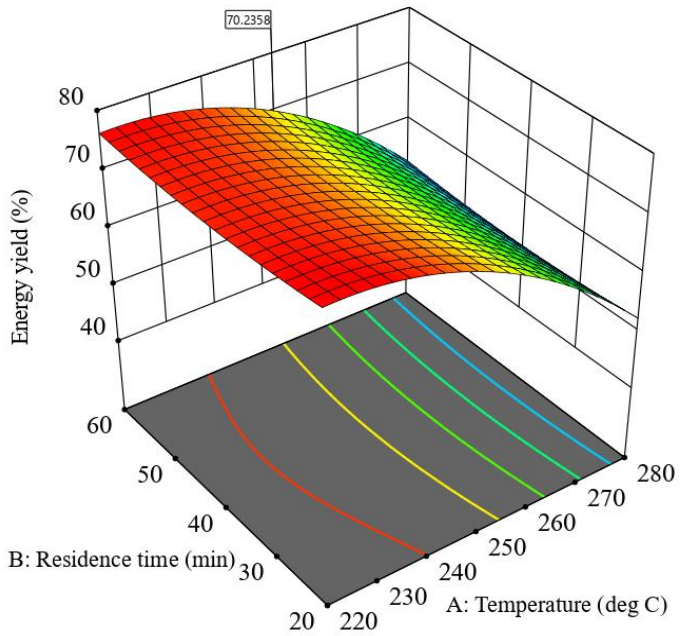
70.2358
Energy yield (%)
80
70
60
50
40
B: Residence time (min)
60
50
40
30
20
A: Temperature (deg C)
220
230
240
250
260
270
280

(b)

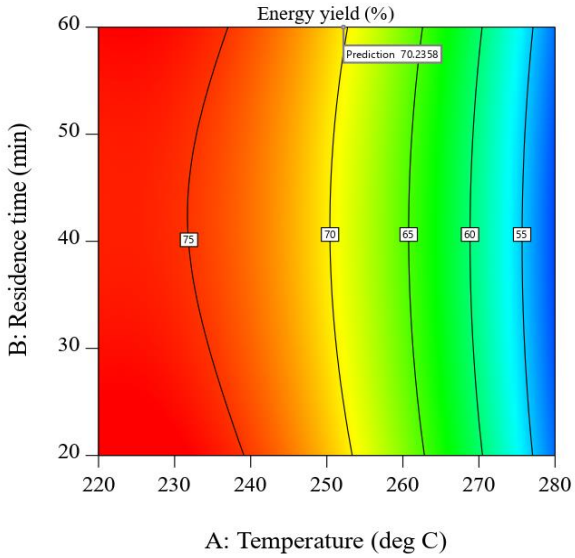
Energy yield (%)
Prediction 70.2358
B: Residence time (min)
60
50
40
30
20
75
70
65
60
55
220
230
240
250
260
270
280
A: Temperature (deg C)

(c)

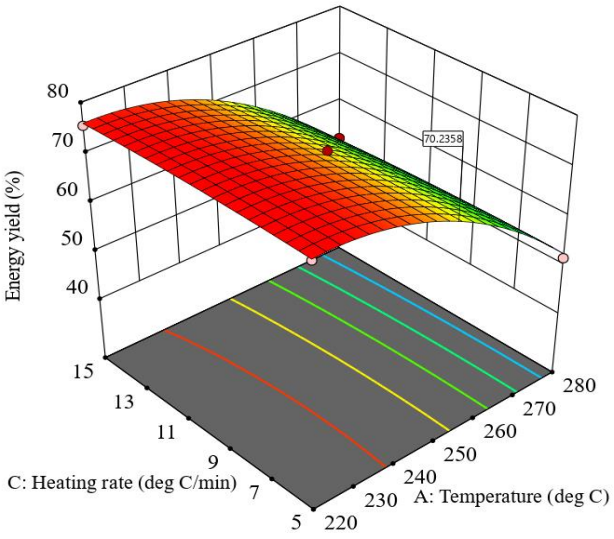
70.2358
Energy yield (%)
80
70
60
50
40
C: Heating rate (deg C/min)
15
13
11
9
7
5
A: Temperature (deg C)
220
230
240
250
260
270
280

(d)

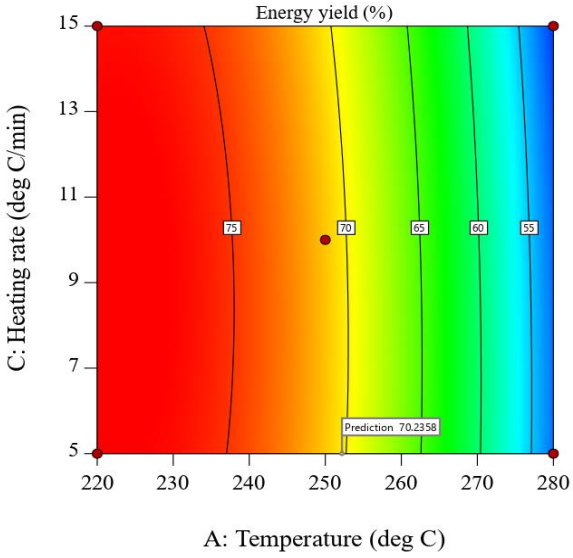
Energy yield (%)
C: Heating rate (deg C/min)
15
13
11
9
7
5
75
70
65
60
55
Prediction 70.2358
220
230
240
250
260
270
280
A: Temperature (deg C)

(e) **(f)**

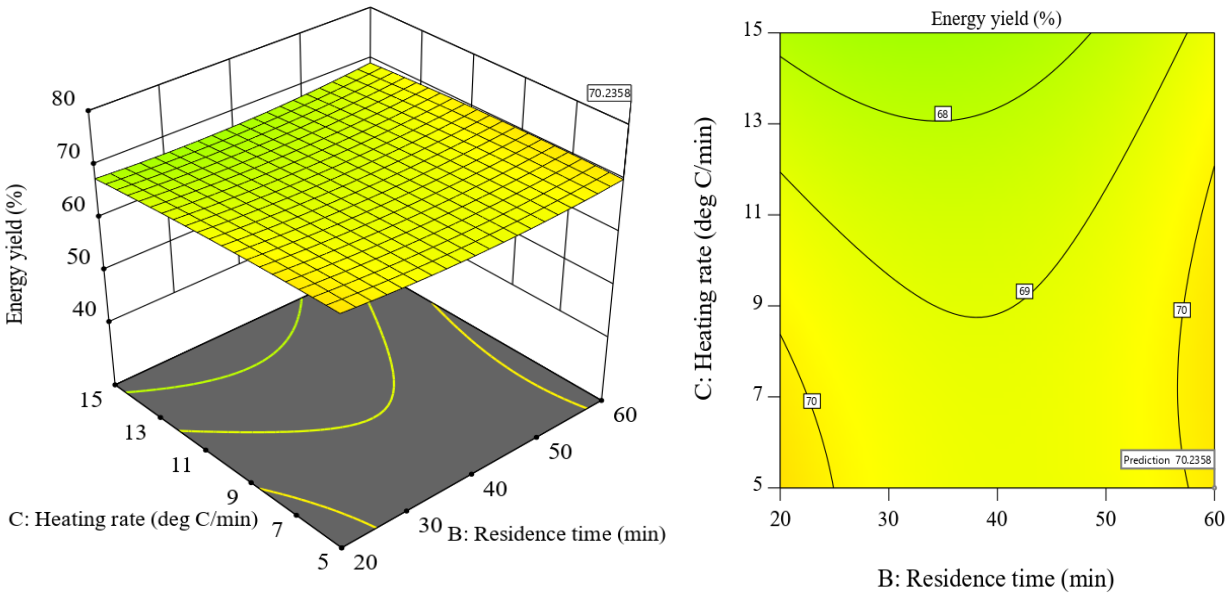

Figure 5.3 Three dimensional response surface and contour plots of EY showing the effect of (a) and (b) temperature and retention time; (c) and (d) temperature and heating rate; (e) and (f) heating rate and retention time.

5.3.3 Optimization of HHV and EY of Torrefied biomass

Twenty experiments have been performed according to the experimental matrix given in Table 5.1. The maximum HHV (25.87 MJ/kg) of TAN was found at 280 ℃, 57 min retention time and 5 ℃/min heating rate (Table 5.3). On the other hand, maximum EY (75.14 %) was obtained at 220 ℃, 20 min retention time and 10 ℃/min heating rate (Table 5.3). It is evident that both HHV and EY attain maximum value at different set of conditions. It may be mentioned that EY indicates energy densification, whereas HHV refers to the direct utilization potential of TAN as solid fuel. Maximum HHV at minimum

EY would be beneficial for using TAN as solid fuel. While maximum EY at minimum HHV would be required in case of biomass densification. In the present study, there was a need to maximize both HHV and EY. As predicted by RSM, the maximum value of HHV and EY are 23.73 MJ/kg and 70.20 %, respectively, obtained at 252 ℃, 60 min retention time and 5 ℃/min heating rate. For validating these data, experiments were performed and it can be seen that the error is less than 2 % (Table 5.3). This clearly suggests that the developed model is in good agreement with the experimental findings.

Table 5.3 Experimental and predicted values of responses at optimum condition

Parameter	**Required optimum values**		
	Maximum HHV and Minimum EY	**Minimum HHV and Maximum EY**	**Maximum HHV and Maximum EY**
Temperature (℃)	280	220	252
Retention time (min)	57	20	60
Heating rate (℃/min)	5	10	5
HHV (MJ/kg) (measured)	25.86	19.98	24.06
HHV (MJ/kg) (predicted)	26.19	19.82	23.73
Error (%)	−1.2	0.8	1.3
Energy yield (%) (measured)	52.91	75.14	71.31
Energy yield (%) (predicted)	52.33	76.34	70.20
Error (%)	1.1	−1.3	1.5
Desirability (%)	98.30	99.40	69.04

5.3.4 Physical and chemical properties of raw and torrefied biomass

The proximate and ultimate analyses data along with HHV and EY at optimized condition are presented in Table 5.4, which clearly shows that MC and VM both decreased as the temperature increased during torrefaction. MC for DAN is 6.24 %, while 1.67 % TAN252-60-5. Besides, the VM also decreased from 80.36% for DAN to 44.78% for TAN252-60-5. The AC of biomass increased from 0.65% for DAN to 1.42% for TAN252-60-5. Ash has strong affinity to deposit in the boiler, pyrolyzer, and gasifier (Cai et al., 2017). So it will be helpful to know the physical and chemical characteristic of ash to prevent such problems of deposition. The FC increased from 12.75% for DAN to 52.13% for TAN252-60-5. This increase in FC and AC was observed during torrefaction because as the temperature increases, rate of devolatilization of (water vapour, methane, ethane, and other lighter hydrocarbon) from biomass also increases which results in relative decrease in MC and VM and relative increase in FC and AC. During torrefaction, loss of hydrogen and oxygen are more compared to the loss of carbon. The relative increase in the carbon content of biomass during torrefaction is responsible for higher HHV. The HHV obtained for DAN, and TAN252-60-5 are 19.31, and 24.06 MJ/kg, respectively. These results are in good agreement with the published literature for similar feedstock.

Table 5.4 Characteristics of DAN and TAN252-60-5

Analysis	**DAN**	**TAN252-60-5**
MC (wt%)	6.24	1.67
AC (wt%)	0.65 (0.69)	1.42 (1.44)
VM (wt%)	80.36 (85.70)	44.78 (44.54)
FC (wt%)	12.75 (13.59)	52.13 (53.01)
O/C	1.09	0.60
H/C	0.17	0.08
HHV (MJ/kg)	19.31 (20.59)	23.73 (24.13)
Solid yield (%)	-	59.90
EY (%)	-	70.22
Geometric mean diameter (mm)	0.53	0.43
FR	0.15	1.19
CI (MJ/kg)	149.43	21.93
VI (MJ/kg)	17.39	13.44
Angle of repose (degree)	38.89	35.75
HR	1.29	1.21
CCI	22.48	17.35
C	0.40	0.35
Bulk density (kg/m^3)	231.45	193.48
Tapped density (kg/m^3)	300.71	235.67
Particle density (kg/m^3)	1251	1156
BET surface area (m^2/g)	-	0.9703
Pore volume (cm^3/g)	-	0.0015
Mean pore diameter (nm)	-	13.69

5.3.5 Fuel and flow properties of torrefied biomass

Table 5.4 presents the combustion indices of the biomass, which are commonly used as crucial parameters in thermochemical conversion processes. In coal-firing power plants, the recommended value of FR is between 0.5-3.0. The FR for DAN and TAN252-60-5 are 0.15 and 1.19, respectively. With increase in temperature, FR of DAN increases since fixed carbon content increases along with decrease in volatile matter. The fuel having higher FR leads to increase in unburnt portion of the fuel, which decreases boiler efficiency during the operation. The fuel which has FR greater than 2 can cause ignition and flammability problem during the application. The reported range of CI and VI for coal are: CI should be less than 23MJ/kg and VI should be greater than 14.5 MJ/kg (Ohm et al., 2015). The calculated value of CI and VI for DAN are 149.43 MJ/kg and 17.39 MJ/kg, respectively. This shows that DAN should not be used as an alternative fuel without prior treatment. After torrefaction, CI and VI for TAN252-60-5, are 21.93 and 13.44, respectively. Transportation and handling are noteworthy processes which involve during the conversion process of biomass. These processes are extremely influenced by flowing ability of biomass. The materials having angle of repose between 31-35^{o} have good flowing property and between 25-30^{o} have excellent flowing property, materials having HR between 1.19-1.25 have fair-flowing properties and between 1.12-1.18 have good flowing properties (Lumay et al., 2012), materials having CCI between 11-15, 16-20 and 21-25 have good, fair and passable flow behavior, respectively (Lumay et al., 2012; Szalay et al., 2015). The angle of repose for DAN and TAN252-60-5 are 38.39, and 35.75, respectively. HR and CCI are important parameters which depict flow behavior of material. The calculated value of HR for DAN and TAN252-60-5 are 1.29 and 1.21, respectively. CCI is a measure of

bulk density, tapped density, moisture content, surface area and cohesiveness of biomass since it varies with all these parameters. CCI of DAN and TAN252-60-5 are 22.48 and 17.35, respectively. DAN torrefied at higher temperature has lesser tendency of agglomeration than the DAN, leading to better flow property. The flowing property of biomass can also be explained by cohesive forces (between the particles) and friction forces (between the wall and the particles) (Szalay et al., 2015)**.** The cohesion coefficient of DAN and TAN252-60-5 are 0.40 and 0.35, respectively, which shows that after torrefaction cohesive force between the particle decreases, which favors the flowing behavior of TAN. This shows that fuel and flow properties of TAN moving toward the properties of coal, which makes it suitable as an alternative source of solid fuel or it, can be blend with coal.

5.3.6 BET surface area and density of raw and torrefied biomass

The surface area, pore diameter and pore volume of were obtained using the BET method. BET surface area, pore diameter and pore volume of TAN252-60-5 were found to be 0.9703 m^2/g, 13.69 nm and 0.0015 cm^3/g, respectively. Similar results were reported by Doddapaneni et al. (Doddapaneni et al., 2018) and Granados et al. (Granados et al., 2017). The variation of density of DAN and TAN252-60-5 are presented in Table 5.4. It was noticed that all three types of densities (bulk, tapped and particle) decreased as the temperature increased during torrefaction. The bulk, tapped and particle densities of DAN were 231.45, 300.71, and 1251 kg/m^3, respectively; and for TAN252-60-5, they were 193.48, 235.67, and 1156 kg/m^3, respectively. The release of volatile matter from DAN at higher temperature creates inside voids, which causes decrease in density along with increase in porosity of TAN. The TAN with increased surface area can be used as an

adsorbent in many processes. Conag et al. (Conag et al., 2017) investigated the bulk and tapped density of switchgrass, sugarcane bagasse and sugarcane leaves. They found that bulk density of switchgrass varied from 50-264 kg/m^3 and bulk density of torrefied switchgrass varied from 68-325 kg/m^3 whereas bulk and tapped density of sugarcane bagasse varies from 46-87 kg/m^3 and 65-125 kg/m^3, respectively.

5.3.7 Thermogravimetric analysis

Figs. 5.4 (a) and (b) show the TGA and DTG analyses of DAN and TAN252-60-5. Each component of biomass (hemicellulose, cellulose and lignin) shows different thermal behavior; hence, they have different thermal degradation temperature. Hemicellulose and cellulose degraded at lower temperature between 200-350 ℃, while lignin decomposes at a wider temperature range between 280-600 ℃ (Ren et al., 2013a). Major mass loss in case of hemicellulose and cellulose occurs between 268 ℃ to 355 ℃ (Yang et al., 2007). Figs 5.4 (a) and (b) show that entire thermal degradation process can be divided into three zones viz. drying (1^{st} zone), devolatilization (2^{nd} zone) and char formation (3^{rd} zone). Drying zone corresponds to removal of moisture and light volatile matter whereas devolatilization zone corresponds to active pyrolysis of DAN or TAN. In char formation zone, disruption and demethylation of lignin leads to char formation (Collard & Blin, 2014). As a representative case, 20 % mass loss was observed for DAN at around 290 ℃; whereas, for TAN, it was observed at 353 ℃. This shift in decomposition temperature may be attributed to lower amount of hemicellulose present in TAN. The char yield in case of DAN is 21%, however in case of TAN252-60-5; char yield is 47%. This increase in char yield is also attributed to the decomposition of hemicellulose and limited decomposition of cellulose during

torrefaction. The shoulder appeared in the DTG curve revealed decomposition of hemicellulose in case of DAN and generally, it was observed at around 300 ℃ (Müller-Hagedorn et al., 2003). In this study, similar shoulder can be seen in Fig. 5.4 (b) for DAN. In case of TAN252-60-5, shoulder disappeared, confirming that hemicellulose has already been degraded during torrefaction. Yang et al. (Yang et al., 2007) illustrated that peaks appeared in DTG curve with maximum weight loss, conforming the presence of cellulose in the biomass. The peaks in DTG curve for DAN and TAN can be seen at temperature around 360 ℃. Comparing DAN and TAN252-60-5, the intensity of peak in case of TAN252-60-5 is lower, confirming the degradation of cellulose in this range of temperature.

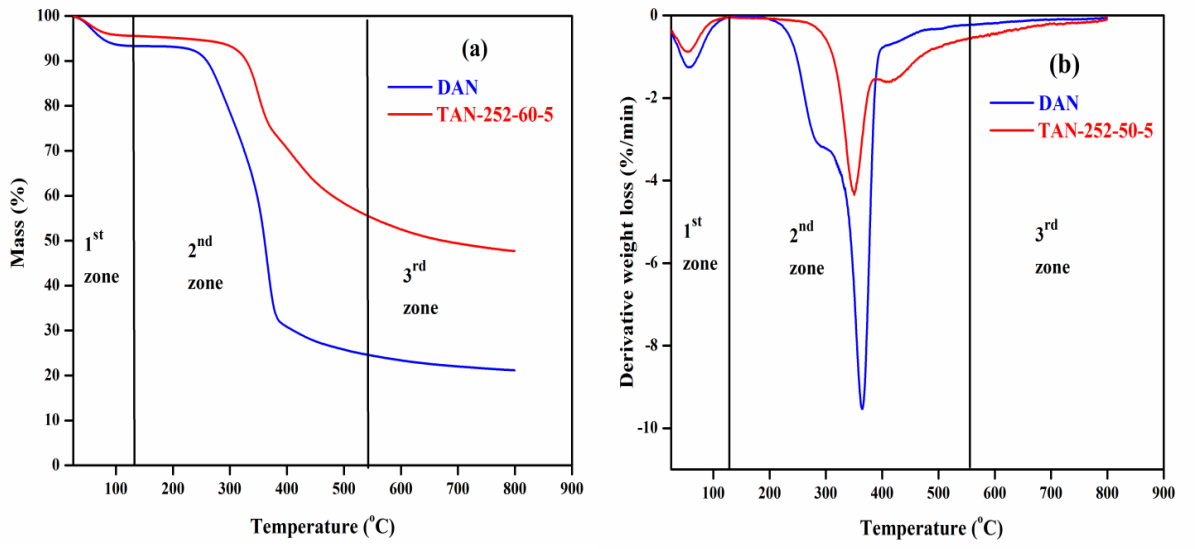

Figure 5.4 Thermogravimetric analyses of DAN and TAN252-60-5 (a) TGA (b) DTG

5.3.8 Fourier transform infrared spectroscopy (FTIR)

FTIR analysis was performed to observe the chemical changes in biomass due to torrefaction (Fig. 5.5). The structural and chemical changes in biomass are mainly due to decomposition of hemicellulose, which occurs mainly in the range of 200 ℃ to 300 ℃. In the wave number range from 4000 to 400 cm^{-1}, the functional groups of concern are O-H, C=O, C=C, C-H, and C-O-C. The characteristic peak between 3400-3100 cm^{-1} corresponds to stretching vibration of O-H bond (Gan et al., 2019) present mainly due to intra and intermolecular hydrogen bonding between alcoholic and phenolic groups present in cellulose and hemicellulose of biomass (Singh et al., 2019a). It can be observed that intensity of O-H bond in TAN250-60-5 has decreased due to torrefaction. Decrease in O-H bond intensity inferred disruption of hemicellulose during torrefaction. The decrease in intensity of peak between 2900-2750 cm^{-1} confirms the decrease of C-H bond stretching of aliphatic groups such as methyl and methelene compounds associated with alkanes and alkenes present in DAN (He et al., 2019). Decrease in intensity of peaks between 1750-1500 cm^{-1} may be attributed to deacetylation reaction, which causes decomposition of ester group present in hemicellulose (Carrasco & Roy, 1992). Between wave number of 600-700 cm^{-1}, intensity of peaks shows the presence of single and cyclic group of aromatic compound (Gomez-Serrano et al., 1996). Thus, as the process temperature increases, the intensity of peaks decreases for TAN252-60-5 in comparison to DAN, conforming structural change of chemical compounds present in DAN like water molecules, carboxyl groups, esters, aldehydes, ketones, acids and aromatic compounds.

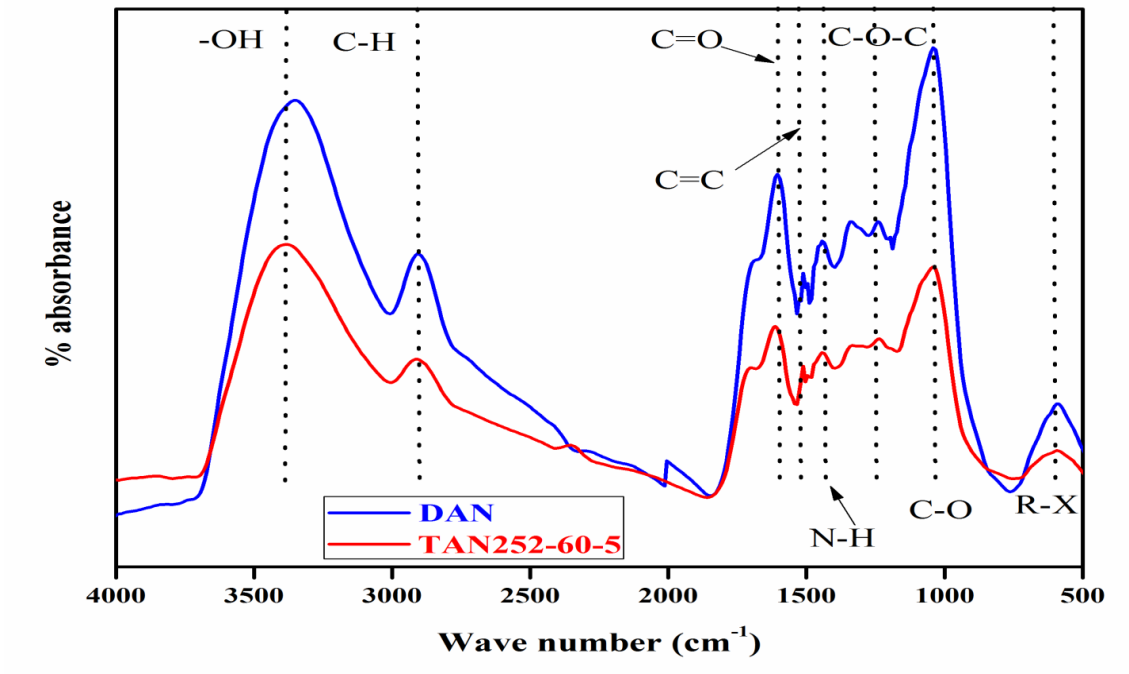

Figure 5.5 FTIR spectra of DAN and TAN252-60-5

5.3.9 Scanning electron microscope (SEM) and energy dispersive X-ray (EDX) analysis

To understand the influence of torrefaction on morphology of biomass, the scanning electron microscope images of DAN and TAN252-60-5 with 5000 magnification are presented in Fig. 5.6. The impact of thermal pretreatment could be seen in Fig. 5.6 (c). Generally, hemicelluloses are branched polysaccharides which contain strong bulky and branched tissues of xylem (Ibrahim et al., 2013). Branched structure on the surface of the DAN elucidates the presence of hemicellulose (Fig. 5.6 (a)). However, in case of TAN, these branched structures started disappearing, suggesting degradation of hemicellulose during torrefaction. The presence of pores is clearly visible for TAN252-60-5. The generation of pores in case of TAN252-60-5 is attributed to lower particle density than

DAN, which may decrease the grinding energy requirement for size reduction of DAN and increase in surface area. These are in agreement with the results reported by Ibrahim et al. (Ibrahim et al., 2013), Bach et al. (Bach & Skreiberg, 2016). Energy dispersive X-ray analysis is used to detect chemical elements present in the sample and to approximate their relative abundance. The EDX images of DAN and TAN252-60-5 are shown in Figs. 5.6 (b) and (d). It can be observed that in case of TAN252-60-5, some useful elements like Nitrogen (N), Calcium (Ca), Magnesium (Mg) and Potassium (K) appear with higher peak intensity along with Carbon (C) and Oxygen (O) than DAN indicating densification due to torrefaction. Oxygen gets reduced due to removal of –OH bonds, which is also supported by the FTIR analysis (Fig. 5.5). The increase in carbon content is also supported by enhanced fixed carbon content due to torrefaction, as presented in Table 5.4.

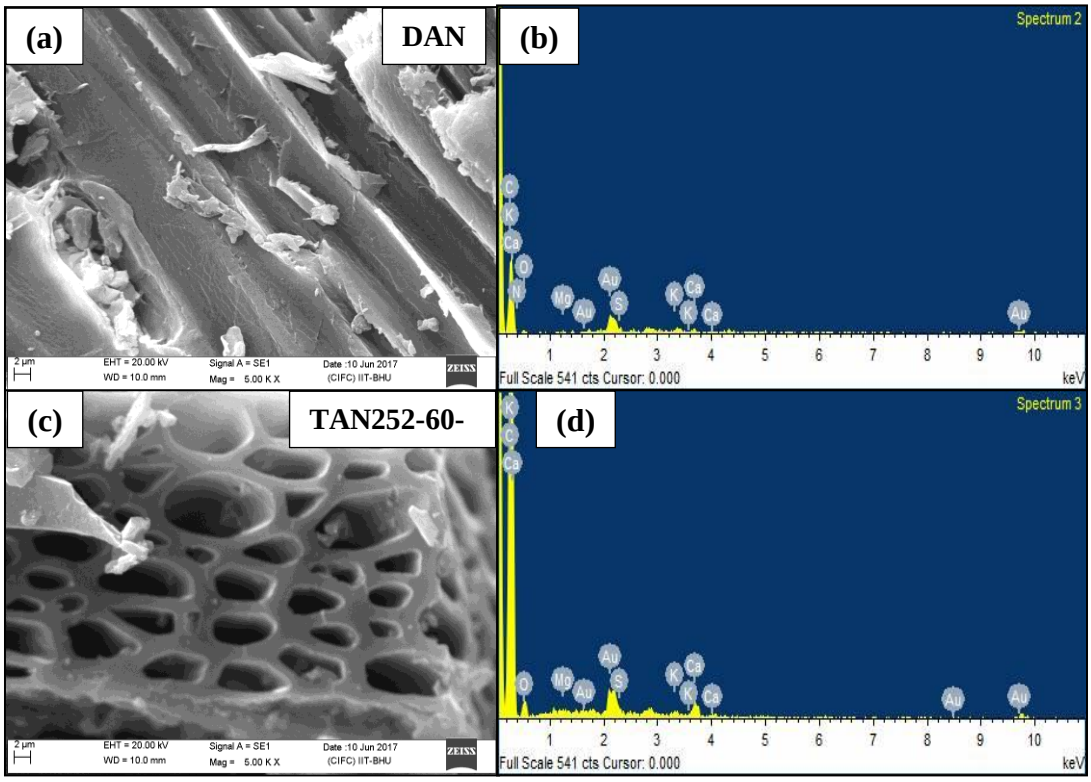

Figure 5.6 SEM and EDX images: (a) and (b) for DAN, (c) and (d) for TAN252-60-5

5.3.10 X-Ray diffraction (XRD) analysis

The major components of biomass are hemicellulose, cellulose and lignin. Among these, hemicellulose and lignin are amorphous in nature and cellulose is crystalline (Zheng et al., 2015). To investigate the effect of torrefaction on crystalline nature of DAN and TAN252-60-5, XRD analysis was performed and crystallinity index (CrI), FWHM of (002) peak and crystal size (L_{002}) were also calculated. The results are shown in Fig. 5.7 and Table 5.5. At 2θ = 22°, the strongest peak with highest intensity originated from 002 crystalline plane. It was observed that relative peak intensity of TAN252-60-5 is lower than the DAN. This shows that crystallinity of biomass decreased after torrefaction. Also, CrI of DAN and TAN252-60-5 was found to be 44.97 and 40.29 %, respectively, which confirm the decrease in crystallinity. The decrease in crystallinity might be due to disruption of intermolecular hydrogen bonding (Wannapeera & Worasuwannarak, 2015) and degradation of cellulose during torrefaction. FWHM of (002) peak increases in case of TAN252-60-5 with respect to DAN. The crystal size decreases in case of TAN252-60-5. Thus the crystal size of biomass decreases upon torrefaction. Similar results were obtained many researchers. Zheng et al. (Zheng et al., 2015) investigated the effect of torrefaction on crystalline behavior of corncob. They found that, at mild torrefaction, CrI of torrefied corncob increased, while at severe torrefaction CrI decreased due to degradation of crystalline cellulose of corncob. Similar results were also obtained by Wen et al. (Wen et al., 2014) during torrefaction of Bamboo.

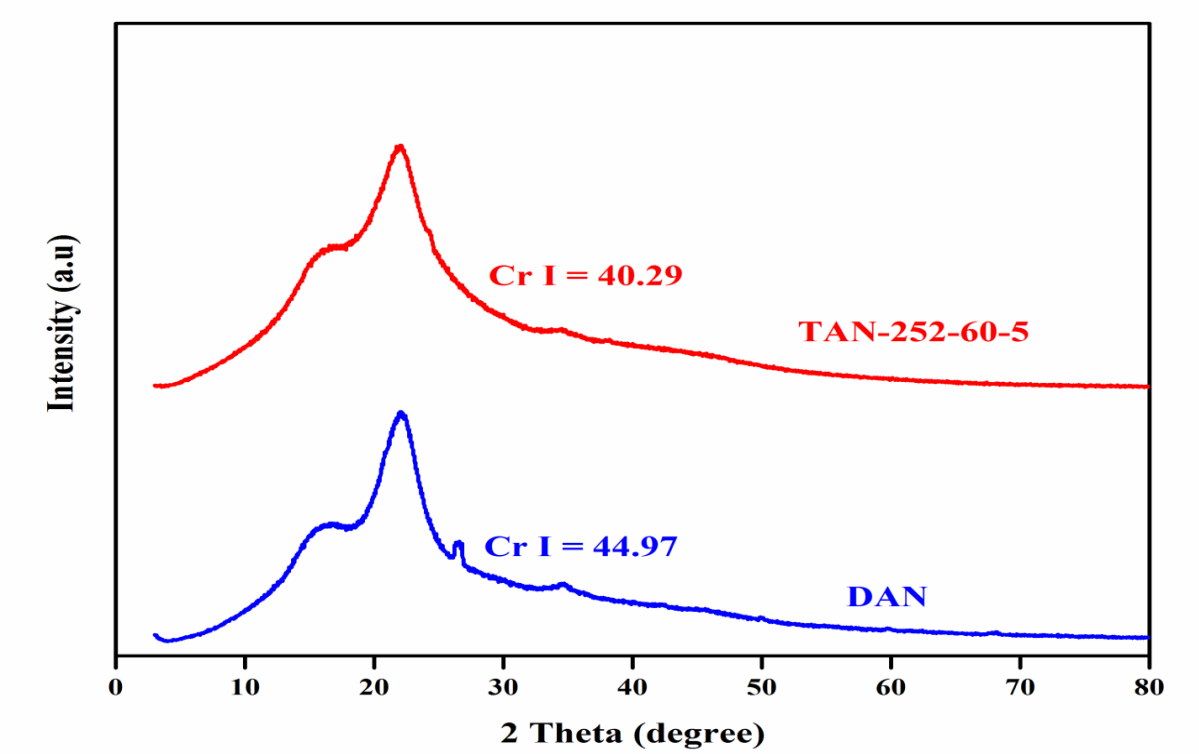

Figure 5.7 XRD spectra of DAN and TAN252-60-5

Table 5.5 Crystalline parameters of DAN and TAN252-60-5

Sample	CrI (%)	2θ (degree)		β^a(degree)	L_{002} (nm)
		I_{002}	I_{am}		
DAN	44.97	21.8	14.9	9.7	0.87
TAN252-60-5	40.29	21.7	14.5	11.5	0.73

[a] Full width at half maximum (FWHM) of (002) peak

5.3.11 Moisture absorption

Fig. 5.8 shows the percentage of moisture absorbed by DAN and TAN252-60-5. DAN and TAN252-60-5 absorbed 8.15 and 4.51 % moisture, respectively from open environment (average relative humidity of 60% $\pm$3) when kept for one day. After 5 days, percentage of moisture absorbed by DAN, and TAN252-60-5 are 34.44, and 7.12%, respectively. The water absorption capacity of biomass is associated with the amount of hemicellulose present in biomass. Hemicellulose contains many hydroxyl group (-OH) which compel biomass to be polar and form hydrogen bonds with water molecules easily. Due to torrefaction, hydroxyl bonds (-OH) in biomass are dissociated and became unsaturated having non-polar characteristics, which diminishes the attraction of biomass to form hydrogen bonds with water molecules (Bach & Skreiberg, 2016). TAN252-60-5 may also absorb less moisture due to deposition of tar, condensing on the surface (Ohm et al., 2015)**.** Tar deposition prevents the capillary rise of water molecules due to blockage of pores inside TAN252-60-5. The torrefaction makes biomass hydrophobic so that it engrosses lesser moistness and offers more stability to biomass when kept in open environment. This suggests that TAN obtained at higher temperature can be stored like coal in open environment, which significantly reduces transport, storage and handling cost of biomass.

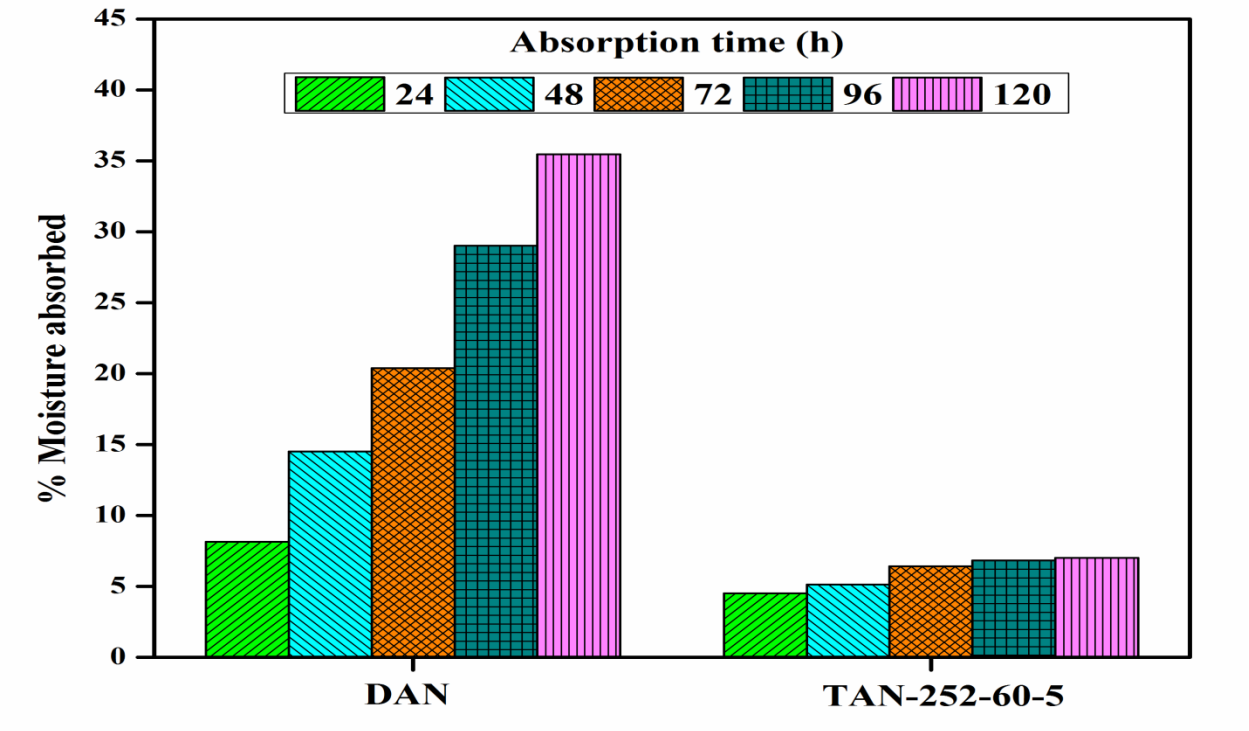

Figure 5.8 Moisture absorption characteristics of DAN and TAN252-60-5.

5.4 Conclusions

The torrefaction of *Acacia nilotica* was carried out in a laboratory scale fixed-bed reactor. The process parameters like temperature, retention time and heating rate were optimized for HHV and EY. A different set of parameters were obtained in case of optimum HHV and EY of TAN individually. The optimum value of temperature, retention time and heating rate to obtain maximum value of HHV and EY combined, were 252 ℃, 60 min, and 5 ℃/min, respectively. It was noted that the effect of temperature on torrefaction was significant, while effect of retention time and heating rate were minimal. Besides, the physical and chemical properties of DAN improved due to torrefaction. For example, MC,

H/C ratio and O/C ratio decreased by 73.23, 52.94 and 46.22 %, respectively; whereas FC content and HHV increased by 75.54 and 18.62 %, respectively. FR increased by 87.39 %; whereas, CI and VI decreased by 83.32 and 22.71 %, respectively. Flow properties such as angle of repose, HR, CCI and cohesion coefficient (C) decreased by 8.04, 6.20, 22.48, and 12.5 %, respectively. Bulk, tapped and particle densities of TAN252-60-5 were decreased by 16.4, 21.62 and 7.59 %, respectively. Moisture sorption test confirmed that TAN252-60-5 absorbed 27.32 % less moisture than DAN when kept in open environment at comparable relative humidity. TGA study suggests that onset of devolatilization shifted to higher temperature in case of TAN and char yield increased during pyrolysis of TAN. Torrefaction has greatly enhanced surface defects and reduced crystallinity of biomass as revealed by SEM-EDX and XRD analysis individually. Overall, it may be concluded that optimization of torrefaction process favors two aspects; first, it may reduce the operational cost during the scaling of process at industrial level. Secondly, TAN has much improved properties than DAN, which can increase the process efficiency during its utilization in pyrolysis, gasification and co-pyrolysis with coal in thermal power plants.

Chapter 6

Pyrolysis of torrefied biomass: Optimization of process parameters using response surface methodology, characterization, and comparison of properties of pyrolysis oil from raw biomass

General background

This chapter aimed to investigate the pyrolysis of torrefied *Acacia nilotica* (TAN-252-60-5) obtained during optimization of torrefaction process as discussed in Chapter 5. Considering pyrolysis oil as the desired product from pyrolysis process, the process parameters such as temperature (400-600 ℃), retention time (30-90 min), heating rate (15-40 ℃/min), and sweeping gas flow rate (40-80 mL/min) were optimized using response surface methodology for maximum pyrolysis oil yield. The raw *Acacia nilotica* (DAN) was also pyrolysed at obtained optimum condition for comparing the physicochemical characteristics of pyrolysis oil from DAN and TAN-252-60-5. The pyrolysis oil obtained from pyrolysis of TAN-252-60-5 (coded as PO-TAN) and from pyrolysis of DAN (coded as PO-DAN) were subjected to FTIR, GC-MS, and ^{13}C NMR analyses along with estimation of water content, pH, viscosity, HHV, etc., for comparing the physicochemical characteristics. In addition, characteristics of pyrolytic gases and biochar obtained at optimum condition form pyrolysis DAN and TAN-252-60-5 were also compared.

6.1 Introduction

The thermochemical processes, for example, combustion, pyrolysis, torrefaction, and gasification, have gained attraction to convert biomass into biofuels due to higher yield of product, lower operational cost, speed of reaction and higher efficiency (Dhanavath et al., 2019). In particular, pyrolysis has gained dominance for conversion of biomass into biochar, pyrolysis oil, and valuable gases (Abas et al., 2018). In pyrolysis process, biomass gets decomposed at elevated temperature in an inert atmosphere (Dai et al., 2019). Pyrolysis oil has been considered as most valuable product from pyrolysis (Guedes et al., 2018). The pyrolysis process is driven by many factors, for example, process temperature (T), retention time (RT), heating rate (HR), sweeping gas flow rate (SGF), and particle size, etc. (Dhyani & Bhaskar, 2018). The optimization of these process parameters becomes very important when it comes to efficiency, economy, and scale-up of pyrolysis reactor system (Singh et al., 2019b).

The pyrolysis oil is an intense dark brown-colored liquid that consists of a large number of chemical compounds (Dhyani & Bhaskar, 2018). Currently, pyrolysis oil is receiving enormous interest since it is regarded as a second-generation biofuel (Lazzari et al., 2019) and may be utilized as a fuel in furnaces, boilers, and engines for generation of heat and power (Zhang et al., 2017) or it may be a good source of various chemicals (Dhyani & Bhaskar, 2018). The pyrolysis of different types of raw biomass and optimization of process parameters for maximum yield of pyrolysis oil has been investigated by many researchers, as mentioned in Chapter 2. However, pyrolysis oil obtained from raw biomass has some drawbacks, for example, high water content, poor volatility, higher acidic value, low heating value, chemical instability, and undesired aging problem (Ro et al., 2018;

Zhang et al., 2017). These characteristics of pyrolysis oil hampered its direct and efficient utilization as fuel (Zhang et al., 2017). Thus, it cannot compete with conventional fuels such as gasoline and diesel. So, there is an urgent demand for upgrading of pyrolysis oil. Various efforts have been made in this field such as catalytic pyrolysis and pretreatment of biomass by torrefaction (Singh et al., 2019b), hydrothermal liquefaction (Nazari et al., 2017) prior to pyrolysis.

The base of the torrefaction is to optimize the operating condition, which can yield improved quality torrefied biomass. However, pyrolysis of that improved torrefied biomass (having maximum HHV and energy yield simultaneously) gained at optimum condition of torrefaction has not been investigated. Less attention has been given towards HHV and energy yield of torrefied biomass. The HHV and energy yield of torrefied biomass are very crucial parameters for energy utilization and densification (Singh et al., 2019b) and play a vital role in deciding quality and quantity of pyrolysis oil obtained from pyrolysis of torrefied biomass. Both these parameters display opposite trend during torrefaction process. The HHV of torrefied biomass increased, while energy yield decreased with temperature. Thus, considering these two parameters, torrefaction process has to be optimized for maximum HHV and energy yield of torrefied biomass. In our previous work (Chapter 6) we have optimized the torrefaction process for maximum HHV and energy yield (Singh et al., 2019b). The optimum condition was attained at 252 ℃, retention time of 60 min, and heating rate of 5 ℃/min. Therefore, in this Chapter, two-stage optimization (optimization of torrefaction process (Stage-1), optimization of pyrolysis process (Stage-2)) of integrated torrefaction-pyrolysis process has been reported.

6.2 Experimental segment

6.2.1 Sample preparation

Torrefied *Acacia nilotica* at optimum torrefaction condition of 252 ℃, 60 min retention time, and 5 ℃/min heating rate (TAN-252-60-5) has been considered as a feedstock for pyrolysis process. Multiple runs of DAN were performed at optimum torrefaction condition for collection of TAN-252-60-5. The detailed discussion about collection, preparation, physicochemical characteristics of DAN has been discussed in Chapter 3.

6.2.2 Design of experimental condition using RSM

To increase the pyrolysis oil yield, it is imperative to know the behavior of each parameter towards the pyrolysis process. This can be done by optimization of process parameters affecting the pyrolysis process. RSM has been considered as one of the most promising and prevalent techniques used for the optimization of process. A three-level, four-factor CCD technique was employed to optimize the independent process variables. The CCD technique was used since it requires minimum set of experimental runs to establish a correlation among independent variables and desired response. Temperature (A), RT (B), HR (C) and SGF (D) in the range of 400-600 ℃, 30-90 min, 15-40 ℃/min and 40-80 mL/min, respectively, were considered as independent process parameters and pyrolysis oil yield was considered as the desired response that needs to be maximized. Table 6.1 represents the coded values of independent process variables. CCD technique consists of axial points (2k), factorial points (2^k), and replicates center points (n_k). The number of experimental runs to be carried out was calculated according to Eq. (6.1):

$$N = 2^k + 2k + n_k = 2^4 + 2(4) + 6 = 30 \quad (6.1)$$

where N signifies number of experimental runs to be carried out, k signifies selected independent variables, and n_k signifies number of replicate central points.

Table 6.1 Coded levels of experimental variables used in CCD method

Independent process variable	Coded experimental levels		
	−1	0	+1
Temperature (℃): A	400	500	600
Retention time (min): B	30	60	90
Heating rate (℃/min): C	15	27.5	40
Sweeping gas flow rate (mL/min): D	40	60	80

The matrix for different experimental conditions is presented in Table 6.2. As per the design matrix, total of 30 experiments were carried out. The yield of pyrolysis oil as the response was correlated with selected independent variables. Few fundamental steps have to be followed during optimization of process variables. First one is to develop a general mathematical relationship among process response and independent variables, given as:

$$Y = f(X_1, X_2, X_3,\ldots\ldots, X_n) \quad (6.2)$$

where Y signifies the desired predicted response, *f* signifies the mathematical relation between desired predicted response and independent process variables, and X_1, X_2,

X_3,…….. X_n signifies n number of independent process variables affecting the desired predicted outcome.

The second step is related to finding the coefficients of developed mathematical co-relation. In CCD technique, usually, a quadratic polynomial equation is suggested for predicting the response. The general quadratic polynomial model of the response can be presented as follows:

$$Y = \beta_0 + \sum_{i=1}^{k} \beta_i X_i + \sum_{i=1}^{k} \beta_{ii} X_i^2 + \sum_{i_{i>j}}^{k} \sum_{j}^{k} \beta_{ij} X_i X_j \quad (6.3)$$

where Y signifies the predicted value of the response, β_0, β_i, β_{ii} , and β_{ij} are constant term and coefficient for linear, quadratic, and interaction terms, respectively, in developed model equation. k signifies the number of independent process variables chosen for optimization of process (here k = 4).

Table 6.2 Experimental design matrix, actual and predicted value of responses

Run	Temp (^{o}C)	Retention time (min)	Heating rate (^{o}C/min)	Sweeping gas flow rate (mL/min)	Pyrolysis oil yield (wt %)	
					Actual	Predicted
1	500 (0)*	60 (0)	27.5 (0)	80 (+1)	33.46	32.91
2	500 (0)	60 (0)	27.5 (0)	60 (0)	31.65	31.63
3	600 (+1)	90 (+1)	40 (+1)	80 (+1)	26.38	26.55
4	600 (+1)	30 (−1)	15 (−1)	40 (−1)	23.76	24.23
5	500 (0)	90 (+1)	27.5 (0)	60 (0)	28.35	28.70
6	400 (−1)	90 (+1)	15 (−1)	80 (+1)	21.93	21.95
7	600 (+1)	90 (+1)	15 (−1)	80 (+1)	22.97	22.86
8	400 (−1)	30 (−1)	40 (+1)	40 (−1)	22.67	23.22
9	500 (0)	60 (0)	27.5 (0)	60 (0)	31.77	31.63
10	400 (−1)	90 (+1)	40 (+1)	40 (−1)	23.60	23.73
11	500 (0)	60 (0)	27.5 (0)	60 (0)	30.93	31.63
12	600 (+1)	30 (−1)	40 (+1)	80 (+1)	25.92	26.56

13	400 (−1)	90 (+1)	15 (−1)	40 (−1)	21.67	21.48
14	400 (−1)	30 (−1)	15 (−1)	40 (−1)	23.95	23.37
15	500 (0)	60 (0)	27.5 (0)	60 (0)	31.92	31.63
16	500 (0)	60 (0)	27.5 (0)	60 (0)	31.67	31.63
17	500 (0)	60 (0)	27.5 (0)	60 (0)	31.41	31.63
18	500 (0)	60 (0)	15 (−1)	60 (0)	30.35	30.98
19	600 (+1)	90 (+1)	40 (+1)	40 (−1)	26.10	25.99
20	500 (0)	60 (0)	40 (+1)	60 (0)	33.51	32.75
21	500 (0)	30 (−1)	27.5 (0)	60 (0)	30.14	29.65
22	400 (−1)	60 (0)	27.5 (0)	60 (0)	24.37	24.08
23	600 (+1)	30 (−1)	15 (−1)	80 (+1)	25.81	25.27
24	500 (0)	60 (0)	27.5 (0)	40 (−1)	32.11	32.51
25	400 (−1)	30 (−1)	15 (−1)	80 (+1)	23.06	23.61
26	600 (+1)	90 (+1)	15 (−1)	40 (−1)	21.85	21.60
27	600 (+1)	30 (−1)	40 (+1)	40 (−1)	26.66	26.23
28	600 (+1)	60 (0)	27.5 (0)	60 (0)	25.88	26.04
29	400 (−1)	30 (−1)	40 (+1)	80 (+1)	22.91	22.75
30	400 (−1)	90 (+1)	40 (+1)	80 (+1)	23.52	23.49

*Values in the parenthesis are coded level in response surface methodology

In third step, ANOVA is employed to analyze the result of optimization process. The yield of pyrolysis oil, obtained from experiments was taken as actual values, while, predicted values were obtained from a software package (Stat-Ease Design-Expert version 11, USA). The statistical fitness of developed model was investigated by several variables provided in ANOVA analysis. The dependence of yield of pyrolysis oil on different independent variables was checked by p and F values. In addition, various determination coefficients such as R^2, R^2_{pred}, and R^2_{adj}, as well as degree of freedom, were also analyzed to authenticate the reliability of the developed model. Further, the impact of individual and interaction terms of independent process variables on pyrolysis oil yield was examined by 3D surface and contour plots.

6.2.3 Experimental process for pyrolysis

The detailed about the experimental setup and procedure for torrefaction has been mentioned in Chapter 3. In this study, similar procedure was followed during pyrolysis. The pyrolysis of TAN-252-60-5 was carried out between 400-600 ℃ with RT 30-90 min, HR 15-40 ℃/min, and SGF 40-80 mL/min as per the experimental design matrix presented in Table 6.2. During each pyrolysis experiment, 4 g of TAN-252-60-5 was used. Every experiment under similar operating conditions was repeated twice for validation of results. The yield of pyrolysis oil, biochar and pyrolytic gases were obtained by using Eq. (6.4)-(6.6):

$$\text{Pyrolysis oil yield (wt \%)} = \frac{\text{Wt. of bio-oil(g)}}{\text{Wt. of TAN-252-60-5 (g)}} \times 100 \quad (6.4)$$

$$\text{Biochar yield (wt \%)} = \frac{\text{Wt. of biochar(g)}}{\text{Wt. of TAN-252-60-5 (g)}} \times 100 \quad (6.5)$$

$$\text{Pyrolytic gas yield (wt \%)} = 100 - (\text{Pyrolysis oil yield} + \text{Biochar yield}) \quad (6.6)$$

Now, considering upgraded pyrolysis oil as desired product from pyrolysis of TAN-252-60-5, the energy yield and energy conversion efficiency can be obtained by using Eq. (6.7) and Eq. (6.8), respectively.

$$\text{Energy yield of pyrolysis oil} = \text{mass yield} \times \frac{HHV\ of\ pyrolysis\ oil}{HHV\ raw\ Acacia\ nilotica} \quad (6.7)$$

$$\text{Energy conversion efficiency} = \frac{Energy\ output}{Energy\ input} \times 100 \quad (6.8)$$

where energy input and energy output can be calculated by using Eq. (6.9) and Eq. (6.10), respectively.

$$\text{Energy input} = \text{weight of DAN} \times \text{HHV of DAN} \quad (6.9)$$

$$\text{Energy output} = \text{weight of pyrolysis oil} \times \text{HHV of pyrolysis oil} \quad (6.10)$$

6.2.4 Analysis of pyrolysis oil, biochar and pyrolytic gases obtained at optimum condition of pyrolysis

The pyrolysis oil obtained from both the feedstocks at optimum conditions were subjected to estimation of physicochemical characteristics. The HHV of pyrolysis oil and biochar was enumerated using a bomb calorimeter (Model C-200, IKA, Germany). The Ramsbottom Carbon residue (RCR- IP 14/65) method was employed for the estimation of carbon residue of pyrolysis oil. ASTM D1298 protocol was employed to estimate the density of pyrolysis oil. The water content of pyrolysis oil was assessed by applying Karl Fischer titrator (ESICO, μP KARL FISCHER moisture titrator) following ASTM D1744 protocol. The viscosity of pyrolysis oil was measured using Brookfield digital viscometer (LVDV-II+Pro). The chemical characteristics, functional groups, and various classes of chemical compounds present in pyrolysis oil were examined by employing FTIR and GC-MS analyses, respectively. Fourier transform infrared spectroscopy (FTIR, Varian 1000, USA) was used to recognize the characteristic peaks associated with various chemical compounds associated with pyrolysis oil and biochar, while GC-MS (model-Shimadzu QP 2010 plus) was used to determine the relative amount of various class of chemical. Helium was used as a carrier gas with 1.21 mL/min flow rate. 1 μL of PO-DAN and PO-TAN-252-60-5 was injected (injector temperature of 260 ℃) into the column (-RXi-5 Sil MS) having dimension of (30 m X 0.25 mm X 0.25 µm). The split ratio of column was 10:1. The initial temperature of GC oven was kept at 50 ℃ (5 min hold) and then heated to 250 ℃ at a rate of 5 ℃/min (again 5 min hold). Finally, the oven heated to 280 ℃ at a rate of 10 ℃/min for holding time of 5 min. The peaks obtained have been identified by using the National Institute of Standards and Technology library (NIST, USA). ^{13}C nuclear magnetic

resonance spectrometry was used to analyze the various type of carbon, and their distribution in PO-DAN and PO-TAN obtained at optimum condition of pyrolysis. The pyrolysis oil was dissolved in deuterated chloroform ($CDCl_3$), and NMR spectra were recorded by Bruker 500 MHz spectrometer (Magnetic system 500'54 ascend ULH) operating at 5 T with a 5 mm BBO BB-1H probe at room temperature with a relaxation delay of 2 s. The standard protocols ASTM E871 for moisture content, ASTM E1755 for ash content, and ASTM E872 for volatile matter were followed to execute proximate analysis of biochar from DAN and TAN-252-60-5. The fixed carbon of both biochars was obtained by difference. The CHNS analyzer instrument and software (EURO EA3000, EURO VECTOR, Italy) was used to investigate the elemental composition of both biochars. The elemental oxygen was obtained by difference considering insignificant sulfur content. The surface characteristics such as morphology and elements that exist on surface of biochar from pyrolysis of DAN and TAN-252-60-5 were studied by Scanning Electron Microscopy (SEM) and Energy-Dispersive X-ray spectroscopy (EDX) (Model JEOL JSM5410, Japan). The pyrolytic gases were analyzed in gas chromatography (GC-TCD Centurion Scientific, model number-5800, New Delhi). Argon was used as carrier gas. The injector, column, and detector temperature were 80, 60, and 150 ℃, respectively.

6.3 Results and discussion

6.3.1 Statistical analysis of developed model

Fig. 6.1 shows the actual and predicted values of response variable (pyrolysis oil yield), where 45° line represents the predicted yield, and the discrete data points represent experimental yield. It is perceived that both actual and predicted values of response are

very close over a wide range of yield of pyrolysis oil; thus, it may be suggested that the developed model excellently represents pyrolysis data. Also, the correlation coefficient (R^2) value is 0.9758, suggesting that developed relation between independent and dependent variables is highly reliable. The polynomial equation between response (pyrolysis oil yield) and variables (T (A), RT (B), HR (C), and SGF (D)) is given by Eq. (6.11).

$$Y_{\text{pyrolysis oil}}\ (\text{wt \%}) = 31.76 + 0.979A - 0.474B + 0.884C + 0.536AC + 0.599BC - 6.01A^2 - 1.90B^2 \quad (6.11)$$

The statistical fitness of developed model has been investigated by ANOVA. The ANOVA is presented in Table 6.3. The statistical fitness of developed model is also confirmed by p-value, which is < 0.005, and higher F-value of 126.59. The model terms having a p-value < 0.0500 are significant. In present developed model, A, B, C, AC, BC, A^2, B^2 are significant model terms. The discrepancy among predicted R^2 and adjusted R^2 should be $<$ 0.2 for reasonable agreement between two coefficients. In this case, predicted R^2 and adjusted R^2 values were 0.9548 and 0.9681, respectively, showing a good agreement. Adequate precision signifies the signal to noise ratio, and its value should be > 4 for significant model. In the case of present developed model, the value of adequate precision was 30.403 showing that developed model can be used for design and scale-up.

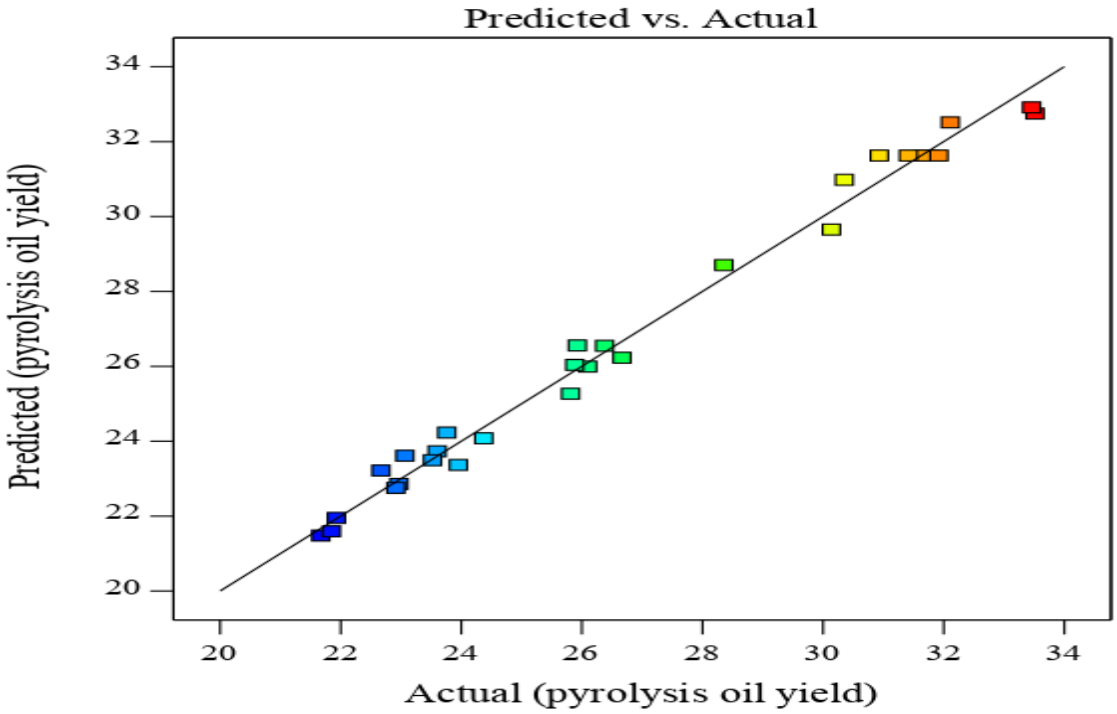

Figure 6.1 Relationship between actual and predicted values of pyrolysis oil

6.3.2 Effect of process variables on yield of pyrolysis oil

6.3.2.1 Individual effect of process parameters

The pyrolysis of biomass was carried out by varying four independent parameters, namely, temperature, heating rate, retention time, and sweeping gas flow rate. The temperature during the pyrolysis supply the required heat for cleavage of bonds associated with biomass (Guedes et al., 2018). As a result, the pyrolysis oil yield increased with increase in temperature, however, after certain temperature, secondary cracking of volatiles dominates, which results in decrease in pyrolysis oil yield and increase in yield of pyrolytic gases

(Guedes et al., 2018). The heating rate during the pyrolysis of biomass significantly affects the yield of pyrolysis oil. In the selected range of heating rate (15-40 ℃/min), the yield of pyrolysis oil increased monotonously with heating rate. Thus, maximum yield of pyrolysis oil was obtained at 40 ℃/min. The higher heating rate during pyrolysis favors the thermal cracking, fragmentation, and depolymerization reaction of biomass, which results in increase in yield of pyrolysis oil (Tripathi et al., 2016). The yield of pyrolysis oil decreased with increase in retention time during pyrolysis of biomass because higher retention time favors cross-linking and repolymerization reaction of biomass, which supports the formation of biochar (Akhtar & Saidina Amin, 2012). The pyrolysis environment also affects the yield of pyrolysis oil. At lower sweeping gas flow rate, the interaction between vapor and solid causes exothermic reaction (Akhtar & Saidina Amin, 2012). As a result, biochar yield increased at lower sweeping gas flow rate. However, at very high sweeping gas flow rate, the condensable vapor might be drained out of the reactor, which may also decrease the yield of pyrolysis oil (Demiral & Şensöz, 2006). Meanwhile, it is important to mention that the effect of individual parameters is also governed by other parameters during pyrolysis process. The interaction of process variables is, therefore, of crucial importance for deciding the yield of pyrolysis oil.

6.3.2.2 Interaction effect of process parameters based on RSM on yield of pyrolysis oil

The effect of process variables (T, RT, HR, and SGF) on the pyrolysis oil yield was examined by 3D surface and contour plots using RSM exported from Design-Expert software. In 3D plots, the impact of two parameters was investigated at one time on

pyrolysis oil yield. The remaining two parameters were kept constant because it is not possible to show the effect of more than two parameters simultaneously on 3D plots (Mohammed et al., 2017c). The significance of individual parameters, their interaction effect with each other, and square of parameters on pyrolysis oil yield was deduced using ANOVA.

Fig. 6.2 (a and b) represent the 3D surface and contour plot for pyrolysis oil yield where the combined influence of temperature and retention time at fixed heating rate (27.5 ℃/min) and sweeping gas flow rate (60 mL/min) was examined. Results displayed that the pyrolysis oil yield increased to a maximum value, then started to decrease as the temperature and retention time continuously increased. An increase in temperature favors the formation of more volatiles; however, after specific temperature, due to secondary cracking reaction, volatiles might be converted into gaseous products such as H_2, CH_4, and CO (Guedes et al., 2018). While, increase in retention time favors the cross-linking and repolymerization reaction, which results in higher bio-char yield (Akhtar & Saidina Amin, 2012). From Table 6.3, it can be observed that temperature (A) is having F-value 33.97 and 244.97 for individual and square terms, respectively, and p-value less than 0.005 for both the terms. For retention time (B), the F-value for individual and square term is 7.96 and 24.35, respectively, and the p-value less was than 0.005 for both the terms. Thus, temperature (A) and retention time (B) individually and their squared terms (A^2, B^2) are significant for maximum yield of pyrolysis oil. However, interaction term (AB) related to temperature and retention time is not significant due to its p-value (0.2049) greater than 0.005. Similarly, the term (AD), which corresponds to the interaction between temperature and sweeping gas flow rate, is not significant because of higher p-value (0.1808). The p-

value of all non-significant terms is not shown in ANOVA table since only significant terms have been considered and mentioned in ANOVA table.

Table 6.3 ANOVA of quadratic model for pyrolysis oil response and corresponding model terms

Source	Sum of square	Degree of freedom	Mean of square	F-value	p-value	Remark
Pyrolysis oil yield						
Model	**450.70**	**7**	**64.39**	**126.59**	**< 0.0001**	Significant
A-Temp	17.28	1	17.28	33.97	< 0.0001	Significant
B-RT	4.05	1	4.05	7.96	0.0100	Significant
C-HR	14.09	1	14.09	27.71	< 0.0001	Significant
AC	4.61	1	4.61	9.07	0.0064	Significant
BC	5.76	1	5.76	11.32	0.0028	Significant
A^2	124.59	1	124.59	244.97	< 0.0001	Significant
B^2	12.38	1	12.38	24.35	< 0.0001	Significant
Residual	4.79	15	0.3191			
Lack of Fit	10.58	17	0.6223	5.10	0.0802	not significant
Pure Error	0.6097	5	0.1219			
Cor Total	461.89	29				
Std. Dev		0.7132		R-Squared		0.9758
Mean		27.01		Adjusted R-Squared		0.9681
C.V		2.64		Predicted R-Squared		0.9548
PRESS		27.24		Adequate Precision		30.407

The coupled impact of temperature and heating rate at fixed retention time and sweeping gas flow rate of 60 min and 60 mL/min, respectively, are displayed in Fig. 6.2 (c and d). The results inferred that pyrolysis oil yield increased with an increase in heating rate, and the maximum yield of pyrolysis oil was attained at the highest value of heating rate. In contrast to temperature, pyrolysis oil yield increased to a maximum value then started to decrease. The thermal cracking and fragmentation of biomass occur with increased heating

rate during pyrolysis, which increases the pyrolysis oil yield (Tripathi et al., 2016). Also, heating rate during pyrolysis significantly affects the depolymerization reaction of biomass, which releases primary volatile components and added to the more liquid condensate (Dhyani & Bhaskar, 2018). Statistically, the individual term related to heating rate (C) and interaction term of heating rate with temperature (AC) is significant since both the terms have a lower p-value than 0.005 (Table 6.3). The F-values for temperature and heating rate are 33.97 and 27.71, respectively. Thus, the temperature influences pyrolysis more markedly than heating rate. However, the squared term related to heating rate (C^2) is not significant due to its higher p-value (0.5103).

Fig. 6.2 (e and f) display the coupled influence of temperature and sweeping gas flow rate at a constant heating rate (27.5 ℃/min) and retention time (60 min). The result shows that the maximum pyrolysis oil yield was obtained at a minimum sweeping gas flow rate in the selected range (40-80 mL/min). At a higher gas flow rate, the vapor formed might be drained out from the condenser. As a result, pyrolysis oil yield decreases, and gaseous yield increases (Guedes et al., 2018). However, at a very low sweeping gas flow rate, retention time of vapor inside the reactor increases, which might result in a secondary cracking reaction of vapor (Tripathi et al., 2016). The statistical analysis confirmed that all the terms (individual, squared, and interaction with temperature) related to the sweeping gas flow rate are not significant for maximum yield of pyrolysis oil because of higher p-value (Table 6.3). The interaction effect of heating rate and retention time is shown in Fig. 6.2 (g and h), while, interaction effect of sweeping gas flow rate and retention time is shown in Fig. 6.2 (i and j). The flat nature of 3D plots indicates that coupled effect of these process variables on the yield of pyrolysis oil is minimal in the selected range of variables. Similar results were

also obtained in case of effect of sweeping gas flow rate and heating rate on pyrolysis oil yield, as shown in Fig. 6.2 (k and l). Thus, based on the F-value obtained from ANOVA, temperature is the most significant parameter followed by heating rate, retention time, and sweeping gas flow rate, respectively, for maximum pyrolysis oil yield.

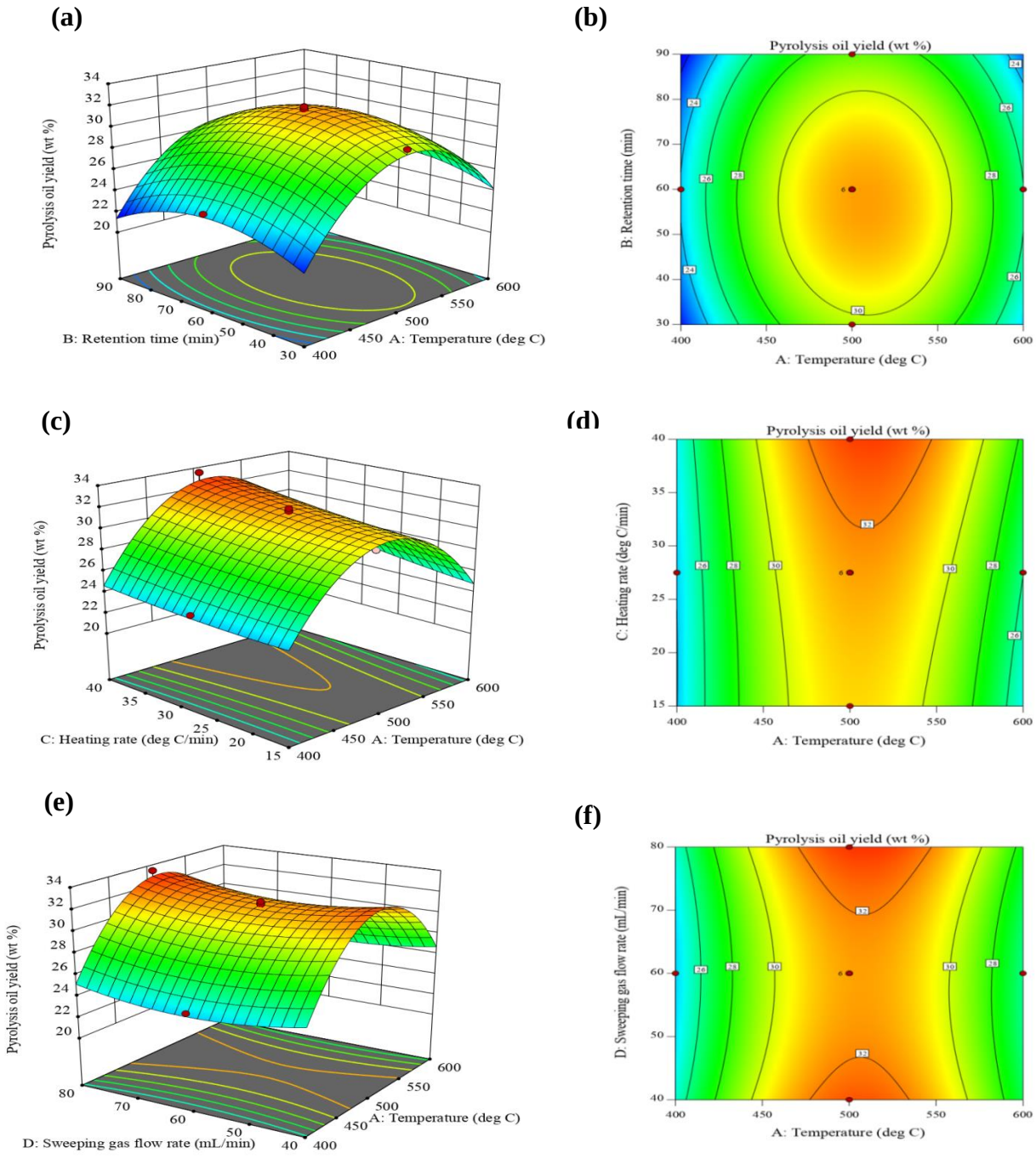

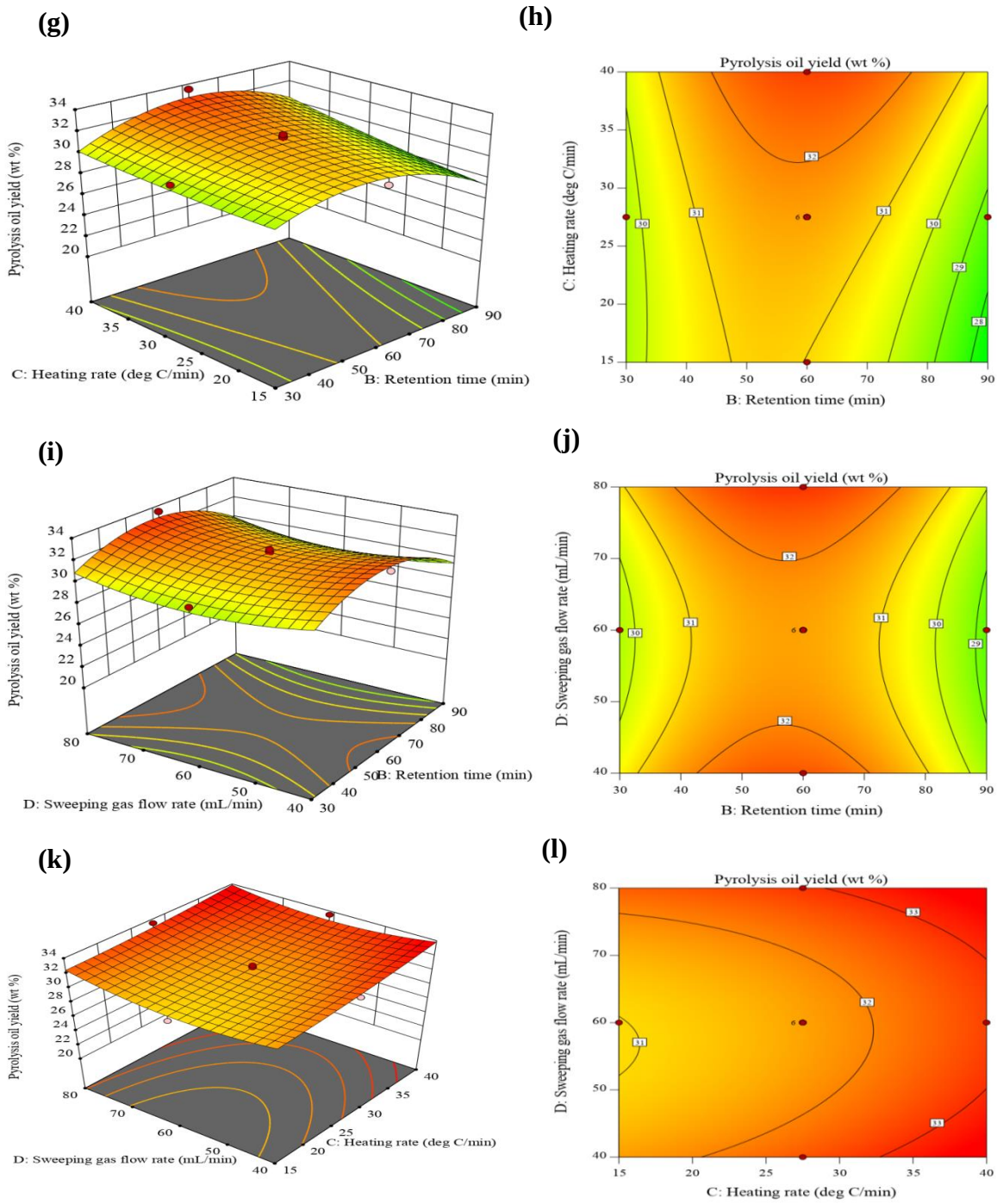

Figure 6.2 Three dimensional response surface and contour plots of pyrolysis oil yield depicting the effect of (a) and (b) temperature and retention time, (c) and (d) temperature and heating rate, (e) and (f) temperature and sweeping gas flow rate, (g) and (h) retention time and heating rate, (i) and (j) retention time and sweeping gas flow rate, (k) and (l) heating rate and sweeping gas flow rate

6.3.3 Validation of process parameters for yield of pyrolysis oil

The optimum condition for the experiment was attained by considering the independent process parameters in experimental range and dependent parameter (pyrolysis oil yield) to be the maximum (Table 6.4). Considering the above conditions, total hundred solutions were provided by the design expert statistical software. However, the solution having the highest desirability was taken into consideration. The optimum values of independent process variables for maximum pyrolysis oil yield (33.56 wt %) were found to be: T of 507.04 ℃, RT of 58.25 min, HR of 38.00 ℃/min, and SGF of 40.53 mL/min. This optimum condition obtained by design expert software was experimentally validated by performing the actual experiments at slightly different conditions (T of 507 ℃, RT of 58 min, HR of 38 ℃/min, and SGF of 40 mL/min) due to instrumental constraints of electric furnace and mass flow controller. The experimental and predicted values are given in Table 6.5. Based on the difference in experimental and predicted value of yield of pyrolysis oil, the error was calculated and mentioned in Table 6.5. The experimental and predicted values for yield of pyrolysis oil were close enough (Error 3.64%) to certify the reliability of developed model. Further, at similar optimum conditions (T of 507 ℃, RT of 58 min, HR of 38 ℃/min, and SGF of 40 mL/min), pyrolysis of DAN was also performed to examine the differences in physicochemical properties of pyrolysis oil from DAN and TAN-252-60-5. During each pyrolysis experiment, 4 g of TAN-252-60-5 and DAN was used. The experiments were carried out in replicate, and average yield of pyrolysis oil was reported. The yield of pyrolysis oil at optimum condition was 34.83 wt % for pyrolysis of TAN-252-60-5, while it was 45.62 wt % for pyrolysis of DAN.

Table 6.4 Independent variables and response as constraints for optimization

Parameters	Objective	Lower limit	Upper limit
Temperature (^{o}C)	In range	400	600
Retention time (min)	In range	30	90
Heating rate (^{o}C/min)	In range	15	40
Sweeping gas flow rate (mL/min)	In range	40	80
pyrolysis oil yield	Maximum	21.67	33.51

Table 6.5 Experimental and predicted values of pyrolysis oil yield at optimum condition

Run	Temp (℃)	RT (min)	HR (℃/min)	SGF (mL/min)	Yield of pyrolysis oil from TAN-252-60-5 (wt %)		Error (%)
					Experimental	Predicted	
1	507	58	38	40	34.58	33.56	2.94
2	507	58	38	40	35.08	33.56	4.33
Average					34.83	33.56	3.64
At similar optimum condition the yield of pyrolysis oil for DAN was 45.62 wt %							

6.3.4 Yield of pyrolysis oil, biochar and pyrolytic gases at optimum condition from pyrolysis of DAN and TAN-252-60-5

Table 6.6 represents the product yield obtained from pyrolysis of DAN and TAN-252-60-5 at optimum condition of pyrolysis of TAN-252-60-5 for maximum pyrolysis oil yield. Results showed that yield of pyrolysis oil was 10.79 wt % lower, while, yield of pyrolytic

gases and biochar was 3.05 and 7.74 wt %, respectively, was higher for TAN-252-60-5 as compared to DAN. These results were in accordance with the published literature (Chen et al., 2016c; Dai et al., 2019; Zheng et al., 2013). The yield of pyrolysis oil is lower due to lower volatile matter of TAN-252-60-5 and decomposition of lighter volatile compounds into CO_2, CO, H_2O, and acetic acid (Boateng & Mullen, 2013b). Also, the higher ash content of TAN-252-60-5 (Singh et al., 2019b) may catalyze the pyrolysis process to decrease the yield of pyrolysis oil by secondary cracking reaction (Yildiz et al., 2015). The solid biochar yield is higher (Boateng & Mullen, 2013b; Singh et al., 2020b) because of higher cross-linking reaction and charring of TAN-252-60-5 during pyrolysis. The energy yield of pyrolysis oil was evaluated by employing Eq. (6.7). The energy yield of pyrolysis oil represents the amount of energy retained in the pyrolysis oil after pyrolysis (Singh et al., 2019b). The energy yield of pyrolysis oil obtained from pyrolysis of DAN and TAN-252-60-5 was found to be 58.42 and 53.15 %, respectively. The lower value of energy yield for pyrolysis oil from TAN-252-60-5 was obtained because of lower pyrolysis oil yield (Chen et al., 2016a). The energy conversion efficiency for pyrolysis oil was evaluated by employing Eq. (6.8) and it was found to be 58.41 and 43.23 % for pyrolysis oil from DAN and TAN-252-60-5, respectively. The lower energy conversion efficiency was noted for pyrolysis of TAN-252-60-5 due to lower yield of pyrolysis oil.

Table 6.6 The average **y**ield of pyrolysis oil, pyrolytic gases and biochar at optimum condition from pyrolysis of DAN and TAN-252-60-5

Yield	Pyrolysis of DAN	Pyrolysis of TAN-252-60-5
Pyrolysis oil (wt %)	45.62	34.83
Pyrolytic gas (wt %)	20.62	23.67
Biochar (wt %)	33.76	41.50

6.3.5 Characteristics of pyrolysis oil obtained at optimum condition of pyrolysis

6.3.5.1 Fourier transform infrared spectroscopy of pyrolysis oil

The FTIR analysis of PO-DAN and PO-TAN obtained at optimum conditions are performed, and their spectra are depicted in Fig. 6.3. The FTIR spectra confirm the existence of various functional groups related to different classes of compounds. The stretching vibration of O-H between 3200-3400 confirms the presence of phenol, alcohol, water; while, vibration of C=O between 1680-1750 cm^{-1} corresponds to aldehyde and ketones (Gupta & Mondal, 2019). The vibration related to C-H stretching and deformation in the waveband of 2855-2926 and 1362-1462 cm^{-1}, respectively, corresponds to presence of alkane in pyrolysis oil (Mandal et al., 2018). The absorption band between 1420- 1610 $cm^{-1}$and 690-900 cm^{-1} ascribes the presence of mono, polycyclic, and substituted aromatic compounds (Isa et al., 2011). Also, for PO-TAN, the intensity of peaks are higher than PO-DAN, indicating the higher amount of aromatic compounds. The reduction of peaks intensity for PO-TAN, between wave number 1100-1260 cm^{-1} attributed to reduction of oxygenated compounds related to alcohol and ether. The FTIR analysis provides a quick technique to identify the class of various chemical compounds (Isa et al., 2011), while gas chromatography-mass spectrometry analysis (GC-MS) can be employed for quantitative analysis of various chemical compounds present in pyrolysis oil.

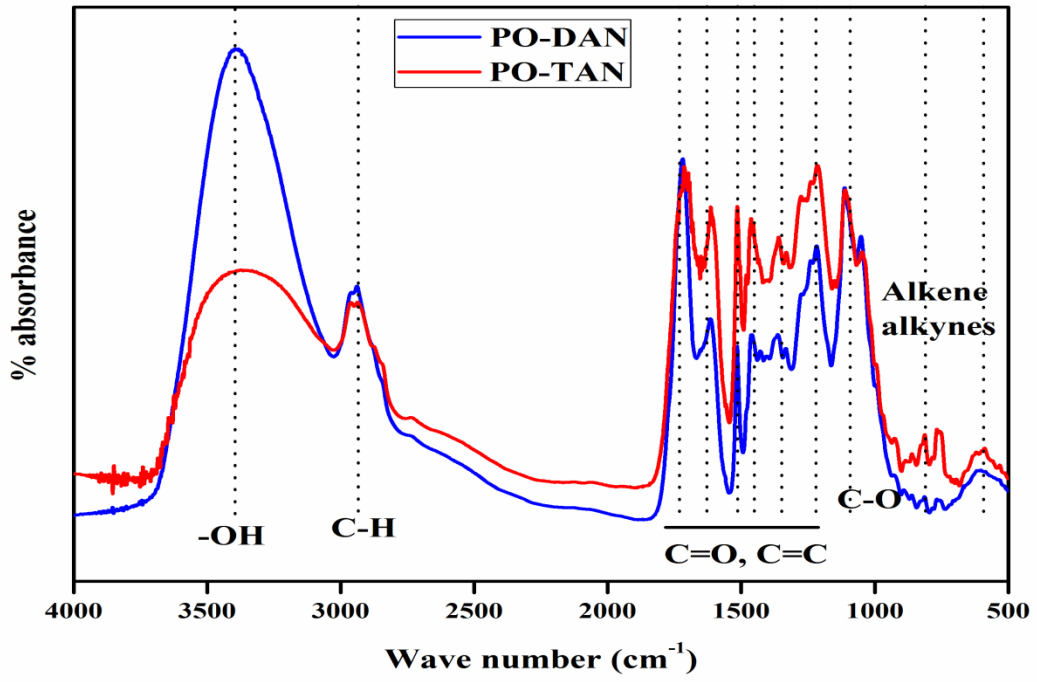

Figure 6.3 FTIR spectra of pyrolysis oil from DAN and TAN-252-60-5 at optimum condition

6.3.5.2 Gas chromatography-mass spectrometry analysis pyrolysis oil

The GC-MS was performed to quantify the various class of chemical compounds exists in PO-DAN and PO-TAN obtained at optimum condition of pyrolysis. The identified chemical compounds are listed in Table 6.7, while GC-MS spectra for PO-DAN and PO-TAN are depicted in Figs. 6.4 (a) and (b). Results showed that PO-DAN and PO-TAN contain various chemical compounds; however, in present study, they were grouped into eight major categories such as acid, aldehydes, ketones, alcohol, esters, phenol derivatives, furan derivatives and sugar derivatives based on their functional groups. It was noted that

quantity of chemical compounds present in both pyrolysis oil varied significantly. Fig. 6.5 depicts the quantitative analysis of various classes of compounds based on the percentage area analyzed by GC-MS analysis. The results showed that PO-TAN contains lower acid, alcohol, and sugar derivatives than PO-DAN. Similar findings were also described by Xin et al. (Xin et al., 2018), Ukaew et al. (Ukaew et al., 2018). This decrease in oxygenated compounds will enhance the stability of pyrolysis oil. It will facilitate the use of pyrolysis oil in bio-refinery at lower cost (Ukaew et al., 2018). Meanwhile, PO-TAN has higher percentage of furan derivatives, phenol derivatives, ketones, and esters than PO-DAN. The decomposition of acetoxy and methoxy groups from hemicellulose results in lower acid content (mainly carboxylic acid) in PO-TAN and ketonization and rearrangement of carboxylic acid results in an increase in ketone content in PO-TAN (Chen et al., 2017). Phenol derivative compounds were mainly formed due to decomposition of lignin present in biomass (Dai et al., 2019).

Table 6.7 Chemical composition of pyrolysis oil identified by GC-MS analysis at optimum condition of pyrolysis of DAN and TAN-252-60-5

Compounds	**Molecular formula**	**Relative content (peak area (%))**	
		PO-TAN	**PO-DAN**
Furan derivatives			
3-Furaldehyde	$C_5H_4O_2$	0.30	0.21
2-Furancarboxaldehyde	$C_5H_4O_2$	10.46	-
2-Furanmethanol	$C_5H_6O_2$	5.62	6.05
Furan, tetrahydro-2,5-dimethoxy-	$C_6H_{13}O_3$	1.04	0.62
2(3H)-Furanone, 5-Methyl-	$C_5H_6O_2$	3.52	5.02
2(5H)-Furanone,5-methyl-	$C_5H_6O_2$	-	0.27
2-Furancarboxaldehyde,-5-Methyl	$C_6H_6O_2$	-	6.45
2-Furanmethanol, Tetrahydro-	$C_5H_{10}O_2$	-	0.44
2-	$C_{16}H_{24}OSi$	-	0.08

Dimethy(trimethylsilylmethyl)silyloxymethyltetrahydrofuran			
Total		**20.94**	**19.14**
Phenol derivatives			
Phenol	C_6H_5OH	3.00	0.97
Phenol, 2-Methyl-	C_7H_8O	-	1.05
Phenol, 2-methoxy-	$C_7H_8O_2$	5.78	
Phenol, 4-methoxy-	$C_7H_8O_2$	-	8.72
Phenol, 2,6-dimethyl-	$C_8H_{10}O$	-	1.25
Creosol	$C_8H_{10}O_2$	3.84	6.05
Phenol, 4-ethyl-2-methoxy-	$C_9H_{12}O_2$	1.62	1.68
2-Methoxy-4-vinylphenol	$C_9H_{10}O_2$	3.79	1.14
Phenol, 2,6-dimethoxy-	$C_8H_{10}O_3$	9.46	9.11
Phenol, 3,4-dimethoxy-	$C_8H_{10}O_3$	-	0.75
3,5-Dimethoxy-4-hydroxytoluene	$C_9H_{12}O_3$	4.63	4.61
Phenol, 2-methoxy-4-(2-propenyl)-	$C_{10}H_{12}O_3$	3.67	0.64
Phenol, 2-methoxy-4-(1-propenyl)-,(E)-	$C_{10}H_{12}O_2$	0.91	-
Phenol, 2,6-dimethoxy-4-(2-propenyl)-	$C_{11}H_{14}O_3$	6.68	0.82
1-Hydroxy-2-methoxy-4-methylbenzene	$C_8H_{10}O_2$	0.37	-
Total		**43.75**	**36.79**
Acids			
dl-3-Methyl-dl-glutamic acid	$C_6H_{11}NO_4$	-	0.54
6-Heptenoic acid, methyl ester	$C_8H_{14}O_2$	-	0.21
Dimethylmalonic acid, dodecyl 3-ethylphenyl ester	$C_{28}H_{56}O_2$	-	0.41
3-Cyclopropenoic acid,-1-butyl, methyl ester	$C_9H_{14}O_2$	-	0.24
2,4-Hexadienedioic acid, 3,4-diethyl-, dimethyl ester, (E,Z)-	$C_8H_{10}O_4$	0.26	-
n-Hexadecanoic acid	$C_{16}H_{32}O_2$	0.60	0.54
Cyclopentanecarboxylic acid	$C_6H_{10}O_2$	0.15	-
Linoelaidic acid	$C_{18}H_{32}O_2$	-	1.90
9-Octadecenoic acid (z)-	$C_{18}H_{34}O_2$	-	0.15
Total		**1.01**	**3.99**
Alcohols			
1-Ethynyl-1-cycloheptanol	$C_8H_{12}O$	-	0.32
1-Penten-3-ol	$C_5H_{10}O$	0.80	0.65
1,2-Benzenediol, 3-methoxy-	$C_7H_8O_3$	0.66	0.28
1,2-Benzenediol, 3-methyl-	$C_7H_8O_2$	-	2.15
1,2,4-Benzenetriol	$C_6H_6O_3$	0.14	-
1-Octen-3-ol, acetate	$C_{10}H_{18}O_2$	0.82	-
3,4-Altrosan	$C_6H_{10}O_5$	0.37	-
trans-Sinapyl alcohol	$C_{11}H_{14}O_4$	0.14	-
Total		**2.93**	**3.40**
Aldehydes			
Benzaldehyde, 4-hydroxy-3-methoxy-	$C_8H_8O_3$	-	0.86
Benzaldehyde, 4-hydroxy-3,5-dimethoxy-	$C_9H_{10}O_4$	0.64	0.64

Coniferyl aldehyde	$C_{10}H_{10}O_3$	0.50	-
trans-Sinapaldehyde	$C_{11}H_{12}O_4$	0.55	-
Total		**1.69**	**1.5**
Ketones			
2-Pentanone, 4-hydroxy-4-methyl-	$C_6H_{12}O_2$	1.45	0.92
3-Penten-2-one, 3,4-dimethyl-	$C_7H_{12}O$	0.42	-
2-Cyclopenten-1-one, 2-methyl-	C_6H_8O	1.15	1.58
Alpha.,.beta.-crotonolactone	$C_4H_4O_2$	2.16	2.16
2-Methyl-3-hexanone	$C_7H_{14}O$	-	0.68
3-Methylcyclopentane-1,2-dione	$C_6H_8O_2$	2.86	3.93
5-Hydroxy-2-heptanone	$C_7H_{14}O_2$	0.30	0.46
Spiro[2.4]heptan-4-one	$C_7H_{10}O$	0.23	-
9-Oxabicyclo[6.1.0]non-6-en-2-one	$C_8H_{10}O_2$	0.14	-
3-Ethylcyclopent-2-en-1-one	$C_7H_{10}O$	-	0.25
4H-pyran-4-one, 3-hydroxy-2-methyl-	$C_6H_6O_3$	-	0.31
Ethanone, 1-(4-hydroxy-3-methoxyphenyl)-	$C_9H_{10}O_3$	0.34	0.25
Ethanone, 1-(4-hydroxy-3,5-dimethoxyphenyl)-	$C_{10}H_{12}O_4$	0.84	0.30
2-Cyclopenten-1-one, 3-ethyl-2-hydroxy-	$C_7H_{10}O_2$	0.54	-
6-Methoxycoumaran-7-ol-3-one	$C_9H_8O_4$	3.61	-
3',5'-Dimethoxyacetophenone	$C_{10}H_{12}O_3$	-	0.41
Total		**14.04**	**11.25**
Sugar derivatives			
1,4:3,6-Dianhydro-.alpha.-d-glucopyranose	$C_6H_8O_4$	0.30	1.47
2,3-Anhydro-d-mannosan	$C_6H_8O_4$	-	0.75
Beta.-D-Glucopyranose, 1,6-anhydro-	$C_6H_{10}O_5$	-	6.39
alpha.-D-Glucopyranose, 4-O-.beta.-D-galactopyranosyl	$C_{12}H_{22}O_{11}$	-	0.42
Total		**0.30**	**9.03**
Esters			
2-(Acetyloxy) Ethyl acetate	$C_7H_{12}O_5$	0.53	
Diethyl Phthalate	$C_{12}H_{14}O_4$	-	0.55
Di-n-octyl phthalate	$C_{24}H_{38}O_4$	0.35	0.31
1,2-Benzenedicarboxylic acid, diethyl ester	$C_{12}H_{14}O_4$	0.51	-
2,4-Hexadienedioic acid, 3,4-diethyl-, dimethyl ester, (E,Z)-	$C_8H_{10}O_4$	0.26+1.24	0.53
Total		**2.89**	**1.53**
Other compounds			
1H-Pyrazole, 3,5-dimethyl-	$C_5H_8N_2$	-	9.34
Bicyclo[2.2.2]octane, 1-fluoro-4-methyl-	$C_9H_{15}F$	-	0.27
Benzene, 1,2,3-trimethoxy-5-methyl-	$C_{10}H_{14}O_3$	3.18	1.91
Butane, 1-chloro-3,3-dimethyl-	$C_6H_{13}Cl$	-	0.32
1,4-Butanediamine, 2,3-dimethoxy-N,N,N',N'-tetramethyl-, [S-(R*,R*)]-	$C_{10}H_{24}N_2O_2$	1.75	-
Total		**4.93**	**11.84**

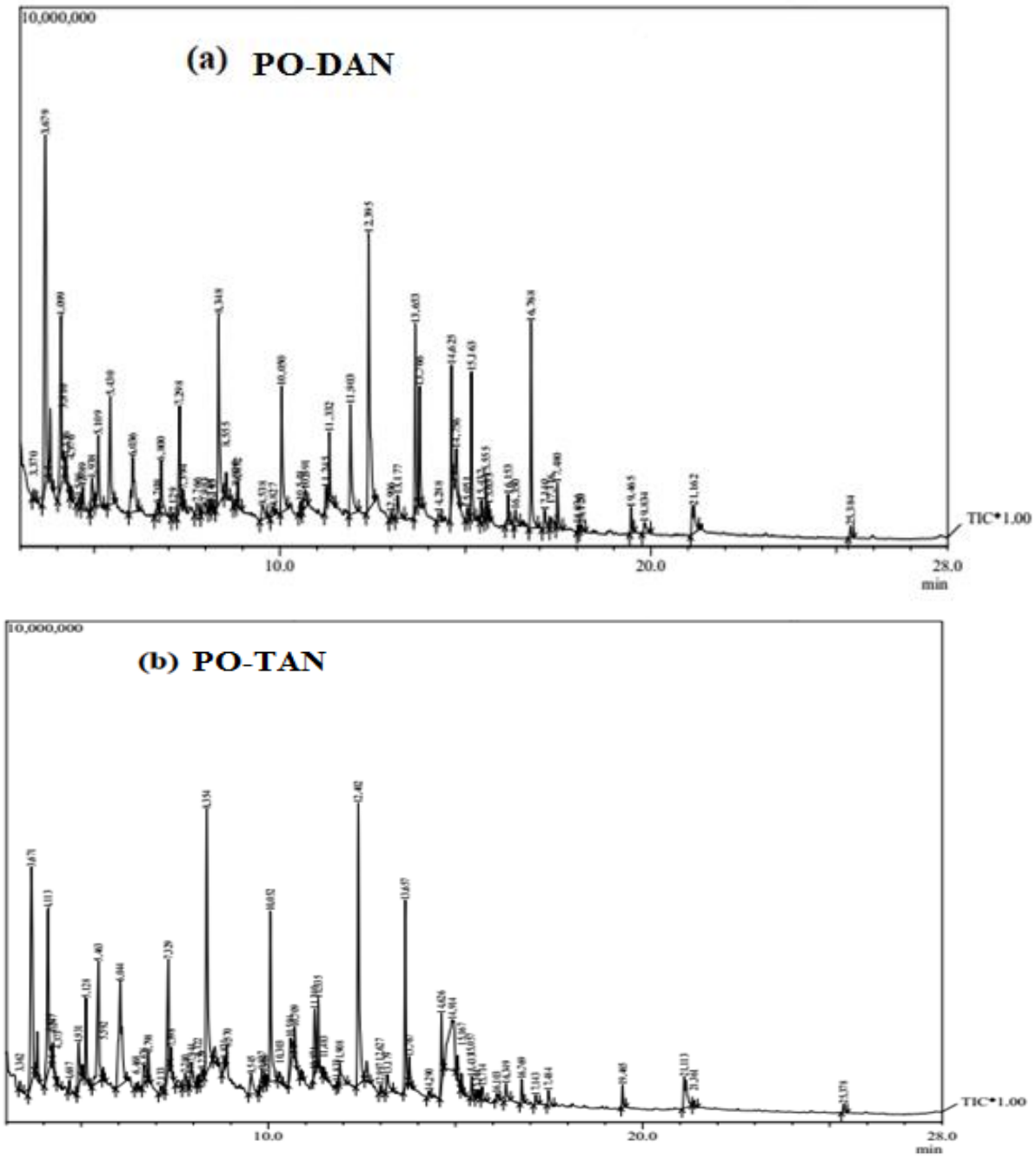

Figure 6.4 GC-MS spectrum of pyrolysis oil from pyrolysis of DAN and TAN-252-60-5 at optimum condition (a) PO-DAN, (b) PO-TAN

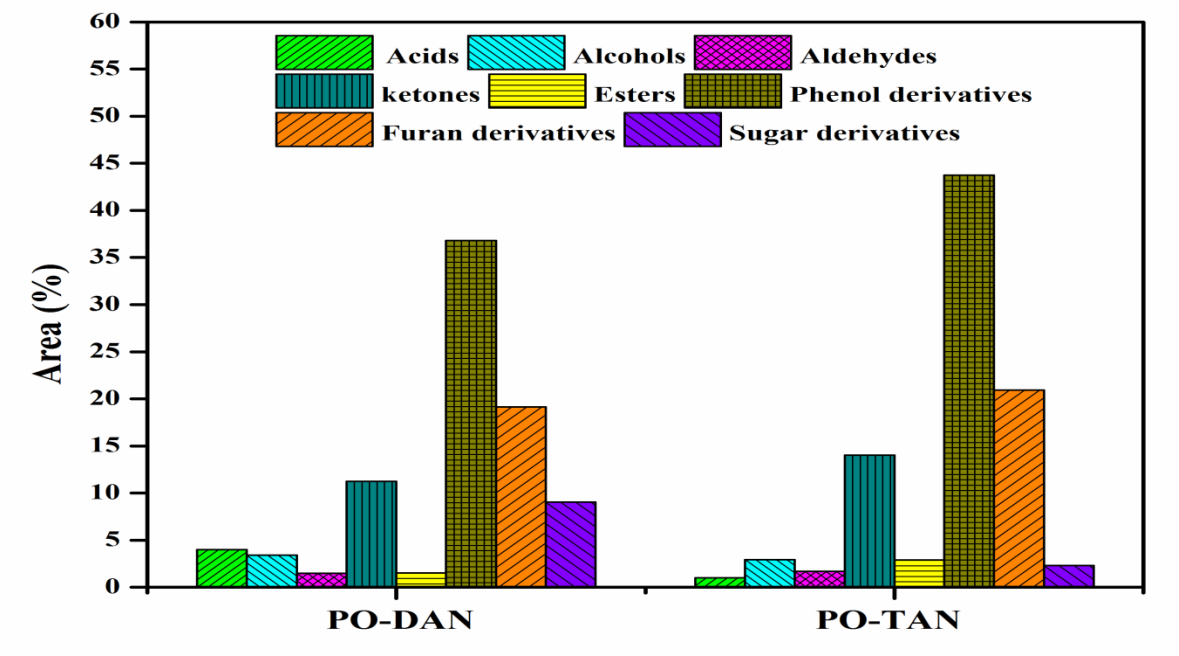

Figure 6.5 The relative amount of different type of compound present in pyrolysis oil from DAN and TAN-252-60-5 obtained at optimum condition

6.3.5.3 ^{13}C NMR analysis of pyrolysis oil

Apart from FTIR analysis, the functional groups and type of carbon present in the pyrolysis oil (PO-DAN and PO-TAN) was also investigated by ^{13}C NMR analysis. The NMR spectra of PO-DAN and PO-TAN are depicted in Fig. 6.6 (a) and (b). The NMR analysis has been considered as a powerful technique to classify the functional groups and type of carbon by dissolving the pyrolysis oil in a suitable solvent and quantify the functional groups by determining the integral area of specific region of spectrum (Negahdar et al., 2016; Xu et al., 2019). The whole NMR spectrum was divided broadly into five chemical shift zones based on the previous work done by Negahdar et al. (Negahdar et al., 2016), Ingram et al. (Ingram et al., 2008), and Joseph et al. (Joseph et al., 2010). The region from 0 to 54 ppm was assigned to alkyl carbon. Also, the alkyl carbon region was sub-divided into primary

alkyl carbon (6-24 ppm) and secondary/tertiary alkyl carbon (24-34 ppm). The chemical shifts from 54 to 70 ppm, 70 to 103 ppm, 103 to 163 ppm, and 163 to 215 ppm were attributed to methoxyl/hydroxyl carbon, carbohydrate carbon, total aromatic carbon, and carbonyl carbon, respectively (Negahdar et al., 2016). Further, the aromatic carbon region was sub-divided into syringyl type carbon (110-112 ppm), guaiacyl type carbon (112-125 ppm). The results related to different types of carbon present in PO-DAN and PO-TAN are presented in Fig. 6.7 (a) and (b), separately. The results showed that total aromatic carbon in PO-DAN and PO-TAN was 24.65 and 34.58 %, respectively. The increase in aromatic carbon in case of PO-TAN may be due to higher lignin content in TAN-252-60-5 than the DAN (Negahdar et al., 2016). The alkyl carbon in PO-DAN and PO-TAN was 36.57 and 28.21 %, respectively. The total alkyl carbon in PO-TAN decreased as compared to PO-DAN. However, primary alkyl carbon in PO-TAN was higher than PO-DAN. This increases the utility of PO-TAN as a fuel. The carbonyl carbon in PO-DAN and PO-TAN was 10.24 and 15.5 %, respectively. The increase in carbonyl carbon may be attributed to an increasing in ketones in case of PO-TAN, as confirmed by GC-MS analysis. A slight decrease in methoxyl/hydroxy carbon was observed in case of PO-TAN (13.16 %) as compared to PO-DAN (15.5 %). This may happen because of decrease in acid content in PO-TAN. The carbohydrate carbon in PO-DAN and PO-TAN was 13.04 and 8.55 %, respectively. The ^{13}C NMR analysis of pyrolysis oil was consistent with the results of GC-MS analysis, as discussed in section 6.3.5.2.

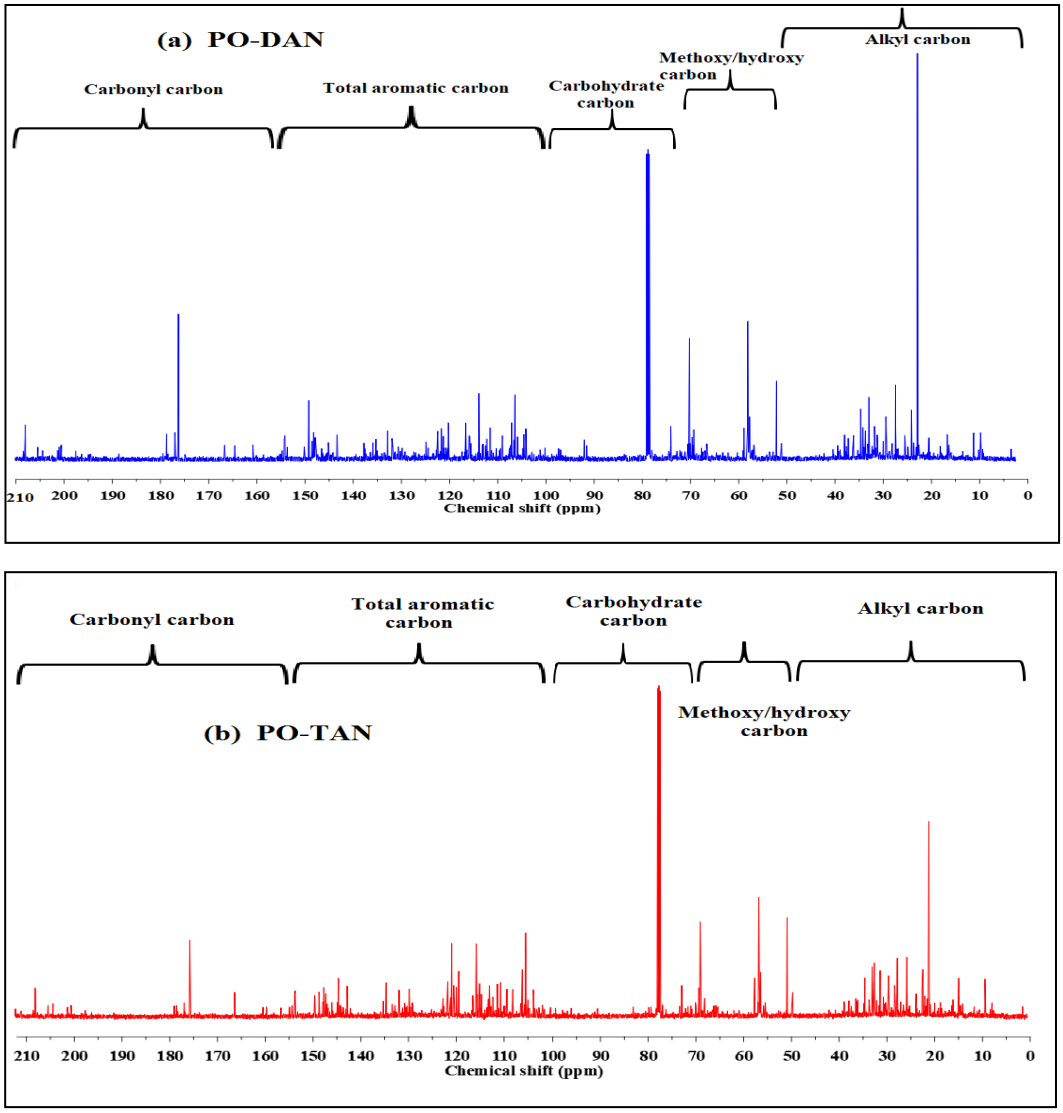

Figure 6.6 ^{13}C NMR spectrum of pyrolysis oil obtained at optimum condition (a) PO-DAN, (b) PO-TAN

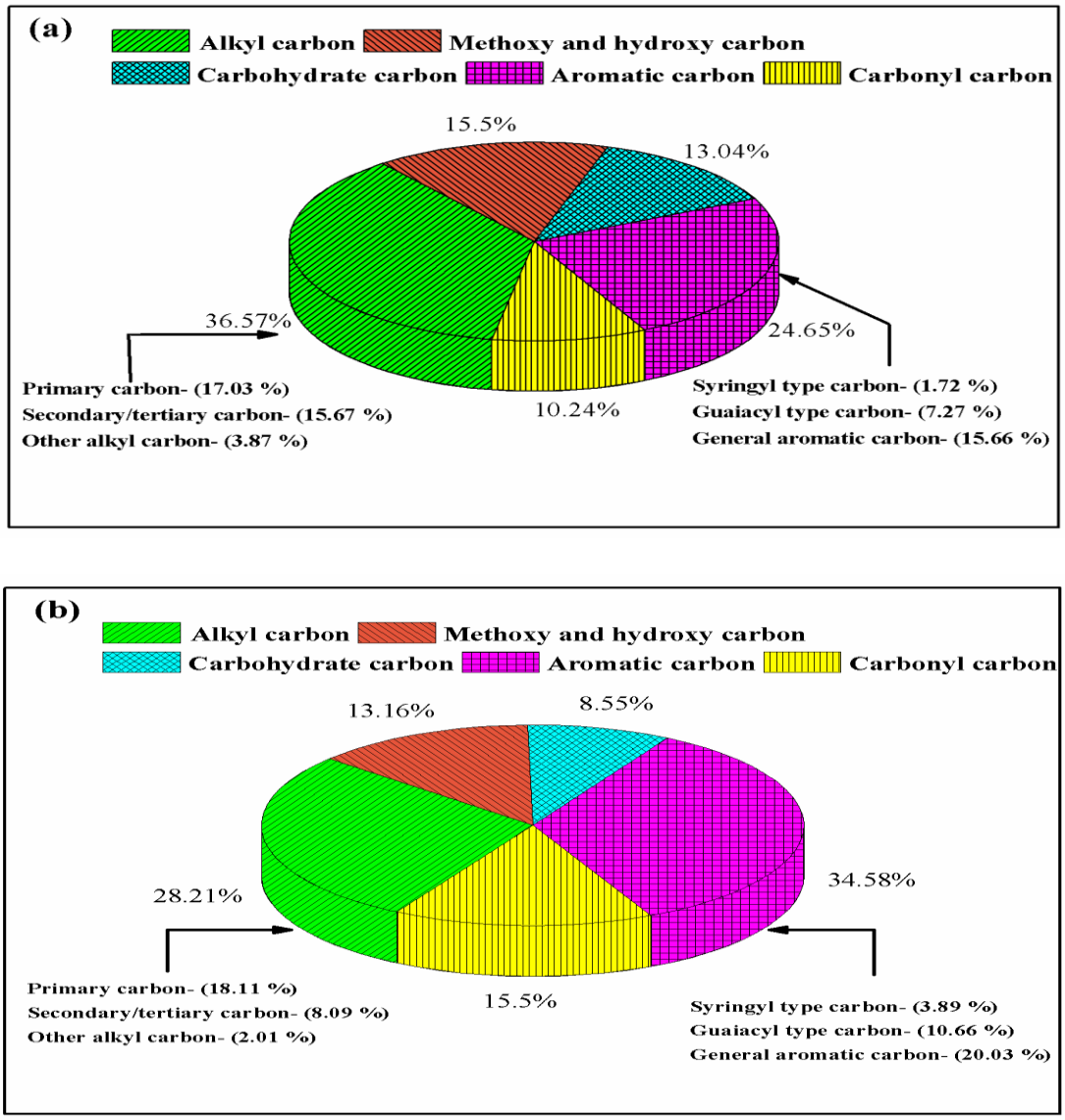

Figure 6.7 The relative amount of different type of carbon present in pyrolysis oil obtained at optimum condition (a) PO-DAN, (b) PO-TAN

6.3.5.4 Physicochemical characteristics of pyrolysis oil

The physicochemical characteristics of pyrolysis oil (PO-DAN and PO-TAN) are mentioned in Table 6.8. The properties of PO-DAN and PO-TAN were compared with standard specification protocol ASTM D7544-12 (ASTM-grade G and ASTM-grade D) (Mohammed et al., 2017c) and physical properties of mineral oils (Dhyani & Bhaskar, 2018). A Minor difference in appearances of PO-TAN and PO-DAN was observed. PO-TAN has an intense dark brownish color with no transparency, while PO-DAN has brownish color having some transparency. The water content of PO-DAN and PO-TAN was found to be 32 and 21 wt %, respectively. The water content in pyrolysis oil is associated with moisture content of native biomass and due to dehydration of pyrolysis products. Lower moisture content in TAN-252-60-5 is attributed to lower water content in PO-TAN. The HHV of PO-DAN and PO-TAN was 24.73 and 30.55 MJ/kg, respectively. The higher HHV of PO-TAN is due to presence of various carbon-rich organic compounds (Mohammed et al., 2017c) and lower water content, which reduces the extra energy consumed in the evaporation of water present in pyrolysis oil. The density of PO-DAN and PO-TAN was 1.098, 1.134 g/cm^3, respectively, while; viscosity was noted to 3.90 and 4.07 cSt, respectively. The lower water content for PO-TAN may be attributed to increasing in density and viscosity. Both the pyrolysis oil (PO-DAN and PO-TAN) show the acidic character having pH value of 2.23 and 3.17, respectively, because of acidic and phenolic compounds present in pyrolysis oil (Mohammed et al., 2017c). However, pH of PO-TAN was 42.15 % higher than the PO-DAN due lower of acidic components. Ramsbottom carbon residue of PO-DAN and PO-TAN was found to be 2.78 and 3.21 wt %, respectively. It depicts the carbon deposition tendency of pyrolysis oil when it is used as a

fuel. The ash content of PO-DAN and PO-TAN was found to be 0.03 and 0.01 wt %, respectively. All physical parameters of PO-DAN and PO-TAN were found in the range of ASTM-grade G and ASTM-grade D. However, PO-TAN has improved properties than PO-DAN. The physical characteristics of both pyrolysis oils vary significantly as compared to mineral oils. This might be due to presence of water and oxygenated compounds present in pyrolysis oil. The higher water and oxygenated compounds attributed to lower heating value and high polarity of pyrolysis oil (Dhyani & Bhaskar, 2018).

Table 6.8 Physicochemical properties of pyrolysis oil (PO-DAN and PO-TAN) at optimum condition and comparison with ASTM grade oil and mineral oils (Dhyani & Bhaskar, 2018; Oasmaa et al., 2009)

Properties	**PO-DAN**	**PO-TAN**	**ASTM-Grade G**	**ASTM-Grade D**	**Heavy fuel oil**	**Light fuel oil**
Appearance	Dark brown	Intense dark brown				
HHV (MJ/kg)	24.73	30.55	Minimum 15	Minimum 15	40.6	42.6
Density (g/cm^3)	1.098	1.134	1.1-1.3	1.1-1.3	0.99-0.995	0.845 (max)
Water content (wt. %)	32	21	Maximum 30	Maximum 30	~0	~0
pH	2.23	3.17	Report	report	-	-
Carbon residue (wt. %)	2.78	3.21	-	-	-	-
Viscosity (cSt)	3.90	4.07	Maximum 125	Maximum 125	180-420	2.0-4.5
Ash content (wt. %)	0.03	0.01	Maximum 0.25	Maximum 0.15	0.08 (max)	0.01 (max)

6.3.6 Characteristics of biochar obtained at optimum condition from pyrolysis of DAN and TAN-252-60-5

6.3.6.1 Proximate and ultimate analyses of biochar

Table 6.9 represents the proximate and ultimate analyses of biochar from pyrolysis of DAN (Biochar-DAN) and TAN-252-60-5 (Biochar-TAN). The moisture content and volatile matter decreased by 29.72 and 31.53 %, while, fixed carbon and ash content increased by 4.58 and 29.58 %, respectively, of Biochar-TAN as compare to Biochar-DAN. The difference in properties of both biochars was associated with the process through which they were obtained. Biochar-DAN was obtained by pyrolysis of DAN, whereas, Biochar-TAN was obtained by thermal treatment of DAN through torrefaction followed by pyrolysis. The intense devolatilization taking place in case of Biochar-TAN results in lesser moisture content and volatile matter and relatively higher fixed carbon and ash content (Dai et al., 2019). Also, in case of Biochar-TAN, the release of hydrogen and oxygen molecules was more prominent than the release of carbon as compared to the Biochar-DAN. The HHV of Biochar-TAN was 10.64 % higher than the Biochar-DAN. The higher HHV of Biochar-TAN was attributed to higher carbon content than Biochar-DAN. The results from proximate and ultimate analysis were similar to the finding of published literature (Chen et al., 2015a; Gogoi et al., 2017).

Table 6.9 Characteristics of biochar obtained at optimum condition from pyrolysis of DAN and TAN-252-60-5

Analysis	Biochar-TAN	Biochar-DAN
Proximate analysis (wt %)		
Moisture content	0.78	1.11
Volatile matter	10.53	15.38
Ash content	8.76	6.97
Fixed carbon*	80.02	76.51
Ultimate analysis (wt %)		
C	86.17	81.38
H	1.01	1.98
N	3.34	2.48
S	BDL	BDL
O*	9.48	14.16
Higher heating value(MJ/kg)	30.55	27.61

*; calculated by difference, BDL; below detection limit

6.3.6.2 SEM-EDX analysis of biochar

Fig. 6.8 (a) and (b) depict the SEM-EDX analysis of Biochar-DAN and Biochar-TAN obtained at optimum condition of pyrolysis. Results showed that surface of both the biochars were heterogeneous, cracked, and having honeycomb-like pore structure (Dhanavath et al., 2019). Biochar-TAN has wide pores as compare to Biochar-DAN because of release of large amounts of volatile matter through intense devolatilization (Dhanavath et al., 2019; Gupta & Mondal, 2019). The pores present on the surface of both biochar may facilitate its potential application in adsorption process (Gupta & Mondal, 2019).

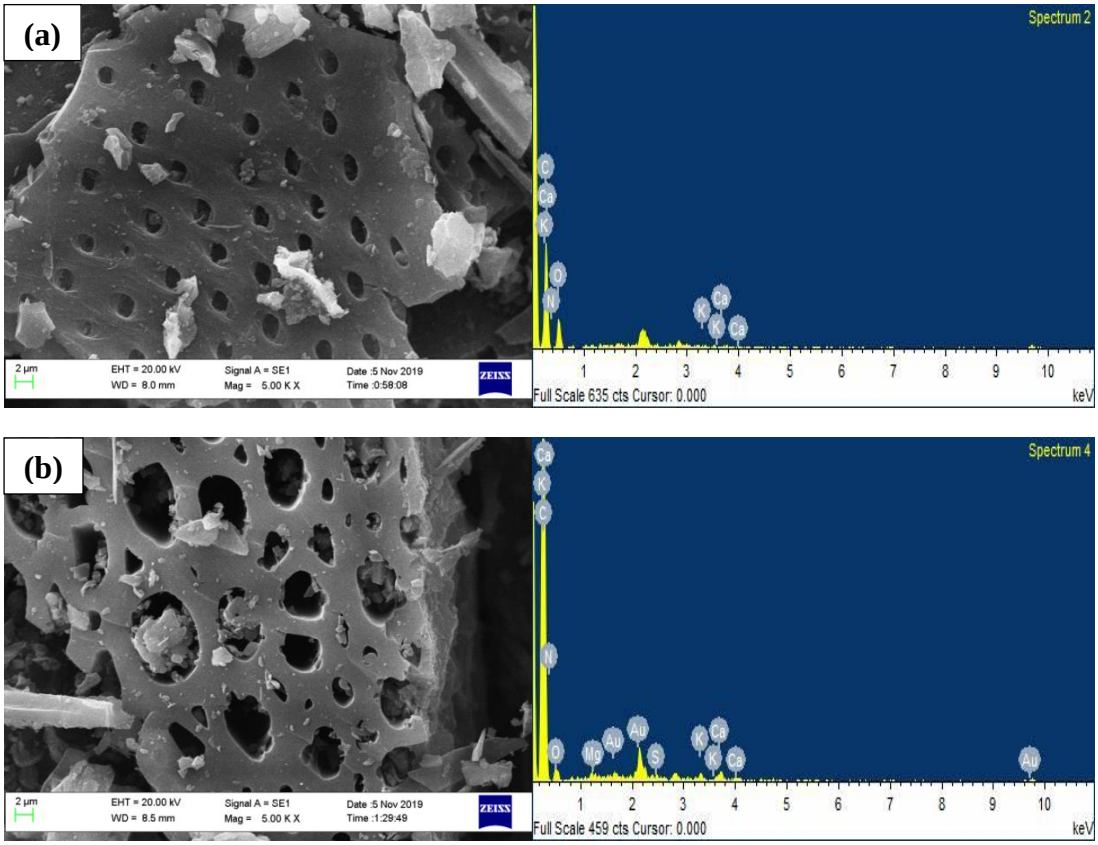

Figure 6.8 SEM-EDX analysis of biochar at optimum condition **(a)** Biochar-DAN **(b)** Biochar-TAN

EDX analysis confirmed that C, K, Ca, O, N existed on the surface of Biochar-DAN, while, C, K, Ca, O, N, Mg existed on the surface of Biochar-TAN. The presence of these macronutrients on the surface of biochar facilitates its utility in soil amendment (Mohammed et al., 2017c). Similar findings were also reported in published literature (Gupta & Mondal, 2019; Mohammed et al., 2017c).

6.3.6.3 FTIR analysis of biochar

The FTIR analysis of Biochar-DAN and Biochar-TAN was performed and their spectra are displayed in Fig. 6.9. The FTIR analysis provides a quick and efficient technique to identify the class of various chemical compounds. The FTIR spectra confirm the presence

of various functional groups associated with biochar. For Biochar-DAN, the peak at 3420.51 cm^{-1} corresponds to stretching vibration of O-H bonded groups such as phenol, alcohol, and water (Gupta & Mondal, 2019). The wavenumber 2925.68 cm^{-1} is ascribed to the stretching and deformation vibration of aliphatic C-H groups. The wavenumber 1688.47 cm^{-1} is assigned to C=O vibration of aldehyde and ketones and C=C aromatic vibrations. The wavenumber 1588.47 cm^{-1} corresponds to secondary amine groups. The wavenumber 1239.84 cm^{-1} is ascribed to deformative vibration of aromatic nitrogen to secondary amine groups. The wavenumber between 876.33- 805.65 cm^{-1} and 757.12-686.51 cm^{-1} ascribe the presence of wagging vibration of C-H bond in aromatic ring and vibration of alkyl halide along with bending vibration of Si-O-Si bond, respectively. Similar results were obtained for Biochar-TAN as well. However, the intensity of peaks for Biochar-TAN was slightly lower than that of Biochar-DAN. This might be due to torrefaction, as considerable rupture of –C-O, -O-H, etc. bonds take place, and there is formation of CO_2 and lighter non-condensable gases (Dai et al., 2019).

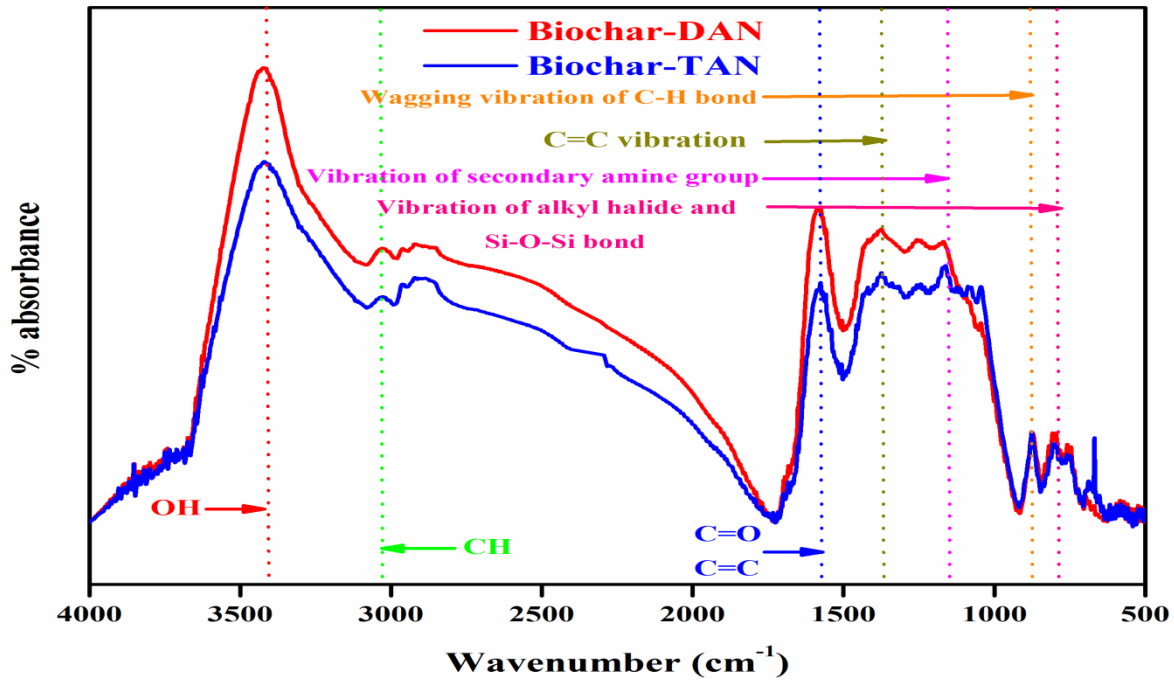

Figure 6.9 FTIR spectra of biochar from DAN and TAN-252-60-5 at optimum condition of pyrolysis

6.3.7 Characteristics of pyrolytic gases obtained at optimum condition from pyrolysis of DAN and TAN-252-60-5

The composition of pyrolytic gases obtained from pyrolysis of DAN and TAN-252-60-5 at optimum condition is displayed in Fig. 6.10. The pyrolytic gases from both the feedstock mainly consist of carbon dioxide (CO_2), carbon monoxide (CO), methane (CH_4) and hydrogen (H_2). Among all gases, the largest amount of CO_2 was present for both the feedstock followed by CO, CH_4, and H_2, respectively. However, significant difference was observed by comparing the composition of pyrolytic gases from DAN and TAN-252-60-5. The mass percentage of CO_2 decreased from 43.05 to 32.71 %, while, mass percentage of

CO, CH_4, and H_2 increased from 32.77 to 35.32, 20.64 to 25.26, 3.54 to 6.70 %, respectively, for pyrolytic gases from TAN-252-60-5 as compared to DAN. CO_2 and CO formed during the pyrolysis as a result of decarboxylation and decorbonylation reactions, respectively (Wang et al., 2018b). Thus, it can be concluded that decarboxylation reaction was more favorable for DAN, while, decarbonylation reaction was more favorable for TAN-252-60-5. The decrease in CO_2 for TAN-252-60-5 pyrolysis was also attributed to degradation of hemicellulose during torrefaction (Konsomboon et al., 2019) The TAN-252-60-5 has higher lignin content as compared to DAN (Singh et al., 2020b). Cleavage of methoxyl group (-OCH_3) through demethoxylation reaction from benzene ring of lignin and presence of large number of alkyl branches in lignin mainly contributed to formation of H_2 and CH_4 (Shen et al., 2010). Small amount of CH_4 was also formed due to breakdown of hemicellulose and cellulose (Yang et al., 2007). The trend of formation of H_2 was in line with CH_4, revealing that generation of H_2 might be complemented by formation of CH_4 (Xin et al., 2013).

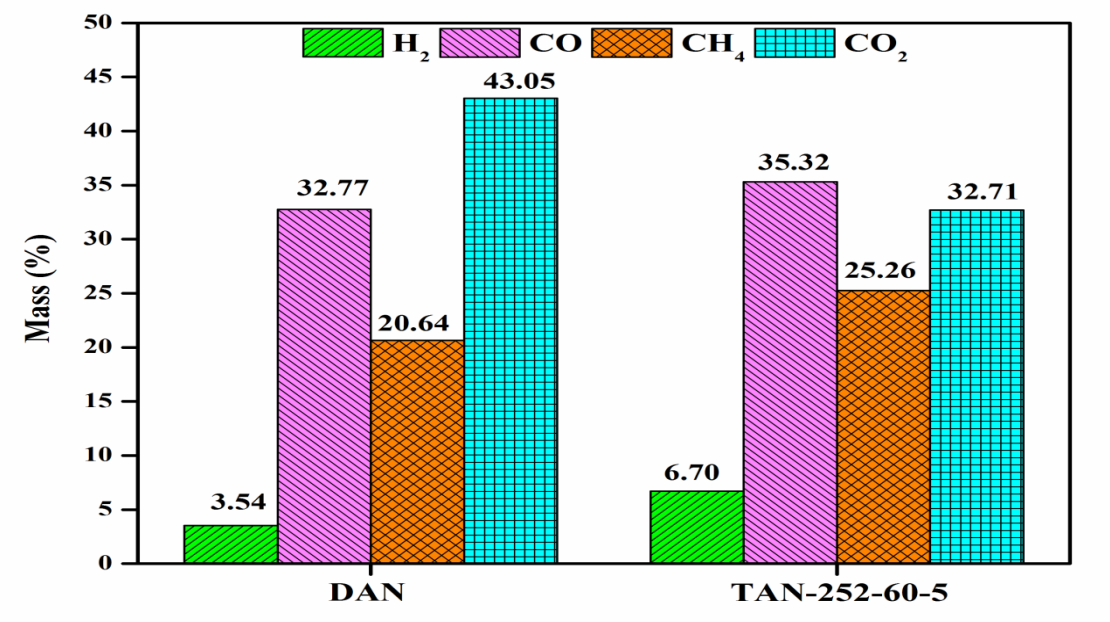

Figure 6.10 Composition of pyrolytic gases from pyrolysis of DAN and TAN-252-60-5 at optimum condition

6.3.8 Mechanism of pyrolysis of TAN-252-60-5

Torrefaction causes physical and chemical modifications in DAN due to which the pyrolysis pathway for TAN-252-60-5 differs from that of DAN because of changes in kinetic parameters, decrease in grinding energy, heat, and mass transfer rate, (Dai et al., 2019). In course of torrefaction, the methenyl groups associated with side chain of hemicellulose are broken, aldose groups detached from main chain of hemicellulose, and all the glycosidic bonds are ruptured; as a result, the hydroxyl bonds of hemicellulose are dehydrated (Dai et al., 2019). The fragmentation of cellulose occurred due to breaking of glycosidic and hydroxyl bonds associated with cellulose (Wang et al., 2017). In addition, slight modification of lignin takes place cleavage of β-O-4 ether bond of benzene ring

associated with lignin (Mahadevan et al., 2016; Wen et al., 2014). The TAN-252-60-5 served better than the DAN since it has lower moisture and oxygen content along with a ruptured surface structure. TAN-252-60-5 has lower activation energy in comparison to DAN (Ren et al., 2013a), which is suggested by loose and porous structure (Singh et al., 2019b). The yield of pyrolysis oil decreases when TAN-252-60-5 is pyrolysed (Boateng & Mullen, 2013b; Chen et al., 2016c), as compared to pyrolysis of DAN; however, there is an enhancement in the characteristics of pyrolysis oil by means of lower water content, oxygenated compounds, and acid content. Also, the amount of total aromatic compounds increases (Chen et al., 2017). The yield of pyrolysis oil is lower due to lower volatile matter of TAN-252-60-5 and decomposition of lighter volatile compounds into CO_2, CO, H_2O, and acetic acid (Boateng & Mullen, 2013b). Also, the higher ash content of TAN-252-60-5 (Singh et al., 2019b) may catalyze the pyrolysis process to decrease the yield of pyrolysis oil by secondary cracking reaction (Yildiz et al., 2015). Also, the pyrolysis of TAN-252-60-5 favors the formation of CH_4 and H_2 as compared to CO_2 and CO (Ren et al., 2013b). The solid biochar yield is higher (Boateng & Mullen, 2013b; Singh et al., 2020b) because of higher cross-linking reaction and charring of TAN-252-60-5 during pyrolysis.

6.3.9 Sustainability of integrated torrefaction-pyrolysis process and implication for cleaner production of pyrolysis oil

Torrefaction was used as a pretreatment step. The desired product was high-quality solid biofuel. However, liquid condensate and gaseous products (CO_2 and CO in large quantity and CH_4 and H_2 in small quantity) are also produced during torrefaction (Chen et al., 2018; Ma et al., 2019). To increase the sustainability of integrated torrefaction-pyrolysis process,

the gaseous products can be used in drying process through combustion of CO, CH_4, and H_2 or may be used to generate heat and electricity for integrated process (Dai et al., 2019). This will reduce the consumption of heat and electricity from external sources. The liquid condensate from torrefaction contains a number of C_1-C_4 oxygenated compounds (Doddapaneni et al., 2017; Liaw et al., 2015) and a large quantity of water (from 40 to 60 wt % depending on the condition of torrefaction) (Chen et al., 2015b; Ma et al., 2019). The liquid condensate may be used to digest CH_4 anaerobically (Doddapaneni et al., 2017; Liaw et al., 2015) or used as a fuel and source of various chemicals after removal of water. Besides, optimization of torrefaction process for high-grade solid biofuel in terms of maximum higher heating value and energy yield can further assist the overall economy, scale-up, and simulation of process by reducing the unnecessary experimental run (Singh et al., 2019b). A general pathway for the sustainability of integrated process is shown in Fig. 6.11.

The pyrolysis oil obtained from pyrolysis of TAN-252-60-5 may have multiple applications, as shown in Fig. 6.12. As mentioned in section 6.3.5.1, the quality of pyrolysis oil obtained from TAN-252-60-5 is superior to pyrolysis oil obtained from DAN in terms of water content, pH value, HHV, etc. In section 6.3.5.3, it is mentioned that oxygen-containing compounds and total acidic compounds in pyrolysis oil from TAN-252-60-5 are lesser as compared to DAN. A pH close to 7 of pyrolysis oil is beneficial as it may reduce the corrosion in fuel system, other equipment, and piping systems during storage and transportation (Dai et al., 2019; Ma et al., 2019). Moreover, decreased water and oxygen-containing compounds may further facilitate upgrading of pyrolysis oil using suitable catalysts because water and oxygen-containing compounds are mainly responsible

for coke formation and deactivation of sites on the surface of a catalysts (Dai et al., 2019). The application of pyrolysis oil has been reported by many authors. For instance, Kurji et al. (Kurji et al., 2016) used the blend of pyrolysis oil for turbine operation. Stamatov et at. (Stamatov et al., 2006) used pyrolysis oil for heating in boilers, furnaces, and kiln and reported that during combustion brighter, shorter and wider flames were observed in case of pyrolysis oil as compared to diesel fuel.

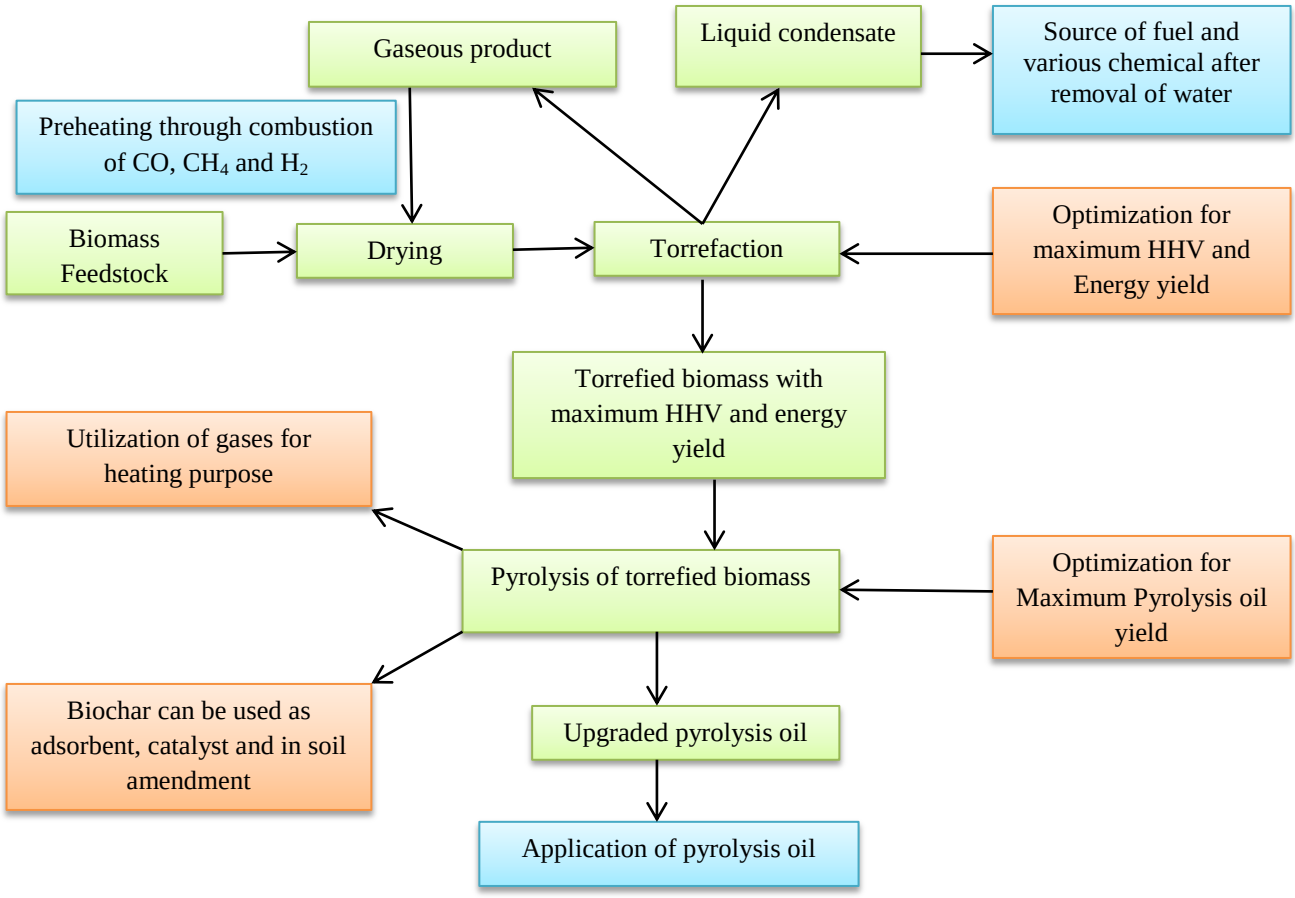

Figure 6.11 Proposed way to increase the sustainability of integrated torrefaction-pyrolysis process

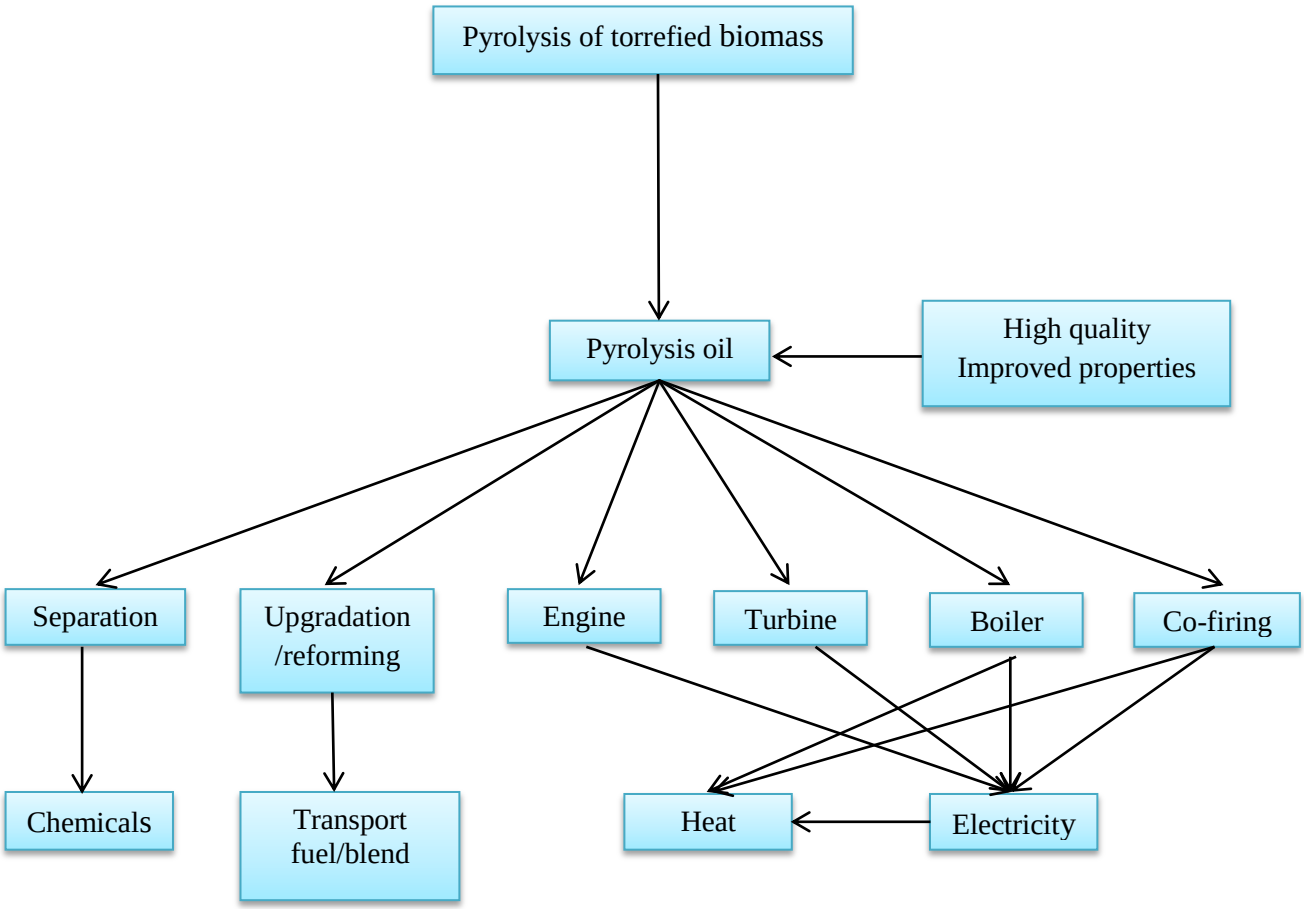

Figure 6.12 Possible applications of pyrolysis oil from pyrolysis of TAN-252-60-5 (adapted from references (Bridgwater, 2012; Dhyani & Bhaskar, 2018))

The biochar obtained from pyrolysis can be used in carbon sequestration, as an adsorbent in wastewater treatment, soil amendment,and as fuel (Dhyani & Bhaskar, 2018). The non-condensable gases produced may be used for external heating in other processes and recycling of gases into the pyrolytic reactor may enhance the heat integration as well as quality of pyrolysis oil (Mante et al., 2012). Besides, pyrolysis oil can be a good source of various chemical for industrial applications such as phenol and phenol derivatives such as

methylphenols, methoxyphenols can be used in resin, food, paints and pharmaceutical industries (Stoikos, 1991), organic acids can be used for the synthesis of levoglucosan, de-icers, hydroxyacetaldehydes and other additives which can be used in fiber manufacturing, fertilizer and pharmaceutical industries (Bogner et al., 2008; Dhyani & Bhaskar, 2018). The aldehydes present in pyrolysis oil can be used as a browning agents for meat, fish, poultry, cheese, and sausages (Ingemarsson et al., 1998). In all these applications, the efficacy of pyrolysis oil from TAN-252-60-5 may be better as compared to pyrolysis oil obtained from DAN.

6.4 Conclusions

Torrefaction improves many properties associated with DAN, while production of solid biofuels is the prime concern. Hence, pyrolysis of TAN-252-60-5 was carried out to obtain high-quality pyrolysis oil. A response surface methodology coupled with central composite design was employed to optimize the process using temperature, retention time and heating rate, and sweeping gas flow rate as independent variables. The main objective was to maximize the yield of pyrolysis oil. To compare the physicochemical characteristics of pyrolysis oil, the DAN was also pyrolysed at the optimum condition, e.g., temperature = 507.04 ℃, retention time = 58.25 min, heating rate = 38.00 ℃/min, sweeping gas flow rate = 40.52 mL/min. It was observed that pyrolysis oil obtained from TAN-252-60-5 was superior in terms of improved HHV, pH, and chemical composition and lower water content, etc. Also, optimization of two processes (torrefaction and pyrolysis) may further facilitate design, scale-up, and simulation of process reactor system. The pyrolysis oil obtained from pyrolysis of TAN-252-60-5 may be used effectively for direct heating in boilers and furnaces or as a blend in fossil-derived fuels. Also, many value-added

chemicals such as phenol and furfural derivatives may be extracted from pyrolysis oil and may be used for manufacturing resin, polymer composites, etc., and as adhesives in cement manufacturing.

Furthermore, to increase the sustainability of integrated process, the energy supplied during the torrefaction process may be offset by utilizing the enthalpy of gaseous products from torrefaction in heat recovery, and liquid products may be utilized as fuel or source of chemical after removal of water. The application of suitable catalysts in pyrolysis of TAN-252-60-5 may further increase the quality of pyrolysis oil and may mitigate the challenges of increased carbon residue and viscosity of pyrolysis oil obtained from TAN-252-60-5.

Thus, it may be concluded that combination of torrefaction with pyrolysis may increase the competitiveness of pyrolysis oil at a commercial scale due to its enhanced quality and improve overall sustainability in the biorefinery process, and also ensure waste minimization.

Chapter 7

Comparative study for removal of aqueous methylene blue using biochar from pyrolysis of raw and torrefied biomass: kinetics, isotherm, thermodynamics and mass transfer studies

General background

This chapter aimed to investigate the performance of biochars from pyrolysis of raw *Acacia nilotica* (Biochar-DAN) and torrefied *Acacia nilotica* (Biochar-TAN) towards removal of aqueous methylene blue (MB) dye using batch adsorption. Both biochars were characterized for physicochemical, BET surface area, SEM-EDX, FTIR and XRD analyses. Impact of time, adsorbent dose, pH, concentration of MB and temperature was examined. A detailed study of adsorption kinetics, isotherm, thermodynamics and mass transfer studies were performed. In addition, the possible mechanism for adsorption of MB onto biochar has been proposed.

7.1 Introduction

Over the last few decades, upsurge in the generation of contaminated water is witnessed due to rapid increase in population as well as industrialization (Güzel et al., 2017). Among various organic and inorganic toxic pollutants, synthetic dyes a kind of organic pollutant from several industries such as paint, textile, leather, paper, and cosmetics, etc. are common pollutant which are severely affecting the water bodies (Karoui et al., 2020; Lyu et al., 2018; Sangon et al., 2018). Methylene blue (MB), a type of cationic dye has vast application in textile dyeing industry, ink manufacturing industry and as an indicator (Mahmoud et al., 2012; Zhai et al., 2019). The MB present in wastewater is non-biodegradable due to its high toxicity and chemical stability (Mahmoud et al., 2012; Zhai et al., 2019). The MB concentration higher that 7 mg/kg can cause abdominal pain, mental disorder, high blood pressure and nausea to human body (Lyu et al., 2018). The treatment of contaminated water is prerequisite and rather imperative as it is imposing serious threat to the aquatic life cycle and creating imbalance to the environment due to its non-biodegradability and carcinogenic effect (Li et al., 2018; Liu et al., 2019; Rafatullah et al., 2010).

The adsorption has already been proven as an efficient and effective method for wastewater treatment, because of its lower operational cost and higher removal efficiency, rapid reaction rate, design and operational simplicity (Lyu et al., 2018; Mahmoud et al., 2012; Zhai et al., 2019), as per the acknowledgement given by the United States Environmental protection Agency (USEPA) (Lyu et al., 2018; Wanassi et al., 2017). In recent years, large number of adsorbents has been synthesized and their efficiency has been tested towards the removal of MB from wastewater. For instance, various type of activated carbon (Benhouria

et al., 2015), zeolites (Yang et al., 2018), and biochar are obtained from different thermochemical routes for instance gasification, pyrolysis, torrefaction, carbonization and hydrothermal of various carbonaceous materials. Nowadays, biochar has gathered huge attention in wastewater treatment processes because it is chemically stable and environmentally friendly (Lyu et al., 2018; Zhang et al., 2020). It is low cost, has high surface area, porosity, and higher carbon content (Trakal et al., 2014). High functionality of biochar surface imparts adsorption potential for toxic substances present in wastewater (Uchimiya et al., 2010). Biochar from thermochemical processes has also been chemically engineered to improve its adsorption capacity (Lyu et al., 2018). However, chemically treated biochars have certain limitations, such as cost and associated problems of release of chemicals (Lyu et al., 2018).

The integrated approach of torrefaction-pyrolysis process can enhance the quality of products (bio-oil, biochar and pyrolytic gases) from pyrolysis process (Dai et al., 2019). Being an energy intensive process, torrefaction can influence the overall economy of the pyrolysis process. Therefore, utilization of by-product such as biochar from integrated process may facilitate the overall economy of the process by making it cost effective. The efficacy of biochar obtained from pyrolysis of variety of native biomass samples as an adsorbent has been comprehensively investigated by various researchers as discussed in Chapter 2. However, studies comparing adsorption efficiency of biochar from pyrolysis of raw and torrefied biomass have not been reported for MB removal. Also, the application of biochar obtained at optimum condition of pyrolysis for maximum bio-oil yield has not been studied so far.

7.2 Material and methods

7.2.1 Material

The Biochar-DAN and Biochar-TAN were used as an adsorbent for the removal of MB dye. The detailed discussion availability, collection and preparation of DAN may be found in Chapter 3. All chemical reagents having analytical grade and methylene blue dye were procured from S.D. Fine-Chem Ltd. and Merck Chemical, India, were used with no further purification.

7.2.2 Experimental procedure for preparation of biochar from pyrolysis of DAN and TAN-252-60-5

The detailed discussion about experimental set-up has been given in Chapter 3. The detailed about the preparation of biochar (Biochar-DAN and Biochar-TAN) has been discussed in Chapter 6 where DAN and TAN has been used for pyrolysis process. The Biochar-DAN and Biochar-TAN were the biochar obtained at optimum condition of pyrolysis for maximum pyrolysis oil yield from pyrolysis of torrefied *Acacia nilotica*. The bio-oil yield was maximum at a temperature of 507 ℃, retention time of 58 min, heating rate of 38 ℃/min and sweeping gas flow rate of 40.52 mL/min.

7.2.3 Characterization of biochar obtained from pyrolysis of DAN and TAN-252-60-5

Proximate and ultimate analyses were performed to characterize Biochar-DAN and Biochar-TAN. The solid addition technique (Liu et al., 2016) was employed to determine

the point of zero charge on the surface of adsorbent (Biochar-DAN and Biochar-TAN) which signifies the net charge density on the surface of adsorbent. The Fourier Transform Infrared Spectroscopy (FTIR) was performed to classify the functional groups present in Biochar-DAN and Biochar-TAN before and after adsorption due to change in vibrational frequency. The surface characteristics such as morphology and elements exist on surface of Biochar-DAN and Biochar-TAN before and after adsorption were studied by Scanning Electron Microscopy (SEM) and Energy-Dispersive X-ray spectroscopy (EDX). The crystalline structure of Biochar-DAN and Biochar-TAN was explored with X-ray Diffraction (XRD) analysis. The XRD spectra were studied at ambient temperature with Cu-Kα monochromatic radiation in the 2θ ranging from 10-80° with 2°/min scanning rate. Table 7.1 represents the specification of various instruments used for characterization of biochar and batch adsorption process.

Table 7.1 Specification of various analytical instruments used for characterization of biochar and batch adsorption process

Analytical instruments	Specification
CHNS analyzer	EURO EA3000, EURO ITALY
FTIR analyzer	Model Varian 1000, USA
SEM-EDX analyzer	Model JEOL JSM5410, Japan
UV- Spectrophotometer	Model 2201, Systronics India
Shaking speed incubator	Model NSW-133, Calton New Delhi, India
pH meter	Model LI 120, Elico, India
BET surface area analyzer	ASAP 2020 Micromeritics, USA
X-ray diffraction analyzer	mini flux II, Rigaku, Japan

7.2.4 Experimental procedure for removal of MB by batch adsorption process

The batch mode adsorption was performed for treatment of aqueous MB solution via Biochar-DAN and Biochar-TAN as adsorbents. Desired quantity of adsorbent was added in 50 mL MB solution of specific concentration in a 100 mL conical flask maintained at fixed pH. The flask was agitated in an incubator at a speed of 150 rpm at 25 ℃ until it attained the equilibrium. After that, the solution was filtered and the supernatant was examined by spectrophotometer to investigate the residual concentration of MB. Table 7.2 represents the variation of different parameters which were studied during the batch adsorption process. The pH of dye solution at desired value was obtained by adjusting the solution with 0.1M HNO_3 and 0.1M KOH solution. Preparation of stock solution of dye, cleaning of flasks and dilution of stock solution to obtain desired concentration of dye solution was done by using double distilled water. The percentage removal of MB and adsorption capacity was obtained by employing Eqs. (7.1) and (7.2), respectively.

$$\% \text{ Removal} = \frac{C_o - C_e}{C_o} \times 100 \quad (7.1)$$

$$q_e = \frac{(C_o - C_e) \times V}{M} \quad (7.2)$$

where C_o and C_e is initial and equilibrium concentration of MB in mg/L. q_e is adsorption capacity of adsorbent in mg/g. V is volume of MB solution in litre (L) and M is mass of adsorbent dose in gram (g).

Table 7.2 Different experimental conditions and their ranges studied during batch adsorption of MB dye

S. No.	Parameters studied	Range of operating parameters				
		pH	Adsorbent dose (g/L)	Temperature (K)	Initial concentration of MB (mg/L)	Equilibrium time (min)
1	Initial pH	2-11	2	298	50	1200
2	Equilibrium time	10	2	298	50	0-1200
3	Adsorbent dose	10	0.2-6	298	50	200
4	Temperature	10	2	293-323	50	200
5	Initial concentration of MB	10	2	298	10-300	200

7.3 Results and discussion

7.3.1 Characteristics of adsorbent Biochar-DAN and Biochar-TAN

7.3.1.1 Proximate and ultimate analyses of Biochar-DAN and Biochar-TAN

The detailed discussion about proximate analysis, ultimate analysis and higher heating value of both biochar (Biochar-DAN and Biochar-TAN) has been given in Chapter 6.

7.3.1.2 Point of zero charge (pH_{pzc}) for Biochar-DAN and Biochar-TAN

The pH_{pzc} of adsorbent is a very crucial parameter to comprehend the adsorption mechanism. It may be defined as the value of pH of solution at which net charge density of adsorbent surface is zero. At a pH of solution lower than the pH_{pzc}, the surface of adsorbent will be mostly positively charged, while, at a pH of solution higher than the pH_{pzc}, the

surface of adsorbent will be mostly negatively charged (Ronix et al., 2017). The point of zero charge allows in predicting the range of pH in which the electrostatic attraction between adsorbate and adsorbent favors the adsorption process. The pH_{pzc} for Biochar-DAN and Biochar-TAN was found to be 8.1 and 7.6, respectively (Fig. 7.1). The lower value of pH_{pzc} in case of Biochar-TAN might be due to lower intensity of functional groups associated with it. Since, Biochar-TAN has been obtained from pyrolysis of TAN which is obtained by thermally treating the DAN during torrefaction.

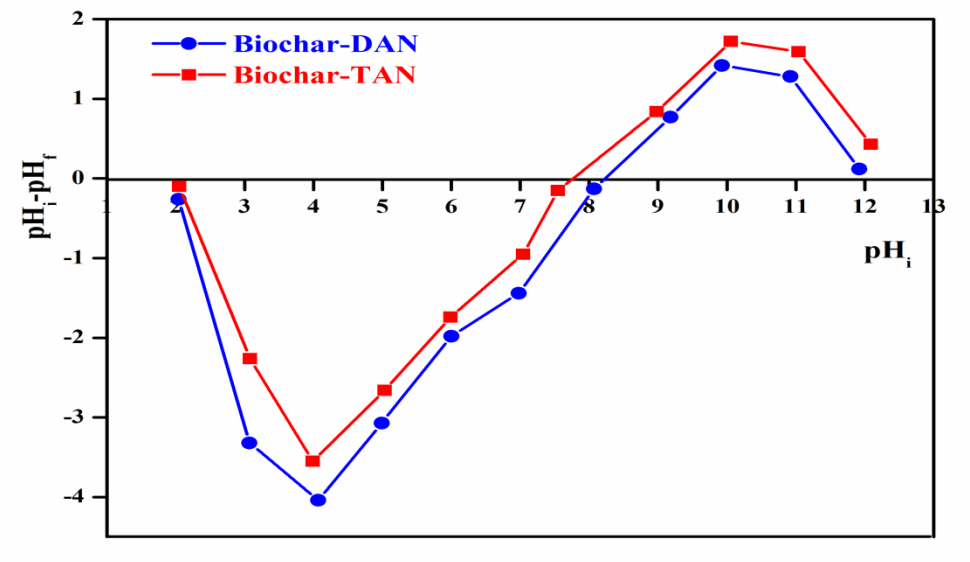

Figure 7.1 Point of zero charge (pH_{pzc}) for Biochar-DAN and Biochar-TAN

7.3.1.3 XRD analysis of Biochar-DAN and Biochar-TAN

Powder X-ray diffraction (XRD) analysis of Biochar-DAN and Biochar-TAN were performed. The results are shown in Fig. 7.2. It can be seen that broad peaks at 2θ value around 22^{o} in both the biochars corresponds to C(002). The C(002) plane was attributed to

parallel and azimuthal orientation of partially carbonized aromatic lamellae (Huang et al., 2009; Mohan et al., 2018). Broad and flat peaks for C(002) plane signifies lower degree of orientation (Huang et al., 2009).

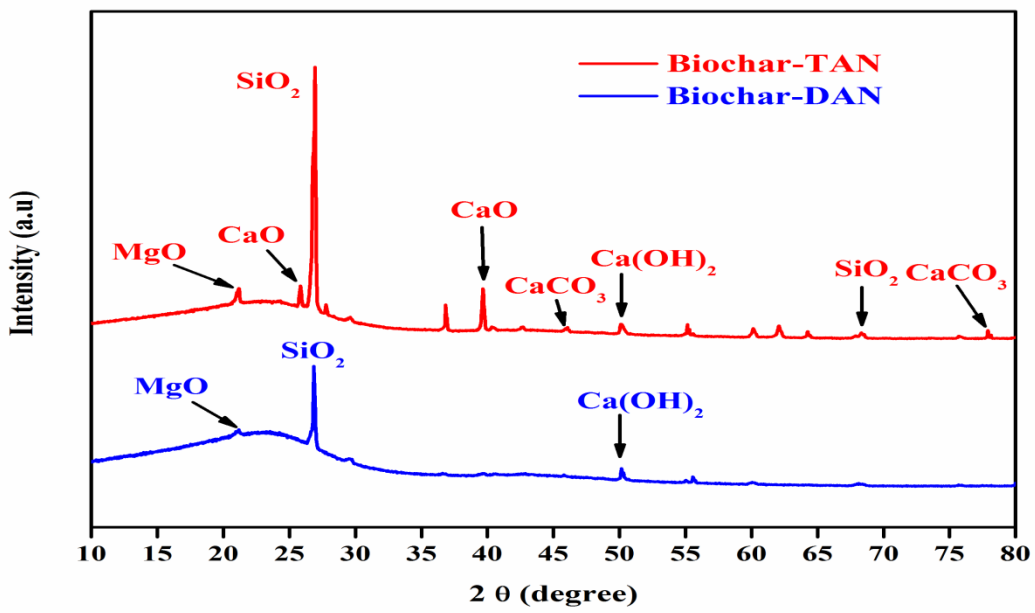

Figure 7.2 XRD analysis of Biochar-DAN and Biochar-TAN

Lui et al. (Liu et al., 2012) also concluded that broad peak between 2θ of 20^o and 30^o corresponds to staking structure of aromatic layer and broadening of peak arises due to small dimension of crystal perpendicular to aromatic layer. The Sharp and small peaks in case of Biochar-DAN at 2θ around 21^o and 50^o corresponds to MgO and $Ca(OH)_2$, while, a sharp and strong peak at 2θ around 27^o corresponds to SiO_2 (Mohan et al., 2018). In case of Biochar-TAN, more sharp and higher intensity peaks than the Biochar-DAN were identified at 2θ around 21^o, 26^o, 27^o, 39^o, 46^o, 50^o, 68^o, and 78^o which corresponds to MgO,

CaO, SiO_2, CaO, $CaCO_3$, $Ca(OH)_2$, SiO_2 and $CaCO_3$, respectively. Similar results can be found in published literatures (Huang et al., 2009; Liu et al., 2012; Mohan et al., 2018).

7.3.1.4 BET surface area and SEM-EDX analysis of Biochar-DAN and Biochar-TAN

The results of BET analysis are given in Table 7.3. The BET surface area of Biochar-DAN and Biochar-TAN was found to be 80.40 and 103.47 m^2/g, individually. The t-plot micropore volume of Biochar-DAN and Biochar-TAN was found to be 0.0641 and 0.0905 cm^3/g, respectively. Further, the BJH adsorption and desorption average pore diameter of Biochar-DAN and Biochar-TAN was noted to be 2.58 and 3.14 nm, and 2.13 and 2.87 nm, respectively. Both the biochars may be categorized as mesoporous material since their average pore size was found between 2 to 50 nm (Fan et al., 2017). Thus, results showed that both the biochar (Biochar-DAN and Biochar-TAN) can be potentially used as adsorbent; however, Biochar-TAN has superior properties than the Biochar-DAN for adsorption process.

Table 7.3 BET surface area analysis of Biochar-DAN and Biochar-TAN

Properties	Biochar-DAN	Biochar-TAN
BET surface area (m^2/g)	80.40	103.47
micropore volume (cm^3/g)	0.0641	0.0905
BJH adsorption average pore diameter (nm)	2.5881	3.1478
BJH desorption average pore diameter (nm)	2.1399	2.8709

Figs. 7.3(a) and (b) depict the SEM-EDX analysis of Biochar-DAN before and after adsorption. Fig. 7.3(a) depicts honeycomb like structure (Fan et al., 2017) of Biochar-DAN before adsorption where wide pores can be seen. EDX analysis confirmed that C, K, Ca, O, N were exist on the surface of Biochar-DAN. The pores present on the surface of Biochar-DAN facilitate its potential in adsorption process. The SEM-EDX analysis of Biochar-DAN after adsorption is depicted in Fig. 7.3(b), where blocked pores can be seen due to

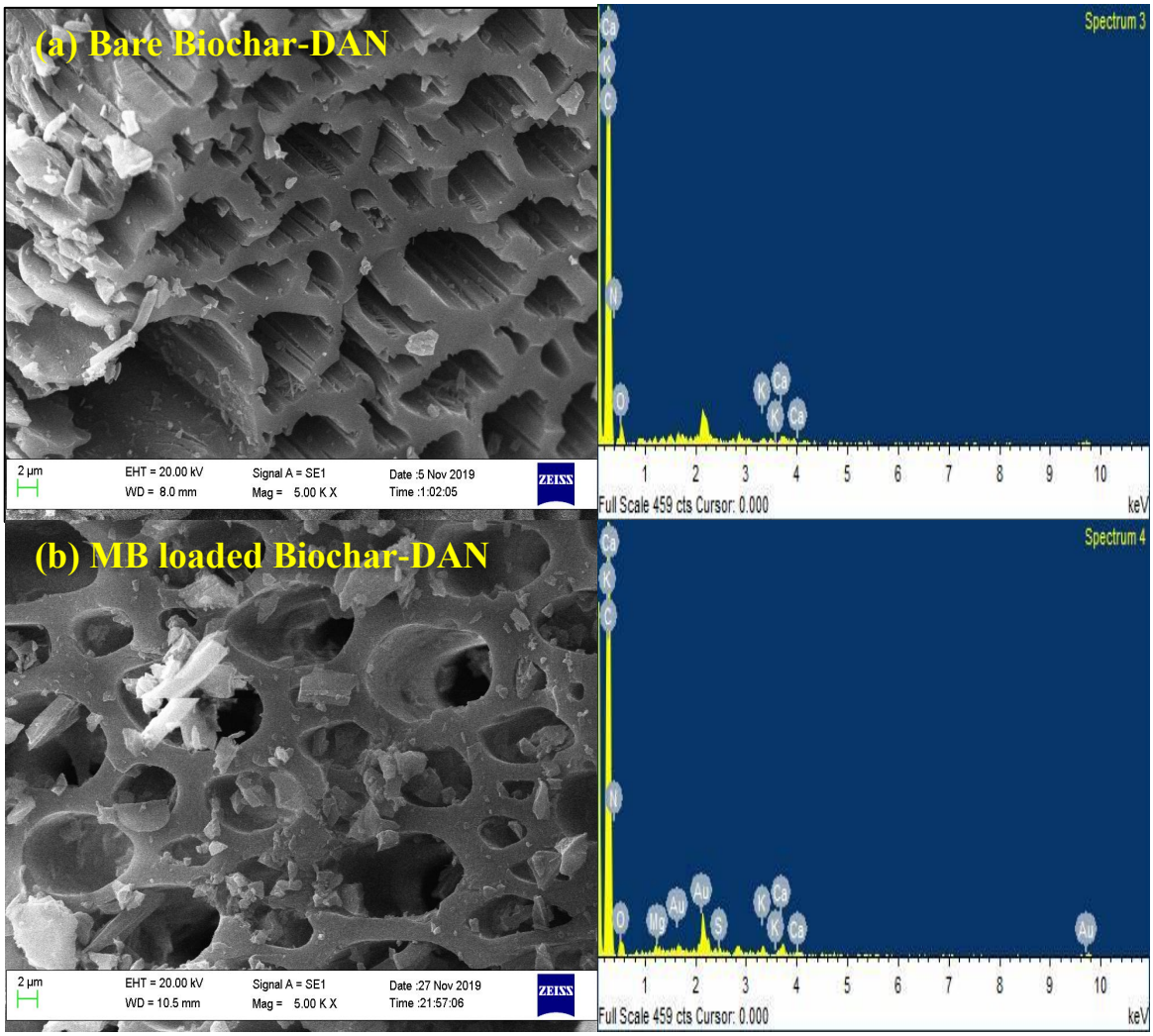

Figure 7.3 SEM-EDX analysis of Biochar-DAN before and after adsorption (a) Bare Biochar-DAN (b) MB loaded Biochar-DAN

layer of matter deposited inside the pores which confirmed the adsorption of MB on biochar. Element S along with C, K, Ca, O, N was perceived on the surface of biochar after adsorption which further confirmed the adsorption of MB.

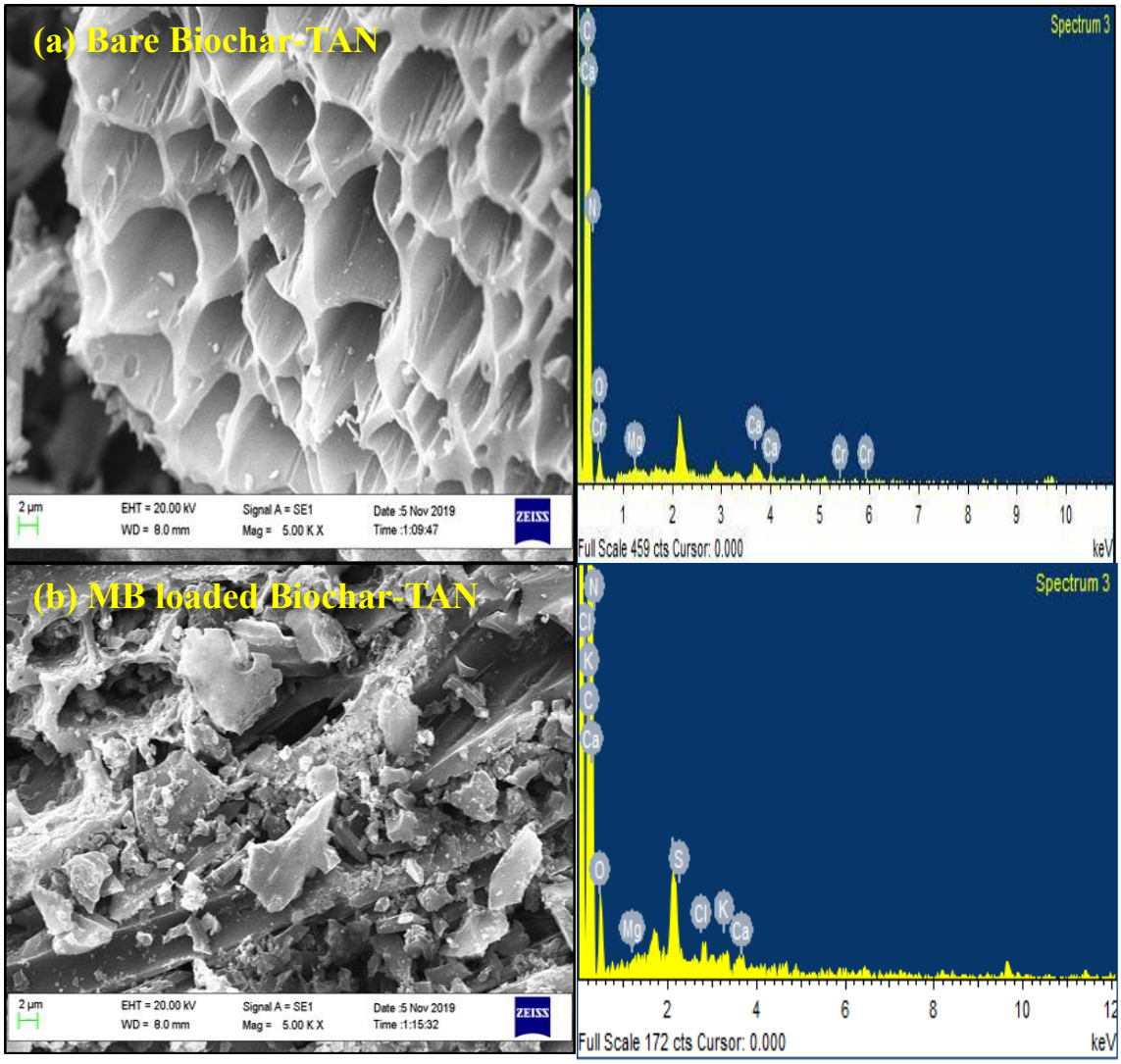

Figure 7.4 SEM-EDX analysis of Biochar-TAN before and after adsorption (a) Bare Biochar-TAN (b) MB loaded Biochar-TAN

Figs. 7.4(a) and (b) present the SEM-EDX of Biochar-TAN before and after adsorption. Biochar-TAN has wider pores than the Biochar-DAN. The EDX analysis confirmed that C, K, Ca, O, N, Mg were existing on the surface of Biochar-TAN. In case of Biochar-TAN after adsorption, filled pores can be seen. Element S and Cl can be seen in EDX image of Biochar-TAN suggesting the adsorption of MB on biochar.

7.3.1.5 FTIR analysis of biochar Biochar-DAN and Biochar-TAN

The FTIR analysis of Biochar-DAN and Biochar-TAN before and after adsorption was performed and their spectra are displayed in Fig. 7.5(a) and (b). The FTIR analysis provides a quick and efficient technique to identify the class of various chemical compounds. The FTIR spectra confirm the presence of various functional groups associated with biochar.

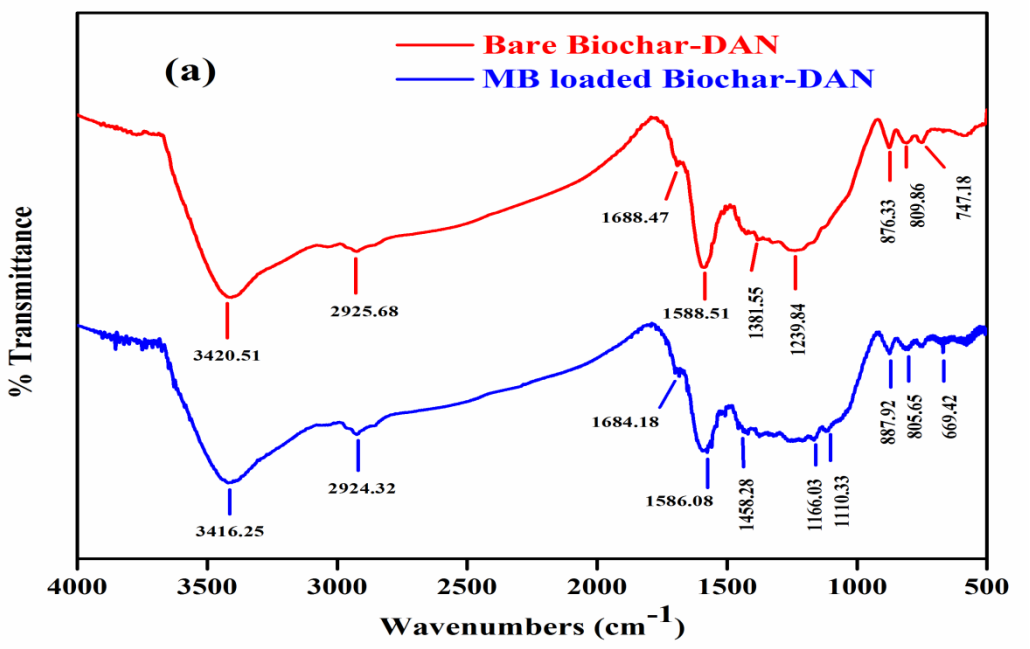

For Biochar-DAN, the peaks at 3420.51 cm^{-1} (before adsorption) and 3416.25 cm^{-1} (after adsorption) correspond to stretching vibration of O-H bonded groups such as phenol,

alcohol, and water (Fan et al., 2017). The wavenumbers 2925.68 cm^{-1} (before adsorption) and 2924.32 cm^{-1} (after adsorption), are ascribed to the stretching and deformation vibration of aliphatic C-H groups. The wavenumbers 1688.47 cm^{-1} (before adsorption) and 1684.18 cm^{-1} (after adsorption) are assigned to C=O vibration of aldehyde, and ketones and C=C aromatic vibrations. The wavenumbers 1588.47 cm^{-1} (before adsorption) and 1586.18 cm^{-1} (after adsorption) correspond to secondary amine groups. The wavenumbers 1239.84 cm^{-1} (before adsorption) and 1166.03 cm^{-1} (after adsorption) are ascribed to deformative vibration of aromatic nitrogen to secondary amine groups. The wavenumber between 876.33- 805.65 cm^{-1} and 757.12-686.51 cm^{-1} ascribe the presence of wagging vibration of C-H bond in aromatic ring and vibration of alkyl halide along with bending vibration of Si-O-Si bond, respectively (Chen et al., 2019).

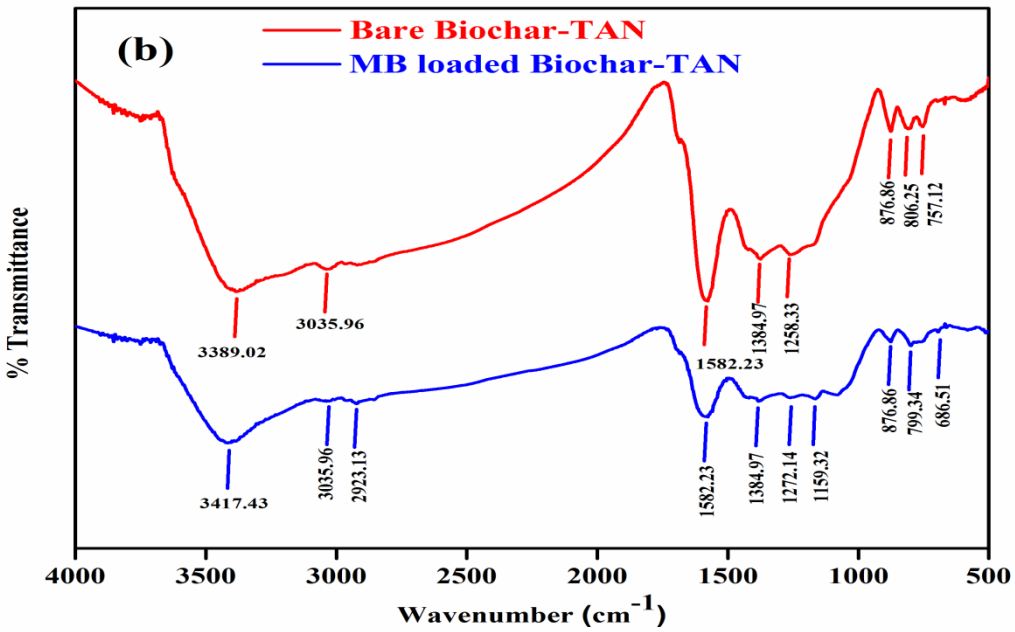

Figure 7.5 FTIR analysis of Biochar-DAN and Biochar-TAN before and after adsorption (a) Bare and MB loaded Biochar-DAN (b) Bare and MB loaded Biochar-TAN

Similar results were obtained for Biochar-TAN as well. The detailed analysis of FTIR spectra and assignment of different wavenumber is presented in Table 7.4. The intensity for Biochar-TAN was slightly lower than that of Biochar-DAN. This might be due to torrefaction as considerable rupture of –C-O, -O-H etc. bonds takes place and there is formation of CO_2 and lighter non-condensable gases. The intensity of functional groups such as –O-H, -C-H, -N-H and -C=O decreased after adsorption of MB on the biochar. This confirmed that these groups have participated in adsorption process. Also, in case of Biochar-DAN, some wavenumbers such as 1381.55, and 747.18 cm^{-1} disappeared, while, some new wavenumbers such as 1458.28, 1110.3, and 669.42 cm^{-1} were identified. Similarly, in case of Biochar-TAN, 757.12 cm^{-1} disappeared, while wavenumber 2923.33, 1159.32, 686.51 cm^{-1} were identified. This might be due to chemisorption on the surface of biochar resulting in formation of new compounds (Ji et al., 2019). The formation of hydrogen bond between –OH group of biochar and oxygen present in MB and electrostatic attraction of cationic MB by large number of –OH groups present in the solution at higher pH are mainly responsible for adsorption of MB on the biochar. In addition, the functional groups having oxygen atoms also form complex with MB molecules through surface complexation resulting in adsorption of MB on the surface of biochar (Fan et al., 2017).

Table 7.4 Functional groups detected in Biochar-DAN and Biochar-TAN before and after adsorption of MB dye

Bare Biochar-DAN (wavenumber cm^{-1})	MB loaded Biochar-DAN	Diff	Assignment	Bare Biochar-TAN	MB loaded Biochar-TAN	Diff	Assignment
3420.51	3416.25	4.26	Bonded -OH groups	3389.02	3417.43	-28.41	Bonded -OH groups
2925.68	2924.32	1.36	Aliphatic C-H group	3035.96	3035.96	0	Aromatic C-H group
1688.47	1684.18	4.29	Assigned to C=O and C=C aromatic vibrations	-	2923.33	-	Aliphatic C-H group
1588.51	1586.08	2.43	Secondary amine groups	1582.23	1582.23	0	Assigned to C=O and C=C aromatic vibrations
1381.55	-	-	-CH bending, $-CH_3$ asymmetric bending	1384.97	1384.97	0	-CH bending, $-CH_3$ asymmetric bending
-	1458.28	-	C-H alkanes in aromatic ring	1258.33	1272.14	-13.81	Ar-N deformation vibration
1239.84	1166.03	73.81	Ar-N deformation vibration	-	1159.32	-	Ar-N deformation vibration
-	1110.3	-	Ar-N deformation vibration	876.86	876.86	-	Wagging vibration of C-H in aromatic ring
876.33	887.92	-11.5	Wagging vibration of C-H in aromatic ring	806.25	799.34	6.91	Wagging vibration of C-H in aromatic ring
809.86	805.65	4.21	Wagging vibration of C-H in aromatic ring	757.12	-	-	Alkyl halide, Bend vibration of Si-O-Si
747.18	-	-	Alkyl halide, Bend vibration of Si-O-Si	-	686.51	-	Alkyl halide, Bend vibration of Si-O-Si
-	669.42	-	Alkyl halide, Bend vibration of Si-O-Si	-	-	-	-

7.3.2 Batch adsorption analysis of MB onto Biochar-DAN and Biochar-TAN

7.3.2.1 Effect of contact time and initial concentration of MB

The contact time for adsorption has obvious effect on adsorption capacity of both biochars. Fig. 7.6(a) and Fig. 7.7(a) display the effect of contact time on adsorption capacity of MB for Biochar-TAN and Biochar-DAN, respectively. The adsorption capacity for both the biochar increased sharply up to first 200 min and then slowly attains stability before reaching to equilibrium. The rapid increase in uptake capacity at the beginning is attributed to fast diffusion of MB molecules from the liquid solution to external surface of adsorbent; while slow and steady uptake capacity after certain time owing to longer diffusion path to interior pores of adsorbent and saturation of active sites for further adsorption (Ji et al., 2019; Li et al., 2018). In addition, uptake capacity increased as the initial concentration of MB increased. At higher concentration of dye, the probability of effective collision between adsorbent and MB molecule increased, resulting in higher adsorption capacity (Alinejad-Mir et al., 2018; Banerjee & Chattopadhyaya, 2017). Furthermore, the adsorption capacity of Biochar-TAN was higher than the Biochar-DAN. This might be due to higher surface area, higher active sites, pore size and surface complexation due to higher concentration of calcium, magnesium and silicon ions on the surface of Biochar-TAN.

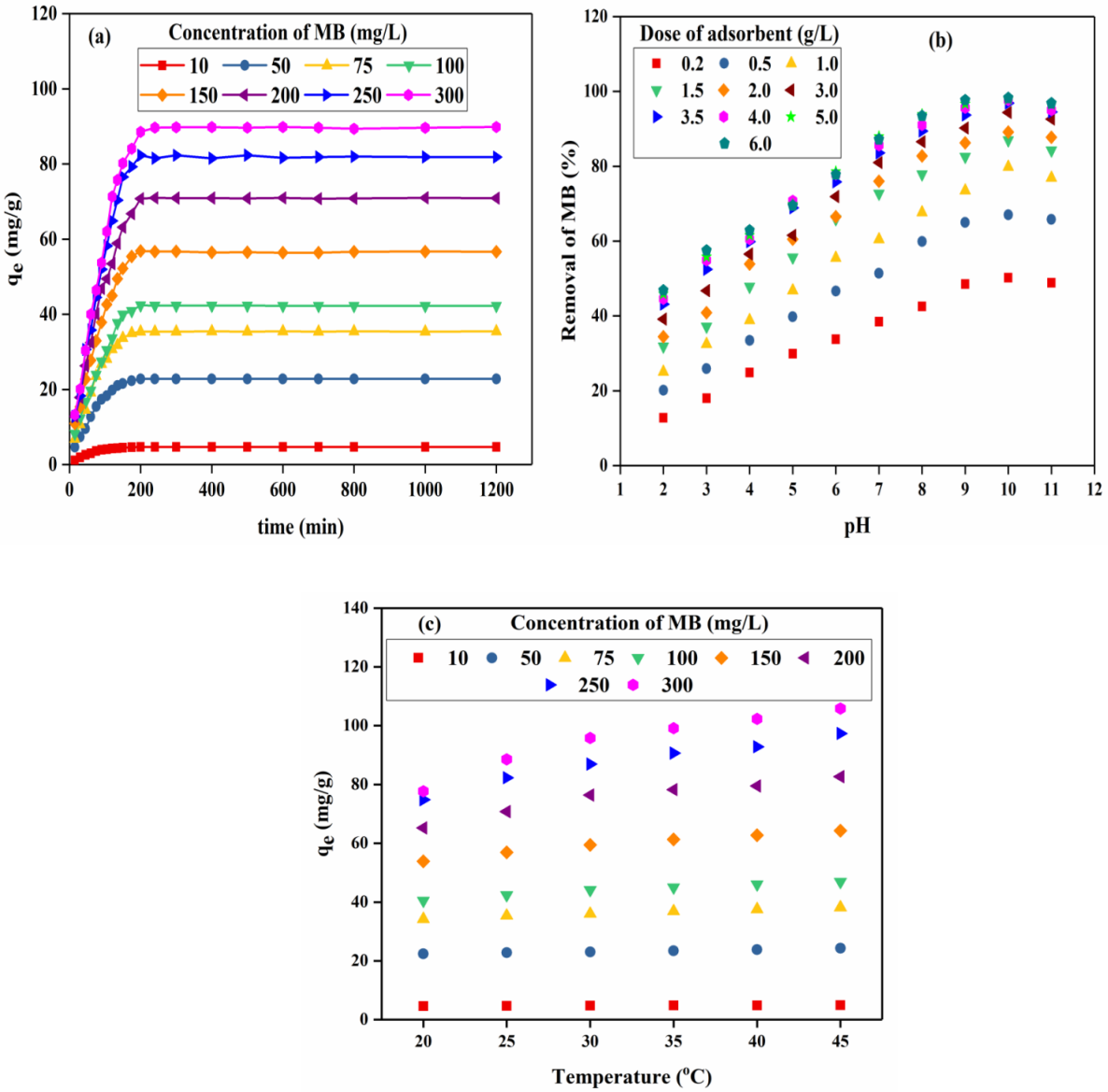

Figure 7.6 Effect of operating parameters on uptake capacity of adsorption process using Biochar-TAN (a) effect of time and concentration (at fixed pH = 10, Temp = 298 K, adsorbent dose = 2 g/L) (b) effect of pH and dose (at fixed Temp = 298 K, MB concentration = 50 mg/L, time = 200 min) (c) effect of temperature and concentration (at fixed pH = 10, adsorbent dose = 2 g/L, time = 200 min)

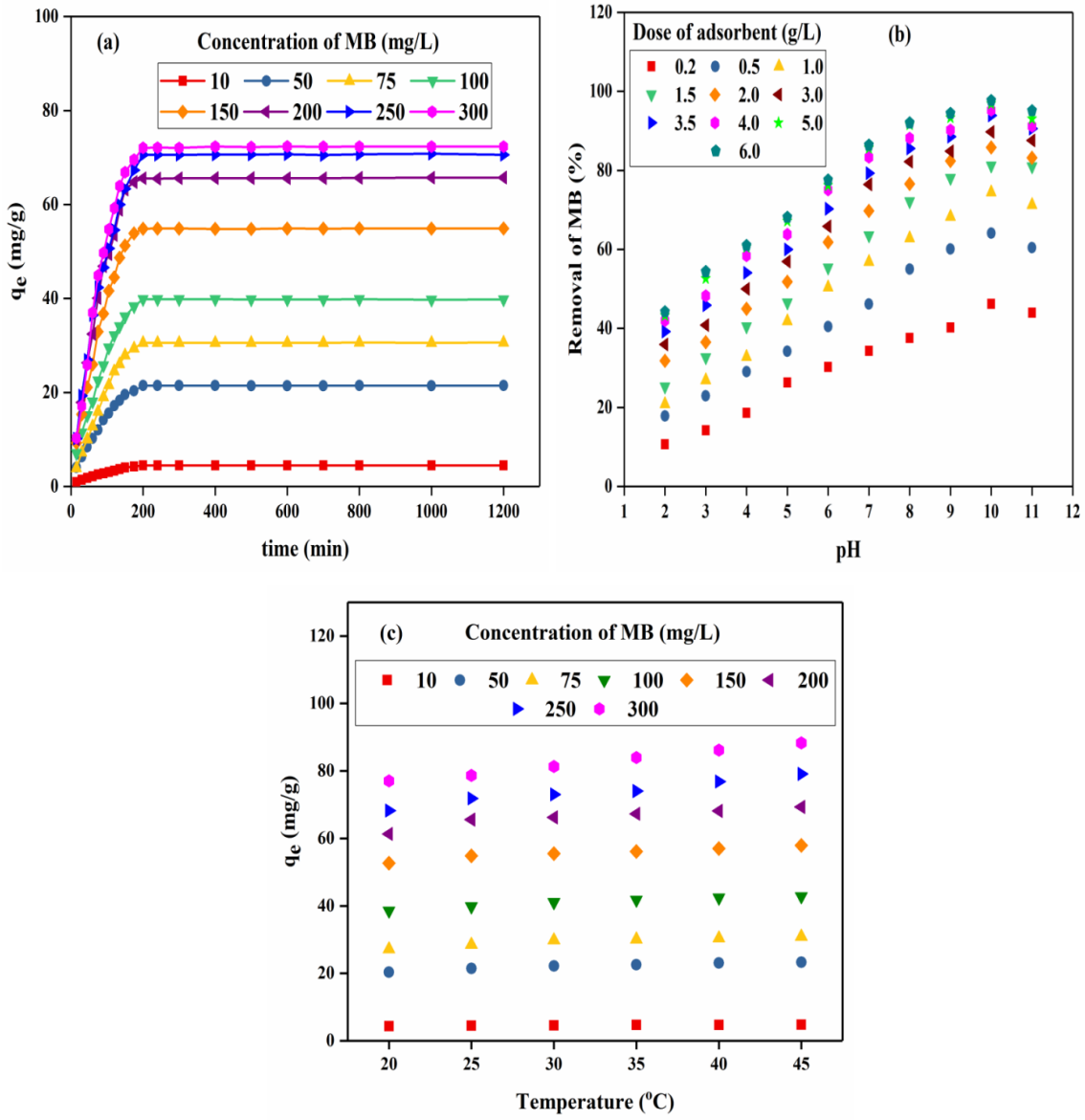

Figure 7.7 Effect of operating parameters on uptake capacity of adsorption process using Biochar-DAN (a) effect of time and concentration (at fixed pH = 10, Temp = 298 K, adsorbent dose = 2 g/L) (b) effect of pH and dose (at fixed Temp = 298 K, MB concentration = 50 mg/L, time = 200 min) (c) effect of temperature and concentration (at fixed pH = 10, adsorbent dose = 2 g/L, time = 200 min)

7.3.2.2 Effect of pH of solution and adsorbent dose

The pH of working solution is a very significant parameter since it affects the charge density and dissociation of functional groups associated with adsorbent as well as structure of MB (Li et al., 2018; Liu et al., 2019). Effect of pH of solution varying from 2.0 to 11.0, for both the biochar (Biochar-TAN and Biochar-DAN) was investigated by different adsorbent dosage varying from 0.2 to 6 g/L for 50 mg/L MB solution and 1200 min adsorption time. The results are displayed in Fig. 7.6(b) and Fig. 7.7(b). It can be perceived at particular dose of adsorbent, the percentage removal increased up to a maximum value at pH 10 and after that percentage removal slightly decreased. Similar finding were also reported by Li et al. (Li et al., 2018), Ji et al. (Ji et al., 2019) for adsorption of MB. The significance of pH can be analyzed based on the pH of solution and point of zero charge for both the adsorbents. MB is accepted as cationic dye having positive charge. The pH_{pzc} for Biochar-DAN and Biochar-TAN was found to be 8.10 and 7.6, respectively. It implies that at pH lower than pH_{pzc}, the adsorbent surface will be positively charged, while, pH greater than pH_{pzc}, it will be negatively charged. Thus, the electrostatic attraction among MB molecules and adsorbent will be stronger at higher pH. However, at pH higher than 10 the steric hindrance among the $-OH^-$ ions might be responsible for reduction in percentage removal of MB.

The adsorbent dose is a crucial parameter for investigating the adsorption capacity of both biochars. The effect of adsorbent dose was examined by changing the adsorbent dose from 0.2 to 6.0 g/L and the results are displayed in Fig. 7.6(b) for Biochar-TAN and Fig. 7.7(b) for Biochar-DAN. It was noticed that as the adsorbent dose increases, the percentage removal of MB for both biochar has increased. This could be attributed to higher surface

area and more number of active adsorption sites with increase in adsorbent dose. However, lower adsorption capacity was noticed at higher adsorbent dose because increase in adsorbent dose, enhance the probability of collision between adsorbent molecules, which resulted in aggregation and overlapping of adsorbent molecules causing lower surface area as well as longer diffusion path for MB molecules (Alinejad-Mir et al., 2018; Ye et al., 2015).

7.3.3 Kinetics and mass transfer study for adsorption of MB onto Biochar-DAN and Biochar-TAN

7.3.3.1 Adsorption kinetics

The adsorption kinetics was performed to investigate the rate of adsorption of MB onto the adsorbent. Also, kinetics of adsorption revealed the rate controlling step as well as mass transfer mechanism associated with movement of molecules of MB from liquid solution to adsorbent surface. For adsorption kinetics, the experiments were performed in time interval of 15-200 min by changing the concentration of MB from 10-300 mg/L and keeping rest of the factor like (pH, adsorbent dose, temperature, and incubator speed) at constant value. In this study, three kinetic models namely, pseudo first order (Eq. 7.3), pseudo second order (Eq. 7.4) and Elovich model (Eq. 7.5) and two mass transfer models such as Weber and Morris (Eq. 7.6) also known as intra-particle diffusion model and Boyd model (Eq. 7.7) were tested.

$$\log(q_e - q_t) = \log q_e - \frac{k_1 t}{2.303} \quad (7.3)$$

$$\frac{t}{q_t} = \frac{t}{q_e} + \frac{1}{k_2 q_e^2} \quad (7.4)$$

$$q_t = \frac{1}{\beta}\ln(\alpha\beta) + \frac{1}{\beta}\ln t \quad (7.5)$$

$$q_t = k_{id}t^{0.5} + C \quad (7.6)$$

$$\ln(1 - F) = -k_{fd}t \quad (7.7)$$

Where q_e is equilibrium uptake capacity (mg/g); q_t is uptake capacity (mg/g) at time t; k_1 is pseudo-first-order rate constant (min^{-1}): k_2 is pseudo-second-order rate constant (g/mg.min); β is constant for desorption (g/mg); α is rate of initial desorption (mg/gmin); k_{id} is rate constant for intra-particle diffusion; C is intercept (mg/g); F is fraction for adsorbed solute at any time t ($F = \frac{q_t}{q_e}$, dimensionless); k_{fd} is constant for liquid film diffusion (sec^{-1}).

The Pseudo first order model was applied to calculate the rate of adsorption of adsorbate onto the surface of adsorbent based on the adsorption capacity. As per the pseudo first order model, initially MB molecules were not present on the surface of adsorbent at the start of adsorption process, however MB molecules start accumulating on the surface of adsorbent until the process reached equilibrium. The theoretical adsorption capacity and rate constant parameters were calculated at different concentrations using Eq. 7.3 and results are shown in Fig. 7.8(a) for Biochar-TAN and Fig. 7.9(a) for Biochar-DAN. The theoretical adsorption capacity ($q_{e,cal}$), first order rate constant (k_1) and correlation coefficient (R^2) for both the biochar are given in Table 5 at different concentrations of MB dye from 10-300 mg/L. The adsorption capacity for Biochar-DAN varies from 5.9563 to 128.9228 mg/g, while, for Biochar-TAN it varies from 5.5195 to 131.492 mg/g, once the concentration varies from 10 to 300 mg/L. The value of k_1 varies from 0.0166 to 0.0244

min^{-1} for Biochar-DAN and for Biochar-TAN it varies from 0.0161 to 0.0234 min^{-1}. R^2 for Biochar-DAN varies from 0.8941 to 0.9629, while for Biochar-TAN it varies from 0.9052 to 0.9876.

The pseudo second order model was employed to describe the dynamics of adsorption process. This model is based on the assumption that chemisorption is the rate determining step and adsorption capacity is proportional to the available active site on the surface of adsorbent. The theoretical adsorption capacity and rate constant parameters were calculated at different concentrations using the Eq. 7.4 and results are shown in Fig. 7.8(b) for Biochar-TAN and Fig. 7.9(b) for Biochar-DAN. The theoretical adsorption capacity ($q_{e,cal}$), pseudo second order rate constant (k_2) and correlation coefficient (R^2) for both the biochar are shown in given in Table 7.5 at different concentrations of MB from 10-300 mg/L. The adsorption capacity for Biochar-DAN varies from 6.4771 to 205.7613 mg/g, while, for Biochar-TAN it varies from 6.4808 to 208.3333 mg/g, once the concentration varies from 10 to 300 mg/L. The value of k_2 varies from 2.33×10^{-3} to 1.96×10^{-5} (g/(mg.min)) for Biochar-DAN and for Biochar-TAN it varies from 2.32×10^{-3} to 1.91×10^{-5} (g/(mg.min)). R^2 for Biochar-DAN varies from 0.9025 to 0.9899, while for Biochar-TAN it varies from 0.8927 to 0.9889. The adsorption affinity or initial rate constant ($V_o= k_2q_e^2$) signifies the rate of adsorption at the beginning. For Biochar-DAN the value of V_o varies from 0.0977 to 0.8479 mg/g.min, while for Biochar-TAN it varies from 0.9744 to 0.8289 mg/g.min. At different concentration of MB dye, the value of k_2 decreased with increase in V_o and $q_{e,cal}$. This revealed that adsorption of MB dye was faster at initial stage when the concentration of MB dye was increased.

Further, Elovich model was also fitted with experimental results. The Elovich model is employed to test the nature of adsorption whether it is physisorption or chemisorption. With the help of Eq. 7.5 the kinetic parameters α and β are calculated and the results are shown in Fig. 7.8(c) for Biochar-TAN and Fig. 7.9(c) for Biochar-DAN. The value of α for Biochar-DAN varies from 0.2597 to 4.0820, while for Biochar-TAN it varies from 0.8862 to 3.8928. The value of β varies from 0.0675 to 1.1164 for Biochar-DAN, while it varies from 0.0512 to 1.3239 for Biochar-TAN. The value of correlation coefficient for Biochar-DAN varies from 0.7811 to 0.8275, while for Biochar-TAN it varies from 0.7385 to 0.8231.

The kinetic model which gives the closest value of experimental and theoretical adsorption capacity along with correlation value nearer to one will be followed during adsorption process. Based on the above criteria it was found that among the tested models the pseudo second order kinetic model was followed during adsorption for both Biochar-DAN and Biochar-TAN as an adsorbent.

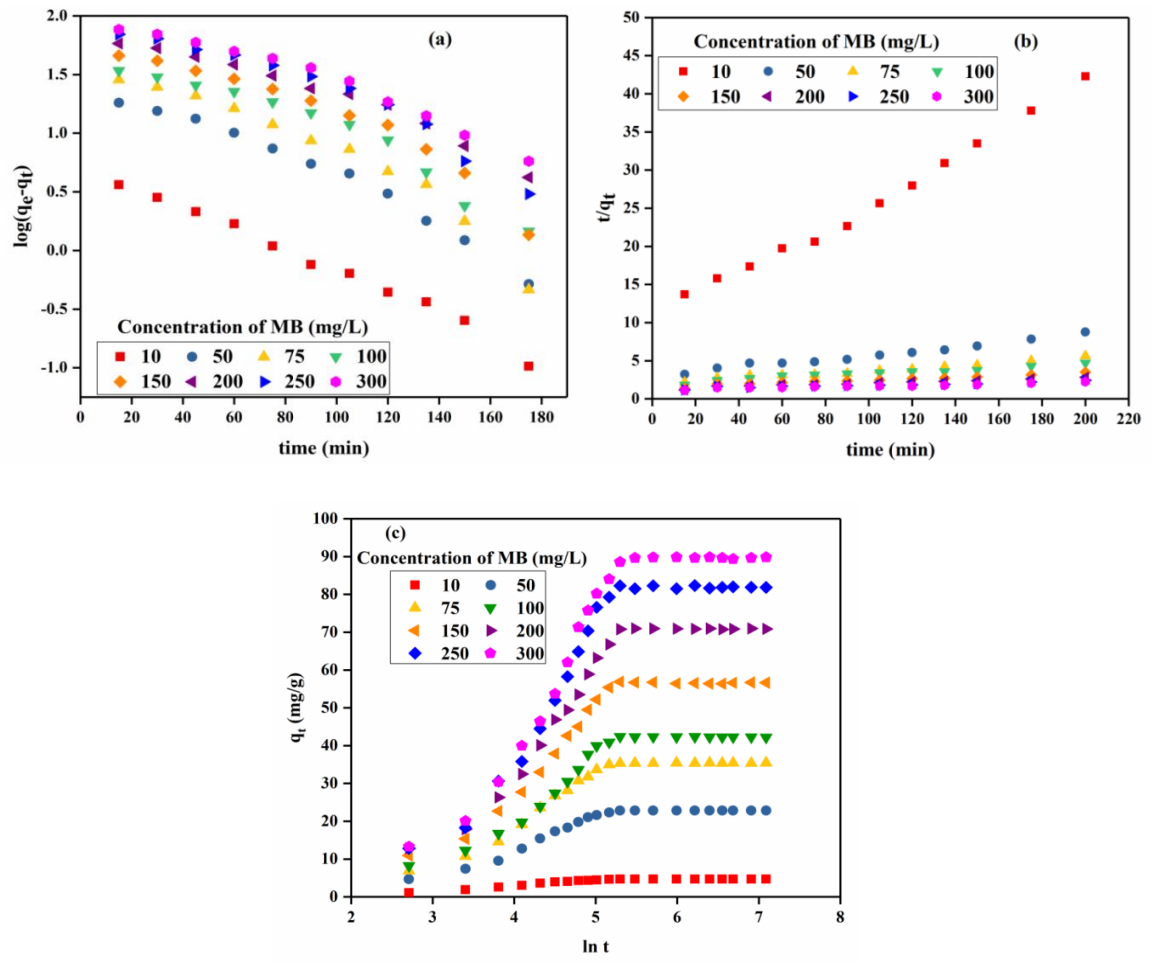

Figure 7.8 Kinetic model for adsorption of MB dye on Biochar-TAN (a) pseudo-first-order (b) pseudo-second-order and (c) Elovich

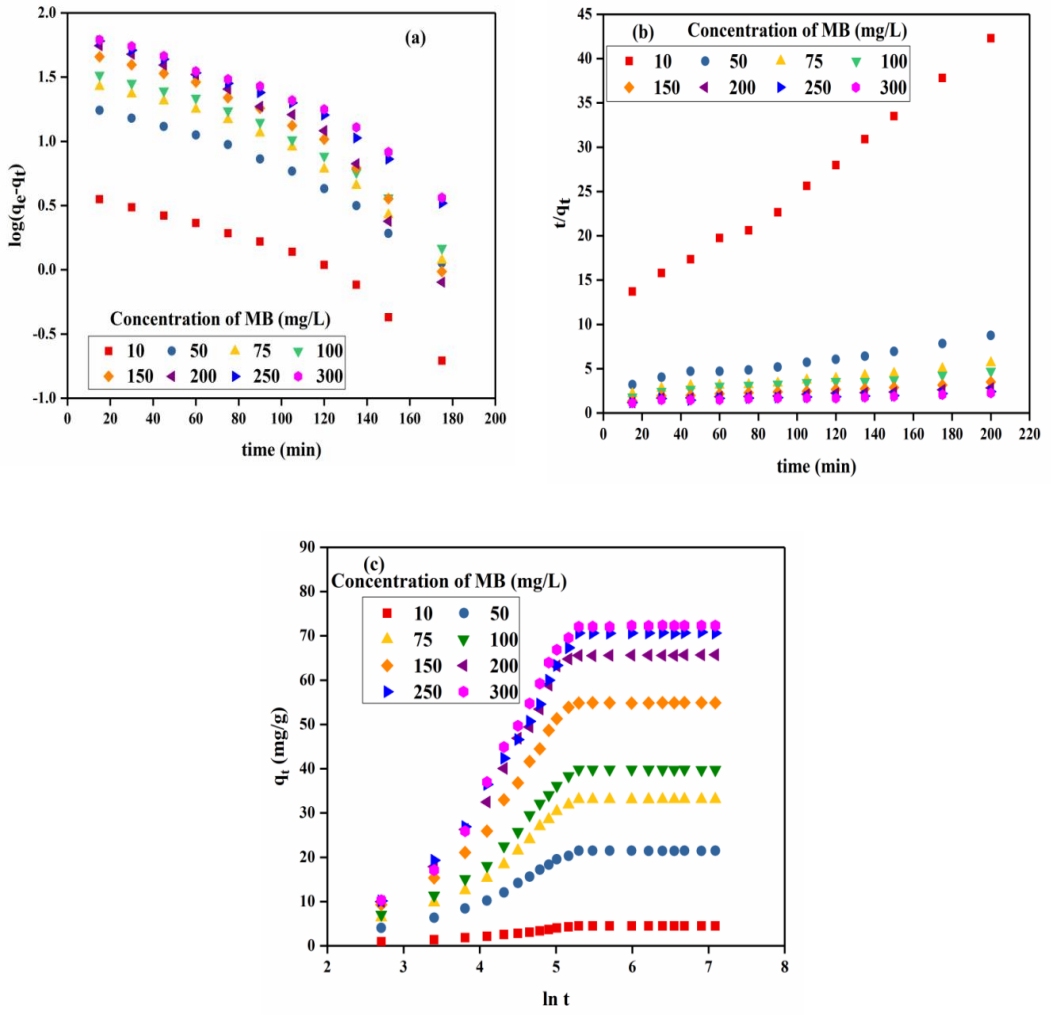

Figure 7.9 Kinetic model for adsorption of MB dye on Biochar-DAN (a) pseudo-first order (b) pseudo-second-order and (c) Elovich

Table 7.5 Adsorption kinetics and related parameters for adsorption of MB dye onto Biochar-DAN and Biochar-TAN

Kinetic model	Parameters	Initial concentration (mg/L)							
		10	50	75	100	150	200	250	300
Biochar-DAN									
Pseudo first order	$q_{e,exp}$(mg/g)	4.4755	21.47	30.588	39.835	54.855	65.58	70.6125	72.075
	$q_{e,cal}$ (mg/g)	5.9563	28.5121	48.8742	59.5634	95.2796	128.9228	94.7850	97.1627
	k_1 (min^{-1})	0.0166	0.0169	0.0186	0.0166	0.0217	0.0244	0.0169	0.0162
	R^2	0.9181	0.9629	0.9402	0.9181	0.9181	0.8941	0.9549	0.9453
Pseudo second order	$q_{e,cal}$ (mg/g)	6.4771	36.9003	60.0240	76.3358	102.3540	131.5789	187.9699	205.7613
	k_2 (g/(mg.min))	2.33×10^{-3}	2.45×10^{-4}	1.34×10^{-4}	8.57×10^{-5}	6.43×10^{-5}	4.45×10^{-5}	2.24×10^{-5}	1.96×10^{-5}
	V_o (mg/g.min)	0.0977	0.3335	0.4827	0.4993	0.6704	0.7704	0.8479	0.8298
	R^2	0.9899	0.9758	0.9695	0.9492	0.9637	0.9526	0.9025	0.9190
Elovich model	β (g/mg)	1.1164	0.2313	0.1493	0.1230	0.0902	0.0759	0.0688	0.0675
	α (mg/g.min)	0.2597	1.2437	1.8923	2.2012	3.2549	4.0820	3.8096	4.0128
	R^2	0.8275	0.8137	0.8048	0.8060	0.7913	0.7811	0.8189	0.7910
Biochar-TAN									
Pseudo first order	$q_{e,exp}$(mg/g)	4.732	22.835	35.404	42.305	56.7225	70.98	81.525	89.67
	$q_{e,cal}$ (mg/g)	5.5195	33.9859	60.2282	65.9629	88.920	92.755	131.492	125.545
	k_1 (min^{-1})	0.0212	0.2180	0.0234	0.0197	0.0198	0.0156	0.0188	0.0161
	R^2	0.9876	0.9650	0.9177	0.9192	0.9052	0.9517	0.9228	0.9601
Pseudo second order	$q_{e,cal}$ (mg/g)	6.4808	36.9003	60.2409	76.3358	103.0927	131.5789	188.6792	208.3333
	k_2 (g/(mg.min))	2.32×10^{-3}	2.45×10^{-4}	1.33×10^{-4}	8.57×10^{-5}	6.34×10^{-5}	4.45×10^{-5}	2.22×10^{-5}	1.91×10^{-5}
	V_o (mg/g.min)	0.9744	0.3335	0.4826	0.4993	0.6738	0.7704	0.7903	0.8289
	R^2	0.9889	0.9761	0.9664	0.9441	0.9601	0.9479	0.8927	0.9109
Elovich model	β (g/mg)	1.3239	0.2382	0.1501	0.1176	0.0883	0.0677	0.0573	0.0512
	α (mg/g.min)	0.8862	2.0813	2.9287	2.5007	3.4518	3.5466	3.8928	3.8371
	R^2	0.7385	0.7673	0.7684	0.7967	0.7981	0.8231	0.7991	0.8174

7.3.3.2 Mass transfer models

7.3.3.2.1 Weber and Morris model

Weber and Morris model was employed to investigate whether the rate controlling step during the adsorption process was film diffusion or intra- particle diffusion (Fan et al., 2017). Fig. 7.10(a) and Fig. 7.11(a) showed the intra-particle diffusion model at different concentration of MB solution ranging from 10 to 300 mg/L for Biochar-TAN and Biochar-DAN respectively. The value of k_{id} and correlation coefficient obtained from the plot are given in Table 7.6. It can be seen that k_{id} value increased with increase in concentration due to higher driving force for adsorption. However, significant increase in k_{id} value was observed up to 150 mg/L and after that minor increase in k_{id} value was observed. This might be due to saturation of adsorbent surface at higher concentration of MB. Also, k_{id} value was higher in case of Biochar-TAN as compared to Biochar-DAN, which can be inferred to faster adsorption rate in case of Biochar-TAN than the Biochar-DAN. In addition, it was found that for both the biochar, the adsorption process was controlled by three stages. In first stage, initial adsorption was controlled by external surface adsorption. The intra-particle diffusion was rate determining step in second stage where gradual adsorption takes place. The third stage of adsorption was associated with final equilibrium stage where intra-particle diffusion gradually slows down due to lower concentration of MB (Wang et al., 2018a). In addition, for each concentration, none of the lines passes through origin, which confirmed that adsorption process was not exclusively governed by internal diffusion, however some other factors such as external diffusion or ion exchange might be responsible for adsorption process.

7.3.3.2.2 Boyd model

Further, Boyd model was also studied to investigate whether external film or internal diffusion controlled the adsorption of MB onto biochar. The Boyd plots for Biochar-TAN and Biochar-DAN at different concentration (10-300 mg/L) are shown in Fig. 7.10(b) and Fig. 7.11(b) respectively. The plots between ln(1-F) and time were used to calculate k_{fd} at different concentrations. The value of k_{fd} and correlation coefficients are presented in Table 7.6. The correlation coefficient for Biochar-TAN varied from 0.9137 to 0.988 and for Biochar-DAN it varied from 0.8940 to 0.9688. For both the biochar (Biochar-DAN and Biochar-TAN) the Boyd plots were non-linear at different concentrations, and did not pass through origin and revealing that it was not only intra-particle diffusion that determined the rate determining factor for adsorption of MB onto biochar. A combined effect of external surface diffusion, intra-particle diffusion and chemical reactions might be responsible for adsorption process.

Table 7.6 Mass transfer models and related parameters for adsorption of MB dye onto Biochar-DAN and Biochar-TAN

	Mass transfer parameters					
	Weber and Morris model			Boyd Model		
C_o (mg/L)	k_{id} (mg/g.min$^{1/2}$)	R^2	C_1 (intercept)	k_{fd} (sec^{-1})	R^2	C_2 (intercept)
Biochar-DAN						
10	0.1018	0.6004	1.9436	0.0165	0.9197	0.2813
50	0.4864	0.5781	9.4275	0.0169	0.9688	0.2836
75	0.7531	0.5709	14.4950	0.0186	0.9406	0.3888
100	0.9123	0.5696	17.2737	0.0182	0.9438	0.3745

150	1.2315	0.5483	24.6453	0.0217	0.9086	0.5521
200	1.4504	0.5324	30.1752	0.0244	0.8941	0.6759
250	1.6275	0.5770	30.4271	0.0168	0.9549	0.2944
300	1.6454	0.5432	31.9215	0.0196	0.9669	0.4135
Biochar-TAN						
10	0.7553	0.7385	0.1208	0.0213	0.9888	0.1541
50	4.1977	0.7673	−2.9453	0.0218	0.9685	0.3978
75	6.6578	0.7684	−5.4718	0.0238	0.9208	0.5496
100	8.5032	0.7967	−10.4071	0.0199	0.9260	0.4526
150	11.3130	0.7981	−13.4410	0.0200	0.9137	0.4526
200	14.7700	0.8231	−21.0720	0.0158	0.9526	0.2673
250	17.4330	0.7991	−26.1550	0.0204	0.9156	0.5390
300	19.5140	0.8174	−31.7550	0.0165	0.9633	0.3409

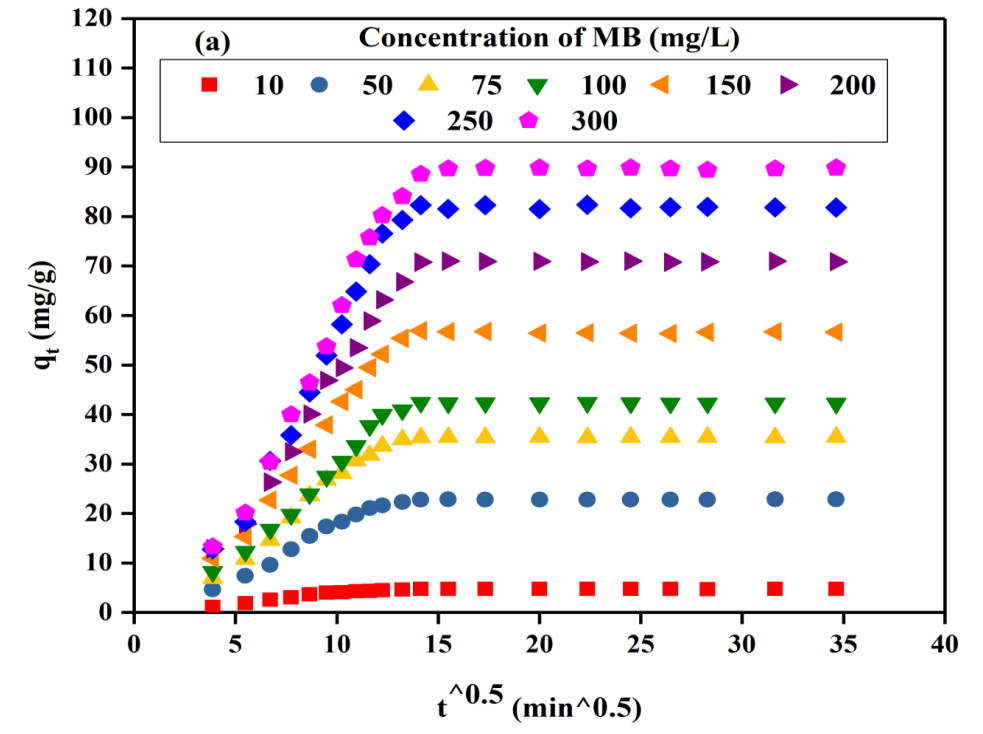

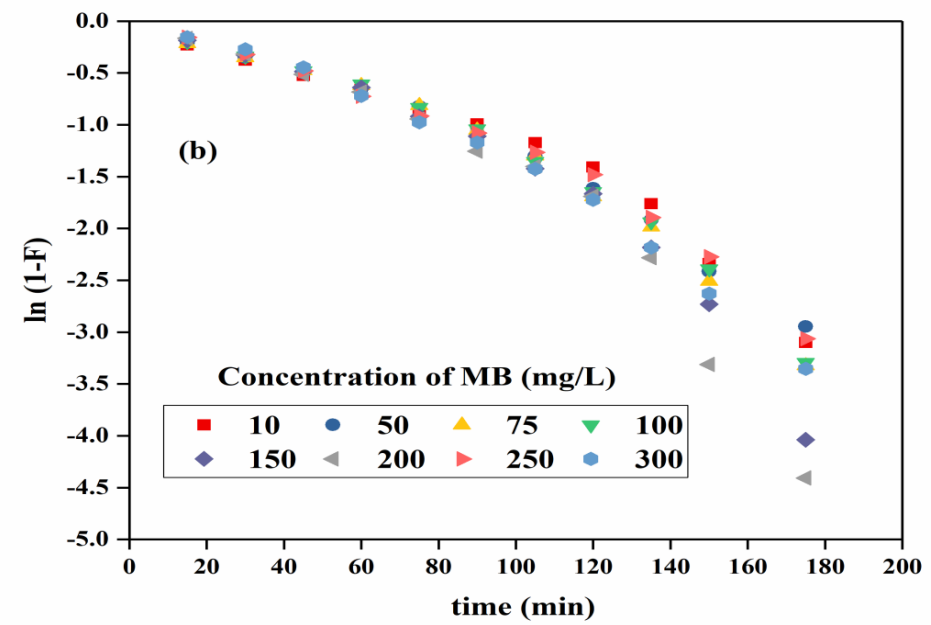

Figure 7.10 Mass transfer model for adsorption of MB dye on Biochar-TAN (a) Weber and Morris model (b) Boyd model

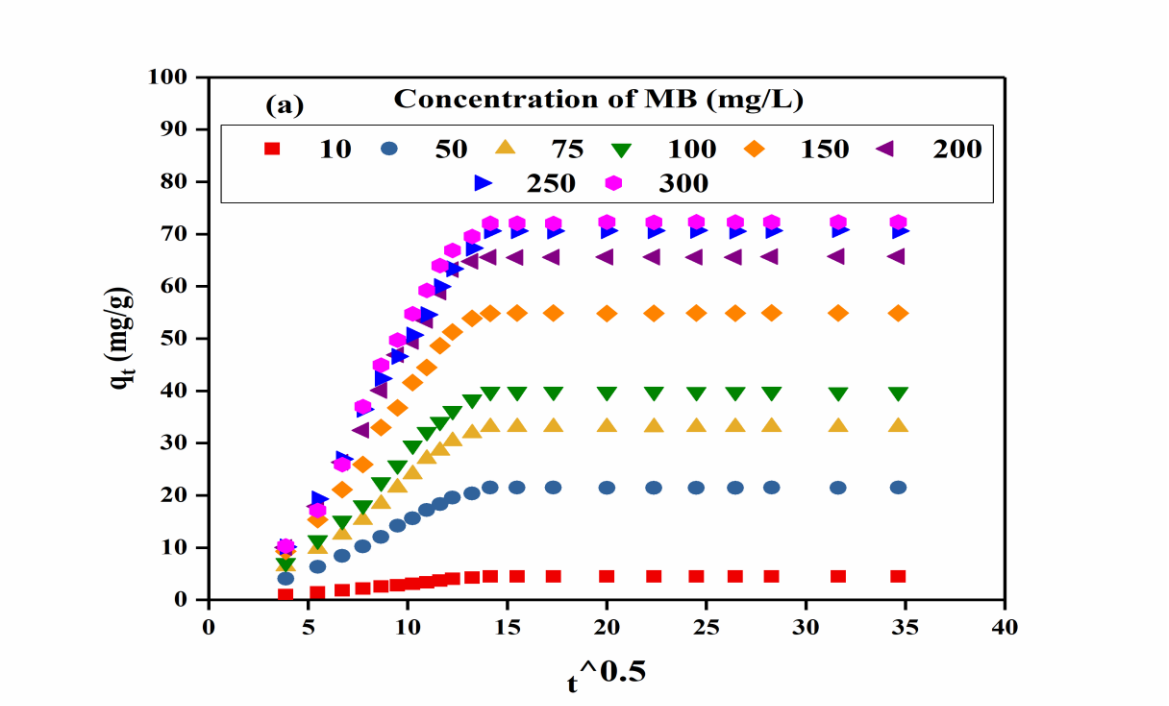

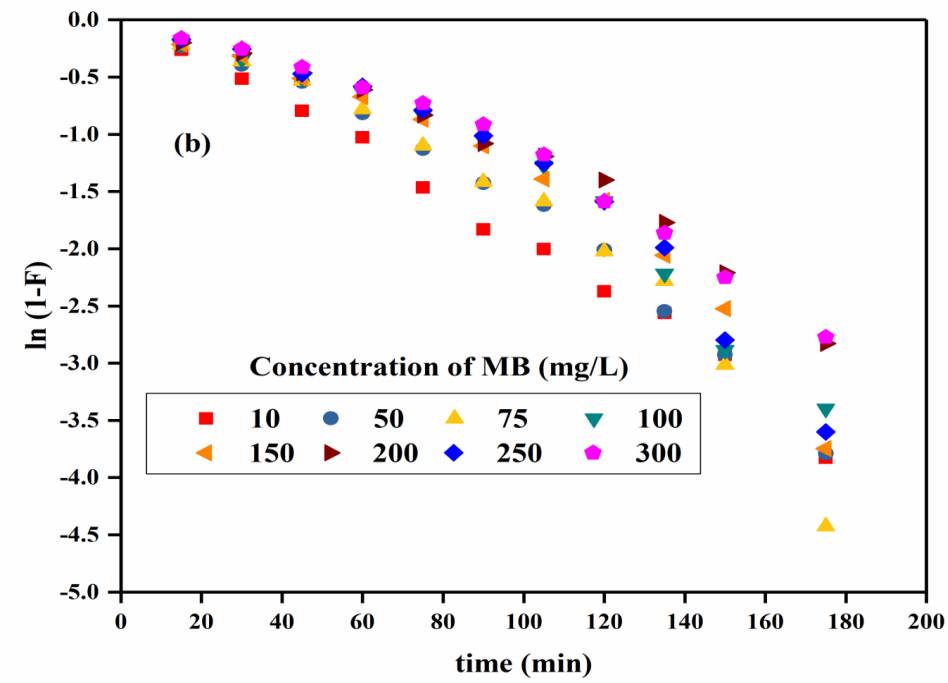

Figure 7.11 Mass transfer model for adsorption of MB dye on Biochar-TAN (a) Weber and Morris model (b) Boyd model

7.3.4 Effect of temperature and isotherms for adsorption of MB onto Biochar-DAN and Biochar-TAN

It is well understood that adsorption is a temperature dependent process. The temperature was varied from 20 to 45 ℃ and adsorption capacity with respect to temperature at different concentration of MB (10-300 mg/L) for Biochar-TAN is shown in Fig. 7.6(c) and for Biochar-DAN is shown in Fig. 7.7(c). At a particular concentration, increase in adsorption capacity is observed with increase in temperature. This might be due to higher mobility of ions at higher temperature and also higher degree of diffusion of MB molecules to the external surface and internal pores of the adsorbent (Saini et al., 2018). Thus, higher

temperature favors the removal of MB (Huang et al., 2019), though the influence of temperature at lower adsorbate concentration was insignificant.

Further, to unveil the adsorption mechanism and distribution of MB in liquid and solid biochar (Biochar-DAN and Biochar-TAN) at equilibrium condition, the adsorption isotherms were fitted with experimental results. In the present study four isotherms namely, Langmuir, Freundlich, Temkin and Sips were fitted with experimental results from both the biochars. The linear and non-linear forms of equations for all the isotherms are given in Table 7.7. The results are shown in Fig. 7.12 for Biochar-TAN and Fig. 7.13 for Biochar-DAN. The parameters calculated for isotherms are presented in Table 7.8. The Langmuir isotherm illustrates the single layer adsorption on specific site of homogeneous surface of adsorbent (Sangon et al., 2018). This model assumes that energy of adsorption is uniform on the surface of adsorbent and no interaction exists between the adsorbed molecules (Saini et al., 2018). The Freundlich isotherm demonstrates the multilayer adsorption process for a heterogeneous surface (Prajapati & Mondal, 2019). Temkin and Pyzhev considered that as a result of adsorbate and adsorbent interaction, the heat associated with adsorption decreased linearly with layer of adsorbed molecules, while, activation energy got distributed homogeneously (Prajapati & Mondal, 2019). The Sips isotherm is derived as a combination and based on limiting behavior of both Langmuir and Freundlich isotherms (Shahryari et al., 2010; Vargas et al., 2011). The maximum adsorption capacity of Biochar-DAN and Biochar-TAN at temperature from 293-318 K was found to be 83.530-89.167 mg/g and 85.959-107.347 mg/g, respectively at fixed concentration of MB dye (50 mg/L) and adsorbent dose (2 g/L). The correlation coefficient (R^2) for Langmuir, Freundlich, Temkin and Sips model for Biochar-TAN was varied between (0.9662-0.9810), (0.9260-

0.9614), (0.9212-0.9500), and (0.9737-0.9818), respectively. And, for Biochar-TAN the value of correlation coefficient varied from (0.9499-0.9822), (0.9765-0.9873), (0.9103-0.9629), and (0.9904-0.9943) for Langmuir, Freundlich, Temkin and Sips model, respectively. Thus, based on the correlation coefficient (R^2), Sips model was found to be followed during adsorption of both Biochar-DAN and Biochar-TAN. The maximum adsorption capacity for both biochar (Biochar-DAN and Biochar-TAN) was found to be 98.2174, and 158.131 mg/g, respectively. The comparable results were also obtained in case of various adsorbents used for removal of MB from aqueous solution (Ji et al., 2019), (Saini et al., 2018), (Liu et al., 2018).

Table 7.7 Linear and non-linear forms of isotherms

Isotherm models	Equation in Nonlinear form	Equation in Linear form	Equation No.
Langmuir isotherm	$q_e = \frac{q_m K_L C_e}{1 + K_L C_e}$	$\frac{C_e}{q_e} = \frac{C_e}{q_m} + \frac{1}{q_m K_L}$ $R_L = \frac{1}{1 + K_L C_O}$	7.8 7.9
Freundlich isotherm	$q_e = K_f C_e^{\frac{1}{n}}$	$\ln q_e = \ln K_f + \frac{1}{n} \ln C_e$	7.10
Temkin isotherm	$q_e = B * \ln(AC_e)$	$q_e = B \ln A + B \ln C_e$ $B (= \frac{RT}{b})$	7.11
Sips isotherm	$q_e = \frac{Q_m (K_s C_e)^{m_s}}{1+(K_s C_e)^{m_s}}$	$\frac{1}{q_e} = \frac{1}{q_m K_s} \left(\frac{1}{C_e}\right)^{1/n} + \frac{1}{q_m}$	7.12

q_e is experimental adsorption capacity (mg/g) at equilibrium; q_m is the maximum adsorption capacity (mg/g) of biochar; K_L is Langmuir constant (L/g); C_e is equilibrium concentration (mg/L) of MB dye in liquid phase; C_o is the initial MB concentration (mg/L); K_f is Freundlich model constant; 1/n is heterogeneity factor constant; R is universal gas constant; T is temperature (K); A is equilibrium binding constant (L/mg); B is Temkin constant associated with enthalpy of adsorption; b is Temkin isotherm constant; K_s and m_s are sips parameters

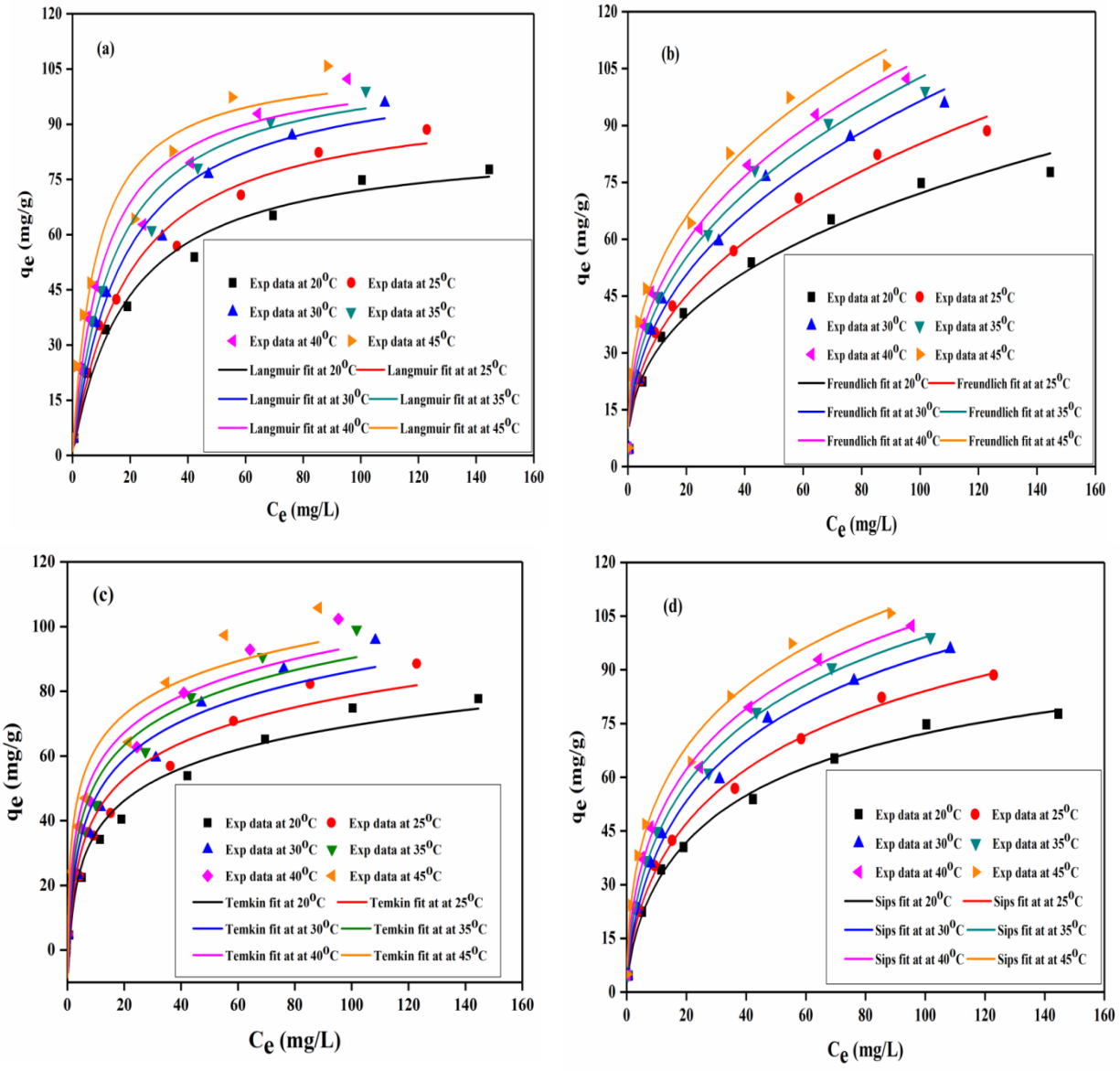

Figure 7.12 Adsorption isotherms for adsorption of MB dye on Biochar-TAN (a) Langmuir isotherm (b) Freundlich isotherm (c) Tempkin isotherm (d) Sips isotherm

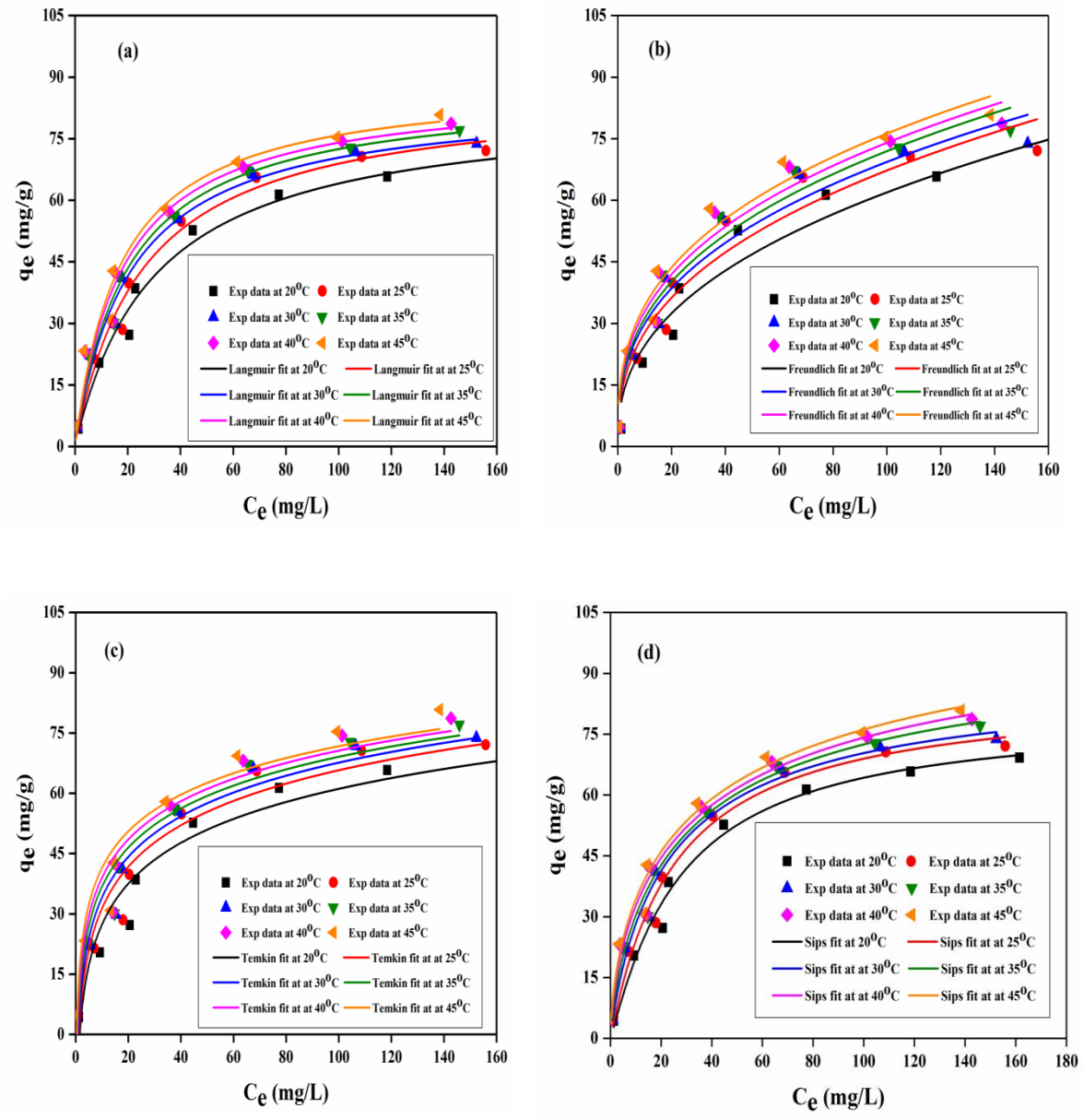

Figure 7.13 Adsorption isotherms for adsorption of MB dye on Biochar-DAN (a) Langmuir isotherm (b) Freundlich isotherm (c) Tempkin isotherm (d) Sips isotherm

Table 7.8 Isotherm and related parameters for adsorption of MB dye onto Biochar-DAN and Biochar-TAN

Isotherm model	Parameters	Temperature (K)					
		293	298	303	308	313	318
Biochar-DAN							
Langmuir	q_m (mg/g)	83.530	86.703	85.165	87.081	87.612	89.167
	K_L (L/mg)	0.0329	0.0387	0.0475	0.0495	0.0544	0.0570
	R_L	0.3780	0.3407	0.2962	0.2877	0.2688	0.2597
	R^2	0.9810	0.9794	0.9837	0.9777	0.9662	0.9651
Freundlich	K_f	9.7477	11.4698	12.923	13.546	14.595	15.428
	n	2.491	2.6037	2.741	2.7577	2.836	2.880
	R^2	0.9312	0.9260	0.9390	0.9527	0.9549	0.9614
Temkin	B	14.6782	14.9444	14.5848	14.0513	13.7453	13.1675
	A (L/mg)	0.6428	0.8134	1.0333	1.3648	1.7033	2.3185
	R^2	0.9324	0.9320	0.9500	0.9375	0.9356	0.9212
Sips	q_m (mg/g)	79.906	85.689	90.091	100.9544	111.230	119.7011
	K_S	0.0363	0.0397	0.0414	0.0333	0.0239	0.0239
	m_s	0.9141	0.9757	1.1188	1.2917	1.5627	1.5627
	R^2	0.9779	0.9753	0.9818	0.9794	0.9737	0.9756
Biochar-TAN							
Langmuir	q_m (mg/g)	85.959	98.2174	106.509	107.651	106.351	107.3474
	K_L (L/mg)	0.0113	0.0515	0.0567	0.0695	0.0913	0.1229
	R_L	0.6389	0.2797	0.2607	0.2234	0.1796	0.1399
	R^2	0.9822	0.9770	0.9799	0.9746	0.9653	0.9499
Freundlich	K_f	13.03	13.77	15.24	17.32	19.65	23.47
	n	2.692	2.528	2.497	2.588	2.711	2.902
	R^2	0.9765	0.9860	0.9841	0.9855	0.9870	0.9873
Temkin	B	124.428	15.931	16.934	16.772	16.472	15.102
	A (L/mg)	1.222	1.388	1.620	2.175	2.950	6.185
	R^2	0.9629	0.9420	0.9294	0.9283	0.9328	0.9103
Sips	q_m (mg/g)	114.654	158.131	162.189	176.5597	199.38	241.4263
	K_S	0.0220	0.0123	0.0163	0.0151	0.0114	0.0069
	m_s	1.4823	1.6345	1.5654	1.6763	1.8607	2.1209
	R^2	0.9943	0.9942	0.9935	0.9936	0.9922	0.9904

7.3.5 Thermodynamic parameters for adsorption of MB onto Biochar-DAN and Biochar-TAN

The thermodynamic parameters for adsorption of MB onto Biochar-DAN and Biochar-TAN at equilibrium were calculated at different temperature ranging from 20-45 ℃ keeping rest of the parameters constant. The Gibb's free energy (ΔG^o), Entropy (ΔS^o) and Enthalpy (ΔH^o) were calculated using Eqs. (7.13)-(7.16) (Saini et al., 2018).

$$\Delta G^o = -RT \ln K_o \quad (7.13)$$

$$K_o = \frac{C_{ad,eq}}{C_{eq}} \quad (7.14)$$

$$\Delta G^o = \Delta H^o - T\Delta S^o \quad (7.15)$$

$$\ln K_o = -\frac{\Delta H^o}{RT} + \frac{\Delta S^o}{R} \quad (7.16)$$

where ΔG^o (kJ/mol), ΔS^o (J/mol.K) and ΔH^o (kJ/mol) are the change in Gibbs free energy, entropy and enthalpy, respectively. T, R and K_o are temperature (K), universal gas constant (8.314 J/mol.K) and the equilibrium constant, respectively. $C_{ad,eq}$ (mg/L) is the amount of MB on the surface of adsorbent at equilibrium. C_{eq} (mg/L) is the equilibrium concentration of dye in the solution.

The values of ΔG^o, ΔS^o and ΔH^o are obtained from the slope and intercept of the van't Hoff plot between $\ln K_o$ versus (1/T). The results are shown in Fig. 7.14(a) and (b) for Biochar-TAN and Biochar-DAN, respectively. The value of ΔG^o, ΔS^o and ΔH^o for both the biochar are listed in Table 7.9. The negative value of Gibbs free energy at different temperature for both the biochar confirmed that the adsorption process is spontaneous and feasible in

nature (Ji et al., 2019). Also, decrease in ΔG^o with temperature revealed that higher temperature favors the adsorption process. The positive values of enthalpy at different temperature indicate that adsorption process is endothermic in nature. The positive value of entropy at different temperature suggested that the randomness at solid/liquid interface during the adsorption process increases (Fan et al., 2017). In addition, lower value of ΔG^o for Biochar-TAN as compared to Biochar-DAN indicates its suitability as an adsorbent for removal of aqueous MB.

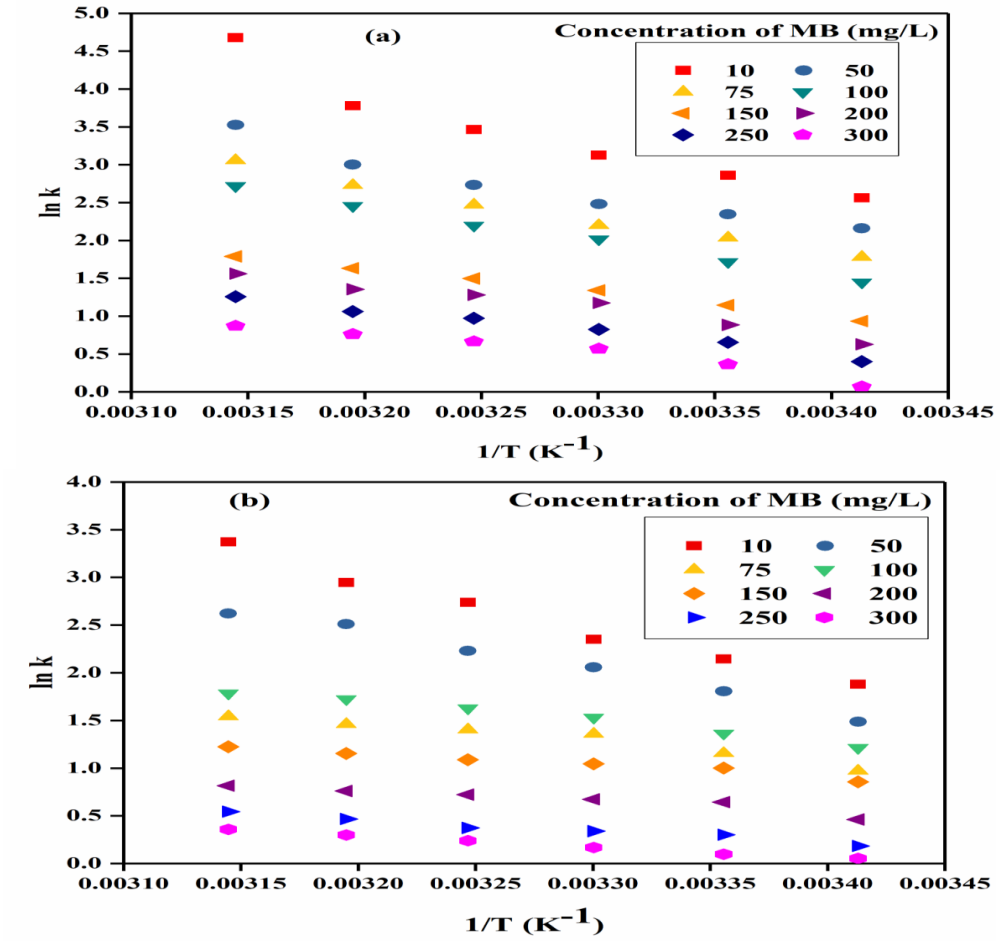

Figure 7.14 van't Hoff plot (a) Biochar-TAN (b) Biochar-DAN

Table 7.9 Thermodynamic parameters for adsorption of MB dye onto Biochar-DAN and Biochar-TAN

Parameters				Temperature (K)					
				293	298	303	308	313	318
C_o (mg/L)	ΔH^o (kJ/mol)	ΔS^o (J/mol.K)	R^2	ΔG^o (kJ/mol)					
Biochar-DAN									
10	45.267	169.672	0.9853	-4.582	-5.312	-5.925	-7.010	-7.668	-8.914
50	35.275	133.173	0.9886	-3.625	-4.473	-5.186	-5.707	-6.534	-6.929
75	16.983	66.571	0.9304	-2.367	-2.863	-3.423	-3.595	-3.799	-4.078
100	17.915	71.509	0.9790	-2.959	-3.384	-3.858	-4.173	-4.490	-4.721
150	10.380	42.834	0.9624	-2.087	-2.482	-2.634	-2.787	-3.005	-3.237
200	9.659	37.294	0.8975	-1.125	-1.597	-1.696	-1.849	-1.979	-2.158
250	10.306	36.827	0.9701	-0.450	-0.748	-0.857	-0.956	-1.217	-1.440
300	9.728	33.558	0.9954	-0.133	-0.243	-0.426	-0.614	-0.780	-0.949
Biochar-TAN									
10	60.267	225.798	0.9100	-6.242	-7.084	-7.878	-8.875	-9.838	-12.371
50	39.785	152.849	0.9171	-5.264	-5.815	-6.254	-6.996	-7.814	-9.320
75	38.619	146.292	0.9843	-4.336	-5.044	-5.541	-6.328	-7.105	-8.083
100	38.823	144.580	0.9966	-3.527	-4.255	-5.084	-5.629	-6.395	-7.196
150	26.147	97.214	0.9952	-2.278	-2.836	-3.379	-3.833	-4.252	-4.732
200	27.489	99.596	0.9531	-1.530	-2.192	-2.961	-3.281	-3.529	-4.129
250	25.107	89.416	0.9761	-0.971	-1.626	-2.081	-2.487	-2.761	-3.328
300	23.578	81.830	0.9367	-0.175	-0.906	-1.437	-1.709	-1.987	-2.310

7.3.6 Possible mechanism for adsorption of MB onto biochars

The adsorption of MB onto biochar is a complex process where multiple phenomenon such as electrostatic attraction, hydrogen bonding, ion exchange, π-π interaction, etc. might be responsible for adsorption process (Fan et al., 2016). The electrostatic attraction occurs as a result of change of pH during the adsorption process (Fan et al., 2017). With increase in

pH, the increase in $-OH^-$ ions in the solution increases the electrostatic attraction force between cationic MB dye (Chen et al., 2019). However, at pH higher than 10 the steric hindrance among the $-OH^-$ ions might reduce the rate of adsorption. The results of kinetics showed that the adsorption of MB onto biochars occurred through physical surface attraction and chemical bonding. Mainly, adsorption of MB proceeds by three steps: (1) diffusion of MB molecules through liquid film surrounding the adsorbent, (2) adsorption of MB molecules on the surface of adsorbent and (3) intra-particle diffusion of MB molecules in-side the pores of adsorbent. The schematic of possible pathways for adsorption of MB is depicted in Fig. 7.15. The FTIR and SEM-EDX analyses revealed the occurrence of -N-H and Si-O-Si functional groups present on the surface of biochar. These groups may contribute in adsorption process MB dye onto biochar through hydrogen bonding and π-π interaction. The inter-molecular hydrogen bond may be formed between nitrogen present in MB dye and hydrogen present on biochar. The inter-molecular hydrogen bonds are associated with adsorption processes and are categorized by means of non-electrostatic attraction (Fan et al., 2017). The –Si-O-Si groups and phenolic sites present on to biochar may participate in adsorption process through π-π interaction. In addition, ion exchange and surface complexation on the surface of biochar might be important mechanism involved during adsorption process. XRD analysis revealed that SiO2, CaO, MgO, $CaCO_3$, and $Ca(OH)_2$ were associated with the surface of biochar which might be proficient physical adsorption spot for the dye molecules (Chen et al., 2019). Comparing the Biochar-TAN and Biochar-DAN, the ion exchange and surface complexation was noteworthy in case of Biochar-TAN as compared to Biochar-DAN. This might be due to significant occurrence of SiO_2, CaO, MgO, $CaCO_3$, and $Ca(OH)_2$ on the surface of Biochar-TAN as

revealed by XRD analysis. Similar results for adsorption mechanism of MB dye onto biochar were also reported in many literatures (Jin et al., 2015; Shi et al., 2014; Sun et al., 2013).

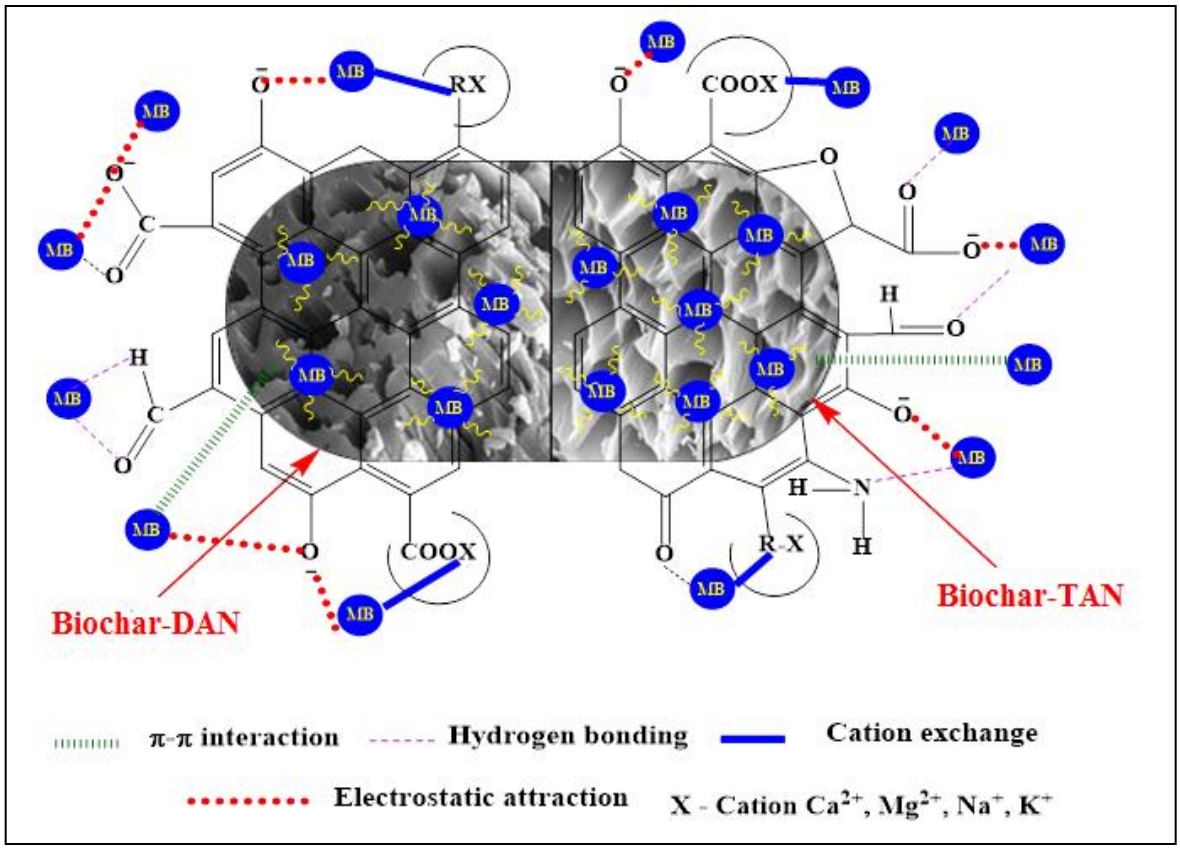

Figure 7.15 Possible mechanisms for adsorption of MB onto biochar

7.4 Conclusions

A comparative study was performed for removal of methylene blue dye from aqueous solution using biochar obtained from pyrolysis of DAN and TAN as an adsorbent. The FTIR analysis showed the decrease in intensity and shifting of peaks which illustrates the

adsorption of MB onto both biochar. The BET surface area of Biochar-DAN and Biochar-TAN was found to be 80.40 and 103.47 m^2/g, respectively, and both biochar can be classified as mesoporous material. The void pores and honey comb like structure of biochar was also revealed by SEM analysis. The maximum adsorption capacity for Biochar-TAN was 158.13 mg/g, while, for Biochar-DAN it was 85.68 mg/g. The higher adsorption capacity of Biochar-TAN towards MB removal was due to higher surface area, pore volume and surface complexation as compared to Biochar-DAN. The Sips isotherm model was best fitted to the experimental results for both biochar as compared to Langmuir, Freundlich and Temkin model. This showed that Langmuir model was followed at lower concentration, while, Freundlich model was followed at higher concentration of MB. The kinetic study for adsorption showed that the pseudo-second-order kinetic model best described the adsorption process of MB dye onto biochar revealing that diffusion through liquid film, adsorption at surface and intra-particle diffusion might be the rate-determining step during adsorption of MB. Additionally, mass transfer studies revealed that both film diffusion and intra-particle diffusion was the rate determining step. The thermodynamic study showed that adsorption of MB onto biochar was endothermic and spontaneous in nature. Further, it was found that four kind of interaction between MB dye and adsorbent were mainly responsible for adsorption process namely, electrostatic attraction, hydrogen bonding, ion exchange and surface complexation and π- π interaction.

Chapter 8

Summary of thesis and scope for future work

This chapter aimed to summerize the results from various aspects of torrefaction of *Acacia nilotica*, pyrolysis of torrefied *Acacia nilotica*, application of biochar from pyrolysis of DAN and TAN towads removal of aqueous methylene blue and finally the scope and recommendation of future work. This chapter has been devided into two parts: (1) summary of thesis and (2) scope for future work.

8.1 Summary of thesis

The pyrolysis of torrefied biomass and comparative study for removal of methylene blue form aqueous solution using biochar from pyrolysis of DAN and TAN as an adsorbent has been performed. The following results can be drawn from present work:

- Fuel and flow characteristics of DAN have been improved after torrefaction and are closure to the properties of coal. The higher heating value (HHV) increased by 28.2 % when DAN was torrefied at 280 ℃ for 40 min.
- Torrefied DAN was found to be less hygroscopic as moisture reabsorbed was 6.61 % (TAN280-40, 120 h) as compared to 35.44 % (DAN, 120 h). Also, the contact angle of TAN280-40 (79.1°/77.5°) was close to 90° confirming the hydrophobic nature.
- The bulk density of torrefied DAN was suitable for use as briquette and co-firing with coal in thermal plants with HR value less than 1.29 and CCI less than about 23. There was significant decrease in volatile matter (57.4 %) with simultaneous increase in fixed carbon content (~4 times). Hence, less volatile matter and high fixed carbon make torrefied *Acacia nilotica* a better solid fuel.
- TGA results showed that devolatilization temperature shifted to higher value and residual char yield increases when torrefied *Acacia nilotica* was pyrolysed.
- ICP-MS analysis revealed that torrefied biomass enriched by important elements such as sodium (Na), potassium (K), calcium (Ca), magnesium (Mg) etc. making it suitable for soil amendment.

- Compositional analysis showed that at lower temperature during torrefaction, the relative cellulose content in the torrefied biomass (TAN-220) is higher than the DAN, while, it goes on decreasing on further increase in temperature. The higher cellulose content attributed to higher activation energy of TAN-220 than DAN.
- The average activation energy of torrefied biomass obtained at 280 ℃ (TAN-280) is 42.39% lower than the DAN. Slight difference between activation energy and enthalpy favors the formation of activated complex. Accordingly, bio-energy generation through pyrolysis can be positively attained. It was noticed that at lower conversion value ($\alpha \leq 0.5$) the diffusion mechanism was rate determining for DAN and TAN-220, however, for TAN-250 and TAN-280, the 2^{nd} order random nucleation model is dominant for rate determination. At higher conversion ($\alpha \geq 0.5$), DAN and TAN-220 follow the 2^{nd} order random nucleation and Avrami-Erofeev models, while, in case of TAN-250 and TAN-280, 3^{rd} order random nucleation is dominant.
- A different set of parameters were obtained in case of optimum HHV and EY of TAN individually. The optimum value of temperature, retention time and heating rate to obtain maximum value of HHV and EY combined, were 252 ℃, 60 min, and 5 ℃/min, respectively.
- It was noted that the effect of temperature on torrefaction was significant, while effect of retention time and heating rate were minimal.
- The physical and chemical properties of DAN improved due to torrefaction. For example, MC, H/C ratio and O/C ratio decreased by 73.23, 52.94 and 46.22 %, respectively; whereas FC content and HHV increased by 75.54 and 18.62 %,

respectively. FR increased by 87.39 %; whereas, CI and VI decreased by 83.32 and 22.71 %, respectively. Flow properties such as angle of repose, HR, CCI and cohesion coefficient (C) decreased by 8.04, 6.20, 22.48, and 12.5 %, respectively. Bulk, tapped and particle densities of TAN252-60-5 were decreased by 16.4, 21.62 and 7.59 %, respectively.

- Torrefaction has greatly enhanced surface defects and reduced crystallinity of biomass as revealed by SEM-EDX and XRD analysis individually.
- Torrefaction improves many properties associated with DAN, while production of solid biofuels is the prime concern. Hence, pyrolysis of TAN-252-60-5 was carried out to obtain high-quality pyrolysis oil.
- The maximum yield of pyrolysis oil (33.59 wt %) was obtained at 507.04 ℃, retention time of 58.25 min, heating rate of 38.00 ℃/min, and sweeping gas flow rate of 40.52 mL/min. Analysis of variance confirmed that pyrolysis of torrefied biomass for maximum pyrolysis oil yield highly depended on temperature followed by heating rate, retention time, and sweeping gas flow rate, respectively.
- It was observed that pyrolysis oil obtained from TAN-252-60-5 was superior in terms of improved HHV, pH, and chemical composition and lower water content, etc. total aromatic carbon, carbonyl carbon, and primary alkyl carbon of pyrolysis oil from torrefied biomass increased by 40.28, 51.36, and 6.34 %, respectively, as compared to pyrolysis oil from DAN. The phenol derivative compounds are increased by 18.91 %. The HHV and pH of pyrolysis oil from torrefied biomass increased by 23.53, 42.15 %, respectively, while water content decreased by 34.37 % as compared to pyrolysis oil from DAN.

- The FTIR analysis showed the decrease in intensity and shifting of peaks which illustrates the adsorption of MB onto both biochar.
- The BET surface area of Biochar-DAN and Biochar-TAN was found to be 80.40 and 103.47 m^2/g, respectively, and both biochar can be classified as mesoporous material. The void pores and honey comb like structure of biochar was also revealed by SEM analysis.
- The maximum adsorption capacity for Biochar-TAN was 158.13 mg/g, while, for Biochar-DAN it was 85.68 mg/g. The higher adsorption capacity of Biochar-TAN towards MB removal was due to higher surface area, pore volume and surface complexation as compared to Biochar-DAN.
- The Sips isotherm model was best fitted to the experimental results for both biochar as compared to Langmuir, Freundlich and Temkin model. This showed that Langmuir model was followed at lower concentration, while, Freundlich model was followed at higher concentration of MB.
- The kinetic study for adsorption showed that the pseudo-second-order kinetic model best described the adsorption process of MB dye onto biochar revealing that diffusion through liquid film, adsorption at surface and intra-particle diffusion might be the rate-determining step during adsorption of MB.
- Additionally, mass transfer studies revealed that both film diffusion and intra-particle diffusion was the rate determining step. The thermodynamic study showed that adsorption of MB onto biochar was endothermic and spontaneous in nature.

- Further, it was found that four kind of interaction between MB dye and adsorbent were mainly responsible for adsorption process namely, electrostatic attraction, hydrogen bonding, ion exchange and surface complexation and π- π interaction.

8.2 Scope for future work

- Catalytic pyrolysis of torrefied biomass can further increase the yield and quality of pyrolysis oil
- Co-pyrolysis of torrefied biomass with other biomass, plastic and municipal solid waste can be possible route for energy generation from waste
- Torrefied biomass can be mixed with coal in thermal power plants to reduce harmful emissions
- In place of fixed bed reactor, fluidized bed reactor can increase the yield of pyrolysis oil due to better heat transfer
- Gasification of torrefied biomass can be used to increase the production of syngas
- Biochar from pyrolysis of torrefied biomass can be used to remove other dyes and heavy metal from waste water
- The efficacy of biochar from pyrolysis of torrefied biomass can be enhanced by chemical modification

Refrences

Abas, F.Z., Ani, F.N., Zakaria, Z.A., "Microwave-assisted production of optimized pyrolysis liquid oil from oil palm fiber," *Journal of Cleaner Production*, **182**(2018)404-413.

Acharjee, T.C., Coronella, C.J., Vasquez, V.R., "Effect of thermal pretreatment on equilibrium moisture content of lignocellulosic biomass," *Bioresource Technology*, **102(7)**(2011)4849-4854.

Agbor, V.B., Cicek, N., Sparling, R., Berlin, A., Levin, D.B., "Biomass pretreatment: fundamentals toward application," *Biotechnology advances*, **29(6)**(2011)675-685.

Ahmad, M.S., Mehmood, M.A., Al Ayed, O.S., Ye, G., Luo, H., Ibrahim, M., Rashid, U., Arbi Nehdi, I., Qadir, G., "Kinetic analyses and pyrolytic behavior of Para grass (Urochloa mutica) for its bioenergy potential," *Bioresource Technology*, **224**(2017)708-713.

Ahmed, M.J., Okoye, P.U., Hummadi, E.H., Hameed, B.H., "High-performance porous biochar from the pyrolysis of natural and renewable seaweed (Gelidiella acerosa) and its application for the adsorption of methylene blue," *Bioresource Technology*, **278**(2019)159-164.

Akhtar, J., Amin, N.S., "A review on operating parameters for optimum liquid oil yield in biomass pyrolysis," *Renewable and Sustainable Energy Reviews*, **16(7)**(2012)5101-5109.

Alinejad-Mir, A., Amooey, A.A., Ghasemi, S., "Adsorption of direct yellow 12 from aqueous solutions by an iron oxide-gelatin nanoadsorbent; kinetic, isotherm and mechanism analysis," *Journal of Cleaner Production*, **170**(2018)570-580.

Alvira, P., Tomás-Pejó, E., Ballesteros, M., Negro, M., "Pretreatment technologies for an efficient bioethanol production process based on enzymatic hydrolysis: a review," *Bioresource technology*, **101(13)**(2010)4851-4861.

Arias, B., Pevida, C., Fermoso, J., Plaza, M., Rubiera, F., Pis, J., "Influence of torrefaction on the grindability and reactivity of woody biomass," *Fuel Processing Technology*, **89(2)**(2008a)169-175.

Asadullah, M., Adi, A.M., Suhada, N., Malek, N.H., Saringat, M.I., Azdarpour, A., "Optimization of palm kernel shell torrefaction to produce energy densified bio-coal," *Energy Conversion and Management*, **88**(2014)1086-1093.

Ates, F., Erginel, N., "Optimization of bio-oil production using response surface methodology and formation of polycyclic aromatic hydrocarbons (PAHs) at elevated pressures," *Fuel Processing Technology*, **142**(2016)279-286.

Ateş, F., Pütün, E., Pütün, A., "Fast pyrolysis of sesame stalk: yields and structural analysis of bio-oil," *Journal of Analytical and Applied Pyrolysis*, **71(2)**(2004)779-790.

Azargohar, R., Nanda, S., Kozinski, J.A., Dalai, A.K., Sutarto, R., "Effects of temperature on the physicochemical characteristics of fast pyrolysis bio-chars derived from Canadian waste biomass," *Fuel*, **125**(2014)90-100.

B. Gratuito, M.K., Panyathanmaporn, T., Chumnanklang, R.A., Sirinuntawittaya, N., Dutta, A, 2008. "Production of activated carbon from coconut shell: Optimization using response surface methodology," *Bioresource Technology*, **99**(2008)4887-4895.

Bach, Q.-V., Gye, H.-R., Song, D., Lee, C.-J., "High quality product gas from biomass steam gasification combined with torrefaction and carbon dioxide capture processes," *International Journal of Hydrogen Energy*, **44(28)**(2019)14387-14394.

Bach, Q.-V., Skreiberg, Ø., "Upgrading biomass fuels via wet torrefaction: A review and comparison with dry torrefaction," *Renewable and Sustainable Energy Reviews*, **54**(2016)665-677.

Bach, Q.-V., Tran, K.-Q., Skreiberg, Ø., "Comparative study on the thermal degradation of dry- and wet-torrefied woods," *Applied Energy*, **185**(2017a)1051-1058.

Bach, Q.-V., Trinh, T.N., Tran, K.-Q., Thi, N.B.D., "Pyrolysis characteristics and kinetics of biomass torrefied in various atmospheres," *Energy conversion and management*, **141**(2017b)72-78.

Bada, S.O., Falcon, R.M.S., Falcon, L.M., "Investigation of combustion and co-combustion characteristics of raw and thermal treated bamboo with thermal gravimetric analysis," *Thermochimica Acta*, **589**(2014)207-214.

Bahng, M.-K., Mukarakate, C., Robichaud, D.J., Nimlos, M.R., "Current technologies for analysis of biomass thermochemical processing: A review," *Analytica chimica acta*, **651(2)** (2009)117-138.

Balarama Krishna, M.V., Chandrasekaran, K., Chakravarthy, S., Karunasagar, D., "An integrated approach based on oxidative pyrolysis and microwave-assisted digestion for the multi-elemental analysis of coal samples by ICP-based techniques, *Fuel*, **158**(2015)770-778.

Banerjee, S., Chattopadhyaya, M., "Adsorption characteristics for the removal of a toxic dye, tartrazine from aqueous solutions by a low cost agricultural by-product," *Arabian Journal of Chemistry*, **10**(2017)S1629-S1638.

Bargali, K., Bargali, S., "Acacia nilotica: A multipurpose leguminous plant," *Nature and Science*, **7(4)** (2009) ISSN 1545-0740.

Baruah, J., Nath, B.K., Sharma, R., Kumar, S., Deka, R.C., Baruah, D.C., Kalita, E., "Recent trends in the pretreatment of lignocellulosic biomass for value-added products," *Frontiers in Energy Research*, **6**(2018) article141.

Ben, H., Ragauskas, A.J., "Comparison for the compositions of fast and slow pyrolysis oils by NMR characterization," *Bioresource Technology*, **147**(2013)577-584.

Benhouria, A., Islam, M.A., Zaghouane-Boudiaf, H., Boutahala, M., Hameed, B., "Calcium alginate–bentonite–activated carbon composite beads as highly effective adsorbent for methylene blue," *Chemical engineering journal*, **270**(2015)621-630.

Bhagwanrao, S.V., Singaravelu, M., "Bulk density of biomass and particle density of their briquettes," *Int J Agric Eng*, **7**(2014) 221-224.

Björk, H., Rasmuson, A., "Moisture equilibrium of wood and bark chips in superheated steam," *Fuel*, **74(12)**(1995)1887-1890.

Bledzki, A.K., Mamun, A.A., Volk, J., "Physical, chemical and surface properties of wheat husk, rye husk and soft wood and their polypropylene composites," *Composites Part A: Applied Science and Manufacturing*, **41(4)**(2010)480-488.

Boateng, A.A., Mullen, C.A., "Fast pyrolysis of biomass thermally pretreated by torrefaction," *Journal of Analytical and Applied Pyrolysis*, **100**(2013b)95-102.

Bogner, J., Pipatti, R., Hashimoto, S., Diaz, C., Mareckova, K., Diaz, L., Kjeldsen, P., Monni, S., Faaij, A., Gao, Q., "Mitigation of global greenhouse gas emissions from waste: conclusions and strategies from the Intergovernmental Panel on Climate

Change (IPCC) Fourth Assessment Report. Working Group III (Mitigation)," *Waste Management & Research*, **26(1)**(2008)11-32.

Boubacar Laougé, Z., Çığgın, A.S., Merdun, H., "Optimization and characterization of bio-oil from fast pyrolysis of Pearl Millet and Sida cordifolia L. by using response surface methodology," *Fuel*, **274**(2020)117842.

Bridgeman, T., Jones, J., Williams, A., Waldron, D., "An investigation of the grindability of two torrefied energy crops," *Fuel*, **89(12)**(2010a)3911-3918.

Bridgeman, T.G., Jones, J.M., Shield, I., Williams, P.T., "Torrefaction of reed canary grass, wheat straw and willow to enhance solid fuel qualities and combustion properties," *Fuel*, **87(6)**(2008)844-856.

Bridgeman, T.G., Jones, J.M., Williams, A., Waldron, D.J., "An investigation of the grindability of two torrefied energy crops," *Fuel*, **89(12)** (2010b)3911-3918.

Bridgewater, A.V., "Biomass fast pyrolysis," *Thermal science*, **8(2)**(2004)21-50.

Bridgwater, A.V., "Review of fast pyrolysis of biomass and product upgrading," *Biomass and Bioenergy*, **38**(2012)68-94.

Buratti, C., Barbanera, M., Lascaro, E., Cotana, F., "Optimization of torrefaction conditions of coffee industry residues using desirability function approach," *Waste Management*, **73**(2018)523-534.

Cai, J., He, Y., Yu, X., Banks, S.W., Yang, Y., Zhang, X., Yu, Y., Liu, R., Bridgwater, A.V., "Review of physicochemical properties and analytical characterization of lignocellulosic biomass," *Renewable and Sustainable Energy Reviews*, **76**(2017)309-322.

Carere, C.R., Sparling, R., Cicek, N., Levin, D.B., "Third generation biofuels via direct cellulose fermentation," *International journal of molecular sciences*, **9(7)**(2008)1342-1360.

Carrasco, F., Roy, C., "Kinetic study of dilute-acid prehydrolysis of xylan-containing biomass," *Wood Science and Technology*, **26(3)**(1992)189-208.

Chandra, R.P., Bura, R., Mabee, W., Berlin, d.A., Pan, X., Saddler, J., "Substrate pretreatment: the key to effective enzymatic hydrolysis of lignocellulosics? in: *Biofuels*, Springer, (2007) pp. 67-93.

Charusiri, W., Numcharoenpinij, N., "Characterization of the optimal catalytic pyrolysis conditions for bio-oil production from brown salwood (Acacia mangium Willd) residues," *Biomass and Bioenergy*, **106**(2017)127-136.

Chen, D., Gao, A., Ma, Z., Fei, D., Chang, Y., Shen, C., "In-depth study of rice husk torrefaction: Characterization of solid, liquid and gaseous products, oxygen migration and energy yield," *Bioresource Technology*, **253**(2018)148-153.

Chen, D., Li, Y., Cen, K., Luo, M., Li, H., Lu, B., "Pyrolysis polygeneration of poplar wood: Effect of heating rate and pyrolysis temperature," *Bioresource Technology*, **218**(2016a)780-788.

Chen, D., Mei, J., Li, H., Li, Y., Lu, M., Ma, T., Ma, Z., "Combined pretreatment with torrefaction and washing using torrefaction liquid products to yield upgraded biomass and pyrolysis products," *Bioresource Technology*, **228**(2017)62-68.

Chen, D., Zheng, Z., Fu, K., Zeng, Z., Wang, J., Lu, M., "Torrefaction of biomass stalk and its effect on the yield and quality of pyrolysis products," *Fuel*, **159**(2015a)27-32.

Chen, Q., Zhou, J., Liu, B., Mei, Q., Luo, Z., "Influence of torrefaction pretreatment on biomass gasification technology," *Chinese Science Bulletin*, **56(14)**(2011)1449-1456.

Chen, S., Qin, C., Wang, T., Chen, F., Li, X., Hou, H., Zhou, M., "Study on the adsorption of dyestuffs with different properties by sludge-rice husk biochar: adsorption capacity, isotherm, kinetic, thermodynamics and mechanism," *Journal of Molecular Liquids*, **285**(2019)62-74.

Chen, W.-H., Kuo, P.-C., "A study on torrefaction of various biomass materials and its impact on lignocellulosic structure simulated by a thermogravimetry," *Energy*, **35(6)**(2010)2580-2586.

Chen, W.-H., Kuo, P.-C., "Torrefaction and co-torrefaction characterization of hemicellulose, cellulose and lignin as well as torrefaction of some basic constituents in biomass," *Energy*, **36(2)**(2011)803-811.

Chen, W.-H., Liu, S.-H., Juang, T.-T., Tsai, C.-M., Zhuang, Y.-Q., "Characterization of solid and liquid products from bamboo torrefaction," *Applied Energy*, **160**(2015b)829-835.

Chen, W.-H., Lu, K.-M., Liu, S.-H., Tsai, C.-M., Lee, W.-J., Lin, T.-C., "Biomass torrefaction characteristics in inert and oxidative atmospheres at various superficial velocities," *Bioresource Technology*, **146**(2013)152-160.

Chen, W.-H., Peng, J., Bi, X.T., "A state-of-the-art review of biomass torrefaction, densification and applications," *Renewable and Sustainable Energy Reviews*, **44**(2015c)847-866.

Chen, Y.-C., Chen, W.-H., Lin, B.-J., Chang, J.-S., Ong, H.C., "Impact of torrefaction on the composition, structure and reactivity of a microalga residue," *Applied Energy*, **181**(2016b)110-119.

Chen, Y., Cao, W., Atreya, A., "An experimental study to investigate the effect of torrefaction temperature and time on pyrolysis of centimeter-scale pine wood particles," *Fuel Processing Technology*, **153**(2016c)74-80.

Chew, J.J., Doshi, V., "Recent advances in biomass pretreatment – Torrefaction fundamentals and technology," *Renewable and Sustainable Energy Reviews*, **15(8)**(2011)4212-4222.

Chin, K.L., H'ng, P.S., Go, W.Z., Wong, W.Z., Lim, T.W., Maminski, M., Paridah, M.T., Luqman, A.C., "Optimization of torrefaction conditions for high energy density solid biofuel from oil palm biomass and fast growing species available in Malaysia," *Industrial Crops and Products*, **49**(2013)768-774.

Ciolkosz, D., Wallace, R., "A review of torrefaction for bioenergy feedstock production," *Biofuels, Bioproducts and Biorefining*, **5(3)**(2011)317-329.

Collard, F.-X., Blin, J., "A review on pyrolysis of biomass constituents: Mechanisms and composition of the products obtained from the conversion of cellulose, hemicelluloses and lignin," *Renewable and Sustainable Energy Reviews*, **38**(2014)594-608.

Conag, A.T., Villahermosa, J.E.R., Cabatingan, L.K., Go, A.W., "Energy densification of sugarcane bagasse through torrefaction under minimized oxidative atmosphere," *Journal of Environmental Chemical Engineering*, **5(6)**(2017)5411-5419.

Cotana, F., Buratti, C., Barbanera, M., Lascaro, E., "Optimization of the steam explosion and enzymatic hydrolysis for sugars production from oak woods," *Bioresource Technology*, **198**(2015)470-477.

Couhert, C., Salvador, S., Commandre, J.-M., "Impact of torrefaction on syngas production from wood," *Fuel*, **88(11)**(2009)2286-2290.

Criado, J.M., "Kinetic analysis of DTG data from master curves," *Thermochimica Acta*, **24(1)**(1978)186-189.

Dacres, O.D., Tong, S., Li, X., Zhu, X., Edreis, E.M.A., Liu, H., Luo, G., Worasuwannarak, N., Kerdsuwan, S., Fungtammasan, B., Yao, H., "Pyrolysis kinetics of biomasses pretreated by gas-pressurized torrefaction," *Energy Conversion and Management*, **182**(2019)117-125.

Dai, L., Wang, Y., Liu, Y., Ruan, R., He, C., Yu, Z., Jiang, L., Zeng, Z., Tian, X., "Integrated process of lignocellulosic biomass torrefaction and pyrolysis for upgrading bio-oil production: A state-of-the-art review," *Renewable and Sustainable Energy Reviews*, **107**(2019)20-36.

Daugaard, D.E., Brown, R.C., "Enthalpy for Pyrolysis for Several Types of Biomass," *Energy & Fuels*, **17(4)**(2003)934-939.

Dawood, S., Sen, T.K., Phan, C., "Adsorption removal of Methylene Blue (MB) dye from aqueous solution by bio-char prepared from Eucalyptus sheathiana bark: kinetic, equilibrium, mechanism, thermodynamic and process design," *Desalination and Water Treatment*, **57(59)**(2016)28964-28980.

Demiral, İ., Şensöz, S., "Fixed-Bed Pyrolysis of Hazelnut (Corylus Avellana L.) Bagasse: Influence of Pyrolysis Parameters on Product Yields," *Energy Sources, Part A: Recovery, Utilization, and Environmental Effects*, **28(12)**(2006)1149-1158.

Demirbas, A., "Combustion of biomass," *Energy sources, Part A: Recovery, utilization, and environmental effects*, **29(6)**(2007)549-561.

Demirbaş, A., "Biomass resource facilities and biomass conversion processing for fuels and chemicals," *Energy conversion and Management*, **42(11)**(2001)1357-1378.

Demirbaş, A., "Mechanisms of liquefaction and pyrolysis reactions of biomass," *Energy Conversion and Management*, **41(6)**(2000)633-646.

Deng, J., Wang, G.-j., Kuang, J.-h., Zhang, Y.-l., Luo, Y.-h., "Pretreatment of agricultural residues for co-gasification via torrefaction," *Journal of Analytical and Applied Pyrolysis*, **86(2)**(2009a)331-337.

Dhanavath, K.N., Bankupalli, S., Sugali, C.S., Perupogu, V., V Nandury, S., Bhargava, S., Parthasarathy, R., "Optimization of process parameters for slow pyrolysis of neem press seed cake for liquid and char production," *Journal of Environmental Chemical Engineering*, **7(1)**(2019)102905.

Dhanavath, K.N., Shah, K., Bankupalli, S., Bhargava, S.K., Parthasarathy, R., "Derivation of optimum operating conditions for the slow pyrolysis of Mahua press seed cake in a fixed bed batch reactor for bio–oil production," *Journal of Environmental Chemical Engineering*, **5(4)**(2017)4051-4063.

Dhyani, V., Bhaskar, T., "A comprehensive review on the pyrolysis of lignocellulosic biomass," *Renewable Energy*, **129**(2018)695-716.

Dhyani, V., Kumar, J., Bhaskar, T., "Thermal decomposition kinetics of sorghum straw via thermogravimetric analysis," *Bioresource Technology*, **245**(2017)1122-1129.

Doddapaneni, T.R.K.C., Jain, R., Praveenkumar, R., Rintala, J., Romar, H., Konttinen, J., "Adsorption of furfural from torrefaction condensate using torrefied biomass," *Chemical Engineering Journal*, **334**(2018)558-568.

Doddapaneni, T.R.K.C., Konttinen, J., Hukka, T.I., Moilanen, A., "Influence of torrefaction pretreatment on the pyrolysis of Eucalyptus clone: A study on kinetics, reaction mechanism and heat flow," *Industrial Crops and Products*, **92**(2016)244-254.

Doddapaneni, T.R.K.C., Praveenkumar, R., Tolvanen, H., Palmroth, M.R., Konttinen, J., Rintala, J., "Anaerobic batch conversion of pine wood torrefaction condensate," *Bioresource Technology*, **225**(2017)299-307.

Dong, Q., Zhang, S., Ding, K., Zhu, S., Zhang, H., Liu, X., "Pyrolysis behavior of raw/torrefied rice straw after different demineralization processes," *Biomass and Bioenergy*, **119**(2018)229-236.

Dorez, G., Ferry, L., Sonnier, R., Taguet, A., Lopez-Cuesta, J.M., "Effect of cellulose, hemicellulose and lignin contents on pyrolysis and combustion of natural fibers," *Journal of Analytical and Applied Pyrolysis*, **107**(2014)323-331.

Doyle, C.D., "Estimating isothermal life from thermogravimetric data," *Journal of Applied Polymer Science*, **6**(24)(1962)639-642.

Edelmann, W., Baier, U., Engeli, H., "Environmental aspects of the anaerobic digestion of the organic fraction of municipal solid wastes and of solid agricultural wastes," *Water science and Technology*, **52(1-2)**(2005)203-208.

Fan, S., Tang, J., Wang, Y., Li, H., Zhang, H., Tang, J., Wang, Z., Li, X., "Biochar prepared from co-pyrolysis of municipal sewage sludge and tea waste for the adsorption of methylene blue from aqueous solutions: kinetics, isotherm, thermodynamic and mechanism," *Journal of Molecular Liquids*, **220**(2016)432-441.

Fan, S., Wang, Y., Wang, Z., Tang, J., Tang, J., Li, X., "Removal of methylene blue from aqueous solution by sewage sludge-derived biochar: adsorption kinetics, equilibrium, thermodynamics and mechanism," *Journal of Environmental Chemical Engineering*, **5(1)**(2017)601-611.

Felfli, F.F., Luengo, C.A., Beat n, P.A., "Wood briquette torrefaction," *Energy for sustainable development*, **9(3)**(2005a)19-22.

Ferreira, M.F.P., Oliveira, B.F.H., Pinheiro, W.B.S., Correa, N.F., França, L.F., Ribeiro, N.F.P., "Generation of biofuels by slow pyrolysis of palm empty fruit bunches: Optimization of process variables and characterization of physical-chemical products," *Biomass and Bioenergy*, **140**(2020)105707.

Gan, Y.Y., Ong, H.C., Ling, T.C., Chen, W.-H., Chong, C.T., "Torrefaction of de-oiled Jatropha seed kernel biomass for solid fuel production," *Energy*, **170**(2019)367-374.

Garg, R., Anand, N., Kumar, D., "Pyrolysis of babool seeds (Acacia nilotica) in a fixed bed reactor and bio-oil characterization," *Renewable Energy*, **96**(2016)167-171.

Ghetti, P., Ricca, L., Angelini, L.,"Thermal analysis of biomass and corresponding pyrolysis products," *Fuel*, **75(5)**(1996)565-573.

Gholami, A., Pourfayaz, F., Hajinezhad, A., Mohadesi, M., "Biodiesel production from Norouzak (Salvia leriifolia) oil using choline hydroxide catalyst in a microchannel reactor," *Renewable Energy*, **136**(2019)993-1001.

Giudicianni, P., Cardone, G., Ragucci, R., "Cellulose, hemicellulose and lignin slow steam pyrolysis: Thermal decomposition of biomass components mixtures," *Journal of Analytical and Applied Pyrolysis*, **100**(2013)213-222.

Gogoi, D., Bordoloi, N., Goswami, R., Narzari, R., Saikia, R., Sut, D., Gogoi, L., Kataki, R., "Effect of torrefaction on yield and quality of pyrolytic products of arecanut husk: an agro-processing wastes," *Bioresource Technology*, **242**(2017)36-44.

Gomez-Serrano, V., Pastor-Villegas, J., Perez-Florindo, A., Duran-Valle, C., Valenzuela-Calahorro, C., "FT-IR study of rockrose and of char and activated carbon," *Journal of Analytical and Applied Pyrolysis*, **36(1)**(1996)71-80.

Goyal, H., Seal, D., Saxena, R., "Bio-fuels from thermochemical conversion of renewable resources: a review," *Renewable and sustainable energy reviews*, **12(2)**(2008)504-517.

Granados, D.A., Basu, P., Chejne, F., Nhuchhen, D.R., "Detailed Investigation into Torrefaction of Wood in a Two-Stage Inclined Rotary Torrefier," *Energy & Fuels*, **31(1)**(2017)647-658.

Granados, D.A., Chejne, F., Basu, P., "A two dimensional model for torrefaction of large biomass particles," *Journal of Analytical and Applied Pyrolysis*, **120**(2016)1-14.

Guedes, R.E., Luna, A.S., Torres, A.R., "Operating parameters for bio-oil production in biomass pyrolysis: A review," *Journal of Analytical and Applied Pyrolysis*, **129**(2018)134-149.

Gupta, G.K., Mondal, M.K., "Bio-energy generation from sagwan sawdust via pyrolysis: Product distributions, characterizations and optimization using response surface methodology," *Energy*, **170**(2019)423-437.

Gupta, G.K., Ram, M., Bala, R., Kapur, M., Mondal, M.K., "Pyrolysis of chemically treated corncob for biochar production and its application in Cr(VI) removal," *Environmental Progress & Sustainable Energy*, **37(5)**(2018)1606-1617.

Gupta, T.B., Lataye, D.H., "Removal of crystal violet and methylene blue dyes using Acacia Nilotica sawdust activated carbon," *Indian Journal of Chemical Technology*, **26(1)**(2019)52-68.

Güzel, F., Sayğılı, H., Akkaya Sayğılı, G., Koyuncu, F., Yılmaz, C., "Optimal oxidation with nitric acid of biochar derived from pyrolysis of weeds and its application in removal of hazardous dye methylene blue from aqueous solution," *Journal of Cleaner Production*, **144**(2017)260-265.

Hagemann, N., Spokas, K., Schmidt, H.-P., Kägi, R., Böhler, M.A., Bucheli, T.D., "Activated Carbon, Biochar and Charcoal: Linkages and Synergies across Pyrogenic Carbon's ABCs," *Water*, **10(2)**(2018)182.

He, Q., Ding, L., Gong, Y., Li, W., Wei, J., Yu, G., "Effect of torrefaction on pinewood pyrolysis kinetics and thermal behavior using thermogravimetric analysis," *Bioresource Technology*, **280**(2019)104-111.

Hoslett, J., Ghazal, H., Mohamad, N., Jouhara, H., "Removal of methylene blue from aqueous solutions by biochar prepared from the pyrolysis of mixed municipal discarded material," *Science of The Total Environment*, **714**(2020)136832.

Hu, Q., Yang, H., Xu, H., Wu, Z., Lim, C.J., Bi, X.T., Chen, H., "Thermal behavior and reaction kinetics analysis of pyrolysis and subsequent in-situ gasification of torrefied biomass pellets," *Energy Conversion and Management*, **161**(2018)205-214.

Huang, J., Liu, J., Chen, J., Xie, W., Kuo, J., Lu, X., Chang, K., Wen, S., Sun, G., Cai, H., Buyukada, M., Evrendilek, F., "Combustion behaviors of spent mushroom substrate using TG-MS and TG-FTIR: Thermal conversion, kinetic, thermodynamic and emission analyses," *Bioresource Technology*, **266**(2018)389-397.

Huang, T., Yan, M., He, K., Huang, Z., Zeng, G., Chen, A., Peng, M., Li, H., Yuan, L., Chen, G., "Efficient removal of methylene blue from aqueous solutions using magnetic graphene oxide modified zeolite," *Journal of colloid and interface science*, **543**(2019)43-51.

Huang, X., Cao, J.-P., Zhao, X.-Y., Wang, J.-X., Fan, X., Zhao, Y.-P., Wei, X.-Y., "Pyrolysis kinetics of soybean straw using thermogravimetric analysis," *Fuel*, **169**(2016)93-98.

Huang, Y., Yin, X., Wu, C., Wang, C., Xie, J., Zhou, Z., Ma, L., Li, H., "Effects of metal catalysts on CO2 gasification reactivity of biomass char," *Biotechnology advances*, **27(5)**(2009)568-572.

Huber, G.W., Iborra, S., Corma, A., "Synthesis of transportation fuels from biomass: chemistry, catalysts, and engineering," *Chemical reviews*, **106**(9)(2006)4044-4098.

Iáñez-Rodríguez, I., Martín-Lara, M.Á., Blázquez, G., Pérez, A., Calero, M., "Effect of torrefaction conditions on greenhouse crop residue: Optimization of conditions to upgrade solid characteristics," *Bioresource Technology*, **244**(2017)741-749.

Ibrahim, R.H.H., Darvell, L.I., Jones, J.M., Williams, A., "Physicochemical characterisation of torrefied biomass," *Journal of Analytical and Applied Pyrolysis*, **103**(2013)21-30.

Ingemarsson, Å., Nilsson, U., Nilsson, M., Pedersen, J.R., Olsson, J.O., "Slow pyrolysis of spruce and pine samples studied with GC/MS and GC/FTIR/FID," *Chemosphere*, **36**(14)(1998)2879-2889.

Ingram, L., Mohan, D., Bricka, M., Steele, P., Strobel, D., Crocker, D., Mitchell, B., Mohammad, J., Cantrell, K., Pittman, C.U., "Pyrolysis of Wood and Bark in an Auger Reactor: Physical Properties and Chemical Analysis of the Produced Bio-oils," *Energy & Fuels*, **22(1)**(2008)614-625.

Isa, K.M., Daud, S., Hamidin, N., Ismail, K., Saad, S.A., Kasim, F.H., "Thermogravimetric analysis and the optimisation of bio-oil yield from fixed-bed pyrolysis of rice husk using response surface methodology (RSM)," *Industrial Crops and Products*, **33(2)**(2011)481-487.

Isahak, W.N.R.W., Hisham, M.W., Yarmo, M.A., Hin, T.-y.Y., "A review on bio-oil production from biomass by using pyrolysis method," *Renewable and sustainable energy reviews*, **16(8)**(2012)5910-5923.

Jahirul, M.I., Rasul, M.G., Chowdhury, A.A., Ashwath, N., "Biofuels production through biomass pyrolysis—a technological review," *Energies*, **5**(12)(2012)4952-5001.

Jenkins, B., Baxter, L., Miles Jr, T., Miles, T., "Combustion properties of biomass," *Fuel Processing Technology*, **54(1-3)**(1998)17-46.

Ji, B., Wang, J., Song, H., Chen, W., "Removal of methylene blue from aqueous solutions using biochar derived from a fallen leaf by slow pyrolysis: Behavior and mechanism," *Journal of Environmental Chemical Engineering*, **7(3)**(2019)103036.

Jin, Z., Wang, X., Sun, Y., Ai, Y., Wang, X., "Adsorption of 4-n-nonylphenol and bisphenol-A on magnetic reduced graphene oxides: a combined experimental and

theoretical studies," *Environmental Science & Technology*, **49(15)**(2015) 9168-9175.

Joseph, J., Baker, C., Mukkamala, S., Beis, S.H., Wheeler, M.C., DeSisto, W.J., Jensen, B.L., Frederick, B.G., "Chemical Shifts and Lifetimes for Nuclear Magnetic Resonance (NMR) Analysis of Biofuels," *Energy & Fuels*, **24(9)**(2010)5153-5162.

Jung, S.-H., Kang, B.-S., Kim, J.-S., "Production of bio-oil from rice straw and bamboo sawdust under various reaction conditions in a fast pyrolysis plant equipped with a fluidized bed and a char separation system," *Journal of Analytical and Applied Pyrolysis*, **82(2)**(2008)240-247.

Jung, S.-J., Kim, S.-H., Chung, I.-M., "Comparison of lignin, cellulose, and hemicellulose contents for biofuels utilization among 4 types of lignocellulosic crops," *Biomass and Bioenergy*, **83**(2015)322-327.

Kadlimatti, H.M., Raj Mohan, B., Saidutta, M.B., "Bio-oil from microwave assisted pyrolysis of food waste-optimization using response surface methodology," *Biomass and Bioenergy*, **123**(2019)25-33.

Kan, T., Strezov, V., Evans, T.J., "Lignocellulosic biomass pyrolysis: A review of product properties and effects of pyrolysis parameters," *Renewable and Sustainable Energy Reviews*, **57**(2016)1126-1140.

Kanwal, S., Chaudhry, N., Munir, S., Sana, H., "Effect of torrefaction conditions on the physicochemical characterization of agricultural waste (sugarcane bagasse)," *Waste management*, **88**(2019)280-290.

Karoui, S., Ben Arfi, R., Mougin, K., Ghorbal, A., Assadi, A.A., Amrane, A., "Synthesis of novel biocomposite powder for simultaneous removal of hazardous ciprofloxacin and methylene blue: Central composite design, kinetic and isotherm studies using Brouers-Sotolongo family models," *Journal of Hazardous Materials*, **387**(2020)121675.

Kastanaki, E., Vamvuka, D., Grammelis, P., Kakaras, E., "Thermogravimetric studies of the behavior of lignite–biomass blends during devolatilization," *Fuel Processing Technology*, **77-78**(2002)159-166.

Katheresan, V., Kansedo, J., Lau, S.Y., "Efficiency of various recent wastewater dye removal methods: A review," *Journal of Environmental Chemical Engineering*, **6**(4)(2018)4676-4697.

Kaur, R., Gera, P., Jha, M.K., Bhaskar, T., "Pyrolysis kinetics and thermodynamic parameters of castor (Ricinus communis) residue using thermogravimetric analysis," *Bioresource Technology*, **250**(2018)422-428.

Keiluweit, M., Nico, P.S., Johnson, M.G., Kleber, M., "Dynamic Molecular Structure of Plant Biomass-Derived Black Carbon (Biochar)," *Environmental Science & Technology*, **44(4)**(2010)1247-1253.

Keivani, B., Gultekin, S., Olgun, H., Atimtay, A.T., "Torrefaction of pine wood in a continuous system and optimization of torrefaction conditions," *International Journal of Energy Research*, **42(15)**(2018)4597-4609.

Khan, A., De Jong, W., Jansens, P., Spliethoff, H., "Biomass combustion in fluidized bed boilers: Potential problems and remedies," *Fuel processing Technology*, **90(1)**(2009)21-50.

Kılıç, M., Pütün, E., Pütün, A.E., "Optimization of Euphorbia rigida fast pyrolysis conditions by using response surface methodology," *Journal of Analytical and Applied Pyrolysis*, **110**(2014)163-171.

Konsomboon, S., Commandré, J.-M., Fukuda, S., "Torrefaction of various biomass feedstocks and its impact on the reduction of tar produced during pyrolysis," *Energy & fuels*, **33(4)**(2019)3257-3266.

Koukios, E.G., "Progress in thermochemical, solid-state refining of biofuels—From research to commercialization," in: *Advances in thermochemical biomass conversion*, Springer, (1993) pp. 1678-1692.

Kumar, R., Strezov, V., Weldekidan, H., He, J., Singh, S., Kan, T., Dastjerdi, B., "Lignocellulose biomass pyrolysis for bio-oil production: A review of biomass pre-treatment methods for production of drop-in fuels," *Renewable and Sustainable Energy Reviews*, **123**(2020)109763.

Kurji, H., Valera-Medina, A., Runyon, J., Giles, A., Pugh, D., Marsh, R., Cerone, N., Zimbardi, F., Valerio, V., "Combustion characteristics of biodiesel saturated with pyrolysis oil for power generation in gas turbines," *Renewable Energy*, **99**(2016)443-451.

Kutlu, O., Kocar, G., "Upgrading lignocellulosic waste to fuel by torrefaction: Characterisation and process optimization by response surface methodology," *International Journal of Energy Research*, **42(15)**(2018)4746-4760.

Lazzari, E., Polidoro, A.d.S., Onorevoli, B., Schena, T., Silva, A.N., Scapin, E., Jacques, R.A., Caramão, E.B., "Production of rice husk bio-oil and comprehensive characterization (qualitative and quantitative) by HPLC/PDA and GC × GC/qMS," *Renewable Energy*, **135**(2019)554-565.

Lazzari, E., Schena, T., Primaz, C.T., da Silva Maciel, G.P., Machado, M.E., Cardoso, C.A.L., Jacques, R.A., Caramão, E.B., "Production and chromatographic characterization of bio-oil from the pyrolysis of mango seed waste," *Industrial Crops and Products*, **83**(2016)529-536.

Lee, J.-W., Kim, Y.-H., Lee, S.-M., Lee, H.-W., "Optimizing the torrefaction of mixed softwood by response surface methodology for biomass upgrading to high energy density," *Bioresource Technology*, **116**(2012)471-476.

Li, Y., Zhang, Y., Wang, G., Li, S., Han, R., Wei, W., "Reed biochar supported hydroxyapatite nanocomposite: Characterization and reactivity for methylene blue removal from aqueous media," *Journal of Molecular Liquids*, **263**(2018)53-63.

Liaw, S.-S., Frear, C., Lei, W., Zhang, S., Garcia-Perez, M., "Anaerobic digestion of C1–C4 light oxygenated organic compounds derived from the torrefaction of lignocellulosic materials," *Fuel Processing Technology*, **131**(2015)150-158.

Liu, J., Wang, Y., Fang, Y., Mwamulima, T., Song, S., Peng, C., "Removal of crystal violet and methylene blue from aqueous solutions using the fly ash-based adsorbent material-supported zero-valent iron," *Journal of Molecular Liquids*, **250**(2018)468-476.

Liu, S., Li, J., Xu, S., Wang, M., Zhang, Y., Xue, X., "A modified method for enhancing adsorption capability of banana pseudostem biochar towards methylene blue at low temperature. *Bioresource Technology*, **282**(2019)48-55.

Liu, S., Ni, C., Su, H., Liu, H., Chen, R., Li, P., Wei, Y., "Exploring the critical dependence of the adsorption of various dyes on the degradation rate using a ferrihydrite surface under visible light," *RSC advances*, **6(37)**(2016)30840-30845.

Liu, Y., Zhao, X., Li, J., Ma, D., Han, R., "Characterization of bio-char from pyrolysis of wheat straw and its evaluation on methylene blue adsorption," *Desalination and Water Treatment*, **46(1-3)**(2010)115-123.

Lloyd, T.A., Wyman, C.E., "Combined sugar yields for dilute sulfuric acid pretreatment of corn stover followed by enzymatic hydrolysis of the remaining solids," *Bioresource Technology*, **96(18)**(2005)1967-1977.

Louwes, A.C., Basile, L., Yukananto, R., Bhagwandas, J.C., Bramer, E.A., Brem, G., "Torrefied biomass as feed for fast pyrolysis: An experimental study and chain analysis," *Biomass and Bioenergy*, **105**(2017)116-126.

Loy, A.C.M., Gan, D.K.W., Yusup, S., Chin, B.L.F., Lam, M.K., Shahbaz, M., Unrean, P., Acda, M.N., Rianawati, E., "Thermogravimetric kinetic modelling of in-situ catalytic pyrolytic conversion of rice husk to bioenergy using rice hull ash catalyst," *Bioresource Technology*, **261**(2018)213-222.

Lu, H., Guo, X., Liu, Y., Gong, X., "Effect of Particle Size on Flow Mode and Flow Characteristics of Pulverized Coal," *KONA Powder and Particle Journal*, **32**(2015)143-153.

Lumay, G., Boschini, F., Traina, K., Bontempi, S., Remy, J.C., Cloots, R., Vandewalle, N., "Measuring the flowing properties of powders and grains," *Powder Technology*, **224**(2012)19-27.

Lyu, H., Gao, B., He, F., Zimmerman, A.R., Ding, C., Tang, J., Crittenden, J.C., "Experimental and modeling investigations of ball-milled biochar for the removal of aqueous methylene blue," *Chemical Engineering Journal*, **335**(2018)110-119.

Ma, Z., Zhang, Y., Shen, Y., Wang, J., Yang, Y., Zhang, W., Wang, S., "Oxygen migration characteristics during bamboo torrefaction process based on the properties of torrefied solid, gaseous, and liquid products," *Biomass and Bioenergy*, **128**(2019)105300.

Magalhães, D., Panahi, A., Kazanç, F., Levendis, Y.A., "Comparison of single particle combustion behaviours of raw and torrefied biomass with Turkish lignites," *Fuel*, **241**(2019)1085-1094.

Mahadevan, R., Adhikari, S., Shakya, R., Wang, K., Dayton, D.C., Li, M., Pu, Y., Ragauskas, A.J., "Effect of torrefaction temperature on lignin macromolecule and product distribution from HZSM-5 catalytic pyrolysis," *Journal of Analytical and Applied Pyrolysis*, **122**(2016)95-105.

Mahmoud, D.K., Salleh, M.A.M., Karim, W.A.W.A., Idris, A., Abidin, Z.Z., "Batch adsorption of basic dye using acid treated kenaf fibre char: equilibrium, kinetic and thermodynamic studies," *Chemical Engineering Journal*, **181**(2012)449-457.

Mallick, D., Poddar, M.K., Mahanta, P., Moholkar, V.S., "Discernment of synergism in pyrolysis of biomass blends using thermogravimetric analysis," *Bioresource Technology*, **261**(2018)294-305.

Mandal, S., Bhattacharya, T.K., Verma, A.K., Haydary, J., "Optimization of process parameters for bio-oil synthesis from pine needles (Pinus roxburghii) using response surface methodology," *Chemical Papers*, **72(3)**(2018)603-616.

Mani, S., Tabil, L.G., Sokhansanj, S., "Grinding performance and physical properties of wheat and barley straws, corn stover and switchgrass," *Biomass and Bioenergy*, **27(4)**(2004)339-352.

Mann, B.F., Chen, H., Herndon, E.M., Chu, R.K., Tolic, N., Portier, E.F., Roy Chowdhury, T., Robinson, E.W., Callister, S.J., Wullschleger, S.D., Graham, D.E., Liang, L., Gu, B., "Indexing Permafrost Soil Organic Matter Degradation Using High-Resolution Mass Spectrometry," *PLOS ONE*, **10**(6)(2015)e0130557.

Manouchehrinejad, M., Yue, Y., de Morais, R.A.L., Souza, L.M.O., Singh, H., Mani, S., "Densification of Thermally Treated Energy Cane and Napier Grass," *BioEnergy Research*, **11(3)**(2018)538-550.

Mante, O.D., Agblevor, F., Oyama, S., McClung, R., "The influence of recycling non-condensable gases in the fractional catalytic pyrolysis of biomass," *Bioresource Technology*, **111**(2012)482-490.

Martín-Lara, M., Ronda, A., Zamora, M., Calero, M., "Torrefaction of olive tree pruning: Effect of operating conditions on solid product properties," *Fuel*, **202**(2017)109-117.

Mehmood, M.A., Ye, G., Luo, H., Liu, C., Malik, S., Afzal, I., Xu, J., Ahmad, M.S., "Pyrolysis and kinetic analyses of Camel grass (Cymbopogon schoenanthus) for bioenergy," *Bioresource Technology*, **228**(2017)7-24.

Meng, J., Park, J., Tilotta, D., Park, S., "The effect of torrefaction on the chemistry of fast-pyrolysis bio-oil," *Bioresource Technology*, **111**(2012)439-446.

Min, F., Zhang, M., Zhang, Y., Cao, Y., Pan, W.-P., "An experimental investigation into the gasification reactivity and structure of agricultural waste chars," *Journal of Analytical and Applied Pyrolysis*, **92(1)**(2011)250-257.

Mishra, G., Kumar, J., Bhaskar, T., "Kinetic studies on the pyrolysis of pinewood," *Bioresource Technology*, **182**(2015)282-288.

Mishra, R.K., Muraraka, A., Mohanty, K., "Optimization of process parameters and catalytic pyrolysis of Cascabela thevetia seeds over low-cost catalysts towards renewable fuel production," *Journal of the Energy Institute*, 93(5)(2020)2033-2043.

Moghtaderi, B., Meesri, C., Wall, T.F., "Pyrolytic characteristics of blended coal and woody biomass," *Fuel*, **83(6)**(2004)745-750.

Mohammed, I.Y., Abakr, Y.A., Kazi, F.K., Yusuf, S., "Effects of pretreatments of Napier grass with deionized water, sulfuric acid and sodium hydroxide on pyrolysis oil characteristics," *Waste and biomass valorization*, **8(3)**(2017a)755-773.

Mohammed, I.Y., Abakr, Y.A., Xing Hui, J.N., Alaba, P.A., Morris, K.I., Ibrahim, M.D., "Recovery of clean energy precursors from Bambara groundnut waste via pyrolysis: Kinetics, products distribution and optimisation using response surface methodology," *Journal of Cleaner Production*, **164**(2017b)1430-1445.

Mohammed, I.Y., Abakr, Y.A., Yusup, S., Kazi, F.K., "Valorization of Napier grass via intermediate pyrolysis: optimization using response surface methodology and pyrolysis products characterization," *Journal of Cleaner Production*, **142**(2017c)1848-1866.

Mohan, D., Abhishek, K., Sarswat, A., Patel, M., Singh, P., Pittman, C.U., "Biochar production and applications in soil fertility and carbon sequestration – a sustainable solution to crop-residue burning in India," *RSC Advances*, **8(1)**(2018)508-520.

Mohan, D., Pittman Jr, C.U., Steele, P.H., "Pyrolysis of wood/biomass for bio-oil: a critical review," *Energy & fuels*, **20(3)**(2006)848-889.

Mokheimer, E.M.A., Hussain, S., Nadeem, M.D., Abdulrahman, A.A.M., "Production Cost–Efficiency Relation for Room Air Conditioners and Its Economic and Environmental Impact," *Journal of Energy Resources Technology*, **139**(6)(2017)061601.

Moralı, U., Şensöz, S., "Pyrolysis of hornbeam shell (Carpinus betulus L.) in a fixed bed reactor: Characterization of bio-oil and bio-char," *Fuel*, **150**(2015)672-678.

Mullen, C.A., Boateng, A.A., Goldberg, N.M., Lima, I.M., Laird, D.A., Hicks, K.B., "Bio-oil and bio-char production from corn cobs and stover by fast pyrolysis," *Biomass and Bioenergy*, **34(1)**(2010)67-74.

Müller-Hagedorn, M., Bockhorn, H., Krebs, L., Müller, U., "A comparative kinetic study on the pyrolysis of three different wood species," *Journal of Analytical and Applied Pyrolysis*, **68-69**(2003)231-249.

Nam, H., Capareda, S., "Experimental investigation of torrefaction of two agricultural wastes of different composition using RSM (response surface methodology)," *Energy*, **91**(2015)507-516.

Nazari, L., Yuan, Z., Ray, M.B., Xu, C.C., "Co-conversion of waste activated sludge and sawdust through hydrothermal liquefaction: optimization of reaction parameters using response surface methodology," *Applied Energy*, **203**(2017)1-10.

Negahdar, L., Gonzalez-Quiroga, A., Otyuskaya, D., Toraman, H.E., Liu, L., Jastrzebski, J.T.B.H., Van Geem, K.M., Marin, G.B., Thybaut, J.W., Weckhuysen, B.M., "Characterization and Comparison of Fast Pyrolysis Bio-oils from Pinewood, Rapeseed Cake, and Wheat Straw Using 13C NMR and Comprehensive GC × GC," *ACS Sustainable Chemistry & Engineering*, **4(9)**(2016)4974-4985.

Niu, Y., Lv, Y., Lei, Y., Liu, S., Liang, Y., Wang, D., Hui, S.e., "Biomass torrefaction: properties, applications, challenges, and economy," *Renewable and Sustainable Energy Reviews*, **115** (2019)109395.

Oasmaa, A., Elliott, D.C., Müller, S., "Quality control in fast pyrolysis bio-oil production and use," *Environmental Progress & Sustainable Energy*, **28(3)**, (2009)404-409.

Ohm, T.-I., Chae, J.-S., Kim, J.-K., Oh, S.-C., "Study on the characteristics of biomass for co-combustion in coal power plant," *Journal of Material Cycles and Waste Management*, **17(2)**(2015)249-257.

Oramahi, H.A., Wahdina, Diba, F., Nurhaida, Yoshimura, T., "Optimization of Production of Lignocellulosic Biomass Bio-oil from Oil Palm Trunk," *Procedia Environmental Sciences*, **28**(2015)769-777.

Pach, M., Zanzi, R., Björnbom, E., "Torrefied biomass a substitute for wood and charcoal," *6th Asia-Pacific International symposium on combustion and energy utilization*, (2002).

Pan, Y.G., Velo, E., Roca, X., Manyà, J.J., Puigjaner, L., "Fluidized-bed co-gasification of residual biomass/poor coal blends for fuel gas production," *Fuel*, **79(11)**(2000)1317-1326.

Pandey, C., Sharma, D., 2005. "Ecology of Acacia nilotica–based traditional agroforestry system in central India," *Bull NIIE*, **15**(2005)109-116.

Park, J., Meng, J., Lim, K.H., Rojas, O.J., Park, S., "Transformation of lignocellulosic biomass during torrefaction," *Journal of Analytical and Applied Pyrolysis*, **100**(2013)199-206.

Phanphanich, M., Mani, S., "Impact of torrefaction on the grindability and fuel characteristics of forest biomass," *Bioresource Technology*, **102(2)**(2011)1246-1253.

Pimchuai, A., Dutta, A., Basu, P., "Torrefaction of agriculture residue to enhance combustible properties," *Energy & Fuels*, **24(9)**(2010)4638-4645.

Pinto, F., Paradela, F., Gulyurtlu, I., Ramos, A.M., "Prediction of liquid yields from the pyrolysis of waste mixtures using response surface methodology," *Fuel Processing Technology*, **116**(2013)271-283.

Poletto, M., Zattera, A.J., Santana, R.M.C., "Thermal decomposition of wood: Kinetics and degradation mechanisms," *Bioresource Technology*, **126**(2012)7-12.

Polidoro, A.d.S., Scapin, E., Lazzari, E., Silva, A.N., dos Santos, A.L., Caramão, E.B., Jacques, R.A., "Valorization of coffee silverskin industrial waste by pyrolysis: From optimization of bio-oil production to chemical characterization by GC × GC/qMS," *Journal of Analytical and Applied Pyrolysis*, **129**(2018)43-52.

Pordesimo, L., Hames, B., Sokhansanj, S., Edens, W., "Variation in corn stover composition and energy content with crop maturity," *Biomass and Bioenergy*, **28(4)**(2005)366-374.

Prajapati, A.K., Mondal, M.K., "Hazardous As(III) removal using nanoporous activated carbon of waste garlic stem as adsorbent: Kinetic and mass transfer mechanisms," *Korean Journal of Chemical Engineering*, **36(11)**(2019)1900-1914.

Prins, M.J., Ptasinski, K.J., Janssen, F.J., 2006a. "Torrefaction of wood: Part 1. Weight loss kinetics," *Journal of analytical and applied pyrolysis*, **77(1)**(2006a)28-34.

Prins, M.J., Ptasinski, K.J., Janssen, F.J., "Torrefaction of wood: Part 2. Analysis of products," *Journal of analytical and applied pyrolysis*, 77**(1)**(2006b)35-40.

Que, W., Jiang, L., Wang, C., Liu, Y., Zeng, Z., Wang, X., Ning, Q., Liu, S., Zhang, P., Liu, S., "Influence of sodium dodecyl sulfate coating on adsorption of methylene blue by biochar from aqueous solution," *Journal of Environmental Sciences*, **70**(2018)166-174.

Rafatullah, M., Sulaiman, O., Hashim, R., Ahmad, A., "Adsorption of methylene blue on low-cost adsorbents: a review," *Journal of hazardous materials*, **177(1-3)**(2010)70-80.

Raj, D., Haokip, V., Chandrawanshi, S., "Acacia nilotica:A Multipurpose Tree and Source of Indian Gum Arabic," *South Indian Journal of Biological Sciences*, **1**(2015)66-69.

Raveendran, K., Ganesh, A., "Adsorption characteristics and pore-development of biomass-pyrolysis char," *Fuel*, **77(7)**(1998)769-781.

Ren, S., Lei, H., Wang, L., Bu, Q., Chen, S., Wu, J., "Thermal behaviour and kinetic study for woody biomass torrefaction and torrefied biomass pyrolysis by TGA," *Biosystems engineering*, **116(4)**(2013a)420-426.

Ren, S., Lei, H., Wang, L., Bu, Q., Chen, S., Wu, J., Julson, J., Ruan, R., "The effects of torrefaction on compositions of bio-oil and syngas from biomass pyrolysis by microwave heating," *Bioresource Technology*, **135**(2013b)659-664.

Repellin, V., Govin, A., Rolland, M., Guyonnet, R., "Energy requirement for fine grinding of torrefied wood," *Biomass and Bioenergy*, **34(7)**(2010)923-930.

Rezaiyan, J., Cheremisinoff, N.P., "Gasification technologies: a primer for engineers and scientists," *CRC press*, (2005).

Ro, D., Kim, Y.-M., Lee, I.-G., Jae, J., Jung, S.-C., Kim, S.C., Park, Y.-K., "Bench scale catalytic fast pyrolysis of empty fruit bunches over low cost catalysts and HZSM-5 using a fixed bed reactor," *Journal of Cleaner Production*, **176**(2018)298-303.

Ronix, A., Pezoti, O., Souza, L.S., Souza, I.P., Bedin, K.C., Souza, P.S., Silva, T.L., Melo, S.A., Cazetta, A.L., Almeida, V.C., "Hydrothermal carbonization of coffee husk: Optimization of experimental parameters and adsorption of methylene blue dye," *Journal of environmental chemical engineering*, **5(5)**(2017)4841-4849.

Rous, eacute, P., "Comparison of Methods for the Measurement of the Angle of Repose of Granular Materials," *Geotechnical Testing Journal*, 37(2014)164-168.

Ru, B., Wang, S., Dai, G., Zhang, L., "Effect of torrefaction on biomass physicochemical characteristics and the resulting pyrolysis behavior," *Energy & Fuels*, **29(9)**(2015)5865-5874.

S. Lam, P., Sokhansanj, S., Bi, X., J. Lim, C., J. Naimi, L., Hoque, M., Mani, S., R. Womac, A., Narayan, S., P. Ye, X., "Bulk Density of Wet and Dry Wheat Straw and Switchgrass Particles," *Applied Engineering in Agriculture*, **24(3)**(2008)351.

Sadaka, S., Negi, S., "Improvements of biomass physical and thermochemical characteristics via torrefaction process," *Environmental Progress & Sustainable Energy*, **28(3)**(2009)427-434.

Saikia, R., Baruah, B., Kalita, D., Pant, K.K., Gogoi, N., Kataki, R., "Pyrolysis and kinetic analyses of a perennial grass (Saccharum ravannae L.) from north-east India: Optimization through response surface methodology and product characterization," *Bioresource Technology*, **253**(2018)304-314.

Saini, J., Garg, V., Gupta, R., "Removal of Methylene Blue from aqueous solution by Fe3O4@ Ag/SiO2 nanospheres: Synthesis, characterization and adsorption performance," *Journal of Molecular Liquids*, **250**(2018)413-422.

Salleh, M.A.M., Mahmoud, D.K., Karim, W.A.W.A., Idris, A., "Cationic and anionic dye adsorption by agricultural solid wastes: A comprehensive review," *Desalination*, **280**(1)(2011)1-13.

Sangon, S., Hunt, A.J., Attard, T.M., Mengchang, P., Ngernyen, Y., Supanchaiyamat, N., "Valorisation of waste rice straw for the production of highly effective carbon based adsorbents for dyes removal," *Journal of cleaner production*, **172**(2018)1128-1139.

Santoso, E., Ediati, R., Kusumawati, Y., Bahruji, H., Sulistiono, D., Prasetyoko, D., "Review on recent advances of carbon based adsorbent for methylene blue removal from waste water," *Materials Today Chemistry*, **16**(2020)100233.

Saratale, R.G., Saratale, G.D., Cho, S.-K., Ghodake, G., Kadam, A., Kumar, S., Mulla, S.I., Kim, D.-S., Jeon, B.-H., Chang, J.S., Shin, H.-S., "Phyto-fabrication of silver nanoparticles by Acacia nilotica leaves: Investigating their antineoplastic, free radical scavenging potential and application in H2O2 sensing," *Journal of the Taiwan Institute of Chemical Engineers*, **99**(2019)239-249.

Scurlock, J.M., Dayton, D.C., Hames, B., "Bamboo: an overlooked biomass resource?," *Biomass and Bioenergy*, **19(4)**(2000)229-244.

Shabbar, S., Janajreh, I., "Thermodynamic equilibrium analysis of coal gasification using Gibbs energy minimization method," *Energy Conversion and Management*, **65**(2013)755-763.

Shahryari, Z., Goharrizi, A.S., Azadi, M., "Experimental study of methylene blue adsorption from aqueous solutions onto carbon nano tubes," *International Journal of Water Resources and Environmental Engineering*, **2(2)**(2010)016-028.

Sharma, R.K., Wooten, J.B., Baliga, V.L., Hajaligol, M.R., "Characterization of chars from biomass-derived materials: pectin chars," *Fuel*, **80(12)**(2001)1825-1836.

Shen, D.K., Gu, S., Luo, K.H., Wang, S.R., Fang, M.X., "The pyrolytic degradation of wood-derived lignin from pulping process," *Bioresource Technology*, **101(15)** (2010)6136-6146.

Shi, L., Zhang, G., Wei, D., Yan, T., Xue, X., Shi, S., Wei, Q., "Preparation and utilization of anaerobic granular sludge-based biochar for the adsorption of methylene blue from aqueous solutions," *Journal of Molecular Liquids*, **198**(2014)334-340.

Sindhu, R., Binod, P., Pandey, A., "Biological pretreatment of lignocellulosic biomass–An overview," *Bioresource Technology*, **199**(2016)76-82.

Singh, R.k., Sarkar, A., Chakraborty, J.P., "Effect of torrefaction on the physicochemical properties of pigeon pea stalk (Cajanus cajan) and estimation of kinetic parameters," *Renewable Energy*, **138**(2019a)805-819.

Singh, S., Chakraborty, J.P., Mondal, M.K., "Optimization of process parameters for torrefaction of Acacia nilotica using response surface methodology and characteristics of torrefied biomass as upgraded fuel," *Energy*, **186**(2019b)115865.

Singh, S., Chakraborty, J.P., Mondal, M.K., "Torrefaction of woody biomass (Acacia nilotica): investigation of fuel and flow properties to study its suitability as a good quality solid fuel," *Renewable Energy*, **153**(2020a)711-724.

Singh, S., Prasad Chakraborty, J., Kumar Mondal, M., "Intrinsic kinetics, thermodynamic parameters and reaction mechanism of non-isothermal degradation of torrefied Acacia nilotica using isoconversional methods," *Fuel*, **259**(2020b)116263.

Slopiecka, K., Bartocci, P., Fantozzi, F., "Thermogravimetric analysis and kinetic study of poplar wood pyrolysis," *Applied Energy*, **97**(2012)491-497.

Song, X., Yang, Y., Zhang, M., Zhang, K., Wang, D., "Ultrasonic pelleting of torrefied lignocellulosic biomass for bioenergy production," *Renewable Energy*, **129**(2018)56-62.

Sriram, A., Swaminathan, G., "Pyrolysis of Musa balbisiana flower petal using thermogravimetric studies," *Bioresource Technology*, **265**(2018)236-246.

Stamatov, V., Honnery, D., Soria, J., "Combustion properties of slow pyrolysis bio-oil produced from indigenous Australian species," *Renewable Energy*, **31(13)**(2006)2108-2121.

Stoikos, T., "Upgrading of biomass pyrolysis liquids to high-value chemicals and fuel additives," in: *Biomass Pyrolysis Liquids Upgrading and Utilization*, Springer, (1991) pp. 227-241.

Stolarski, M.J., Szczukowski, S., Tworkowski, J., Klasa, A., "Yield, energy parameters and chemical composition of short-rotation willow biomass," *Industrial Crops and Products*, **46**(2013)60-65.

Strandberg, M., Olofsson, I., Pommer, L., Wiklund-Lindström, S., Åberg, K., Nordin, A., "Effects of temperature and residence time on continuous torrefaction of spruce wood," *Fuel Processing Technology*, **134**(2015)387-398.

Sumalinog, D.A.G., Capareda, S.C., de Luna, M.D.G, "Evaluation of the effectiveness and mechanisms of acetaminophen and methylene blue dye adsorption on activated biochar derived from municipal solid wastes," *Journal of Environmental Management*, **210**(2018)255-262.

Sun, L., Wan, S., Luo, W., "Biochars prepared from anaerobic digestion residue, palm bark, and eucalyptus for adsorption of cationic methylene blue dye: Characterization, equilibrium, and kinetic studies," *Bioresource Technology*, **140**(2013)406-413.

Szalay, A., Kelemen, A., Pintye-Hódi, K., "The influence of the cohesion coefficient (C) on the flowability of different sorbitol types," *Chemical Engineering Research and Design*, **93**(2015)349-354.

Tan, I.A.W., Ahmad, A.L., Hameed, B.H., "Optimization of preparation conditions for activated carbons from coconut husk using response surface methodology," *Chemical Engineering Journal*, **137(3)**(2008)462-470.

Tillman, D.A., "Biomass cofiring: the technology, the experience, the combustion consequences," *Biomass and bioenergy*, **19(6)**(2000)365-384.

Tong, S., Xiao, L., Li, X., Zhu, X., Liu, H., Luo, G., Worasuwannarak, N., Kerdsuwan, S., Fungtammasan, B., Yao, H., "A gas-pressurized torrefaction method for biomass wastes," *Energy Conversion and Management*, **173**(2018)29-36.

Tooyserkani, Z., Sokhansanj, S., Bi, X., Lim, J., Lau, A., Saddler, J., Kumar, L., Lam, P.S., Melin, S., "Steam treatment of four softwood species and bark to produce torrefied wood," *Applied Energy*, **103**(2013)514-521.

Trakal, L., Šigut, R., Šillerová, H., Faturíková, D., Komárek, M., "Copper removal from aqueous solution using biochar: Effect of chemical activation," *Arabian Journal of Chemistry*, **7(1)**(2014)43-52.

Tripathi, M., Sahu, J.N., Ganesan, P., "Effect of process parameters on production of biochar from biomass waste through pyrolysis: A review," *Renewable and Sustainable Energy Reviews*, **55**(2016)467-481.

Tsai, W., Lee, M., Chang, Y., "Fast pyrolysis of rice husk: Product yields and compositions," *Bioresource Technology*, **98(1)**(2007)22-28.

Tumuluru, J.S., Heikkila, D.J., "Biomass Grinding Process Optimization Using Response Surface Methodology and a Hybrid Genetic Algorithm," *Bioengineering*, **6(1)**(2019)12.

Turmanova, S.C., Genieva, S.D., Dimitrova, A.S., Vlaev, L.T., "Non-isothermal degradation kinetics of filled with rise husk ash polypropene composites." *Express Polymer Letters*, **2**(2008)133-146.

Uchimiya, M., Lima, I.M., Thomas Klasson, K., Chang, S., Wartelle, L.H., Rodgers, J.E., "Immobilization of heavy metal ions (CuII, CdII, NiII, and PbII) by broiler litter-derived biochars in water and soil," *Journal of agricultural and food chemistry*, **58(9)**(2010)5538-5544.

Ukaew, S., Schoenborn, J., Klemetsrud, B., Shonnard, D.R., "Effects of torrefaction temperature and acid pretreatment on the yield and quality of fast pyrolysis bio-oil from rice straw," *Journal of Analytical and Applied Pyrolysis*, **129**(2018)112-122.

Vamvuka, D., Kakaras, E., Kastanaki, E., Grammelis, P., "Pyrolysis characteristics and kinetics of biomass residuals mixtures with lignite," *Fuel*, **82(15)**(2003)1949-1960.

van der Stelt, M.J.C., Gerhauser, H., Kiel, J.H.A., Ptasinski, K.J., "Biomass upgrading by torrefaction for the production of biofuels: A review," *Biomass and Bioenergy*, **35(9)**(2011)3748-3762.

Vargas, A.M., Cazetta, A.L., Kunita, M.H., Silva, T.L., Almeida, V.C., "Adsorption of methylene blue on activated carbon produced from flamboyant pods (Delonix regia): Study of adsorption isotherms and kinetic models," *Chemical Engineering Journal*, **168(2)**(2011)722-730.

Vasco-Correa, J., Ge, X., Li, Y., 2016. "Biological pretreatment of lignocellulosic biomass," in: *Biomass Fractionation Technologies for a Lignocellulosic Feedstock Based Biorefinery*, Elsevier, pp. 561-585.

Vassilev, S.V., Baxter, D., Andersen, L.K., Vassileva, C.G., "An overview of the composition and application of biomass ash. Part 1. Phase–mineral and chemical composition and classification," *Fuel*, **105**(2013)40-76.

Vecino Mantilla, S., Gauthier-Maradei, P., Álvarez Gil, P., Tarazona Cárdenas, S., "Comparative study of bio-oil production from sugarcane bagasse and palm empty fruit bunch: Yield optimization and bio-oil characterization," *Journal of Analytical and Applied Pyrolysis*, **108**(2014)284-294.

Vieira, F.R., Romero Luna, C.M., Arce, G.L.A.F., Ávila, I., "Optimization of slow pyrolysis process parameters using a fixed bed reactor for biochar yield from rice husk," *Biomass and Bioenergy*, **132**(2020)105412.

Vlaev, L.T., Georgieva, V.G., Genieva, S.D., "Products and kinetics of non-isothermal decomposition of vanadium(IV) oxide compounds" *Journal of Thermal Analysis and Calorimetry*, **88(3)**(2007)805-812.

Vlaev, L.T., Markovska, I.G., Lyubchev, L.A., "Non-isothermal kinetics of pyrolysis of rice husk," *Thermochimica Acta*, **406(1)**(2003)1-7.

Volpe, R., Zabaniotou, A.A., Skoulou, V., "Synergistic effects between lignin and cellulose during pyrolysis of agricultural waste," *Energy & fuels*, **32(8)**(2018)8420-8430.

Vuthaluru, H.B., "Thermal behaviour of coal/biomass blends during co-pyrolysis," *Fuel Processing Technology*, 85(2)(2004)141-155.

Vyazovkin, S., Burnham, A.K., Criado, J.M., Pérez-Maqueda, L.A., Popescu, C., Sbirrazzuoli, N., "ICTAC Kinetics Committee recommendations for performing kinetic computations on thermal analysis data," *Thermochimica Acta*, **520(1)**(2011)1-19.

Wanassi, B., Hariz, I.B., Ghimbeu, C.M., Vaulot, C., Hassen, M.B., Jeguirim, M., "Carbonaceous adsorbents derived from textile cotton waste for the removal of Alizarin S dye from aqueous effluent: kinetic and equilibrium studies," *Environmental Science and Pollution Research*, **24**(11)(2017)10041-10055.

Wang, G., Luo, Y., Deng, J., Kuang, J., Zhang, Y., "Pretreatment of biomass by torrefaction," *Chinese Science Bulletin*, **56(14)**(2011)1442-1448.

Wang, H., Xie, R., Zhang, J., Zhao, J., "Preparation and characterization of distillers' grain based activated carbon as low cost methylene blue adsorbent: Mass transfer and equilibrium modeling," *Advanced Powder Technology*, **29**(1)(2018a)27-35.

Wang, S., Dai, G., Ru, B., Zhao, Y., Wang, X., Xiao, G., Luo, Z., "Influence of torrefaction on the characteristics and pyrolysis behavior of cellulose," *Energy*, **120**(2017)864-871.

Wang, X., Wu, J., Chen, Y., Pattiya, A., Yang, H., Chen, H., "Comparative study of wet and dry torrefaction of corn stalk and the effect on biomass pyrolysis polygeneration," *Bioresource Technology*, **258**(2018b)88-97.

Wannapeera, J., Fungtammasan, B., Worasuwannarak, N., "Effects of temperature and holding time during torrefaction on the pyrolysis behaviors of woody biomass," *Journal of Analytical and Applied Pyrolysis*, **92(1)**(2011a)99-105.

Wannapeera, J., Fungtammasan, B., Worasuwannarak, N., "Effects of temperature and holding time during torrefaction on the pyrolysis behaviors of woody biomass," *Journal of Analytical and Applied Pyrolysis*, **92(1)**(2011b)99-105.

Wannapeera, J., Worasuwannarak, N., "Examinations of chemical properties and pyrolysis behaviors of torrefied woody biomass prepared at the same torrefaction mass yields," *Journal of Analytical and Applied Pyrolysis*, **115**(2015)279-287.

Wen, J.-L., Sun, S.-L., Yuan, T.-Q., Xu, F., Sun, R.-C., "Understanding the chemical and structural transformations of lignin macromolecule during torrefaction," *Applied Energy*, **121**(2014)1-9.

Worasuwannarak, N., Sonobe, T., Tanthapanichakoon, W., "Pyrolysis behaviors of rice straw, rice husk, and corncob by TG-MS technique," *Journal of Analytical and Applied Pyrolysis*, **78(2)**(2007)265-271.

Xin, S., Mi, T., Liu, X., Huang, F., "Effect of torrefaction on the pyrolysis characteristics of high moisture herbaceous residues," *Energy*, **152**(2018)586-593.

Xin, S., Yang, H., Chen, Y., Wang, X., Chen, H., "Assessment of pyrolysis polygeneration of biomass based on major components: Product characterization and elucidation of degradation pathways," *Fuel*, **113**(2013)266-273.

Xu, L., Cheng, J.-H., Liu, P., Wang, Q., Xu, Z.-X., Liu, Q., Shen, J.-Y., Wang, L.-J., "Production of bio-fuel oil from pyrolysis of plant acidified oil," *Renewable Energy*, **130**(2019)910-919.

Xu, Y., Chen, B., "Investigation of thermodynamic parameters in the pyrolysis conversion of biomass and manure to biochars using thermogravimetric analysis," *Bioresource Technology*, **146**(2013)485-493.

Yaman, S., "Pyrolysis of biomass to produce fuels and chemical feedstocks," *Energy Conversion and Management*, 45**(5)**(2004)651-671.

Yan, W., Acharjee, T.C., Coronella, C.J., Vasquez, V.R., "Thermal pretreatment of lignocellulosic biomass," *Environmental Progress & Sustainable Energy*, **28(3)**(2009)435-440.

Yang, H., Yan, R., Chen, H., Lee, D.H., Zheng, C., "Characteristics of hemicellulose, cellulose and lignin pyrolysis," *Fuel*, **86(12)**(2007)1781-1788.

Yang, Q., Ren, S., Zhao, Q., Lu, R., Hang, C., Chen, Z., Zheng, H., "Selective separation of methyl orange from water using magnetic ZIF-67 composites," *Chemical Engineering Journal*, **333**(2018)49-57.

Yang, X., Ma, F., Yu, H., Zhang, X., Chen, S., "Effects of biopretreatment of corn stover with white-rot fungus on low-temperature pyrolysis products," *Bioresource Technology*, **102(3)**(2011)3498-3503.

Yang, Y., Sun, M., Zhang, M., Zhang, K., Wang, D., Lei, C., "A fundamental research on synchronized torrefaction and pelleting of biomass," *Renewable Energy*, **142**(2019)668-676.

Yang, Z., Kumar, A., Huhnke, R.L., "Review of recent developments to improve storage and transportation stability of bio-oil," *Renewable and Sustainable Energy Reviews*, **50**(2015)859-870.

Ye, J., Cong, X., Zhang, P., Hoffmann, E., Zeng, G., Wu, Y., Zhang, H., Fan, W., "Phosphate Adsorption onto Granular-Acid-Activated-Neutralized Red Mud: Parameter Optimization, Kinetics, Isotherms, and Mechanism Analysis," *Water, Air, & Soil Pollution*, **226(9)**(2015)306.

Yildiz, G., Ronsse, F., Venderbosch, R., van Duren, R., Kersten, S.R., Prins, W., "Effect of biomass ash in catalytic fast pyrolysis of pine wood," *Applied Catalysis B: Environmental*, **168**(2015)203-211.

Yu, Y., Zeng, Y., Zuo, J., Ma, F., Yang, X., Zhang, X., Wang, Y., "Improving the conversion of biomass in catalytic fast pyrolysis via white-rot fungal pretreatment," *Bioresource technology*, **134**(2013)198-203.

Yuan, X., He, T., Cao, H., Yuan, Q., "Cattle manure pyrolysis process: kinetic and thermodynamic analysis with isoconversional methods," *Renewable Energy*, **107**(2017)489-496.

Yue, Y., Singh, H., Singh, B., Mani, S., "Torrefaction of sorghum biomass to improve fuel properties," *Bioresource Technology*, **232**(2017)372-379.

Zaror, C., Pyle, D., "The pyrolysis of biomass: A general review," *Proceedings of the Indian Academy of Sciences Section C: Engineering Sciences*, **5**(4)(1982)269.

Zhai, S., Li, M., Wang, D., Zhang, L., Yang, Y., Fu, S., "In situ loading metal oxide particles on bio-chars: Reusable materials for efficient removal of methylene blue from wastewater," *Journal of Cleaner Production*, **220**(2019)460-474.

Zhang, L., Xu, C., Champagne, P., "Overview of recent advances in thermo-chemical conversion of biomass," *Energy Conversion and Management*, **51(5)**(2010)969-982.

Zhang, L., Xu, S., Zhao, W., Liu, S., "Co-pyrolysis of biomass and coal in a free fall reactor," *Fuel*, **86(3)**(2007)353-359.

Zhang, P., O'Connor, D., Wang, Y., Jiang, L., Xia, T., Wang, L., Tsang, D.C.W., Ok, Y.S., Hou, D., "A green biochar/iron oxide composite for methylene blue removal," *Journal of Hazardous Materials*, **384**(2020)121286.

Zhang, S., Chen, T., Xiong, Y., Dong, Q., "Effects of wet torrefaction on the physicochemical properties and pyrolysis product properties of rice husk," *Energy Conversion and Management*, **141**(2017)403-409.

Zheng, A., Zhao, Z., Chang, S., Huang, Z., He, F., Li, H., "Effect of Torrefaction Temperature on Product Distribution from Two-Staged Pyrolysis of Biomass," *Energy & Fuels*, **26(5)**(2012)2968-2974.

Zheng, A., Zhao, Z., Chang, S., Huang, Z., Zhao, K., Wei, G., He, F., Li, H., "Comparison of the effect of wet and dry torrefaction on chemical structure and pyrolysis behavior of corncobs," *Bioresource Technology*, **176**(2015)15-22.

Zheng, A., Zhao, Z., Huang, Z., Zhao, K., Wei, G., Wang, X., He, F., Li, H., "Catalytic Fast Pyrolysis of Biomass Pretreated by Torrefaction with Varying Severity," *Energy & Fuels*, **28(9)**(2014)5804-5811.

Zheng, A.Q., Zhao, Z.L., Chang, S., Huang, Z., Wang, X.B., He, F., 2013. "Effect of torrefaction on structure and fast pyrolysis behavior of corncobs," *Bioresource Technology,* **128**(2013)370.

Zheng, Y., Tao, L., Yang, X., Huang, Y., Liu, C., Gu, J., Zheng, Z., "Effect of the torrefaction temperature on the structural properties and pyrolysis behavior of biomass," *BioResources*, **12(2)**(2017)3425-3447.

Publications

(1) **Satyansh Singh**, Jyoti Prasad Chakraborty, Monoj Kumar Mondal. "Torrefaction of woody biomass (Acacia nilotica): Investigation of fuel and flow properties to study its suitability as a good quality solid fuel". **Renewable Energy 153 (2020) 711-724.** https://doi.org/10.1016/j.renene.2020.02.037

(2) **Satyansh Singh**, Jyoti Prasad Chakraborty, Monoj Kumar Mondal. "Intrinsic kinetics, thermodynamic parameters and reaction mechanism of non-isothermal degradation of torrefied *Acacia nilotica* using isoconversional methods". **Fuel 259 (2020) 116263.** https://doi.org/10.1016/j.fuel.2019.116263

(3) **Satyansh Singh**, Jyoti Prasad Chakraborty, Monoj Kumar Mondal. "Optimization of process parameters for torrefaction of *Acacia Nilotica* and characteristics of torrefied biomass as upgraded fuel". **Energy 186 (2019) 115865.** https://doi.org/10.1016/j.energy.2019.115865

(4) **Satyansh Singh**, Jyoti Prasad Chakraborty, Monoj Kumar Mondal. "Pyrolysis of torrefied biomass: Optimization of process parameters using response surface methodology, characterization, and comparison of properties of pyrolysis oil from raw biomass". **Journal of Cleaner Production 272 (2020) 122517**. https://doi.org/10.1016/j.jclepro.2020.122517

(5) **Satyansh Singh**, Anuj Kumar Prajapati, Jyoti Prasad Chakraborty, Monoj Kumar Mondal. "Comparative study for removal of aqueous methylene blue using biochar from pyrolysis of raw and torrefied biomass: kinetics, isotherm, thermodynamics and mass transfer studies". **Journal of Cleaner Production (under review)**.

Conferences

(1) Satyansh Singh, Jyoti Prasad Chakraborty, Monoj Kumar Mondal. "In-depth characteristics of products from torrefaction of woody biomass". **(BEHSD 2018)** Lucknow.

(2) Delivered oral presentation in **Chemcon-2017** organized by IICHE at Haldia Institute of Technology, West Bengal. **(Best paper award for oral presentation).**

(3) Participated in a workshop INSPIRE-2017 organized by IIT BHU, Varanasi.

(4) Participated as delegate in the 73rd Annual Convention and International conference of the **OTAI, 2018**.

(5) Presented poster titled "Efficient gasification through torrefied biomass" on **Institute day** April, 2016 organized by **IIT (BHU) Varanasi**.